NUREG/CR-6452
BMI-2195

The Second International Piping Integrity Research Group (IPIRG-2) Program

Final Report
October 1991-April 1996

Manuscript Completed: January 1997
Date Published: March 1997

Prepared by
A. Hopper, G. Wilkowski, P. Scott, R. Olson, D. Rudland,
T. Kilinski, R. Mohan, N. Ghadiali, D. Paul

Battelle
505 King Avenue
Columbus, OH 43201

M. Mayfield, NRC Project Manager

Prepared for
Division of Engineering Technology
Office of Nuclear Regulatory Research
U.S. Nuclear Regulatory Commission
Washington, DC 20555-0001
NRC Job Code D2060

DISCLAIMER

ABSTRACT

The IPIRG-2 program was an international group program managed by the U.S. NRC and funded by organizations from 15 nations. The emphasis of the IPIRG-2 program was the development of data to verify fracture analyses for cracked pipes and fittings subjected to dynamic/cyclic load histories typical of seismic events. The scope included: (1) the study of more complex dynamic/cyclic load histories, i.e., multi-frequency, variable amplitude, simulated seismic excitations, than those considered in the IPIRG-1 program, (2) crack sizes more typical of those considered in Leak-Before-Break (LBB) and in-service flaw evaluations, (3) through-wall-cracked pipe experiments which can be used to validate LBB-type fracture analyses, (4) cracks in and around pipe fittings, such as elbows, and (5) laboratory specimen and separate effect pipe experiments to provide better insight into the effects of dynamic and cyclic load histories. Also undertaken were an uncertainty analysis to identify the issues most important for LBB or in-service flaw evaluations, updating computer codes and databases, the development and conduct of a series of round-robin analyses, and analyst's group meetings to provide a forum for nuclear piping experts from around the world to exchange information on the subject of pipe fracture technology.

CONTENTS

Page

EXECUTIVE SUMMARY xxi

ACKNOWLEDGMENTS xxvii

NOMENCLATURE xxix

PREVIOUS REPORTS IN SERIES xli

1.0 INTRODUCTION 1-1

1.1 Historical Perspective 1-1
1.2 Rationale and Objective Behind the IPIRG-2 Program 1-12
1.3 Structure of the IPIRG-2 Program 1-13
1.4 Structure of the IPIRG-2 Final Report 1-15
1.5 References 1-15

2.0 MATERIAL PROPERTY EVALUATIONS 2-1

2.1 General Material Property Evaluations of IPIRG-2 Materials 2-1

2.1.1 Tensile Test Results 2-1
2.1.2 Fracture Toughness Results from Monotonic C(T) Specimen Tests 2-2

2.2 Cyclic Effects on Small Scale Specimen Fracture 2-5

2.2.1 Analysis Approaches to Account for Cyclic Loading Effects 2-5
2.2.2 Cyclic C(T) Experiments 2-6
2.2.3 Fractographic Results 2-20

2.3 References 2-21

3.0 FULL-SCALE PIPE EXPERIMENTS 3-1

3.1 Experimental Procedures 3-1
3.2 6-Inch Nominal Diameter Through-Wall-Cracked Pipe Experiments 3-1

3.2.1 Japanese STS410 TWC Pipe Experiments 3-2
3.2.2 Intermediate Stress Ratio Experiment 3-4
3.2.3 Dynamic, Monotonic, Pressurized Through-Wall-Cracked Pipe Experiment 3-5
3.2.4 Comparison of J-R Curves Between the IPIRG-1 and IPIRG-2 6-Inch Nominal Diameter, Unpressurized, TWC Pipe Experiments 3-5

CONTENTS

Page

3.3 16-Inch Nominal Diameter Pipe and Fitting Experiments 3-9

3.3.1 Experimental Facilities 3-9
3.3.2 Simulated Seismic Pipe-System Experiments 3-14
3.3.3 Single-Frequency Pipe-System Experiments 3-22

3.4 References 3-29

4.0 ANALYSIS OF EXPERIMENTS 4-1

4.1 Fracture Analysis Prediction Methodologies 4-1

4.1.1 "Intuitively Consistent" Flaw Size Definition 4-1
4.1.2 Material Property Data to be Used in Fracture Analyses 4-3
4.1.3 Description of Fracture Prediction Analysis Methods 4-6
4.1.4 Description of Failure Avoidance Criteria 4-15
4.1.5 Elbow Fracture Mechanics Analyses 4-17

4.2 6-Inch Nominal Diameter Through-Wall-Cracked Pipe Moment Predictions 4-20

4.2.1 Prediction of Dynamic TWC Pipe Response Using Dynamic Material Properties 4-20
4.2.2 Maximum Moment Predictions for Japanese STS410 Carbon Steel Pipe 4-29
4.2.3 Cyclic TWC Pipe Moment Predictions Using Cyclic J-R Curves 4-30

4.3 16-Inch Nominal Diameter Straight Pipe Maximum Stress Predictions 4-35

4.3.1 Simulated-Seismic, Surface-Cracked Pipe Experiments 4-35
4.3.2 Elbow Girth Weld Pipe Experiments 4-39
4.3.3 Short Surface-Cracked Pipe Experiments 4-42
4.3.4 Short Through-Wall-Cracked Pipe Experiments 4-44

4.4 Comparison of Maximum Stress Predictions from Failure Avoidance Criteria with Experimental Data for 16-Inch Diameter Straight Pipe Experiments 4-51

4.4.1 Approach 1 Fracture Ratios 4-51
4.4.2 Approach 2 Fracture Ratios 4-53

4.5 16-Inch Diameter Elbow Maximum Stress Predictions 4-54

4.5.1 Development of a Simplified Failure Avoidance Analysis Procedure for Cracks in Fittings 4-57

4.6 References 4-72

CONTENTS

Page

5.0 ADDITIONAL TECHNICAL DEVELOPMENTS AND ANALYSES 5-1

5.1 Development and Improvement of Computer Codes 5-1

5.1.1 NRCPIPE - Version 3.0 for Windows 5-1
5.1.2 NRCPIPES - Version 3.0 for Windows 5-2
5.1.3 IP2ELBOW - Version 1.0 for Windows 5-4
5.1.4 SQUIRT - Version 2.4 for DOS 5-5
5.1.5 QA of Computer Programs 5-6

5.2 Development and Improvements of Databases 5-7

5.2.1 AXIALCK 5-7
5.2.2 CIRCUMCK 5-7
5.2.3 ELBOWCK 5-8
5.2.4 TEECK 5-8
5.2.5 PIFRAC 5-8
5.2.6 QA OF DATABASES 5-9

5.3 Uncertainty Analyses 5-11

5.3.1 Uncertainty Analyses Relative to LBB 5-13
5.3.2 Uncertainty Analyses Relative to In-Service Flaw Evaluations 5-22
5.3.3 Ranking of Significance of Various Factors Investigated 5-28

5.4 Comparison of Pre-Test Ultrasonic Examination of Test Flaws with Post-Test Measurements 5-28

5.5 References 5-33

6.0 TASK 5 - INFORMATION EXCHANGE SEMINARS AND WORKSHOPS 6-1

6.1 LBB Seminars 6-1
6.2 Round-Robin Analyses 6-1

6.2.1 Problem Set A: Evaluations of Fracture Properties and Pipe Loads 6-1
6.2.2 Problem Set B: Crack-Opening and Leak-Rate Evaluations 6-3
6.2.3 Problem Set C: Dynamic Analysis of Cracked Pipes 6-5
6.2.4 Problem Set D: Fracture Evaluations of Elbows 6-6

6.3 Fracture Analyst's Group Meetings 6-6

6.3.1 First Meeting 6-6
6.3.2 Second Meeting 6-8
6.3.3 Third Meeting 6-9
6.3.4 Fourth Meeting 6-12

Page

6.4 Summary 6-13
6.5 References 6-13

7.0 SUMMARY AND DISCUSSION OF RESULTS 7-1

7.1 Key Results from the Material Property Evaluations 7-1

7.1.1 Discussion of Loading Rate Effects on the Tensile and Fracture Toughness Properties of Ferritic Nuclear Grade Piping Steels 7-1
7.1.2 Discussion of Cyclic Effects on the Fracture Toughness of Nuclear Grade Steels 7-2

7.2 Key Results from the Straight Pipe and Elbow Fracture Analyses 7-6

7.2.1 Straight Pipe Fracture Analyses 7-6
7.2.2 Key Results From the Flawed Fittings Fracture Analyses 7-27

7.3 Key Results from Other Issues Studied in the IPIRG-2 Program 7-34

7.3.1 Discussion of Results from Uncertainty Analysis 7-34
7.3.2 Discussion of Computer Codes and Databases 7-36
7.3.3 Seminars and Workshops 7-37

7.4 References 7-38

8.0 CONCLUSIONS 8-1

8.1 Conclusions Related to the Major Issues Which Formed the Rationale and Basis for the Formation and Conduct of the IPIRG-2 Program 8-1

8.1.1 Developing a Better Understanding of Dynamic and Cyclic Load Effects on Material Properties and Their Impact on the Behavior of Cracked Pipe Sections 8-1
8.1.2 Effect of More Complex Load Histories on the Fracture Behavior of Cracked Pipe Sections 8-5
8.1.3 Behavior of Smaller Crack Sizes When Subjected to Dynamic/Cyclic Load Histories 8-6
8.1.4 Behavior of Cracks Adjacent to Elbows 8-7
8.1.5 Behavior of Cracks in Elbows 8-7

8.2 Other Key Observations and Conclusions from the IPIRG-2 Program 8-8

8.2.1 Effect of Flaw Size Definition on the Predictions of the Load-Carrying Capacity of a Cracked Pipe Section 8-8
8.2.2 Inherent Inaccuracy Associated with the ASME Section XI Z-Factor Approaches 8-9

CONTENTS

Page

8.2.3 Inherent Inaccuracy Associated with the R6 Revision 3 Option 1 and ASME Code Case N-494-3 FAD Approaches 8-10
8.2.4 Conclusions from Uncertainty Analyses 8-10

8.3 References 8-11

CONTENTS

Page

LIST OF FIGURES

1.1 STA pipe system for dynamic flawed pipe tests (Ref. 1.21) 1-6

1.2 Piping System 1 configuration evaluated in EPRI/NRC Piping Reliability Program (Ref. 1.25) 1-6

1.3 Effect of cyclic loading on fracture toughness as measured by the crack-tip-opening-angle (CTOA) on through-wall-cracked pipe (a) Incremental plastic displacement, (b) Effect of stress ratio (R) and incremental plastic displacement 1-8

1.4 Artist's conception of the test configuration used in IPIRG-1 1-9

1.5 Modeling of a multilinear moment-rotation curve 1-10

1.6 Plot of the ratio of the maximum experimental stress to the Net-Section-Collapse predicted stress for the IPIRG-1 pipe system and companion experiments showing the effect of the various stress components on the fracture behavior 1-11

2.1 $J_{QS,\,cyc}/J_{QS,\,mono}$ for DP2-A23 stainless steel cyclic experiments (Experiment 1.3-3 on stainless steel pipe A8II) 2-10

2.2 Crack growth per cyclic for a variety of cyclic DP2-A23 stainless steel experiments 2-11

2.3 $J_{QS,\,cyc}/J_{QS,\,mono}$ for DP2-F30 carbon steel cyclic experiments 2-12

2.4 Crack growth per cycle for the cyclic DP2-F30 carbon steel experiments 2-12

2.5 $J/J_{QS,\,mono}$ for carbon steel and stainless steel submerged-arc welds and base metals 2-13

2.6 Experimental J versus calculated J for dynamic, cyclic (R = -1) experiments 2-14

2.7 J-R curve comparison for a DP2-A23 stainless steel specimen tested at R = -1 2-15

2.8 J-R curves from C(T) specimens machined from Pipe DP2-A8I 2-17

2.9 J-R curves from C(T) specimens machined from Pipe DP2-A8II 2-17

2.10 Several J-R curves for comparison with Experiment 1.3-3 2-19

2.11 General view of three additional DP2-A23 stainless steel cyclic C(T) specimens 2-20

3.1 Fixtures used in the 6-inch diameter, unpressurized, through-wall-cracked pipe experiments 3-2

3.2 Experimental setup for Experiment 1-9 3-6

Page

3.3 Moment-rotation response for Experiment 1-9 3-6

3.4 J-R curves for STS410 and A106 Grade B carbon steel TWC pipe experiments 3-7

3.5 J-R curves for A106 Grade B carbon steel TWC pipe experiments 3-8

3.6 Quasi-static, monotonic pipe bend test fixture used for the 16-inch nominal diameter straight pipe experiments 3-11

3.7 Quasi-static, monotonic, elbow test facility 3-11

3.8 Artist's conception of the IPIRG pipe loop experimental facility 3-12

3.9 Schematic of primary restraint system used for the IPIRG-2 straight pipe-system experiments 3-12

3.10 Modifications to pipe-system test loop for the elbow girth weld and elbow pipe-system experiments 3-14

3.11 Actuator displacement-time history for the SSE forcing function 3-17

3.12 Actuator displacement-time history for the "Test" forcing function 3-17

3.13 Response spectra of actuator motion for the simulated seismic load history 3-18

3.14 Comparison of the elastically-calculated stresses for actual plant piping systems to the crack section stresses for the IPIRG simulated seismic pipe-system experiments 3-18

3.15 Comparison of the moment-rotation responses for the stainless steel, base-metal, simulated-seismic experiment (1-1) with the companion stainless steel, base-metal, single-frequency pipe-system experiment (1.3-3) from IPIRG-1 (Ref. 3.9) 3-20

3.16 Comparison of the moment-CMOD responses for the carbon steel, base-metal, simulated-seismic experiment (1-2) and the companion carbon steel, base-metal, single-frequency, pipe-system experiment (1.3-2) from IPIRG-1 (Ref. 3.9) 3-20

3.17 Comparison of the moment-rotation responses for the short-through-wall-cracked, simulated-seismic experiment (1-7) and the quasi-static, monotonic, four-point bend, short-through-wall-cracked pipe experiment (1-8) 3-21

3.18 Actuator displacement versus time history for single-frequency pipe-system experiments 3-22

Page

3.19 Comparison of the moment-rotation responses for the short-surface crack, stainless steel weld, single-frequency, pipe-system experiment conducted as part of IPIRG-2 (1-5) and the companion short surface crack, stainless steel weld, quasi-static, monotonic, pressure and four-point bend experiment from IPIRG-2 (1-6) and the companion long surface-crack, stainless steel weld, single-frequency, pipe-system experiment (1.3-5) from IPIRG-1 (Ref. 3.9) (a) Experiments 1-5 and 1-6, (b) Experiments 1-5 and 1.3-5 3-24

3.20 Comparison of the moment-rotation responses for the carbon steel, elbow girth weld single-frequency, pipe-system experiment conducted as part of IPIRG-2 (1-3) and the companion carbon steel elbow, girth weld, quasi-static, monotonic, pressure and bend experiment (1-4) from IPIRG-2 3-25

3.21 Moment-time response of the seven, single-frequency, pipe-system experiments from IPIRG-1 (Ref. 3.9) and IPIRG-2 which used the same single-frequency forcing function 3-26

3.22 Moment versus crack-mouth-opening displacement for carbon steel elbow experiments 3-27

3.23 Moment versus crack-mouth-opening displacement for stainless steel elbow experiments 3-28

4.1 Nomenclature for weld crack geometry 4-2

4.2 Nomenclature and assumed stress distribution for the Net-Section-Collapse analysis 4-8

4.3 Nomenclature and key parameter definitions for Dimensionless-Plastic-Zone-Parameter analysis 4-9

4.4 Ratio of experimental failure stress to Net-Section-Collapse predicted failure stress as a function of the Dimensionless-Plastic-Zone-Parameter (DPZP) 4-11

4.5 Reduced thickness analogy for SC.ENG1 and SC.ENG2 analysis methods 4-14

4.6 Failure assessment diagram (FAD) for R6 Revision 3 Option 1 analysis method 4-17

4.7 Variation of J with applied bending moment for axially and circumferentially cracked elbows and circumferentially cracked straight pipe (a) $R_m/t = 10$, (b) $R_m/t = 20$ 4-19

4.8 Load versus pipe displacement at the load point for Experiments 4.2-1 and 3.3-1 4-22

4.9 Load versus load-line displacement for STS410 C(T) specimen tests 4-22

4.10 Quasi-static and dynamic load versus displacement records for carbon steel C(T) specimens (a) DP2-F30, (b) D2-F29 4-24

Page

4.11 Comparison of quasi-static and dynamic J-R curves for C(T) specimens removed from pipe materials DP2-F30 (Experiment 1.2-8), IP-F13 (Experiment 4.2-1), and DP2-F22 (Experiment 1-9) (a) DP2-F30, (b) IP-F13, (c) DP2-F22 4-27

4.12 Normalized dynamic-maximum-moment predictions versus pipe diameter for carbon steel TWC pipe 4-28

4.13 Normalized maximum moment predictions versus pipe diameter for stainless steel TWC pipe 4-34

4.14 Normalized maximum moment predictions versus pipe diameter for carbon steel TWC pipe 4-35

4.15 Moment-CMOD response for stainless steel, base metal, simulated-seismic, pipe-system experiment (1-1) 4-38

4.16 Moment-CMOD response for stainless steel, base metal, single-frequency, pipe-system experiment (1.3-3) from IPIRG-1 (Ref. 4.2) 4-38

4.17 Comparison of weld cross-section geometry for straight pipe-to-pipe and elbow-to-straight pipe girth welds 4-41

4.18 Moment-rotation response for the stainless steel weld short surface-cracked pipe-system experiment (1-5) and the stainless steel weld long surface-cracked pipe-system experiment (1.3-5) from IPIRG-1 (Ref. 4.2) 4-42

4.19 Schematic of patch used to seal the two combined pressure and bend through-wall-cracked pipe experiments 4-45

4.20 Moment-CMOD response for the short through-wall-cracked pipe-system experiment (1-7) 4-46

4.21 Quasi-static, monotonic and dynamic, monotonic J-R curves for A106 Grade B carbon steel pipe material (DP2-F23) used in the two short through-wall-cracked pipe experiments 4-47

4.22 Photographs showing differences in angled crack growth in TWC pipe experiments (a) Experiment 1-7, (b) Experiment 1-8 4-48

4.23 Effect of angled crack growth on moment-rotation response (a) IPIRG-1 Subtask 1.2 6-inch Schedule 120 A106 Grade B experimental results, (b) Schematic showing increase in $dm/d\phi$ with more axial crack growth 4-49

4.24 Calculated moment across the crack due to the presence of the curve plate seal 4-50

4.25 Design stress versus fracture analyses limit-load definitions 4-58

Page

4.26 Comparison of applied J versus moment for the axially-cracked SC.ELB3 elbow analysis and four straight pipe analyses (SC.TNP1, SC.TNP2, SC.ENG1, and SC.ENG2) (a) $R_m/t = 5$, (b) $R_m/t = 10$, (c) $R_m/t = 20$ 4-60

4.27 The applied J as a function of the ratio of moments for the straight pipe to moments for an axial-flank-cracked elbow 4-62

4.28 Ratio of the moments for the straight pipe to moments for an axial-flank-cracked elbow as a function of the stress indices B_2 and C_2 4-63

4.29 Ratio of the moments for the straight pipe to moments for an axial-flank-cracked elbow as a function of the stress indices B_2 and C_2 with the experimental data for EDF Experiment Y6135 shown for a comparison 4-65

4.30 Comparison of applied J versus moment for the circumferentially-cracked SC.ELB1 and SC.ELB2 elbow analyses and four straight pipe analyses (SC.TNP1, SC.TNP2, SC.ENG1, and SC.ENG2) (a) $R_m/t = 5$, (b) $R_m/t = 10$, (c) $R_m/t = 20$ 4-67

4.31 The applied J as a function of the ratio of moments for the straight pipe to moments for a circumferentially cracked elbow (a) Using the SC.ELB1 analysis, (b) Using the SC.ELB2 analysis 4-68

4.32 Ratio of the moments for the straight pipe to moments for a circumferentially cracked elbow as a function of the stress indices B_2 and C_2 (a) Using the SC.ELB1 analysis, (b) Using the SC.ELB2 analysis 4-69

4.33 Ratios of moments for the straight pipe to moments for a circumferentially cracked elbow as a function of the stress indices B_2 with the IPIRG-2 elbow experimental data shown for comparison 4-72

5.1 Comparison of calculated crack lengths for a given leak rate for various default crack morphology parameters (corrosion-fatigue crack using the SQUIRT2 program) 5-14

5.2 Comparison of calculated leak rates between current SQUIRT Version 2.4 and NUREG/CR-6004 COD dependant crack morphology models (small leak rates) 5-14

5.3 Conditional failure probability for a crack in a SAW in a 28-inch nominal diameter Schedule 80 TP304 stainless steel pipe for various combinations of normal operating and N+SSE stresses 5-16

5.4 Ratio of NSC to EPFM maximum loads (Z-factor) when keeping the circumferential TWC length equal to 30 percent of the circumference for stainless steel base metal pipe and varying the toughness to account for quasi-static and dynamic/cyclic effects 5-18

Page

5.5 Comparison of maximum loads for 3.785 lpm (1 gpm) leaking cracks that were off-centered during leakage but centered during N+SSE loading versus angle from center of off-centered crack to the bending plane 5-19

5.6 Conditional failure probability for a crack in the base metal of a 28-inch nominal diameter Schedule 80 TP304 stainless steel pipe for various crack orientations (off-centered cracks) 5-20

5.7 Effects of restrained bending from axial loading on COD normalized by the unrestrained COD 5-20

5.8 Ratio of leak rates, with and without residual stresses, as a function of applied loads 5-22

5.9 Ratio of NSC to EPFM maximum loads (Z-factor) for surface-cracked TP304 stainless steel pipe ($R_m/t = 10$) showing the effect of quasi-static and dynamic/cyclic toughness and comparisons with experimental data 5-23

5.10 Statistical results of depth/thickness ratio from the 1989 EPRI Round-Robin data (Ref. 5.31) (a) Original EPRI data (b) Battelle determination of mean, standard deviation, and coefficient of variance (COV) 5-25

5.11 Ratio of actual maximum moment, $M_{baseline}$, to mean maximum moment, M_{UT}, for uncertainty in UT crack depth measurement as a function of a/t (28-inch nominal diameter Schedule 80 TP304 stainless steel pipe with the crack in the base metal) 5-26

5.12 Maximum moments for circumferentially surface-cracked 28-inch nominal diameter Schedule 80 pipe with the crack in the base metal (a) Net-Section-Collapse analysis values, (b) SC.TNP1 J-estimation scheme values 5-27

5.13 Pre- and post-test flaw depth measurements for Experiment 2-1, carbon steel elbow containing an internal fatigue-sharpened surface crack (Elbow IP2-FE18) 5-31

5.14 Pre- and post-test flaw measurements for Experiment 2-2, carbon steel elbow containing an internal fatigue-sharpened surface crack (Elbow IP2-FE16) 5-31

5.15 Comparison of UT flaw sizing of carbon steel piping data to EPRI UT round robin mean curve for stainless steel pipe 5-32

7.1 Load-displacement-crack growth records from a GE/EPRI TWC pipe prediction and C(T) specimens illustrating the need to change δ_{cyc}/δ_i after crack initiation to produce comparable cyclic crack growth between the two specimen types (a) GE/EPRI J-estimation scheme prediction of TWC pipe Experiment 4131-5 (Pipe DP2-A23) (J-R curve used in the calculation is inserted figure), (b) C(T) specimen results 7-5

7.2 Sketch of an "off-centered" crack showing the angle ψ between the crack centerline where the bending stresses are highest and the location along the crack front where the crack is the deepest 7-7

Page

7.3 Calculated number of cycles to maximum moment as a function of pipe diameter based on a cyclic dJ/da crack growth analysis 7-13

7.4 Response spectra for the simulated-seismic forcing function used in IPIRG-2 7-15

7.5 Comparison of moment-CMOD response for the stainless steel base metal, simulated-seismic, pipe-system experiment conducted as part of IPIRG-2 (Experiment 1-1) and the stainless steel base metal, single-frequency, pipe-system experiment conducted as part of IPIRG-1 (Experiment 1.3-3) (a) Experiment 1-1, (b) Experiment 1.3-3 7-16

7.6 Comparison of the experimental moment-rotation response with the SC.TNP1 predicted moment-rotation response for Experiment 1-3 7-18

7.7 Comparison of the experimental moment-rotation response with the SC.TNP1 predicted moment-rotation response for Experiment 1-5 7-18

7.8 Comparison of flow stresses using actual tensile data (average of yield and ultimate) and flow stresses based on S_m(Code) and S_m(Actual) values 7-22

7.9 Comparison of ASME Section XI Appendix C Z-factors with calculated Z-factors from the Dimensionless-Plastic-Zone-Parameter analysis using both the "Best-Fit" and "95-percent Confidence Level" curves 7-24

7.10 Comparison of ASME Section XI Appendix H Z-factors with calculated Z-factors from the Dimensionless-Plastic-Zone-Parameter analysis using both the "Best-Fit" and "95-percent Confidence Level" curves 7-24

7.11 Ratio of the maximum bending stress using the NRCPIPES R6 analysis-to-the NSC stress as a function of the ratio of the pressure stress-to-the maximum bending stress using the NRCPIPES Version 3.0 R6 analysis 7-27

7.12 Prediction of maximum moment as a function of crack depth for the Net-Section-Collapse, SC.TNP1, DPZP, R6, ASME Appendix H, SC.ELB1, and SC.ELB2 analysis methods with experimental moments from the two carbon steel elbow experiments (Experiments 2-1 and 2-2) shown for comparison 7-30

7.13 Prediction of maximum moment as a function of crack depth for the Net-Section-Collapse, SC.TNP1, DPZP, R6, ASME Appendix C, SC.ELB1, and SC.ELB2 analysis methods with experimental moments from the two stainless steel elbow experiments (Experiments 2-3 and 2-4) shown for comparison 7-30

7.14 Ratio of moments for the straight pipe to moments for an axial-flank-cracked elbow as a function of the stress index B_2 with the experimental data for EDF Experiment Y6135 shown for comparison 7-32

Page

7.15 Ratio of moments for the straight pipe to moments for a circumferential-cracked elbow as a function of the stress index B_2 with the IPIRG-2 elbow experimental data shown for comparison 7-32

7.16 The parameter Υ^e_x (equal to $M^{pipe}/M^{elbow})|_J$) as a function of the stress index B_2 for both the axial flank Υ^e_a and circumferential extrados Υ^e_c crack cases for both the SC.TNP1 and SC.TNP2 straight pipe analysis methods 7-33

CONTENTS

Page

LIST OF TABLES

1.1 Timeline of nuclear industry milestones and major pipe fracture research programs 1-2

1.2 Matrix of full-scale pipe and elbow experiments conducted as part of the IPIRG-2 program .. 1-14

2.1 Piping materials evaluated during IPIRG-2 2-1

2.2 Tensile test results from IPIRG-2 2-3

2.3 Fracture toughness test results from IPIRG-2 from monotonic C(T) specimen tests 2-4

2.4 Advantages and disadvantages of several analysis methods for assessing cycle load effects on the load-carrying capacity of cracked pipes 2-7

2.5 Cyclic-load C(T) test matrix 2-8

2.6 Cyclic-load C(T) fracture toughness summary 2-9

3.1 Test matrix for Japanese STS410 TWC pipe experiments 3-3

3.2 Summary of key results from Experiments 4.2-1, 4.2-2, 4.2-3, and 3.3-1 3-3

3.3 Experimental results for A106 Grade B 6-inch diameter TWC pipe experiments 3-4

3.4 Key results for 6-inch diameter, dynamic, monotonic, pressurized through-wall-cracked pipe experiment 3-5

3.5 Listing of 16-inch diameter IPIRG-2 and companion experiments from related programs 3-10

3.6 Comparison of damping values and first four natural frequencies for the IPIRG-1 and IPIRG-2 pipe loop facilities 3-13

3.7 Key results from 16-inch diameter simulated seismic pipe-system experiments conducted as part of IPIRG-2 and companion experiments from IPIRG-2 and related programs (Refs. 3.8, 3.9, and 3.10) 3-19

3.8 Key results from 16-inch diameter single-frequency pipe-system experiments conducted as part of IPIRG-2 and companion experiments from IPIRG-2 and related programs (Refs. 3.8, 3.9, and 3.10) 3-23

3.9 Key results from 16-inch nominal diameter, long-radius elbow, single-frequency, pipe-system and quasi-static, monotonic, pressure and bend companion experiments conducted as part of IPIRG-2 3-27

4.1 Tensile properties of pipe materials used in IPIRG-2 and companion pipe experiments 4-5

Page

4.2 Extrapolated J_D-R curve constants for the pipe materials used in the IPIRG-2 and companion pipe experiments 4-7

4.3 Maximum moment ratios for Experiment 1.2-8 4-25

4.4 Maximum moment ratios for Experiment 4.2-1 4-25

4.5 Maximum longitudinal stress ratios for Experiment 1-9 4-25

4.6 Comparison of maximum experimental moments with Net-Section-Collapse, DPZP, GE/EPRI, LBB.ENG2, and R6 predictions for the 6-inch nominal diameter STS410 through-wall-cracked pipe experiments 4-30

4.7 Predictions of stainless steel, cyclic, TWC pipe response using a variety of J-R curves 4-31

4.8 Predictions of carbon steel, cyclic, TWC pipe response using a variety of J-R curves 4-33

4.9 Results of fracture ratio calculations for the two simulated-seismic, surface-cracked, pipe-system experiments (1-1 and 1-2) plus two companion quasi-static, four-point bend (4112-8 and EPRI 13S) and two companion single-frequency, pipe-system experiments (1.3-2 and 1.3-3) 4-37

4.10 Results of fracture ratio calculations for the two elbow girth weld experiments plus the companion straight pipe girth weld experiments 4-40

4.11 Results of fracture ratio calculations for the two short surface-cracked pipe experiments plus the companion long surface-cracked pipe experiments 4-43

4.12 Results of fracture ratio calculations for the two 16-inch diameter through-wall-cracked pipe experiments conducted as part of IPIRG-2 Task 1 4-46

4.13 Comparison of maximum experimental stresses for IPIRG-2 straight pipe surface-cracked pipe experiments and companion experiments with maximum stress predictions from ASME Section XI and R6 Revision 3 Option 1 4-52

4.14 Fracture ratios for Task 2 elbow experiments 4-56

4.15 Parameters used in analyses of axial, flank, surface-cracked elbows 4-59

4.16 Parameters in EDF axial, flank, surface-cracked, elbow Experiment Y6135 4-64

4.17 Parameters in IPIRG-2 circumferential, extrados, surface-crack, elbow experiments 4-71

5.1 Ranking of various technical issues investigated that affect LBB evaluations 5-29

Page

5.2 Ranking of various technical issues investigated that affect in-service flaw evaluations 5-30

7.1 Comparison of maximum moment predictions between using the "intuitively consistent" and ASME Code crack size definitions for the SC.TNP1 analysis method for seven experiments which considered cracks in welds 7-8

7.2 Comparison of fracture ratios for two dynamic, monotonic, experiments (1.2-8 and 4.2-1) for two analysis methods (LBB.ENG2 and LBB.NRC) using the quasi-static stress-strain curve and two different J-R curves (quasi-static and dynamic) 7-10

7.3 Comparison of fracture ratios (experimental to predicted maximum loads) for two quasi-static, cyclic (R = -1) pipe experiments (1.2-4 and 1.2-5) for two analysis methods (LBB.ENG2 and LBB.NRC) using four different J-R curves 7-12

7.4 Ranking of various technical aspects investigated in uncertainty study that affect LBB evaluations 7-35

7.5 Ranking of various technical aspects investigated in uncertainty study that affect in-service flaw evaluations 7-36

EXECUTIVE SUMMARY

The Second International Piping Integrity Research Group (IPIRG-2) program was an international group program managed by the United States Nuclear Regulatory Commission (U.S. NRC) and funded by a consortium of organizations from 15 nations. The unifying goal of the IPIRG-2 program was the development of data for the verification of fracture analyses for cracked pipes and fittings subjected to dynamic and/or cyclic load histories. The dynamic/cyclic load histories used in the IPIRG-2 program tended to be more complex than those used in the IPIRG-1 program. In addition, the IPIRG-2 program explored different crack geometries/locations than had been considered in the earlier IPIRG-1 pipe-system experiments, and laboratory specimen and separate effect pipe experiments were conducted to provide better insight into the effects of dynamic and cyclic load histories.

The IPIRG-2 program was structured into five tasks:

Task 1 - Pipe System Experiments with Flaws in Straight Pipe and Welds
Task 2 - Fracture of Flawed Fittings
Task 3 - Cyclic and Dynamic Load Effects on Fracture Toughness
Task 4 - Resolution of Issues from IPIRG-1 and Related Programs
Task 5 - Seminars, Workshops, and Program Management

The scope and purpose of Task 1 was to build upon past work through the development of pipe fracture data in areas where data were lacking at the beginning of the IPIRG-2 program. The specific areas of interest to this effort included:

- the effects of simulated-seismic load histories,
- the behavior of cracks at geometric discontinuities such as at an elbow/straight pipe girth weld,
- the behavior of smaller surface cracks than those considered in IPIRG-1, and
- the behavior of short through-wall-cracks subjected to dynamic/cyclic load histories.

A total of five dynamic pipe-system and four quasi-static experiments were conducted in Task 1.

Task 2 involved compiling a database of past pipe fitting fracture tests, developing elbow fracture analyses, development of cracked elbow experimental data, development of a simplified method that could be used for code implementation and validation of the fracture analyses. Four 16-inch diameter elbow experiments with circumferential surface cracks along the extrados of the test elbows were conducted, two quasi-static bend and two dynamic pipe-system experiments. For each loading conditions, both carbon and stainless steel elbows were tested.

Task 3 focussed on the resolution of differences in toughness values observed between laboratory specimen and full-scale pipe experimental data resulting from load history effects, such as the cyclic and dynamic loading effects that can occur during a seismic event. This task involved laboratory C(T) specimen tests, full-scale dynamic and/or cyclic pipe experiments, supporting finite element analyses, and sensitivity analyses.

Executive Summary

the carbon steel SAW investigated, if the weld crown was ground off (i.e., during UT inspection), then the typically more accurate analyses overpredicted the failure load by 10 to 20 percent.

(17) When accounting for the actual strength of the pipes tested, the degree of inaccuracy associated with the ASME Section XI Appendices C and H approaches are comparable. The Z-factor approaches for both criteria will tend to under predict the experiment moment by a factor of approximately 1.5 for 16-inch diameter pipe for a material with strength properties near the strength properties provided in Section II of the ASME Code. This level of inaccuracy will increase with pipe diameter.

(18) The ASME definition of flow stress for ferritic steels ($2.4S_m$) underestimates the strength of the A106 Grade B carbon steels evaluated in this and related programs while the ASME definition of flow stress for austenitic steels ($3S_m$) overestimates the strength of the TP304 stainless steels evaluated in this and related programs. It might be that one flow stress definition could be established for both materials.

(19) The degree of inaccuracy associated with the R6 Revision 3 Option 1 approach and ASME Code Case N-494-3 (without the ASME applied safety factors) are comparable if the same material property data and a consistent flaw size definition are used for the two analyses. Furthermore, the degree of inaccuracy associated with these FAD-based approaches is comparable to that for the ASME Appendices C and H approaches (without the ASME applied safety factors), if one accounts for the differences in material property data. It is of note that there is a problem with the coding of the L_r term for the R6 analysis in the NRCPIPES code for the case where the pressure stress is a significant factor of the bending stress.

(20) The technical issues which were found from an uncertainty analyses to be highly significant or important for LBB evaluations were:

(a) The LBB failure probability is controlled more by normal operating stresses than SSE stresses, and hence, aspects that affect crack-opening displacement (COD) predictions at normal operating stresses are more important than pipe fracture aspects.

(b) The effect of restraint of pressure induced bending on the COD for a circumferential through-wall crack in a small diameter pipe changed the LBB failure loads by a factor of nine (compared with the safety factor of $\sqrt{2}$). This effect may also be important for intermediate diameter pipe.

(c) The effect of residual stresses for thin-walled pipe (believed to be less than 25mm in thickness but may vary with joint design and welding parameters) can significantly reduce the crack-opening displacements for leak-rate analyses,

(d) The COD-dependent crack morphology model parameters for very small leak rates (< 3.5 lpm) appears to rectify problems with the friction factor equations in existing leak rate codes.

(21) The technical issues which were found from an uncertainty analysis to be highly significant or important for in-service flaw evaluations was:

(a) Using statistics from a 1989 EPRI UT round robin, the uncertainty in the ultrasonic flaw sizing for deep cracks ($a/t > 0.5$), especially for long crack lengths, had a significant affect on the failure moments, whereas, for short crack lengths ($\theta/\pi < 0.25$) and/or shallow cracks ($a/t < 0.25$), the uncertainty in the flaw depth size does not significantly affect the failure moments.

(b) Cyclic load effects on the toughness of stainless steel base metal caused elastic-plastic fracture rather than limit-load failure, hence for Service Level C and D loads, an EPFM correction (Z-factor) is needed in the ASME Section XI pipe flaw evaluation criteria for austenitic base metals.

ACKNOWLEDGMENTS

The IPIRG Program was an international group program coordinated by the U.S. Nuclear Regulatory Commission's Electrical, Materials, and Mechanical Engineering Branch of the Office of Nuclear Regulatory Research under Contract No. NRC-04-91-063 to Battelle. Mr. Michael Mayfield was the U.S. NRC program manager. Dr. Allen Hopper was the Battelle program manager.

The members of the IPIRG-2 Program and their representatives to the IPIRG Technical Advisory Group (TAG) were:

Bulgaria	
- CUAEPP	Mr. Y. Yanev
Canada	
- AECB(*)	Dr. B. Jarman(**), Mr. J. K. Pereira
- Ontario Hydro	Mr. M. Kozluk
Czech Republic	
- NRI	Dr. J. Zdárek, Dr. M. Brumovsky, Dr. P. Kadečka, Mr. J. Palyza
France	
- EDF(*)	Mr. C. Faidy(**), Mr. P. Le Delliou
- CEA	Ms. F. Gantenbein, Mr. E. Debec-Mathet
- Framatome	Dr. Ph. Gilles
Hungary	
- HAEC	Mr. A. Fehérvári
Italy	
- ANPA-DISP(*)	Dr. C. Maricchiolo(**)
Japan	
- CRIEPI(*)	Dr. K. Kashima(**), Mr. N. Miura
- Hitachi	Mr. J. Kawahata, Mr. K. Murayama
- Mitsubishi Heavy Industry	Mr. H. Yokota
- Toshiba	Mr. K. Kitsukawa
- IHI	Mr. H. Ogata, Mr. H. Sugino

(*) Contractual organization.

(**) TAG representative at end of program.

Lithuania	
- VATESI	Mr. P. Vaisnys
Republic of China	
- INER/AEC(*)	Dr. Li-Fu Lin(**)
Republic of Korea	
- KINS(*)	Dr. J. B. Lee(**), Dr. Y. H. Choi, Dr. Y. -W. Park
- SKKU	Dr. Y. J. Kim
Slovak Republic	
- VUJE	Dr. L. Kupca
- NRA	Dr. J. Misak
Sweden	
- SKI(*)	Dr. G. Hedner
- SAQ	Dr. B. Brickstad(**)
Switzerland	
- KKL(*)	Mr. R. Wanner(**)
- HSK	Dr. D. H. Njo
United Kingdom	
- Nuclear Electric(*)	Dr. T. C. Chivers(**), Dr. J. Darlastan
United States	
- U.S. NRC-RES(*)	Mr. M. Mayfield(**)
- U.S. NRC-NRR(*)	Mr. K. Wichman(**)
- EPRI(*)	Mr. S. Gosselin(**), Dr. Y. K. Tang

We would like to express our appreciation for the support and interest of the IPIRG members in this program.

Visiting scientists who stayed at Battelle during the IPIRG-2 program were: Dr. Y. H. Choi of KINS (Korea), Dr. C. Maricchiolo of ANPA-DISP (Italy), and Mr. N. Miura of CRIEPI (Japan). We would like to thank them for their contributions to this program.

We would like to thank others at Battelle who have helped in these efforts. Technicians who have contributed include: Mr. J. Anthony, Mr. E. Blakesley, Mr. R. Gertler, Mr. P. Held, Mr. P. Mincer, Mr. M. Oliver, Mr. D. Rider, Mr. D. Shoemaker, and Mr. G. Wall. We also would like to recogonize Mrs. V. Kreachbaum and Ms. Brenda Fuller for their assistance in preparing this report.

---

* Contractual organization.

** TAG representative at end of program.

NOMENCLATURE

1. SYMBOLS

a	Crack depth
a_{max}	Crack depth at the deepest location along the crack front
a_i	Initial crack length for a C(T) specimen
a_1	Crack depth referenced to the inside pipe surface for weld crack experiments
a_2	Crack depth referenced to the inside surface of the counterbore for weld crack experiments
â	Length of reduced section of pipe in LBB.ENG and SC.ENG analyses
B_2	Stress indice from ASME code
C	Circumferential
C_1	Statistically-based parameter from plastic zone size screening criteria
C_2	Stress indice from ASME code
C_3	Coefficient in power-law extrapolated J-R curve-fit expression
c	Distance from neutral bending axis
D	Pipe diameter
da/dN	Crack growth per cycle
d_{cb}	Depth of weld counterbore
D_i	Inside pipe diameter
D_m	Mean pipe diameter
D_o	Outside pipe diameter
E	Elastic modulus
f_1	Function in GE/EPRI J-estimation scheme for calculating elastic component of J

g	Unit of gravity
h	Characteristic bend parameter of a curved pipe or butt welded elbow
H(a/t)	Function in SC.ENG1 and SC.ENG2 J-estimation schemes
H_B	Function in LBB.ENG2 J-estimation scheme
h_{wc}	Height of weld crown
h_1	Function in EPRI/GE J-estimation scheme to calculate plastic contribution of J
$\hat{h}$	A constraint parameter defined as the ratio of the hydrostatic stress to the effective stress
I	Area moment of inertia
I_B	Function in LBB.ENG2 J-estimation scheme
J	J-integral fracture parameter
$J_{applied}$	Applied value of the J-integral
J_D	Deformation theory J
J_e	Elastic component of J
J_i	J at crack initiation
J_{Ic}	Plane strain J at crack initiation by ASTM813
J_M	Modified form of J
J_p	Plastic component of J
$J_{QS, mono}$	J for quasi-static, monotonic loading history
$J_{QS,cyc}$	J for quasi-static, cyclic loading history
$J_{dyn,cyc}$	J for dynamic, cyclic loading history
$J_{dyn,mono}$	J for dynamic, monotonic loading history
J_R	Crack growth resistance
K	LEFM stress intensity factor fracture parameter

K_I	Applied linear elastic stress intensity factor
K_{Ic}	Material toughness expressed in terms of K
K_r	Ratio of K_I to $K_r(a)$ from R6 analysis
L	Length parameter in SC.TNP analyses
L_B	Function in LBB.ENG2 J-estimation scheme
L_r	Load ratio in R6 analysis
m	Exponent in power-law extrapolated J-R curve-fit expression
M	Moment
M^{elbow}	Maximum predicted moment from a cracked-elbow analysis
$M_{baseline}$	Actual maximum moment
M_L^c	Net-Section-Collapse moment for a circumferentially surface-cracked pipe used in SC.ENG1 and SC.ENG2 analyses
M_L^d	Net-Section-Collapse moment for an uncracked pipe with a reduced thickness, t_e, used in SC.ENG1 and SC.ENG2 analyses
M_o	Limit moment for a cracked pipe under pure bending
M_{NSC}	Moment at Net-Section-Collapse
$M_{Max.Pred.}$	Predicted maximum moment
M^{pipe}	Maximum predicted moment from a cracked straight pipe analysis
M^B_{Pred}	Predicted moment for pure bending
M^{B+T}_{Pred}	Predicted moment for bending plus tension
M^B_{NSC}	Net-Section-Collapse predicted moment for pure bending
M^{B+T}_{NSC}	Net-Section-Collapse predicted moment for bending plus tension
M_{UT}	Mean maximum moment accounting for uncertainty in UT crack depth measurements
n	Ramberg-Osgood strain-hardening exponent
P	Total stress at maximum load

p	Pressure
P_e	Thermal expansion stress
P_m	Membrane stress
P_{NSC}	Net-Section-Collapse analysis predicted failure stress
Q	Constraint parameter
Q_m	Constraint parameter
r	Constant in power-law extrapolation J-R curve fit having a value of unity and same dimensions as Δa
R	Stress or load ratio, i.e., minimum stress (load)/maximum stress (load)
$R_{effective}$	Effective stress ratio for a pipe experiment accounting for the stress contribution due to internal pipe pressure
R_{el}	Bend radius of elbow
R_m	Mean pipe radius
S_m	ASME code design stress intensity
S_m(Actual)	S_m based on measured tensile properties
S_m(Code)	S_m based on Code properties
S_u	ASME Section II Part D ultimate strength
S_y	ASME Section II Part D yield strength
t	Pipe wall thickness
T	Thickness of C(T) specimen
t_1	Wall thickness of the pipe referenced to the inside pipe surface and excluding the weld crown height
t_2	Wall thickness of the pipe referenced to the inside surface of the counterbore and excluding the weld crown height
t_3	Wall thickness of the pipe referenced to the inside pipe surface and including the weld crown height

t_4	Wall thickness of the pipe referenced to the inside surface of the counterbore and including the weld crown height
t_e	Reduced wall thickness representation of cracked section in LBB.ENG2 method
t_{elbow}	Wall thickness of elbow
t_{pipe}	Wall thickness of pipe
V	Compliance function from GE/EPRI J-estimation scheme method
w	Width of C(T) specimen
Z	Stress multipliers in Section XI to account for low toughness
α	Ramberg-Osgood parameter
β	Angle from bottom of pipe to neutral bending axis
δ	Displacement
δ_{cyc}	Incremental cyclic plastic displacement from a cyclic test
δ_i	Displacement at crack initiation from a monotonic test
Δa	Change in crack length or depth, i.e., crack growth
ΔJ	Cyclic J-integral (Dowling approach)
ΔM_{NSC}	Difference in NSC predicted moments for pure bending and bending plus tension cases
ϵ	Strain
ϵ_o	Ramberg-Osgood reference strain
λ	Parameter is SQUIRT leak rate code
ψ	Angle between the crack centerline and the location along the crack front where the crack is the deepest
η-factor	Method for estimating fracture toughness of a pipe experiment from the experimental moment-rotation or load-displacement relationship
ϕ	Pipe rotation
σ	Stress

σ_b	Bending stress
$\sigma_B^{NSC(\sigma_y)}$	Net-Section-Collapse bending stress in R6 analysis using the yield strength in lieu of the flow stress in the analysis
$\sigma_{B_{analysis}}$	Predicted bending stress from the analysis
$\sigma_{B_{max}}$	Maximum bending stress
$\sigma_{B_{min}}$	Minimum bending stress
$\sigma_{B_{expt}}$	Experimental bending stress at maximum moment
σ_f	Flow stress
σ_m	Membrane stress due to internal pipe pressure
σ_N	Normal stress
σ_{N+SSE}	Normal plus SSE stress
σ_o	Ramberg-Osgood reference stress
σ_{SL-A}	Service Level A stress
σ_u	Ultimate strength
σ_y	Yield strength
θ	Half crack angle
Υ^e_a	Geometric stress multiplier related to the stress indices B_2 which gives the predicted moment for an axial crack in a pipe relative to the predicted moment for an axial crack in an elbow
Υ^e_c	Geometric stress multiplier related to the stress indices B_2 which gives the predicted stress for a circumferential crack in a pipe relative to the predicted stress for a circumferential crack in an elbow
Υ^f_x	General geometric stress multiplier related to B_2 stress indices which gives the predicted stress for a cracked pipe relative to the predicted stress for a cracked fitting where f stands for the type of fitting and x is the crack orientation

2. ACRONYMS AND INITIALISMS

3D	Three dimensional
ACS	Aged cast stainless steel
AECB	Atomic Energy Control Board (Canada)
AIT	American Institute of Taiwan
ANPA-DISP	Agenzia Najionale per la Protezion dell'Ambiarte (Italy)
ANL	Argonne National Laboratory (U.S.)
ASCE	American Society of Civil Engineers
ASME	American Society of Mechanical Engineers
ASTM	American Society for Testing and Materials
BCD	Battelle-Columbus Division (U.S.)
BWR	Boiling Water Reactor
BWROG	BWR Owner's Group
B&W	Babcock and Wilcox (U.S.)
CCP	Center-cracked panel specimen
CEA	Commissariat A L'Energie Atomique (France)
CEGB	Central Electric Generating Board, now Nuclear Electric (United Kingdom)
CMOD	Crack-mouth-opening displacement
COD	Crack-opening displacement
COV	Coefficient of variance
CPOF	Conditional probability of failure
CRIEPI	Central Research Institute of Electric Power Industry (Japan)
CS	Carbon steel

CSBM	Carbon steel base metal
CSW	Carbon steel weld
CTOA	Crack-tip-opening angle
C(T)	Compact (Tension)
CUAEPP	Commercial Use of Atomic Energy for Peaceful Purposes agency (Bulgaria)
d-c	Direct current
d-c EP	Direct-current electric potential
DEGB	Double-ended guillotine break
DEN	Double-edge-notch specimen
DOS	Disk operating system
DPZP	Dimensionless plastic-zone parameter
DP^3II	Degraded Piping Program - Phase II
DSA	Dynamic strain aging
DTRC	David Taylor Research Center (U.S.)
Dyn	Dynamic
DW	Dead Weight
EDF	Electricité de France
EDM	Electric-discharge machine
EPFM	Elastic-plastic fracture mechanics
EPRI	Electric Power Research Institute (U.S.)
FAD	Failure assessment diagram
FEM	Finite element method
FC	Fatigue crack
Freq.	Frequency

GE	General Electric (U.S.)
HAEC	Hungarian Atomic Energy Commission
HDR	Heissdampfreaktor (An experimental reactor facility in Germany)
HSK	Hauptabteilung für die Sicherheit der Kernanlagen (Switzerland)
IGSCC	Intergranular-stress-corrosion crack
IHI	Ishikawajima-Harima Heavy Industries (Japan)
INER/AEC	Institute of Nuclear Energy Research/Atomic Energy Commission (Republic of China)
IPIRG-1	First International Piping Integrity Research Group
IPIRG-2	Second International Piping Integrity Research Group
JAERI	Japanese Atomic Energy Research Institute
J-R	J-resistance (curve)
J_D-R	J-resistance curve based on deformation theory
J_M-R	J-resistance curve based on modified J
KfK	Kernfortschangszantran Karlsruhe (Germany)
KINS	Korean Institute of Nuclear Safety
KKL	Kernkraftwerk Leibstadt AG (Switzerland)
LBB	Leak-Before-Break
L-C	Orientation that indicates crack plane is normal to longitudinal axis (L) and crack growth direction is circumferential (C)
LDD	Load-line displacement
LEFM	Linear-elastic-fracture mechanics
L-R	Orientation that indicates crack plane is normal to the longitudinal axis (L) and crack growth direction is radial (R) through the pipe wall
L-T	Orientation that indicates crack plane is normal to the longitudinal axis (L) and crack growth direction is transverse (T)

LWR	Light water reactor
MEA	Materials Engineering Associates (U.S.)
MIC	Microbiologically-induced corrosion
Mono	Monotonic
MPA	Staatliche Materialprüfungsanstalt (Germany)
MTS	Material Testing Systems
N	Normal
N/A	Not applicable
NDE	Nondestructive evaluation
NRA	Nuclear Regulatory Authority (Slovak Republic)
NRC	Nuclear Regulatory Commission (U.S.)
NRC-NRR	Nuclear Regulatory Commission - Office of Nuclear Reactor Regulation (U.S.)
NRC-RES	Nuclear Regulatory Commission - Office of Nuclear Reactor Research (U.S.)
NRI	Nuclear Research Institute (Czech Republic)
NSC	Net-Section-Collapse (analysis)
NUPEC	Nuclear Power Engineering Test Center (Japan)
OBE	Operational Basis Earthquake
PC	Personal computer
PICEP	Pipe Crack Evaluation Program
PIFRAC	Piping fracture mechanics material property database
PS	Pipe system
PSD	Power spectral density
PVP	Pressure Vessel and Piping
PWR	Pressurized Water Reactor

QA	Quality assurance
QS	Quasi-static
ROC-AEC	Republic of China - Atomic Energy Commission
SAM	Seismic anchor motion
SAW	Submerged-arc weld
SC	Surface crack
Sch.	Schedule
SEN(B)	Single-edge notch (bend) specimen
SEN(T)	Single-edge notch (tension) specimen
SIA	Structural Integrity Associates (U.S.)
Sim.	Simulated
SKI	Statens Kärnkraftinspektion (Swedish Nuclear Power Inspectorate)
SKKU	Sung Kyun Kwan University (Korea)
SMAW	Shielded-metal-arc weld
SMiRT	Structural Mechanics in Reactor Technology
SMN	Sharp machine notch
SQUIRT	Seepage Quantification of Upsets In Reactor Tubes (Leak rate and crack opening area computer code)
SRP	Standard Review Plan
SS	Stainless steel
SSBM	Stainless steel base metal
SSE	Safe shutdown earthquake
SSW	Stainless steel weld
TAG	Technical Advisory Group

TIG	Tungsten-inert-gas weld
TWC	Through-wall crack
U.S.	United States
U.S. NRC	United States Nuclear Regulatory Commission
UT	Ultrasonic testing
UTS	Ultimate tensile strength
VATESI	State Nuclear Energy Safety Inspection of the Republic of Lithuania
VTT	Technical Research Centre of Finland
VUJE	Vyskumny Ustav Jadravyeh Elektrarni (Nuclear Power Plant Research Institute of Slovakia)

PREVIOUS REPORTS IN SERIES

Reports from this Program

"Summary of Results from the IPIRG-2 Round-Robin Analyses," NUREG/CR-6337, BMI-2186, January 1996.

"IPIRG-2 Task 1 - Pipe System Experiments With Circumferential Cracks in Straight-Pipe Locations," NUREG/CR-6389, BMI-2187, February 1997.

"The Effect of Cyclic and Dynamic Loads on Carbon Steel Pipe," NUREG/CR-6438, BMI-2188, February 1996.

"Design of the IPIRG-2 Simulated Seismic Forcing Function," NUREG/CR-6439, BMI-2189, February 1996.

"The Effect of Cyclic and Dynamic Loading on the Fracture Resistance of Nuclear Piping Steels," NUREG/CR-6440, BMI-2190, December 1996.

"Deterministic and Probabilistic Evaluations for Uncertainty in Pipe Fracture Parameters in Leak-Before-Break and In-Service Flaw Evaluations," NUREG/CR-6443, BMI-2191, June 1996.

"Fracture Behavior of Circumferentially Surface-Cracked Elbows," NUREG/CR-6444, BMI-2192, December 1996.

"Development of a J-Estimation Scheme for Internal Circumferential and Axial Surface Cracks in Elbows," NUREG/CR-6445, BMI-2193, June 1996.

"Fracture Toughness Evaluations of TP304 Stainless Steel Pipes," NUREG/CR-6446, BMI-2194, February 1997.

Reports from the IPIRG-1 Program

"Evaluation and Refinement of Leak-Rate Estimation Models," NUREG/CR-5128, BMI-2164, Revision 1, June 1994.

"Loading Rate Effects on Strength and Fracture Toughness of Pipe Steels Used in Task 1 of the IPIRG Program," Topical Report, NUREG/CR-6098, BMI-2175, October 1993.

"Stability of Cracked Pipe Under Inertial Stresses," NUREG/CR-6233, BMI-2177, Volume 1, August 1994.

Previous Related Documents from NRC's Short Cracks in Piping and Piping Welds Program

"Short Cracks in Piping and Piping Welds," First Semiannual Report, NUREG/CR-4599; BMI-2173, Vol. 1, No. 1, March 1991.

"Short Cracks in Piping and Piping Welds," Second Semiannual Report, NUREG/CR-4599, BMI-2173, Vol. 1, No. 2, April 1992.

"Short Cracks in Piping and Piping Welds," Third Semiannual Report, NUREG/CR-4599, BMI-2173, Vol. 2, No. 1, September 1992.

"Short Cracks in Piping and Piping Welds," Fourth Semiannual Report, NUREG/CR-4599, BMI-2173, Vol. 2, No. 2, February 1993.

"Short Cracks in Piping and Piping Welds," Fifth Semiannual Report, NUREG/CR-4599, BMI-2173, Vol. 3, No. 1, October 1993.

"Short Cracks in Piping and Piping Welds," Sixth Semiannual Report, NUREG/CR-4599, BMI-2173, Vol. 3, No. 2, March 1994.

"Short Cracks in Piping and Piping Welds," Progress Report, NUREG/CR-4599, BMI-2173, Vol. 4, No. 1, April 1995.

"Assessment of Short Through-Wall Circumferential Cracks in Pipes," NUREG/CR-6235, BMI-2178, April 1995.

"Fracture Behavior of Short Circumferential Short-Surface-Cracked Pipe," NUREG/CR-6298, BMI-2183, November 1995.

"Fracture Evaluations of Fusion Line Cracks in Nuclear Pipe Bimetallic Welds," NUREG/CR-6297, BMI-2182, April 1995.

"Effect of Dynamic Strain Aging on the Strength and Toughness of Nuclear Ferritic Piping at LWR Temperatures," NUREG/CR-6226, BMI-2176, October 1994.

"Effects of Toughness Anisotropy and Combined Loading on Fracture Behavior of Ferritic Nuclear Pipe," NUREG/CR-6299, BMI-2184, April 1995.

"Refinement and Evaluation of Crack-Opening Analyses for Circumferential Through-Wall Cracks in Pipes," NUREG/CR-6300, April 1995.

"Probabilistic Pipe Fracture Evaluations for Leak-Rate Detection Applications," NUREG/CR-6004, BMI-2174, April 1995.

"Stainless Steel Submerged Arc Weld Fusion Line Toughness," NUREG/CR-6251, BMI-2180, April 1995.

"Validity Limits in J-Resistance Curve Determination: Volume 1: An Assessment of the J_M Parameter," NUREG/CR-6264, BMI-2181, Vol. 1, February 1995.

"Validity Limits in J-Resistance Curve Determinations: Volume 2: A Computational Approach to Ductile Crack Growth Under Large-Scale Yielding Condition," NUREG/CR-6264, BMI-2181, Vol. 2, February 1995.

Previous Related Documents from NRC's Degraded Piping Program - Phase I Reports

"The Development of a Plan for the Assessment of Degraded Nuclear Piping by Experimentation and Tearing Instability Fracture Mechanics Analysis," NUREG/CR-3142, Vols. 1 and 2, June 1983.

Previous Related Documents from NRC's Degraded Piping Program - Phase II Reports

"Degraded Piping Program - Phase II," Semiannual Report, NUREG/CR-4082, BMI-2120, Vol. 1, Oct. 1984.

"Degraded Piping Program - Phase II," Semiannual Report, NUREG/CR-4082, BMI-2120, Vol. 2, June 1985.

"Degraded Piping Program - Phase II," Semiannual Report, NUREG/CR-4082, BMI-2120, Vol. 3, March 1986.

"Degraded Piping Program - Phase II," Semiannual Report, NUREG/CR-4082, BMI-2120, Vol. 4, July 1986.

"Degraded Piping Program - Phase II," Semiannual Report, NUREG/CR-4082, BMI-2120, Vol. 5, Dec. 1986.

"Degraded Piping Program - Phase II," Semiannual Report, NUREG/CR-4082, BMI-2120, Vol. 6, April 1988.

"Degraded Piping Program - Phase II," Semiannual Report, NUREG/CR-4082, BMI-2120, Vol. 7, March 1989.

"Degraded Piping Program - Phase II," Semiannual Report, NUREG/CR-4082, BMI-2120, Vol. 8, March 1989.

"NRC Leak-Before-Break (LBB.NRC) Analysis Method for Circumferentially Through-Wall Cracked Pipes Under Axial Plus Bending Loads," Topical Report, NUREG/CR-4572, BMI-2134, March 1986.

"Elastic-Plastic Finite Element Analysis of Crack Growth in Large Compact Tension and Circumferentially Through-Wall-Cracked Pipe Specimen--Results of the First Battelle/NRC Analysis Round Robin," Topical Report, NUREG/CR-4573, BMI-2135, September 1986.

"An Experimental and Analytical Assessment of Circumferential Through-Wall Cracked Pipes Under Pure Bending," Topical Report, NUREG/CR-4574, BMI-2136, June 1986.

"Predictions of J-R Curves With Large Crack Growth From Small Specimen Data," Topical Report, NUREG/CR-4575, BMI-2137, September 1986.

"An Assessment of Circumferentially Complex-Cracked Pipe Subjected to Bending," Topical Report, NUREG/CR-4687, BMI-2142, September 1986.

"Analysis of Cracks in Stainless Steel TIG Welds," Topical Report, NUREG/CR-4806, BMI-2144, November 1986.

"Approximate Methods for Fracture Analyses of Through-Wall Cracked Pipes," Topical Report, NUREG/CR-4853, BMI-2145, January 1987.

"Assessment of Design Basis for Load-Carrying Capacity of Weld-Overlay Repair," Topical Report, NUREG/CR-4877, BMI-2150, February 1987.

"Analysis of Experiments on Stainless Steel Flux Welds," Topical Report, NUREG/CR-4878, BMI-2151, February 1987.

"Experimental and Analytical Assessment of Circumferentially Surface-Cracked Pipes Under Bending," Topical Report, NUREG/CR-4872, BMI-2149, April 1987.

Other Related Program Reports

"Validation of Analysis Methods for Assessing Flawed Piping Subjected to Dynamic Loading," NUREG/CR-6234, ANL-94/22, BMI-2178, August 1994.

1.0 INTRODUCTION

The Second International Piping Integrity Research Group (IPIRG-2) Program was an international group program managed by the U. S. Nuclear Regulatory Commission (U.S. NRC) and funded by a consortium of organizations from 15 nations: Bulgaria, Canada, Czech Republic, France, Hungary, Italy, Japan, Korea, Lithuania, Republic of China, Slovak Republic, Sweden, Switzerland, United Kingdom, and the United States. The individuals participating in the IPIRG-2 Program and their organizations are listed in the Acknowledgments.

The IPIRG-2 Program was a continuation of the First IPIRG Program (IPIRG-1). The scope of IPIRG-2 included the development of data for the verification of fracture analyses for cracked pipe and fittings subjected to dynamic and/or cyclic load histories. The dynamic/cyclic load histories of IPIRG-2 tended to be more complex than those for IPIRG-1, i.e., multi-frequency, variable amplitude, simulated seismic excitations in IPIRG-2 versus constant frequency, increasing amplitude excitations in IPIRG-1. In addition, the scope of IPIRG-2 included the study of smaller crack sizes, with an associated increase in plasticity in the uncracked pipe, through-wall-cracked pipe test specimens, and cracks in and around piping components, such as elbows.

This report will begin by providing an historical perspective leading up to the development of the IPIRG-2 program. As part of this discussion some of the relevant past pipe fracture programs conducted at Battelle and other organizations will be discussed. In addition, the state-of-the-art in pipe fracture technology prior to the formation of the IPIRG-2 program will be discussed. This discussion will lead naturally into the technical reasons the various participants joined the program.

Next we will present the scope and structure of the various tasks which made up the IPIRG-2 program.

This section concludes with a brief description of the structure and contents of this report.

1.1 Historical Perspective

The IPIRG-2 program is the latest program in a continuum of research programs aimed at developing a better understanding of the fracture behavior of pressurized nuclear plant piping. As part of one of Battelle's presentations to the IPIRG Technical Advisory Group (TAG), a time line of pipe fracture technology, research programs, and nuclear industry milestones was presented. Table 1.1 is a summary of that time line. This is briefly summarized below.

The early 1960's marked the beginning of the nuclear power generation era with the first commercial nuclear power plants becoming operational. It was not long afterwards that the first observations of intergranular stress corrosion cracking (IGSCC) were made. As early as 1965 cracks in 6-inch nominal diameter Type 304 stainless steel bypass lines associated with the recirculation loop of the Dresden I boiling water reactor (BWR) were discovered. From 1965 to 1974 cracks were found in six BWRs (Ref. 1.1). All affected piping was Type 304 stainless steel with nominal pipe diameters of 8-inch or less. All of the cracks were attributed to IGSCC due to a combination of weld residual stresses, material sensitization, and high oxygen content in the water. Shortly after discovering the IGSCC cracks at

Table 1.1 Timeline of nuclear industry milestones and major pipe fracture research programs

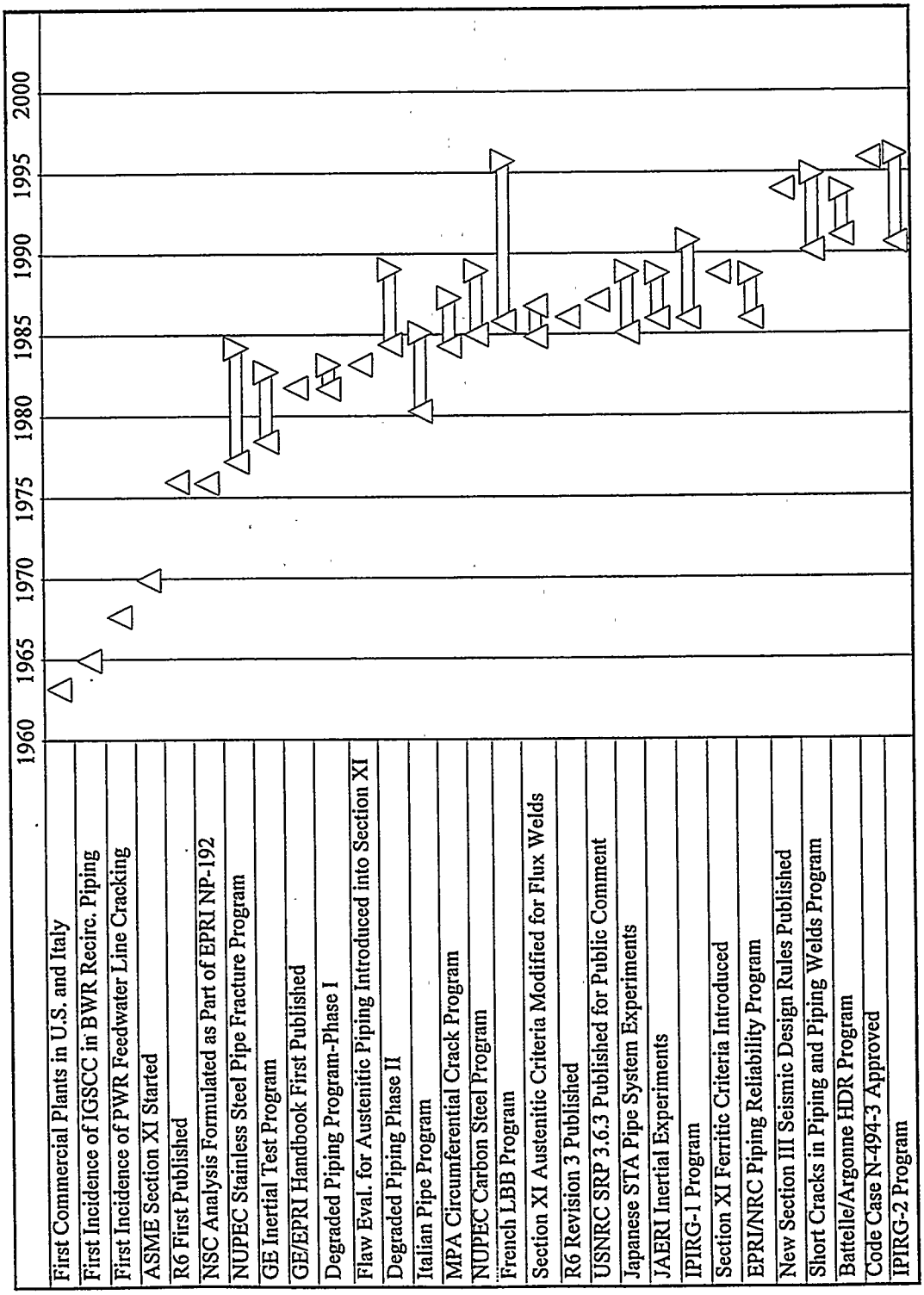

Dresden I, the first incidence of cracking in a feedwater piping system was discovered at the San Onofre pressurized water reactor (PWR). Cracks were subsequently found in the feedwater piping adjacent to the steam generators in 15 of the 32 PWRs inspected (Ref. 1.2). Analyses of the operating conditions for these plants suggested that thermal fatigue was the most probable cause for this feedwater line cracking. Temperature differences of over 200 C (392 F) between the top (hot) and bottom (cold) of the piping were observed adjacent to the steam generator inlet during hot standby.

In partial response to these cracking issues, the ASME Code initiated the Section XI committee in 1970. By the mid-1970's, IGSCC was starting to be become a widespread problem. IGSCC in larger diameter piping systems was discovered then. Examples include cracks found in 26-inch diameter welds in a German BWR and in a 12-inch diameter riser pipe in Japan. In response to the growing IGSCC problem, the Electric Power Research Institute (EPRI) initiated the first in a series of pipe fracture programs aimed at developing validated fracture criteria for circumferentially-cracked pipe (Ref. 1.3). As part of this Battelle/EPRI program, a new limit-load analysis method for circumferentially-cracked pipe was developed, i.e., the Net-Section-Collapse (NSC) analysis. This analysis eventually became the basis for a number of flaw evaluation criteria embodied in such documents as the ASME Code.

At this time, the U.S. NRC was also involved in addressing the issue of circumferentially-cracked nuclear power plant piping systems. One of their earliest entries into this field was the Degraded Piping Program - Phase I (Ref. 1.4). The scope of this program was to develop a cogent plan for assessing the integrity of degraded nuclear power plant piping systems for continued operation. Early on it was realized that conventional linear-elastic-fracture-mechanics (LEFM), which was well established at that time, would not be sufficient to address the problem at hand (Ref. 1.5). It was obvious that nonlinear, elastic-plastic-fracture mechanics (EPFM) analyses, such as those being developed by General Electric (GE) under the sponsorship of EPRI (Ref. 1.6), would be required. One of the key findings from the Degraded Piping Program - Phase I was the realization of the need for the definition of a more extensive program to develop and experimentally validate the necessary EPFM methodologies.

This was the scope of the Degraded Piping Program - Phase II (Ref. 1.7), which began at Battelle-Columbus in 1984. As part of the Phase II effort, a number of EPFM J-estimation scheme analysis methods were developed, both for through-wall-cracked and finite length surface-cracked pipe. Prior to and concurrent with this effort, other J-estimation schemes were being developed at other organizations (Refs. 1.6, 1.8, 1.9, and 1.10). In addition, two interactive computer programs (NRCPIPE and NRCPIPES) were developed which facilitated the use of these methods.

One of the larger tasks associated with Phase II of the Degraded Piping program was a task to develop full-scale pipe fracture experimental data to be used to validate these analysis methods. The scope of the Degraded Piping Program experiments included a number of loading conditions (four-point bending, compliant four-point bending, pressure, and combined pressure and bending) and pipe materials (both austenitics and ferritics and their associated weldments) for both small and large diameter pipe. However, the scope was limited to the evaluation of relatively large cracks, for which the plasticity in the test specimen would be limited to the crack section. In addition, only quasi-static loading rates were considered. These limitations were recognized, however, during the development of the Degraded Piping program, and plans were included for the development of a follow-on program to address the fracture behavior of cracked nuclear grade piping systems subjected to dynamic and cyclic load histories, such as may be experienced during a seismic event. The objective of another task in the Degraded Piping

Program - Phase II was to develop such a program and to solicit support of other organizations worldwide. By soliciting international cooperation, it was hoped that an international consensus within the worldwide nuclear community (both industry and regulators) on the issues of pipe fracture could be reached. In addition, it was felt that by consolidating their respective resources, and avoiding duplication of effort, larger, more complex experiments could be conducted. The program which evolved was the First International Piping Integrity Research Group (IPIRG-1) Program (Ref. 1.11). The IPIRG-1 program was initiated at Battelle-Columbus in July of 1986.

During this period, when Battelle and the U.S. NRC were heavily involved in the Degraded Piping Programs, other organizations were conducting their own independent pipe fracture research programs. In the late 70's and early 80's, a pipe instability program evaluating Type 304 stainless steel pipe was conducted at the Nuclear Power Engineering Test Center (NUPEC) in Japan (Ref. 1.12). NUPEC followed this program with a second program aimed at demonstrating the Leak-Before-Break (LBB) concept for both BWR and PWR carbon steel piping systems (Ref. 1.13).

In the early 1980's, researchers in Italy were conducting their own pipe experiments on 2- to 12-inch nominal diameter pipes with the objective of developing a better understanding of the fracture behavior of cracked pipes in order to set new more realistic, yet conservative, design criteria than the existing guillotine break criteria and to prepare new in-service flaw acceptance criteria, particularly for stainless steel BWR piping subjected to IGSCC (Ref. 1.14).

In addition, scientists and engineers in Germany were becoming involved in their own research initiatives for assessing the integrity of circumferentially flawed piping. In 1984, the first circumferentially-cracked pipe tests within the Phenomenological Pipe and Vessel Burst Test Program (Ref. 1.15) were being conducted at MPA Stuttgart. This was a major multi-year initiative aimed at developing verified flaw acceptance criteria for defective piping, specifically main coolant line piping associated with pressurized water reactor (PWR) primary systems. These experiments typically involved relatively large diameter (800 mm [31.5-inch]), heavy-wall (47 mm [1.85 inch] thick) ferritic test specimens. Also, at about this same time, researchers in France were initiating their own program with the goal of validating the Leak-Before-Break concept for their specific application (Ref. 1.16).

Progress was also being made at this time in transferring the technology from these research programs into the appropriate codes and standards. Flaw evaluation procedures for austenitic piping first appeared in Article IWB-3640 of ASME Section XI in 1983 and subsequently in Code Case N-436 that eventually became Appendix C of Section XI. These procedures were subsequently modified to account for low toughness stainless steel flux welds through the inclusion of special stress multipliers (i.e., Z-factors) in the Winter 1985 Addendum of the Code. The fracture toughness data used in the development of these Z-factors came from some Westinghouse C(T) specimen tests (Ref. 1.17). The mid 1980s also marked the publication of the third revision to the R6 document (Ref. 1.18). This flaw assessment document, used extensively in Europe, was first published by the Central Electricity Generating Board (CEGB) in the United Kingdom in 1976. In 1989 the flaw evaluation procedures for ferritic piping were introduced into Section XI of the ASME Code, i.e., Article IWB-3650 and subsequently in Code Case N-463 that eventually became Appendix H of Section XI. A third code case, N-494-3, based on a failure assessment diagram approach, much in the motif of the R6 Level 1 procedures, and applicable to both austenitic and ferritic piping was approved by the main committee of Section XI in 1996.

A common denominator among each of the experimental programs described above was the load histories applied. Each involved the application of relatively slow quasi-static bend or tension or compliant bend or tension load histories. Little had been done to further the basic understanding of the fracture behavior of cracked pipe subjected to more complex load histories, such as might occur in a seismic event.

One exception was some pioneering work carried out by GE San Jose (Ref. 1.19). Researchers at GE studied the behavior of cracked pipe subjected to high rate dynamic loadings. This program was funded by the BWR Owner's Group (BWROG) and involved 4-inch nominal diameter stainless steel pipe tested at room temperature and without internal pipe pressure. These experiments involved constant amplitude, fully reversed, cyclic inertial loading.

In addition to the GE San Jose dynamic experiments, researchers at the Japan Atomic Energy Research Institute (JAERI) conducted a similar series of inertially-loaded pipe fracture experiments (Ref. 1.20) later in the decade. The big difference between these experiments and those conducted at GE San Jose (Ref. 1.19) was that a number of the test specimens for the JAERI experiments were pressurized. The GE experiments were not. An observation from these JAERI experiments was that the failure loads were much less than the Net-Section-Collapse predicted loads using the initial crack sizes. This was attributed to low-cycle fatigue crack growth.

At about the same time that JAERI was conducting these inertially-loaded pipe experiments, the National Research Center for Disaster Prevention, also in Japan, was undertaking a series of dynamic, cyclic pipe system experiments. These were pressurized, room temperature experiments (Ref. 1.21). The pipe system, shown in Figure 1.1, was fabricated from 4-inch and 6-inch nominal diameter pipe. Both cracked and uncracked pipe system experiments were conducted. One of the key findings from this program was that complete pipe breaks (i.e., DEGBs) occurred within 4 to 7 cycles after surface crack penetration during the long surface-cracked pipe experiments. Note that a similar observation was made in one of the Degraded Piping Program experiments (i.e., Experiment 4115-7), in which the stainless steel test specimen severed into two pieces as soon as the 360-degree internal surface crack penetrated the pipe wall thickness. The applied loading for this experiment was quasi-static, compliant four-point bending. These observations, along with the conclusions drawn in Reference 1.22 for complex-cracked pipe, which indicated that the fracture resistance of the complex crack geometry was especially low, suggest that the stipulation in the U.S. NRC LBB criteria (Refs. 1.23 and 1.24) which precludes the application of LBB to piping systems susceptible to IGSCC is a prudent one.

During this same time period, i.e., the second half of the decade of the 80s, the U.S. NRC and EPRI were cooperating in a series of experiments looking at the behavior of an uncracked pipe system, see Figure 1.2, subjected to a dynamic cyclic load history (Ref. 1.25). The failure mode of these uncracked pipe system experiments was not fracture, but instead fatigue ratcheting. One of the outcomes of this joint program was the development of a new set of seismic design rules for Section III of the ASME Code which are in Article NB-3656 of Section III of the 1995 Edition of the ASME Boiler and Pressure Vessel Code. These rules were subsequently not endorsed by the U.S. NRC, and to this date they continue to be debated by various committees and subcommittees in ASME.

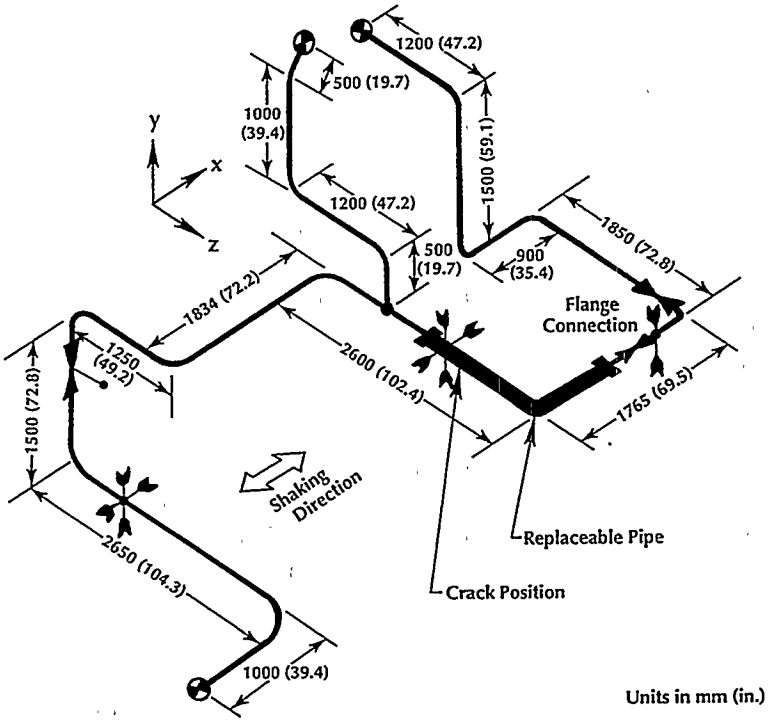

Figure 1.1 STA pipe system for dynamic flawed pipe tests (Ref. 1.21)

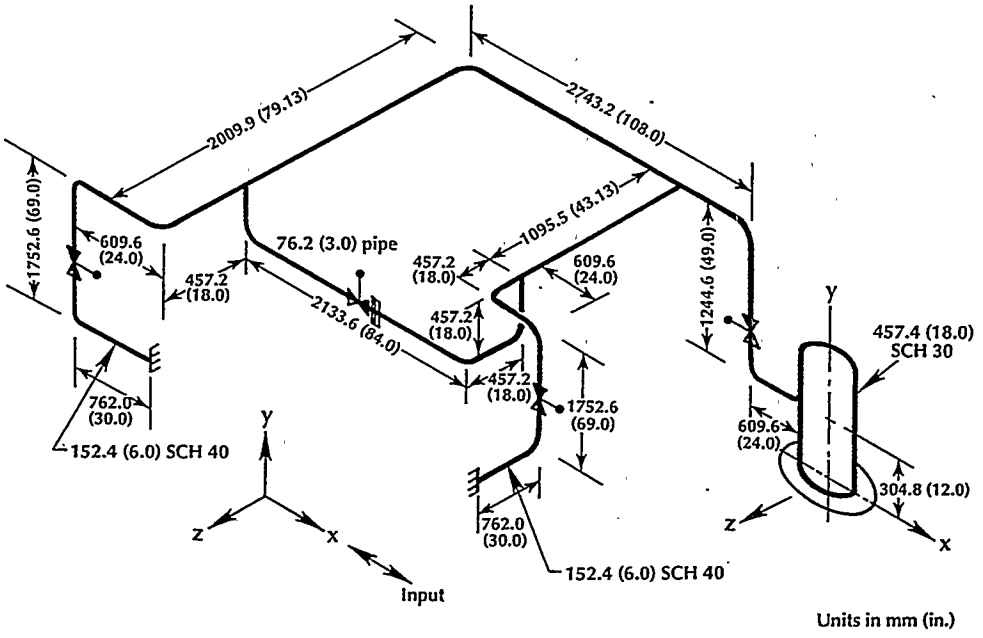

Figure 1.2 Piping System 1 configuration evaluated in EPRI/NRC Piping Reliability Program (Ref. 1.25)

This summarizes the state of pipe fracture technology as the first IPIRG program was getting underway. Significant progress had been made in the understanding of the basic problems associated with cracked nuclear power plant piping systems. However, there remained a number of key technical issues still to be addressed. Analysis methods to assess the fracture behavior of cracked nuclear piping systems had been developed and verified for a number of conditions. What was lacking was an understanding of the effect of dynamic and cyclic load histories, especially at elevated temperatures, and a basic understanding of the effects of inertial and displacement-controlled stresses on the fracture behavior of cracked piping.

Like its predecessor, the Degraded Piping Program, the IPIRG-1 program involved material characterization efforts using laboratory size specimens and full-scale pipe experiments. Note, however, unlike the Degraded Piping Program, the extent of analytical development in this program was minimal. As part of the main experimental task, both separate effects straight pipe and combined inertial and displacement-controlled pipe system experiments were conducted. From the pure inertially loaded separate effects experiments (Ref. 1.26), it was concluded that inertial loading should be considered more as a load-controlled load than a displacement-controlled load. For each of these experiments there were very few cycles (i.e., two to four) between the attainment of maximum load for the experiment and the occurrence of a double-ended-guillotine-break (DEGB). A number of significant conclusions were also reached as a result of the displacement-controlled separate effects experiments (Refs. 1.27 and 1.28). For one, it was shown that both the load-carrying capacity and moment-rotation response (which is indicative of the overall fracture toughness) of the carbon steel pipe tested decreased dramatically with increasing strain rate. Similar findings were observed from the laboratory tensile and fracture toughness tests for this material. This decrease in strength and fracture toughness, and ultimately load-carrying capacity, was attributed to dynamic strain aging (DSA) effects (Ref. 1.29). DSA is a condition associated with many carbon steels operating in the temperature range of 150 C (300 F) to 370 C (700 F). It involves interactions between highly mobile nitrogen and carbon atoms dissolved in the steel and moving dislocations associated with plastic strain. It can affect both the tensile strength and fracture toughness properties of the affected material and varies with strain rate. Unlike the case for the ferritic steels, the strength, toughness, and ultimately load-carrying capacity of the austenitic steel evaluated in these experiments was not adversely affected by strain rate. In fact, the toughness actually showed a significant increase in several cases. In addition, there were also effects of cyclic loading observed. For both the ferritic and austenitic steels evaluated, cyclic loading, especially fully-reversed cyclic loading, lowered the moment-rotation curves for the experiments. It was observed that the crack-tip-opening-angle (CTOA), which is a measure of the fracture toughness for these through-wall-cracked pipe experiments, was dependent not only on the stress ratio (R) but also the increment of plastic displacement between load cycles, see Figure 1.3.

The IPIRG-1 Program also included a series of combined inertial and displacement-controlled pipe system experiments. One major difference between these pipe system experiments and those conducted earlier in Japan, was the pipe diameter. The pipe diameter for these experiments was 406 mm (16 inch) in contrast to that for the Japanese pipe system experiments, i.e., 4-inch and 6-inch nominal diameter. The smaller pipe diameter used in the Japanese experiments tended to create a situation in which fully-plastic (limit-load) conditions would be expected regardless of the toughness of the material. By evaluating larger diameter pipes in the IPIRG-1 pipe system experiments, it was anticipated that the fracture process for the higher toughness steels would be governed by fully-plastic (limit-load) conditions and by elastic-plastic fracture mechanics (EPFM) for the lower toughness steels. In order to conduct these pipe system experiments, a special experimental pipe loop facility had to be designed and constructed, see Figure 1.4. The philosophy driving the design of this facility was that it should be a facility which could be easily

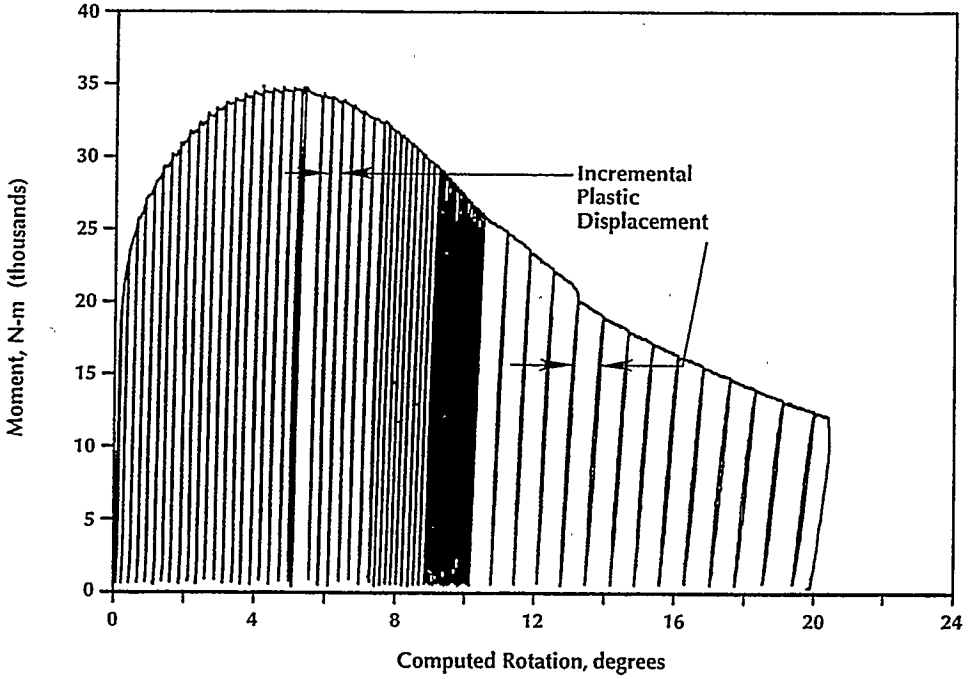

(a) Incremental plastic displacement

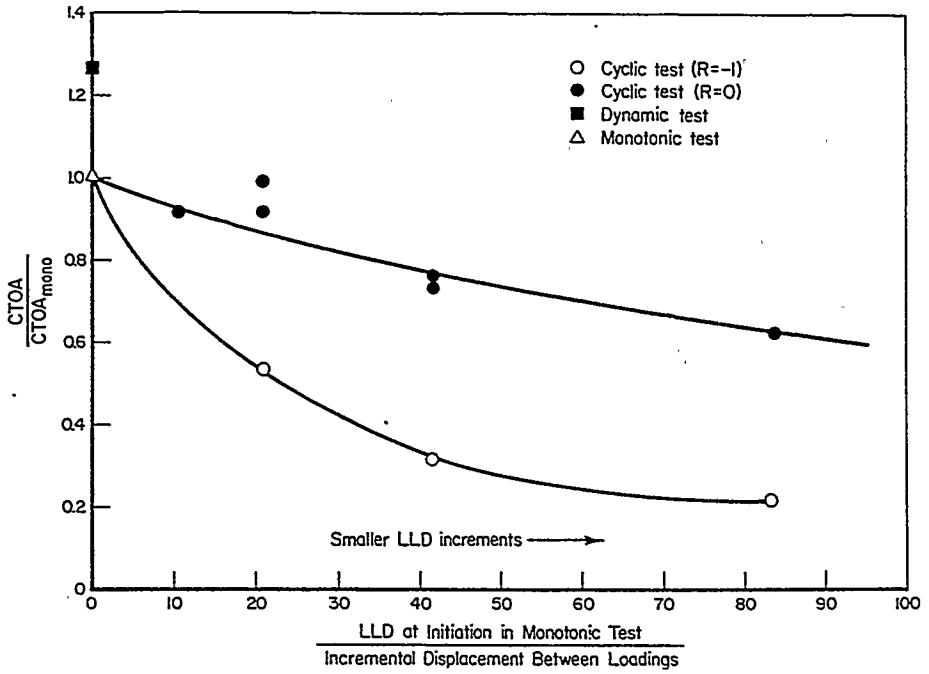

(b) Effect of stress ratio (R) and incremental plastic displacement

Figure 1.3 Effect of cyclic loading on fracture toughness as measured by the crack-tip-opening-angle (CTOA) on through-wall-cracked pipe

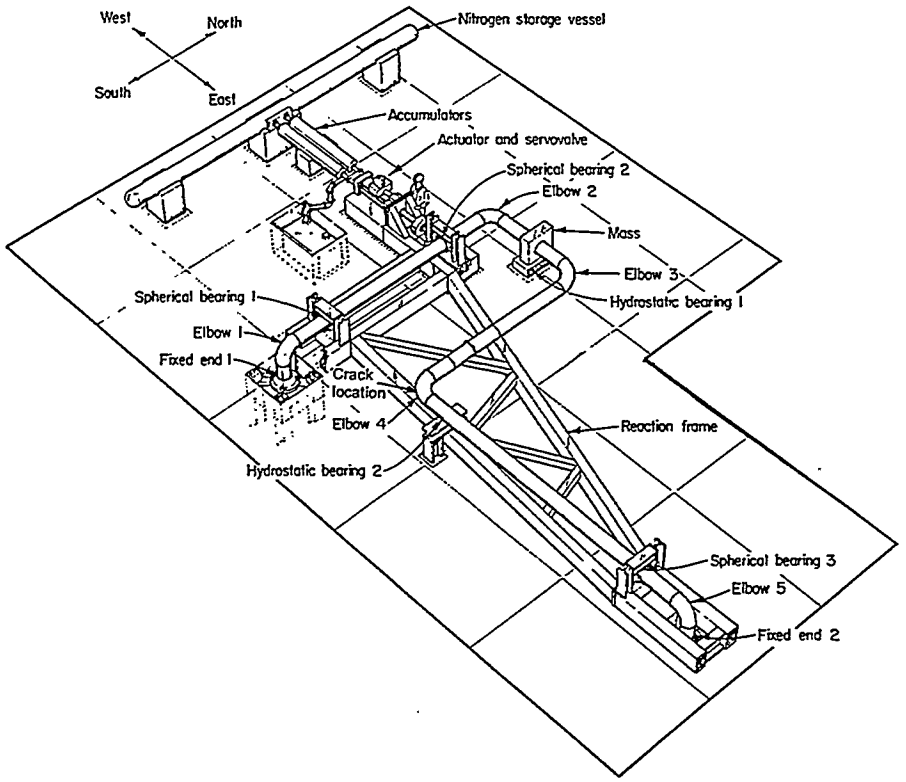

Figure 1.4 Artist's conception of the test configuration used in IPIRG-1

modeled using the finite element method and such that the model could be used to benchmark or validate new analysis methodologies. As such, the constructed pipe loop included a number of specially designed pieces of hardware to facilitate the description of the imposed boundary conditions.

This design process for these pipe system experiments was based on finite element analysis. The commercial finite element package ANSYS was chosen for these analyses. One of the advancements in the technology developed as part of this design process was a means of mathematically describing the moment-rotation relationship for the crack section within the finite element model. The initial concept involved the use of a special nonlinear spring element embodied in the library of elements in the ANSYS finite element code. Unfortunately, it was discovered that this element type did not properly model the unloading behavior of the crack during cyclic loading. As a result, a new nonlinear spring representation of the crack was devised by combining a series of spring and slider elements in the ANSYS library of element types (Ref. 1.30), see Figure 1.5. This crack model was very effective at predicting the fracture behavior of the IPIRG pipe system experiments, at least up to the instant of surface crack penetration. It was not capable of making the transition in crack section compliance as the surface crack transitioned from a surface crack to a through-wall crack. This spring-slider model was eventually enhanced in the early 1990's as part of a program Battelle undertook for the U.S. NRC which validated pipe fracture analyses for dynamic load histories (Ref. 1.31). The enhancement involved the incorporation of a series of truss elements in series with the spring-slider elements.

During the IPIRG-1 Program, one uncracked and five cracked-pipe system experiments were conducted. The five cracked-pipe system experiments involved five different materials, i.e., a carbon and stainless

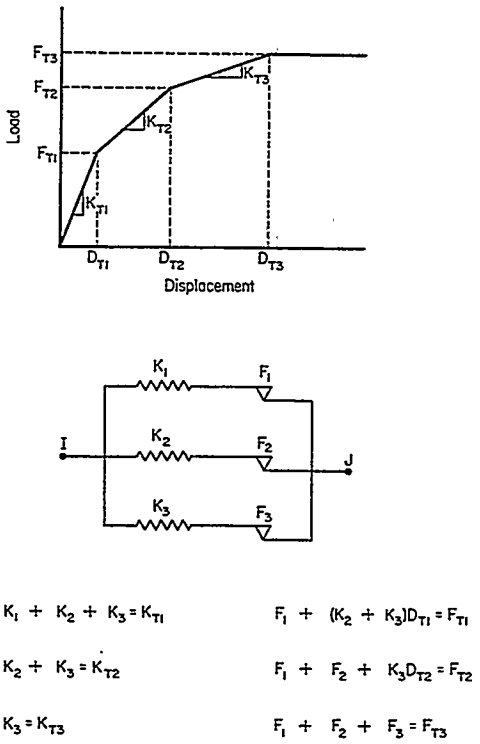

Figure 1.5 Modeling of a multilinear moment-rotation curve

steel and their associated weldments and a section of aged cast stainless steel. The cracks in each of these experiments were nominally the same, i.e., 50 percent of the pipe circumference in length and 66 percent of the pipe wall thickness in depth. The forcing function applied to each experiment was an increasing amplitude sinusoidal single-frequency excitation. One of the key findings from these pipe system experiments was that the global secondary stresses (i.e., thermal expansion and seismic anchor motion stresses) provided a contribution to the fracture that was equal to that contributed by the pressure and inertial stresses, if the pipe loop stresses at failure were below the yield strength of the pipe. This condition occurred in these pipe system experiments due to the relatively large crack sizes tested. Figure 1.6 shows a plot of the ratio of the maximum experimental stress to the predicted stress for the five IPIRG-1 pipe system experiments as well as the five companion quasi-static, monotonic four-point bend experiments from References 1.7 and 1.32. The experimental stresses in this figure have been normalized by the Net-Section-Collapse predicted stresses to account for differences in pipe size, crack size, and material strength. The stresses for the IPIRG-1 pipe system experiments have been delineated by the various stress components, i.e., primary membrane plus bending and secondary seismic anchor motion and thermal expansion stresses. As can be seen in Figure 1.6, the total stress (primary plus secondary) for the IPIRG-1 pipe system experiments agreed quite closely with the total stress for the companion quasi-static experiments. If the global secondary stresses (i.e., thermal expansion and seismic anchor motion stresses) were not considered for the IPIRG-1 pipe system experiments, then the maximum experimental stresses would only be a fraction of the maximum stresses for the quasi-static experiments. This finding is in conflict with the flaw evaluation procedures embodied in ASME Section XI. In both the Appendix C (for

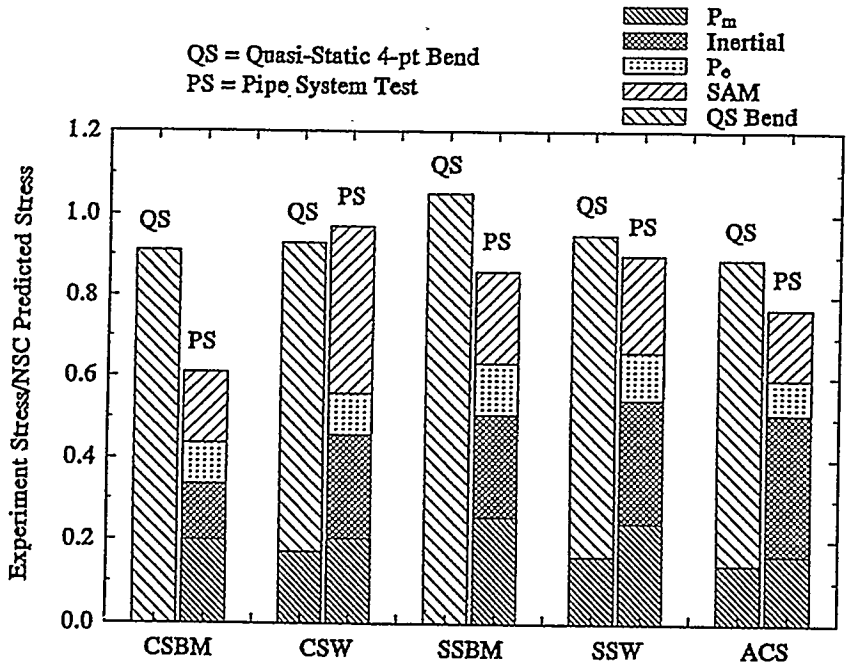

Figure 1.6 Plot of the ratio of the maximum experimental stress to the Net-Section-Collapse predicted stress for the IPIRG-1 pipe system and companion experiments showing the effect of the various stress components on the fracture behavior

austenitic piping) and Appendix H (for ferritic piping) flaw evaluation procedures, the thermal stresses are included with a safety factor of 1.0 while the primary stresses are included with a full safety factor of 1.39 for emergency and faulted conditions or 2.77 for normal and test conditions. In fact, for the case of cracks in stainless steel base metals, the Appendix C criteria ignore the secondary stresses completely. Seismic anchor motion stresses are not explicitly used in the current ASME Section XI flaw evaluation criteria.

Conversely, the R6 method assumes that global secondary stresses contribute to fracture to the same degree as do primary stresses, while local secondary stresses, i.e., weld residual stresses, may contribute in the elastic regime. The findings from the IPIRG-1 pipe system experiments tend to support the R6 position more so than that of the ASME position.

Near the end of the IPIRG-1 program, the U.S. NRC initiated another pipe fracture program at Battelle; the Short Cracks in Piping and Piping Welds Program (Ref. 1.33). The scope of this program was similar in nature to that of the Degraded Piping Program - Phase II (Ref. 1.7) in that it was a combined analytical and experimental program, and the loading conditions for the pipe experiments tended to be quasi-static, monotonic bending plus internal pipe pressure. However, unlike the Degraded Piping Program - Phase II, smaller crack sizes were considered in both the analysis and experimental efforts, for which plasticity remote from the crack section would be expected. In addition there were a number of specific issues addressed in the Short Cracks Program, which had not been addressed in detail in any of the prior pipe fracture experiments, i.e., cracks in the fusion line of bimetallic welds, stainless steel weld fusion line cracks, anisotropy effects, combined loading with torsional stresses, dynamic strain aging effects,

crack-opening-area predictions, probabilistic pipe fracture evaluations for leak-rate-detection applications, etc. The Short Cracks Program, which began in March of 1990, came to a conclusion in February of 1995.

Finally, in the early 1990's Battelle and Argonne National Laboratory (ANL) conducted a joint research program for the U.S. NRC to evaluate the ability of current engineering analysis methods to predict the behavior of the HDR Test Group E31 series of dynamically-loaded flawed piping experiments (Ref. 1.31). The major finding from this program was that the nonlinear spring methodology developed in IPIRG-1 resulted in much better predictions of these water hammer-loaded experiments than did conventional 3-dimensional finite element analysis.

1.2 Rationale and Objective Behind the IPIRG-2 Program

From the beginning of the first Battelle/EPRI program (Ref. 1.3) to the end of the Short Cracks (Ref. 1.33) and HDR (Ref. 1.31) Programs, the state-of-the-art in pipe fracture technology has increased dramatically. The state-of-the-art in pipe fracture analysis in the mid 1970s was simple limit-load analysis. Now, the state-of-the-art included nonlinear spring representations of the crack using sophisticated J-estimation schemes to calibrate the moment-rotation response of the nonlinear spring. In addition, the database of pipe fracture experiments has grown from a few relatively small diameter, unpressurized, room temperature, quasi-static four-point bend experiments to over 700 circumferentially-cracked pipe experiments encompassing a wide variety of pipe diameters, loading conditions, and test conditions (Ref. 1.34).

Even with this explosion in technology and understanding of the problem, there remained a number of holes in the technology at the end of the IPIRG-1 and Short Cracks Programs which still needed to be addressed. Addressing these remaining issues was the impetus behind the development of the IPIRG-2 program. These issues included:

The behavior of cracked-pipe sections subjected to more complex load histories such as may occur during an actual seismic event,

The behavior of smaller crack sizes, including both short surface-cracked and short through-wall-cracked pipes, when subjected to dynamic/cyclic load histories, and

The behavior of cracks in and adjacent to fittings, such as elbows.

In addition, a more basic understanding of dynamic and cyclic load effects on material properties was needed.

1.3 Structure of the IPIRG-2 Program

The IPIRG-2 program was structured with five basic tasks. Task 1 involved the assessment of the fracture behavior of pipe system experiments with cracks in straight pipe and welds*. There were a total of eight pipe experiments conducted as part of this effort, five pipe system experiments and three quasi-static bend companion experiments, see Table 1.2. There were seven technical subtasks associated with Task 1. The first three had to do with refurbishing and upgrading the IPIRG pipe loop experimental facility. As part of the last IPIRG-1 pipe system experiment (i.e., Experiment 1.3-7), the pipe loop facility experienced significant damage. Before a pipe system experiment could be conducted as part of IPIRG-2, this facility had to be rebuilt. In addition, special hardware (i.e., restraint systems) to preclude the possibility of a repeat of the accident associated with Experiment 1.3-7 had to be designed and constructed. Finally, additional accumulator capacity, required for the longer duration simulated seismic pipe system experiments, had to be incorporated into the overall facility design.

The last four subtasks associated with Task 1 involved the conduct of the nine Task 1 pipe experiments, see Table 1.2.

Task 2 involved the development of experimental data and fracture analyses to evaluate the fracture behavior of cracked pipe fittings, specifically elbows**. There were three subtasks associated with Task 2. Subtask 2.1 involved the conduct of a survey and assessment of flawed fitting data. Associated with Subtask 2.1 were five activities, which involved the consolidation of information from service experience and prior experimental and analytical research. The results from these activities were used to more effectively plan and carry out Subtasks 2.2 and 2.3 of this program. These activities included:

Reviewing and compiling a database of crack locations for cracks found in service in pipe fittings in nuclear and non-nuclear applications,

Reviewing and compiling a database of existing experimental research on flawed fittings (elbows and tees),

Comparing the failure stress levels for the flawed fitting experiments with the predicted failure stresses from existing flaw assessment methodologies developed for straight pipe,

Reviewing fabrication methods for fittings to assess how material properties may be affected, and

Describing the experimental difficulties associated with testing flawed fittings.

---

* For further details regarding Task 1 of the IPIRG-2 program, the reader is referred to the IPIRG-2 Task 1 Final Report, NUREG/CR-6389.

** For further details regard Task 2 of the IPIRG-2 program, the reader is referred to the IPIRG-2 Final Report, NUREG/CR-6444.

Table 1.2 Matrix of full-scale pipe and elbow experiments conducted as part of the IPIRG-2 program

Expt. No.	Nominal Pipe Diameter, inch	Crack Location	Material	Crack Geometry[1]	Internal Pipe Pressure, MPa	Loading History[2]
1-1	16	Straight pipe base metal	TP304	SC	15.5	Simulated seismic pipe system
1-2	16	Straight pipe base metal	A106B	SC	15.5	Simulated seismic pipe system
1-3	16	Elbow girth weld	A106B SAW	SC	15.5	Single frequency pipe system
1-4	16	Elbow girth weld	A106B SAW	SC	15.5	QS, monotonic, bend
1-5	16	Straight pipe weld	TP304 SAW	SC	15.5	Single frequency pipe system
1-6	16	Straight pipe weld	TP304 SAW	SC	15.5	QS, monotonic, 4-point bend
1-7	16	Straight pipe base metal	A106B	TWC	15.5	Simulated seismic pipe system
1-8	16	Straight pipe base metal	A106B	TWC	15.5	QS, monotonic, 4-point bend
1-9	6	Straight pipe base metal	A106B	TWC	15.5	Dynamic, monotonic, 4-point bend
2-1	16	Elbow extrados	A106B	SC	15.5	Single frequency pipe system
2-2	16	Elbow extrados	A106B	SC	15.5	QS, monotonic, bend
2-3	16	Elbow extrados	WP304L	SC	15.5	Single frequency pipe system
2-4	16	Elbow extrados	WP304L	SC	15.5	QS, monotonic, bend
3.3-1	6	Straight pipe base metal	STS410	TWC	0	QS, monotonic, 4-point bend
3.3-2	6	Straight pipe base metal	A106B	TWC	0	QS, cyclic (R=-0.6), 4-point bend
4.2-1	6	Straight pipe base metal	STS410	TWC	0	Dynamic, monotomic, 4-point bend
4.2-2	6	Straight pipe base metal	STS410	TWC	0	Dynamic, cyclic (R=-1), 4-point bend
4.2-3	6	Straight pipe weld	STS410TIG	TWC	0	Dynamic, cyclic (R=-1), 4-point bend

(1) SC = Surface crack; TWC = Through-wall crack.
(2) QS = Quasi-static.

Subtask 2.2 involved (1) the conduct of a survey and assessment of existing J-estimation scheme methods applicable to fittings, and to modify those methods as appropriate, and (2) the development of valid J-estimation scheme methods for cases where applicable analytical methods do not currently exist. Finally, the third subtask associated with Task 2, i.e., Subtask 2.3, involved the development of full-scale experimental data for the case of cracks in pipe fittings. There were four full-scale experiments associated with this subtask, see Table 1.2, all which involved internal circumferential surface cracks in the extrados of 90-degree long-radius elbows.

Task 3 involved the resolution of differences in toughness values observed between laboratory specimen and full-scale pipe experimental data resulting from load history effects such as the cyclic and dynamic loading effects that can occur during a seismic event*. This task involved laboratory C(T) specimen tests, full-scale dynamic and/or cyclic pipe experiments, see Table 1.2, supporting finite element analyses, and sensitivity analyses.

Task 4 was a task included in the overall program to address a series of unrelated, unresolved, issues left over from IPIRG-1 and other related programs. Associated with this task were (1) an effort to resolve

* For further details regard Task 3 of the IPIRG-2 program, the reader is referred to the IPIRG-2 Task 3 Final Report, NUREG/CR-6440.

discrepancies between experimental results and finite element analyses, (2) a series of pipe experiments on a Japanese carbon steel pipe material (Ref. 1.35), see Table 1.2, (3) the conduct of an uncertainty analysis to assess which parameters are of most importance in a fracture analyses*, and (4) the management and upkeep of the various computer codes (i.e., NRCPIPE, NRCPIPES, SQUIRT, and IP2ELBOW) and databases (CIRCUMCK, AXIALCK, ELBOWCK, TEECK, and PIFRAC) developed as part of this and related programs.

Task 5 involved the development and conduct of the information exchange seminars and workshops (i.e., round robins and analysts group meetings) conducted during the IPIRG-2 program (Ref. 1.36). Task 5 also included the required program management activities (i.e., report generation, cost tracking, etc.) associated with the IPIRG-2 contract.

1.4 Structure of the IPIRG-2 Final Report

Sections 2.0, 3.0, and 4.0 of this report present the results of the material property evaluations, the pipe experiments, and the analysis of the pipe experiments, respectively. The primary focus of Section 2.0 is on the effects of cyclic load histories on the fracture toughness of the nuclear grade pipe steels evaluated in this program. In Section 3.0, the results from both a series of 6-inch nominal diameter separate effects pipe experiments and a series of 16-inch diameter straight pipe and elbow experiments conducted as part of IPIRG-2 are discussed. In Section 4.0, the results from a series of analyses of the pipe experiments conducted as part of this program and other companion experiments from related programs (Refs. 1.7, 1.11, 1.27, and 1.32) are presented. Section 5.0 presents the results from Task 4 of the IPIRG-2 program, i.e., Resolution of Issues from IPIRG-1 and Related Programs. The main focus of this section is the presentation of the results from an uncertainty analysis conducted as part of Subtask 4.5. Section 6.0 presents the results from Task 5 of this program, i.e., Information Exchange Seminars and Workshops. Section 7.0 is the Discussion of Results section in which the results from the IPIRG-2 program are discussed in light of the objectives of the program. Finally, Section 8.0 is the Conclusions section.

1.5 References

1.1 "Investigation and Evaluation of Stress-Corrosion Cracking in Piping of Light Water Reactor Plants," by the Pipe Crack Study Group, NUREG-0531, February 1979.

1.2 Goldberg, A., and others, "Evaluation of Cracking in Feedwater Piping Adjacent to the Steam Generator in Nine Pressurized Water Reactor Plants," NUREG/CR-1603, October 1980.

1.3 Kanninen, M. F., and others, "Mechanical Failure Predictions for Sensitized Stainless Steel Piping with Circumferential Cracks," EPRI Report NP-192, September 1976.

* For further details regarding this uncertainty analysis, the reader is referred to NUREG/CR-6443.

1.4 Kanninen, M. F., and others, "The Development of a Plan for the Assessment of Degraded Nuclear Piping by Experimentation and Tearing Instability Fracture Mechanics Analysis," NUREG/CR-3142, June 1983.

1.5 Kanninen, M. F., and others, "A Critical Survey on the Application of Plastic Fracture Mechanics to Nuclear Pressure Vessels and Piping," *Nuclear Engineering and Design*, Vol. 67, pp 27-55, 1981.

1.6 Kumar, V., and others, "An Engineering Approach for Elastic-Plastic Fracture Analysis," EPRI Report NP-1931, July 1981.

1.7 Wilkowski, G. M., and others, "Degraded Piping Program - Phase II - Summary of Technical Results and Their Significance to Leak-Before-Break and In-Service Flaw Acceptance Criteria, March 1984-January 1989," NUREG/CR-4082, Vol. 8, March 1989.

1.8 Klecker, R., and others, "NRC Leak-Before-Break (LBB.NRC) Analysis Method for Circumferentially Through-Wall-Cracked Pipes Under Axial Plus Bending Loads," NUREG/CR-4572, May 1986.

1.9 Paris, P. C., and Tada, H., "The Application of Fracture Proof Design Methods Using Tearing Instability Theory to Nuclear Piping Postulating Circumferential Through-Wall Cracks," NUREG/CR-3464, September 1983.

1.10 Kumar, V., and others, "Advances in Elastic-Plastic Analysis," EPRI Report NP-3607, August 1984.

1.11 Schmidt, R. A., and others, "The International Piping Integrity Research Group (IPIRG) Program--An Overview," SMiRT-11 Proceedings, Paper G23/1, August 1991.

1.12 Yagawa, G., and others, "Research Activities on Fracture Mechanics for Nuclear Piping in Japan," *Nuclear Engineering and Design*, Vol. 98, pp 231-241, 1987.

1.13 Takumi, K., "Results of the Japanese Carbon Steel Pipe Fracture Program," Proceedings of the Seminar on Leak-Before-Break: Further Developments in Regulatory Policies and Supporting Research, NUREG/CP-0109, February 1990.

1.14 Milella, P. P., "Outline of Nuclear Piping Research Conducted in Italy," *Nuclear Engineering and Design*, Vol. 98, pp 219-229, 1987.

1.15 Sturm, D., "Recent Results and Future Programmes of Pipe Fracture Tests in MPA Stuttgart," Proceedings of the Seminar on Leak-Before-Break: Progress in Regulatory Policies and Supporting Research, NUREG/CP-0092, March 1988.

1.16 Faidy, C., and others, "Developments in Leak Before Break Approach in France," NUREG/CP-0092, pp 69-82, March 1988.

1.17 Landes, J. D. and McCabe, D. E., "Elastic-Plastic Methodology to Establish R-Curves and Instability Criteria - Topical Report on Toughness Characterization of Austenitic Stainless Steel Pipe Weldments," AWI CP-86-003, February 1986.

1.18 Milne, I., and others, "Assessment of the Integrity of Structures Containing Defects,", R/H/R6-Rev. 3, Published by Central Electricity Generating Board, England, May 1986.

1.19 Hale, D. A., and others, "The Growth and Stability of Stress Corrosion Cracks in Large-Diameter BWR Piping," EPRI Report NP-2472 Vol. 2, July 1982.

1.20 Murakami, E, and others, "Crack Growth of Nuclear Piping Under Dynamic Loading," ASME PVP special publication PVP 167, pp 115-120, July 1987.

1.21 Ogawa, N., "Experimental Study of Piping Stability Under Strong Earthquake," ASME PVP special publication PVP 150, pp 69-80, July 1988.

1.22 Kramer, G., and Papaspyropoulos, V., "An Assessment of Circumferentially Complex-Cracked Pipe Subjected to Bending," NUREG/CR-4687, October 1986.

1.23 "Report to the U. S. Nuclear Regulatory Commission Piping Review Committee," Prepared by the Pipe Break Task Group, NUREG/CR-1061, Vol. 3, November 1984.

1.24 Published for public comment on "Standard Review Plan, Section 3.6.3 Leak-Before-Break Evaluation," *Federal Register*, Vol. 52, No. 167, Notices, pp 32626 to 32633, Friday, August 28, 1987.

1.25 "Piping and Fitting Dynamic Reliability Program," Final Report for EPRI Contract RP 1543-15, Report TR-102792, Vols. 1-5, 1995.

1.26 Scott, P., and others, "Stability of Cracked Pipe Under Inertial Stresses - Subtask 1.1 Final Report," NUREG/CR-6233, Vol. 1, August 1994.

1.27 Scott, P., and others, "The Effect of Dynamic and Cyclic Loading During Ductile Tearing on Circumferentially Cracked Pipe: Experimental Results," PVP Vol. 280, pp 207-220, June 1994.

1.28 Wilkowski, G., and others, "The Effect of Dynamic and Cyclic Loading During Ductile Tearing on Circumferentially Cracked Pipe: Analytical Results," PVP Vol. 280, pp 221-240, June 1994.

1.29 Marschall, C. W., and others, "Effect of Dynamic Strain Aging on the Strength and Toughness of Nuclear Ferritic Piping at LWR Temperatures," NUREG/CR-6226, October 1994.

1.30 Olson, R., and others, "The Next Generation Analysis Methodology for Cracked Pipe Systems Subjected to Dynamic Loads," ASME PVP, Vol. 275-1, pp 159-172, June 1994.

1.31 Olson, R. J., and others, "Validation of Analysis Methods for Assessing Flawed Piping Subjected to Dynamic Loading," NUREG/CR-6234, August 1994.

1.32 Kanninen, M. F., and others, "Instability Predictions for Circumferentially Cracked Type 304 Stainless Steel Pipes Under Dynamic Loadings," EPRI Report NP-2347, April 1982.

1.33 Wilkowski, G. M., and others, "Short Cracks in Piping and Piping Welds - Semiannual Report: March-September 1990," NUREG/CR-4599, Vol. 1, No. 1, May 1991.

1.34 Wilkowski, G. M., and others, "Short Cracks in Piping and Piping Welds - Semiannual Report: March 1993-December 1994," NUREG/CR-4599, Vol. 4, No. 1, April 1995.

1.35 Rudland, D. L., Scott, P. M., and Wilkowski, G. M., "The Effect of Cyclic and Dynamic Loads on Carbon Steel Pipe," NUREG/CR-6438, February 1996.

1.36 Rahman, S., Olson, R., and Wilkowski, G., "Summary of Results from the IPIRG-2 Round-Robin Analyses," NUREG/CR-6337, February 1996.

2.0 MATERIAL PROPERTY EVALUATIONS

This section of the report discusses the material property evaluations conducted in this program. In addition to the standard quasi-static tensile and fracture toughness tests, dynamic tensile and fracture toughness tests were conducted. Furthermore, a series of quasi-static, cyclic and dynamic, cyclic fracture toughness tests were conducted to understand how the load history affects the fracture toughness of these nuclear grade piping steels.

2.1 General Material Property Evaluations of IPIRG-2 Materials

Table 2.1 shows a list of the piping materials used in the IPIRG-2 program.

Table 2.1 Piping materials evaluated during IPIRG-2

Pipe Experiment Number[1]	Loading	Material	Battelle Designation
1-1	Simulated Seismic	16-inch TP304	DP2-A8I[2]
1-2	Simulated Seismic	16-inch A106 Grade B	DP2-F29[2]
1-3 (1-4)	Single Frequency	16-inch A106 Grade B SAW	DP2-F29W[2] DP2-F55W (plate)
1-5 (1-6)	Single Frequency	16-inch TP304 SAW	DP2-A8W[2]
1-7 (1-8)	Simulated Seismic	16-inch A106 Grade B	DP2-F23
1-9	Dynamic, Monotonic	6-inch A106 Grade B	DP2-F22
2-1 (2-2)	Single Frequency	16-inch A106 Grade B Elbow	IP2-FE17
2-3 (2-4)	Single Frequency	16-inch WP304L Elbow	IP2-AE1
4.2-1 (3.3-1)	Dynamic, Monotonic	6-inch STS410 Pipe	IP-F13
4.2-2	Dynamic, Cyclic (R = -1)	6-inch STS410 Pipe	IP-F13
4.2-3	Dynamic, Cyclic (R = -1)	6-inch STS410 TIG Weld	IP-F16W
3.3-2	Quasi-static, Cyclic (R = -0.6)	6-inch A106 Grade B	DP2-F30[2]

(1) Number in parentheses are companion quasi-static monotonic experiment numbers.
(2) Material characterized in IPIRG-1 (Ref. 2.1).

Each of these pipe materials was well characterized and the results are discussed below. In addition to these pipe materials, dynamic material property tests were conducted on a 10-inch nominal diameter A106 Grade B (DP2-F9) carbon steel pipe and a 30-inch nominal diameter STS49 (IP-F1) carbon steel pipe.

2.1.1 Tensile Test Results

Tensile specimens were machined from the pipes such that their tensile axes were parallel to the pipes axis. Weld tensile specimens were taken transverse to the weld with the gage section entirely in weld metal. All specimens were machined without flattening and were taken from the midwall location of the pipes.

Quasi-static tensile tests employed round bar specimens with a 6.35 mm (0.25 inch) diameter by 25.4 mm (1 inch) long gage section. The dynamic tensile tests employed flat, pin-loaded specimens. Typically, all dynamic tensile specimens had a gage length of 25.4 mm (1.0 inch), a gage width of 6.35 mm (0.25 inch), and a gage thickness of 3.18 mm (0.125 inch). However, several of the IP-F13 and IP-F16W specimens had a gage length of 8.89 mm (0.35 inch). Due to the small size of the TIG weld (IP-F16W), the gage length for these weld dynamic specimens was reduced. The corresponding base metal specimens (IP-F13) were manufactured with the same gage length in order to eliminate material property scatter due to specimen geometry differences. However, one specimen from the IP-F13 material was machined with a 25.4 mm (1.0 inch) gage length to document the difference in the stress-strain response. Dynamic testing rates used in this effort corresponded to loading rates a piping system may experience during a high amplitude, low frequency, seismic event.

All tensile tests were performed in an 88.9 kN (20,000 lb) capacity servohydraulic MTS testing machine. Two different methods were used to measure strain during the course of these tests. The optical strain measuring device used in the IPIRG-1 program was initially used. However, it was found that the data the optical device produced were erroneous. Therefore, another device that makes use of a high-temperature, fast-response clip gage was established and implemented. Table 2.2 shows a listing of the tensile results for the materials tested in this program.

2.1.2 Fracture Toughness Results from Monotonic C(T) Specimen Tests

Standard fracture toughness specimens were of the compact (tension), C(T), design and contained side grooves to a depth of 10-percent per side*. These specimens were machined from the pipe thickness without flattening the pipe and were machined in the L-C orientation; that is, the longitudinal direction was the loading direction while the circumferential direction was the crack growth direction. The specimens were fatigue precracked according to the specifications in ASTM E1152-87, "Standard Test Method for Determining J-R Curves", to produce an initial average crack length of about 0.54w. Displacement rates in the quasi-static tests were set to cause crack initiation in about 10 minutes. In the dynamic tests, the displacement rates were selected to cause crack initiation in about 0.2 seconds. The quasi-static specimens were tested in a screw-driven Instron machine with a 133.4 kN (30,000 pound) capacity. The dynamic tests were run in a servohydraulic MTS test frame with a 89 kN (20,000 pound) capacity. The direct-current electric potential (d-c EP) method was used to detect crack initiation and to monitor crack growth during the C(T) tests (Ref. 2.2). A listing of the fracture toughness results for the specimens tested in this investigation are shown in Table 2.3.

Also shown in Table 2.3 are data from Pipe DP2-A8. It has been shown** that there are two distinct lots of material for the 16-inch nominal diameter, Schedule 100, TP304 stainless steel pipe labeled DP2-A8. These materials have different chemical compositions and toughness values. However, there was little difference in the stress-strain response between the two lots. The two lots of material have been given the designations DP2-A8I and DP2-A8II.

---

* Note, the cyclic base metal C(T) specimens discussed in the next section were not side grooved in order to better simulate the crack growth behavior of a TWC.

** The reader is referred to NUREG/CR-6446.

Table 2.2 Tensile test results from IPIRG-2

Specimen Number	Test Temperature, C	Strain Rate s^{-1}	UTS, ksi	UTS, MPa	σ_{ys}, ksi	σ_{ys}, MPa	Final Elong., Percent
DP2-F22-1t	288	2×10^{-4}	85.3	588	37.5	259	26.1
DP2-F22-2t	288	2×10^{-4}	85.2	587	37.0	255	27.1
DP2-F22B	288	0.99	76.3	526	47.5	327	20.7
DP2-F23-3t	288	2×10^{-4}	74.6	514	32.2	223	33.0
DP2-F23-4t	288	2×10^{-4}	72.3	498	30.5	210	32.7
DP2-F23A	288	1.0	64.1	442	39.7	273	29.9
DP2-F23B	288	1.0	65.4	451	33.9	234	30.2
DP2-F23C	288	1.0	66.8	461	39.0	269	28.9
DP2-F9A	288	0.91	62.9	433	42.7	294	29.5
DP2-F9B	288	1.05	68.1	470	44.7	308	24.3
DP2-F9-5	288	4×10^{-4}	76.6	528	34.7	239	26.5
IP-F1-1h	288	1.1	76.1	525	46.7	322	28.7
IP-F1-2h	288	1.1	72.0	496	44.6	308	27.0
IP-F1-1	288	4×10^{-4}	84.6	583	35.1	242	31.2
IP-FE17-T1	288	2×10^{-4}	65.2	208	30.2	449	28.3
IP-FE17-T2	288	2×10^{-4}	64.8	215	31.2	446	29.1
IP-FE17-T3	288	2×10^{-4}	65.6	210	30.5	452	28.2
IP-FE17-T4	288	2×10^{-4}	64.4	203	29.5	444	29.5
IP-FE17-HT1	288	1.0	58.6	265	38.5	404	30.4
IP-FE17-HT2	288	1.0	59.9	274	39.7	413	30.4
IP-FE17-HT3	288	1.0	56.1	249	36.1	387	21.9
IP-FE17-HT4	288	1.0	58.6	192	27.9	404	25.2
IP-F13-T1	300	4×10^{-4}	71.4	493	31.3	216	28.5
IP-F13-T2	300	4×10^{-4}	71.6	494	31.5	217	28.3
IP-F13-T4	300	1.0	59.9	413	26.1	180	48.5
IP-F13-T6	300	9.9	61.4	423	32.5	224	42.6
IP-F13-T7	300	12.0	60.6	418	37.1	256	41.6
IP-F13-T8	300	1.4	62.5	431	37.8	261	48.0
IP-F13-T9	288	8×10^{-2}	63.0	434	29.1	201	50.0
IP-F13-T10	288	3×10^{-2}	65.0	448	28.0	193	50.5
IP-F13-T11	300	4×10^{-4}	72.3	499	32.2	222	53.0
IP-F13-T12	300	4×10^{-4}	72.1	497	28.9	199	52.2
IP-F13-T13	300	3×10^{-4}	71.1	490	30.4	210	33.4
IP-F16-T2w	300	4×10^{-4}	97.4	672	69.6	480	36.3
IP-F14-T1w	300	4×10^{-4}	103.7	715	80.0	552	36.6
IP-F16-T3w	300	12	76.3	526	60.9	420	33.3
IP-F16-T4w	300	1.4	85.2	587	58.3	402	33.2
IP-F14-T2w	300	1.6	90.1	621	65.1	449	34.2
DP2-F55W-T1	288	2×10^{-4}	88.2	608	47.6	328	30.1
DP2-F55W-T2	288	2×10^{-4}	89.2	615	56.5	390	30.6
IP2-AE1-T1	20	2×10^{-4}	96.1	662	47.1	325	75.0
IP2-AE1-T2	20	2×10^{-4}	94.4	651	47.9	330	73.0
IP2-AE1-T3	288	2×10^{-4}	59.2	408	29.0	200	47.0
IP2-AE1-T4	288	2×10^{-4}	59.6	411	27.2	188	46.0
IP2-AE1-HT1	288	0.80	59.1	407	33.5	231	52.0
IP2-AE1-HT2	288	0.80	59.6	411	30.3	209	50.0
IP2-AE1-HT3	288	0.85	62.7	432	30.9	213	50.0

Table 2.3 Fracture toughness test results from IPIRG-2 from monotonic C(T) specimen tests

Specimen Number	Approximate Time to Crack Initiation, seconds	J at Initiation		dJ/da[1]	
		kJ/m^2	in-lb/in^2	MJ/m^3	in-lb/in^3
DP2-F22-3	600	77.1	440	108.3	15,710
DP2-F22-5	600	65.3	373	94.19	13,660
DP2-F22-2	0.2	43.6	249	42.71	6,190
DP2-F23-1	600	74.3	424	104.6	15,170
DP2-F23-2	600	69.3	396	159.5	23,132
DP2-F23-3	0.2	94.9	542	98.5	14,290
DP2-F23-4	0.2	115	659	99.5	14,440
IP-F1-1d	0.2	387	2,210	131.4	19,100
IP-F1-2d	0.2	278	1,590	167.6	24,300
IP-F1-8	600	366	2,090	153.6	22,300
DP2-F9-1d	0.2	96	549	43.0	6,240
DP2-F9-2d	0.2	137	785	27.4	3,970
DP2-F9-19	600	147	840	103.8	15,050
IP-F13-1	600	389	2,224	222.5	32,270
IP-F13-2	600	368	2,101	201.4	29,210
IP-F13-4	10	371	2,119	177.7	25,780
IP-F13-5	0.2	395	2,257	165.6	24,020
IP-F13-6	0.2	507	2,897	177.0	25,670
IP-F13-7	10	446	2,545	200.3	29,040
IP-F16-1w	600	833	4,754	181.1	26,270
IP-F16-2w	600	689	3,936	240.9	34,940
IP-F16-3w	10	411	2,346	359.4	52,120
IP-F16-4w	10	459	2,619	353.9	51,330
IP-F16-5w	0.2	638	3,642	321.6	46,640
IP-F16-6w	0.2	435	2,483	354.6	51,430
DP2-F55W-2	600	65.4	373	46.3	6,720
DP2-F55W-3	0.2	91.3	521	86.4	12,500
DP2-F55W-4	0.2	106	605	99.4	14,400
IP-FE17-1	0.2	373	2,130	207.8	30,140
IP-FE17-2	0.2	349	1,995	193.8	28,100
IP-FE17-3	600	533	3,042	249.9	36,250
IP-FE17-4	600	317	1,812	306.6	44,470
IP2-AE1-1	600	1,116	6,347	144.9	21,000
IP2-AE1-5	600	1,062	6,065	90.9	13,200
IP2-AE1-2	0.2	1,377	7,863	200.0	29,000
IP2-AE1-3	0.2	1,341	7,659	123.0	17,800
A8I-12a	600	854	4,876	481	69,720
A8I-9a	0.2	1,302	7,430	500	72,470
A8II-17	600	546	3,118	255	37,000
A8II-20	0.2	815	4,655	310	45,000

(1) Determined for crack extensions between 0.15 and 1.5 mm (0.006 to 0.06 inch).

2.2 Cyclic Effects on Small Scale Specimen Fracture

In the IPIRG-1 (Ref 2.3) program, a series of cyclic 6-inch diameter TWC pipe tests was conducted. The results from these experiments suggest that fully reversed cyclic loading degrades the fracture toughness of nuclear piping materials. To examine whether the cyclic toughness degradation effect observed in the 6-inch diameter TWC experiments is present in small scale specimens, a series of cyclic, C(T) and cyclic, single-edge notched tension [SEN(T)] experiments was conducted. Quasi-static, cyclic C(T) experiments were run on an A106 Grade B carbon steel base metal, three TP304 stainless steel base metals (DP2-A23, DP2-A8I, and DP2-A8II), an A106 Grade B carbon steel submerged-arc weld (SAW), and a TP304 stainless steel SAW. Only the stainless steel base metal was used in the SEN(T) experiments. Dynamic, cyclic C(T) experiments were conducted on a stainless steel and carbon steel SAW and two stainless steel base metals in order to address the combined effect of dynamic and cyclic loading. In addition to the experiments, several analyses were completed. A series of finite element analyses was run on both the C(T) and SEN(T) geometries in order to attempt to predict the cyclic experimental behavior and to verify the estimates of J using the upper envelope of the load-displacement curve. Also, a fractographic analysis was conducted on one of the stainless steel and carbon steel base metals in order to determine the mechanism behind the observed cyclic toughness degradation.

2.2.1 Analysis Approaches to Account for Cyclic Loading Effects

There are two parameters that are important in evaluating cyclic loading effects: (1) R-ratio (minimum/maximum load), and (2) the cyclic plastic displacement increment, δ_{cyc}/δ_i. For a cracked structure, cyclic loading alters the stress and strain fields ahead of the crack. During this loading, a compressive plasticity zone is formed within the original tensile plastic zone. The damage that occurs due to this plasticity dictates the amount of ductile tearing resistance directly ahead of the crack. Hence, the R-ratio, which dictates the magnitude of the compressive loads, is important in evaluating cyclic effects. Also, the magnitude of the crack growth per cycle becomes important. If the crack growth per cycle is large, then the crack will grow out of the damaged material and into virgin material. However, if the crack growth per cycle is small, the crack is always growing in highly damaged material. Additionally, the cyclic damage might accumulate differently for a stationary crack than a growing crack. Therefore, δ_{cyc}/δ_i (the cyclic plastic displacement/displacement to reach crack initiation in a monotonic test) can be used as a parameter in studying cyclic effects.

There are three separate methods that could be used in conjunction with these parameters to evaluate the effects of cyclic loading during ductile tearing on the fracture toughness of nuclear piping steels. The first is a detailed finite element analysis. Even though this analysis will be the most theoretically correct, time and cost constraints dictate that simpler analyses or estimation methods be used.

Another method for evaluating cyclic loading effects is the Dowling low cycle fatigue analysis methodology. In the presence of plasticity at the crack tip, Dowling (Ref. 2.4) calculated a cyclic J-integral, ΔJ, by integrating the load-displacement test record on a cycle by cycle basis and using the results in an η-factor type of analysis. These results can then be compared with high cycle fatigue crack growth da/dN versus ΔJ data for validation of the general methodology.

The third method employs accounting for the cyclic effects on the J-R curve of the material. From the experimental test record, the "upper envelope" of the load-displacement-crack growth record is extracted

and used in an η-factor type analysis to produce a cyclic J-R curve. With this method, the decrease in the load-carrying capacity is embedded directly into the J-integral calculation.

Table 2.4 lists some of the main advantages and disadvantages with each of the methods described above. For the assessments made in the IPIRG-2 program, it was determined that it would be easier to implement the "upper envelope" cyclic J-R curve approach rather than to try to implement the other methods. The upper envelope method is computationally manageable and can be integrated into the existing LBB framework with relative ease.

2.2.2 Cyclic C(T) Experiments

The C(T) specimens used in this cyclic study that were machined from pipe were done so without flattening and were machined from the L-C orientation, i.e., loads were applied in the direction of the pipe axis and the crack growth direction was circumferential. The C(T) specimens that were machined from a plate weld were machined in the L-T orientation; that is, the longitudinal direction was the loading direction while the specimen width direction (along the length of the weld) was the crack growth direction. The DP2-A23 and DP2-F30 base metal specimens and the carbon steel weld specimens were of the ½T C(T) size, while the stainless steel weld, the DP2-A8I, and DP2-A8II specimens were of the 1T C(T) size. The DP2-F30 base metal specimens, the stainless steel weld specimens, the DP2-A8I, and DP2-A8II specimens were about 80 percent of the standard thickness because of the smaller wall thicknesses of those particular pipes. The DP2-A23 and DP2-F30 C(T) specimens were not sidegrooved in order to better simulate the crack growth behavior of a TWC pipe. The weld specimens and the DP2-A8I and DP2-A8II specimens were sidegrooved to a depth of 10 percent per side in order to match previous material characterization results.

Table 2.5 shows the test matrix for the cyclic C(T) specimen tests. In this test matrix, δ_{cyc}/δ_i is the cyclic plastic displacement increment and is identical to the ratio used in the cyclic TWC pipe experiments (Ref. 2.3). These experiments were conducted with the same BASIC control program that was described in Reference 2.3.

The direct-current electric potential (d-c EP) method was used to monitor crack initiation and growth in all C(T) specimen tests. This method has been shown to be reliable in past programs (Refs. 2.1 and 2.3). For these tests, the point of crack initiation was estimated from the point of departure from linearity of the d-c EP versus displacement graph. Beyond the initiation point, crack extension was calculated using the Johnson equation (Ref. 2.2) which was modified as described in Reference 2.1. A J-Resistance curve was then calculated from the load-displacement-crack growth history using the procedure described in ASTM E1152-87, "Standard Test Method for Determining J-R Curves". Note, for the cyclic experiments, the upper envelope of the load-displacement curve was used in calculating the J-R curves. Table 2.6 shows the fracture toughness summary for the cyclic-load experiments.

2.2.2.1 DP2-A23 Stainless Steel and DP2-F30 Carbon Steel Results

Figure 2.1 shows $J_{QS,\,cyc}/J_{QS,\,mono}$ as a function of stress ratio for the DP2-A23 stainless steel base metal cyclic tests. The ratio $J_{QS,\,cyc}/J_{QS,\,mono}$ is a measure of the decrease in J when going from a monotonic to a cyclic loading history. In order to make a comparison between the C(T) and TWC pipe experiments, the J values were taken at a crack extension equal to 30 percent of the initial C(T) specimen ligament, which is

Table 2.4 Advantages and disadvantages of several analysis methods for assessing cyclic load effects on the load-carrying capacity of cracked pipes

Aspect	Detailed FEM Analyses	Dowling Operational ΔJ Approach	Cyclic J-R Curve Approach
Theoretical validity	Can be assessed by various integral fracture parameters	Empirical modification in compressive load region. Transformation to J_D needed process. Application to ΔJ values above J_{Ic} needs verification.	Violates J_D theory. Validation by FEM needed.
Ease of Application	Impractical at this time	Much more complicated than current analysis methods	Consistent with current LBB and in-service flaw evaluation analysis procedures
Material property needs	If a damage mechanism unexplainable by other than continuum mechanics occurs (i.e., void flattening), then load-history specific material property data needed.	Extrapolation of high cycle fatigue crack growth curve. (Fracture toughness not a consideration.)	Trend curve of the effects of cyclic and dynamic loading on J-R curve needed. Similitude from specimen to structural cyclic J-R curves needed to be shown.
Additional requirements	Knowledge of the load history, i.e., global loads and displacements	Knowledge of the load-history , i.e., loads, displacements, and when crack closure occurs.	Knowledge of the load history, i.e., R-ratio, incremental cyclic plastic displacement. These load-history corrections on the toughness may change during the course of a seismic event, so simplification is required.
Additional advantages	Can consider each individual cycle in detail		Readily lends itself to dynamic cracked-pipe analysis
More disadvantages	High time and computer costs		

Table 2.5 Cyclic-load C(T) test matrix

Material	Loading rate	δ_{cyc}/δ_i	Stress Ratio	Specimen Identification
TP304 DP2-A23	Quasi-static	n/a	1	A23-2c
		0.1	0	A23-4c, A23-21c
			-0.3	A23-13c
			-0.6	A23-14c
			-0.8	A23-17c
			-1	A23-5c, A23-20c
		0.2	0	A23-6c
			-0.6	A23-16c
			-0.8	A23-18c
			-1	A23-7c
		0.025	0	A23-11c, A23-22c
			-0.6	A23-15c
			-0.8	A23-19c
			-1	A23-12c
A106B DP2-F30	Quasi-static	n/a	1	F30-1c
		0.1	0	F30-2c, F30-7c
			-0.3	F30-12c
			-0.6	F30-4c
			-0.8	F30-5c
			-1	F30-3c, F30-6c
TP304 SAW DP2-A8W4	Quasi-static	0.1	-0.6	A8W4-103c, A8W4-104c
			-1	A8W4-101c, A8W4-102c
	Dynamic (4 Hz)	0.1	-0.6	A8W4-108c
			-1	A8W4-106c, A8W4-107c
A106 B SAW DP2-F40W	Quasi-static	n/a	1	F40W-1c
		0.1	-0.6	F40W-7c
			-1	F40W-5c, F40W-8c
	Dynamic (4 Hz)	n/a	1	F40W-4c
		0.1	-0.6	F40W-12c, F40W-13c
			-1	F40W-10c, F40W-11c
TP304 DP2-A8I	Quasi-static	n/a	1	A8I-12a
		0.1	-0.3	A8I-13
			-1	A8I-14
	Dynamic (4 Hz)	n/a	1	A8I-9a
		0.1	-0.3	A8I-22, A8I-23
TP304 DP2-A8II	Quasi-static	n/a	1	A8II-17
		0.1	-0.3	A8II-21
			1	A8II-18
	Dynamic (4 Hz)	n/a	1	A8II-20
		0.1	-0.3	A8II-15, A8II-16

Table 2.6 Cyclic-load C(T) fracture toughness summary

Specimen Identification	Loading Rate	Stress Ratio, R	δ_{cyc}/δ_i	J at Initiation, kN/m	J at Initiation, lb/in	dJ/da[a], MN/m²	dJ/da[a], lb/in²
A23-2c	QS	1	N/A[b]	1124	6,418	130.1	18,870
A23-4c	QS	0	0.1	1150	6,566	75.6	10,960
A23-21c	QS	0	0.1	862	4,924	156.0	22,620
A23-13c	QS	-0.3	0.1	877	5,010	194.0	28,140
A23-14c	QS	-0.6	0.1	799	4,565	177.6	25,760
A23-17c	QS	-0.8	0.1	536	3,061	219.5	31,830
A23-5c	QS	-1	0.1	455	2,598	79.0	11,460
A23-20c	QS	-1	0.1	253	1,449	85.8	12,440
A23-6c	QS	0	0.2	1013	5,788	400.0	58,010
A23-16c	QS	-0.6	0.2	850	4,858	203.0	29,440
A23-18c	QS	-0.8	0.2	857	4,896	202.0	29,300
A23-7c	QS	-1	0.2	343	1,963	72.5	10,510
A23-11c	QS	0	0.025	1405	8,025	230.6	33,440
A23-22c	QS	0	0.025	959	5,479	164.2	23,810
A23-15c	QS	-0.6	0.025	726	4,146	68.0	9,860
A23-19c	QS	-0.8	0.025	291	1,665	120.9	17,530
A23-12c	QS	-1	0.025	157	900	132.8	19,260
F30-1c	QS	1	N/A[b]	98.3	561	79.8	11,430
F30-2c	QS	0	0.1	94.2	537	93.2	13,530
F30-3c	QS	-1	0.1	63.2	360	32.7	4,750
F30-4c	QS	-0.6	0.1	76.4	436	46.2	6,700
F30-5c	QS	-0.8	0.1	82.1	468	21.6	3,150
F30-6c	QS	0	0.1	75.5	431	26.6	3,870
F30-7c	QS	-1	0.1	106.3	606	100.8	14,620
F30-12c	QS	-1	0.1	81.4	464	44.2	6,420
A8W4-110	QS	1	N/A[b]	55	315	135	19,550
A8W4-107	QS	1	N/A[b]	140	800	180	26,140
A8W4-101c	QS	-1	0.1	39	225	30.2	4,380
A8W4-102c	QS	-1	0.1	57	328	38.3	5,560
A8W4-103c	QS	-0.6	0.1	46	265	72.9	10,570
A8W4-104c	QS	-0.6	0.1	59	336	62.6	9,080
A8W4-106c	QS	-1	0.1		254	55.0	7,980
A8W4-107c	QS	-1	0.1	34	192	46.8	6,790
A8W4-108c	QS	-0.6	0.1	61	343	72.6	10,530
F40W-1c	QS	1	N/A[b]	65.5	374	29.3	4,250
F40W-4c	QS	1	N/A[b]	56.4	322	113.2	16,400
F40W-5c	QS	-1	0.1	30.1	172	26.2	3,800
F40W-7c	QS	-0.6	0.1	47.3	270	29.3	4,250
F40W-8c	QS	-1	0.1	30.3	173	33.6	4,870
F40W-10c	QS	-1	0.1	38.6	220	43.3	6,280
F40W-11c	QS	-1	0.1	33.7	192	37.2	5,390
F40W-12c	QS	-0.6	0.1	48.5	277	56.5	8,190
F40W-13c	QS	-0.6	0.1	33.4	191	58.8	8,530
A8I-12a	QS	1	N/A[b]	854	4876	481	69,720
A8I-9a	DYN	1	N/A[b]	1,302	7,430	500	72,470
A8I-13	QS	-0.3	0.1	952	5,435	287	41,600
A8I-14	QS	-1	0.1	356	2,032	214	31,000
A8II-15	DYN	-0.3	0.1	395	2,260	123	17,840
A8II-16	DYN	-0.3	0.1	376	2,147	138	20,010
A8II-17	QS	1	N/A[b]	546	3,118	255	37,000
A8II-18	QS	-1	0.1	313	1,786	116	16,800
A8II-20	DYN	1	N/A[b]	815	4,655	310	45,000
A8II-21	QS	-0.3	0.1	652	3,722	240	34,800
A8I-22	DYN	-0.3	0.1	1,297	7,404	340	49,300
A8I-23	DYN	-0.3	0.1	1,269	7,248	401	58,200

(a) Calculated between crack extensions of 0.15 mm (0.006 inch) and 1.5 mm (0.06 inch).
(b) Monotonic test.

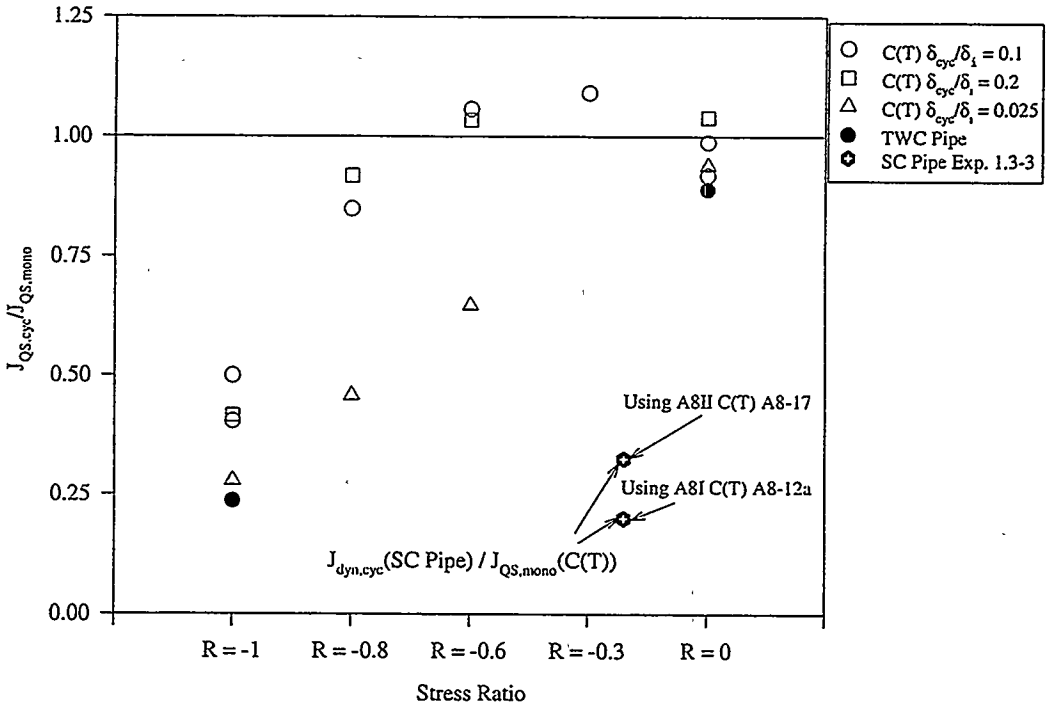

Figure 2.1 $J_{QS,cyc}/J_{QS,mono}$ for DP2-A23 stainless steel cyclic experiments (Experiment 1.3-3 on stainless steel pipe A8II)

the maximum allowable crack extension for a C(T) specimen (Ref. 2.5). The amount J decreases with decreasing stress ratio is a function of the cyclic plastic displacement increment (δ_{cyc}/δ_i). For the smaller cyclic plastic displacement increments ($\delta_{cyc}/\delta_i = 0.025$), the J value drops significantly at the intermediate stress ratio (R = -0.6), while at the larger cyclic plastic displacement increments ($\delta_{cyc}/\delta_i = 0.1$ and 0.2), the decrease is minimal until a stress ratio of -0.8. This indicates that at smaller cyclic plastic displacement increments, either there is a greater loss in apparent toughness due to the crack growing in highly damaged material or contributions to the crack growth from fatigue have become substantial.

Each of the DP2-A23 stainless steel TWC pipe test results fall slightly below the C(T) specimen results in Figure 2.1. The cyclic C(T) specimen tests tend to slightly underestimate the effect of cyclic loading on the TWC pipe J response at this particular crack extension. Overall, the C(T) tests do a reasonable job of predicting the decrease in toughness under cyclic loading.

Figure 2.2 shows a comparison between the cyclic TWC pipe and the cyclic C(T) specimen crack growth per cycle for this stainless steel (DP2-A23). In Figure 2.2, Labels A, C, and E show R = -1 crack growth comparison results for the DP2-A23 stainless steel specimens at cyclic plastic displacement increments (δ_{cyc}/δ_i) of 0.1, 0.2 and 0.025, respectively. Labels B, D, and F show the same comparisons, but for the R = 0 case. From Figure 2.2, the cyclic C(T) tests severely underpredict the crack growth per cycle for the TWC pipe tests. However, doubling δ_{cyc}/δ_i after crack initiation in the C(T) specimens would produce crack growth that better matches the crack growth in the TWC pipe. As shown in Figure 2.2, the C(T)

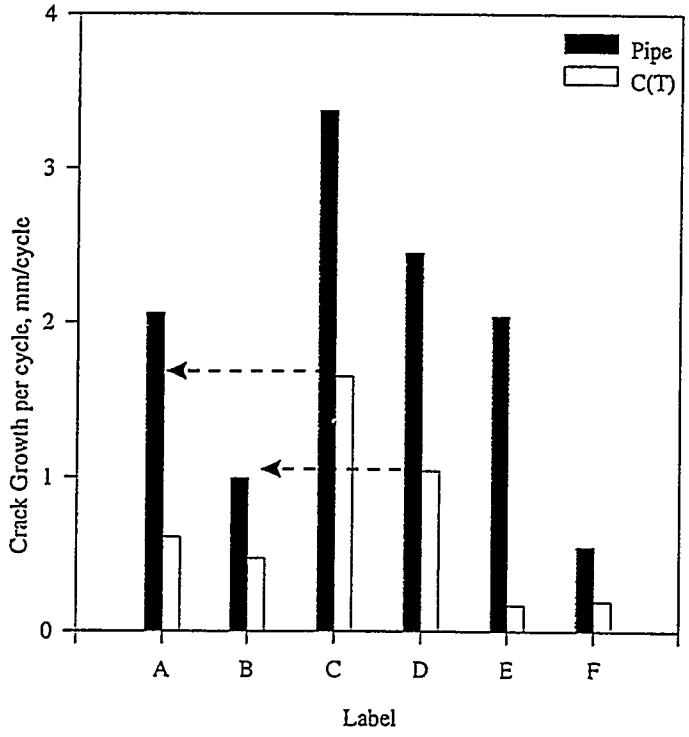

Label	R	δ_{cyc}/δ_i	Material
A	-1	0.1	A23
B	0	0.1	A23
C	-1	0.2	A23
D	0	0.2	A23
E	-1	0.025	A23
F	0	0.025	A23

Figure 2.2 Crack growth per cyclic for a variety of cyclic DP2-A23 stainless steel experiments

results under Label D ($R = 0$, $\delta_{cyc}/\delta_i = 0.2$) match well with the TWC pipe results of Label B ($R = 0$, $\delta_{cyc}/\delta_i = 0.1$). It has been shown* that the problem of similitude between a C(T) specimen and TWC pipe can be overcome by using a pipe analysis with the appropriate dynamic loading to determine the δ_{cyc}/δ_i parameter for control of the C(T) test. The calculated δ_{cyc}/δ_i parameter may change after crack initiation and would probably be much different for a TWC pipe than for a SC pipe.

Figure 2.3 shows the ratio $J_{QS,\,cyc}/J_{QS,\,mono}$ for the DP2-F30 carbon steel base metal C(T) and TWC pipe experiments. Again, note that this ratio is a measure of the relative decrease in resistance due to cyclic loading and cannot be used to directly compare the cyclic C(T) J-R curves to the cyclic TWC pipe J-R curves. The cyclic C(T) results follow the same trend as the TWC pipe experimental results. This indicates that for this material the relative decrease in resistance due to cyclic loading is approximately the same for the C(T) and pipe geometries.

Figure 2.4 shows the average crack growth per cycle for the DP2-F30 carbon steel specimens tested. Clearly, at a cyclic plastic displacement increment of 0.1, the C(T) specimens does not accurately predict the crack growth per cycle in a TWC pipe experiment.

* For details, the reader is referred to NUREG/CR-6440

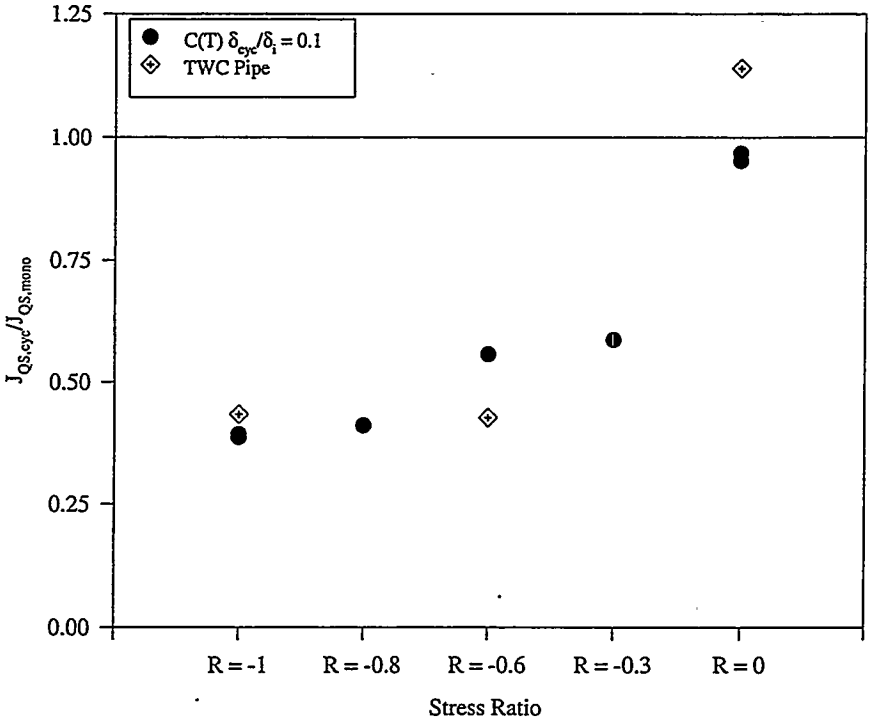

Figure 2.3 $J_{QS,\,cyc}/J_{QS,\,mono}$ for DP2-F30 carbon steel cyclic experiments

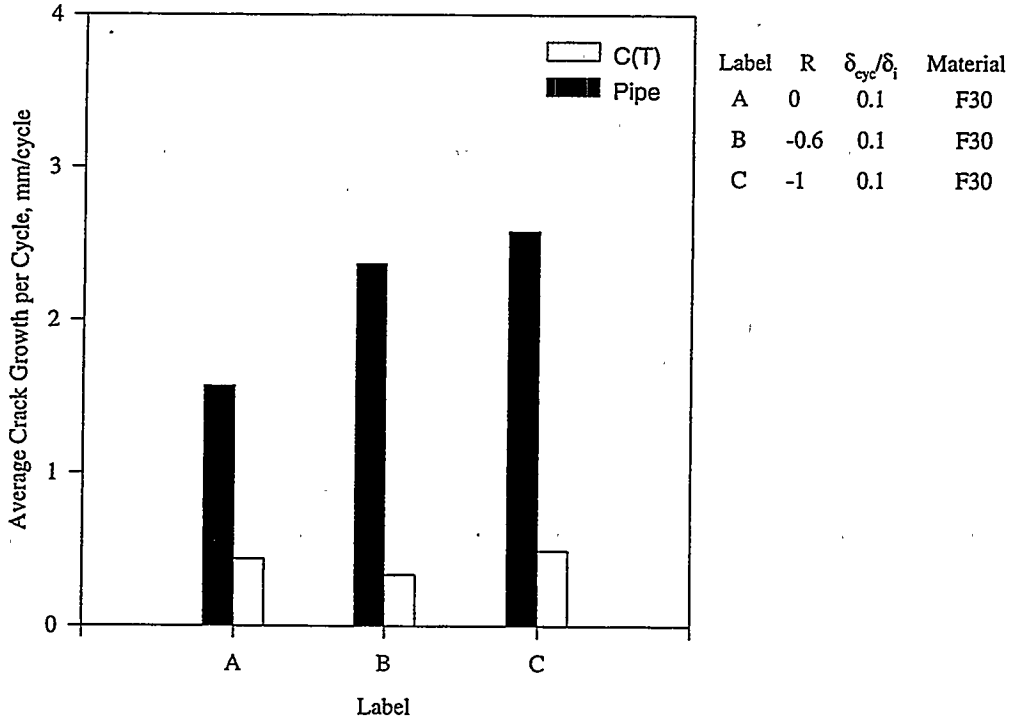

Label	R	δ_{cyc}/δ_i	Material
A	0	0.1	F30
B	-0.6	0.1	F30
C	-1	0.1	F30

Figure 2.4 Crack growth per cycle for the cyclic DP2-F30 carbon steel experiments

2.2.2.2 Submerged-Arc Weld Results

Figure 2.5 shows $J/J_{QS, mono}$ for the carbon and stainless steel SAW C(T) specimen tests. Also shown in this figure are results from a series of base metal TWC pipe experiments. For the carbon and stainless steel SAW C(T) tests, dynamic, monotonic loading significantly increased the resistance as compared with the quasi-static, monotonic tests, whereas for the base metal pipe experiments dynamic loading had no effect on the stainless steel and lowered the resistance of the carbon steel as compared with the quasi-static resistance.

Furthermore, all materials shown in Figure 2.5 were adversely affected by the cyclic loading. For the carbon steel SAW tests, the resistance under dynamic loading was 100 percent greater than the quasi-static, monotonic resistance, while the resistance at quasi-static, cyclic (R = -1) loading was 40 percent less than the quasi-static, monotonic loading resistance. If these two factors were strictly additive, the dynamic, cyclic (R = -1) resistance would be 60 percent higher than the quasi-static, monotonic resistance. Clearly, this is not the case as evident in Figure 2.5.

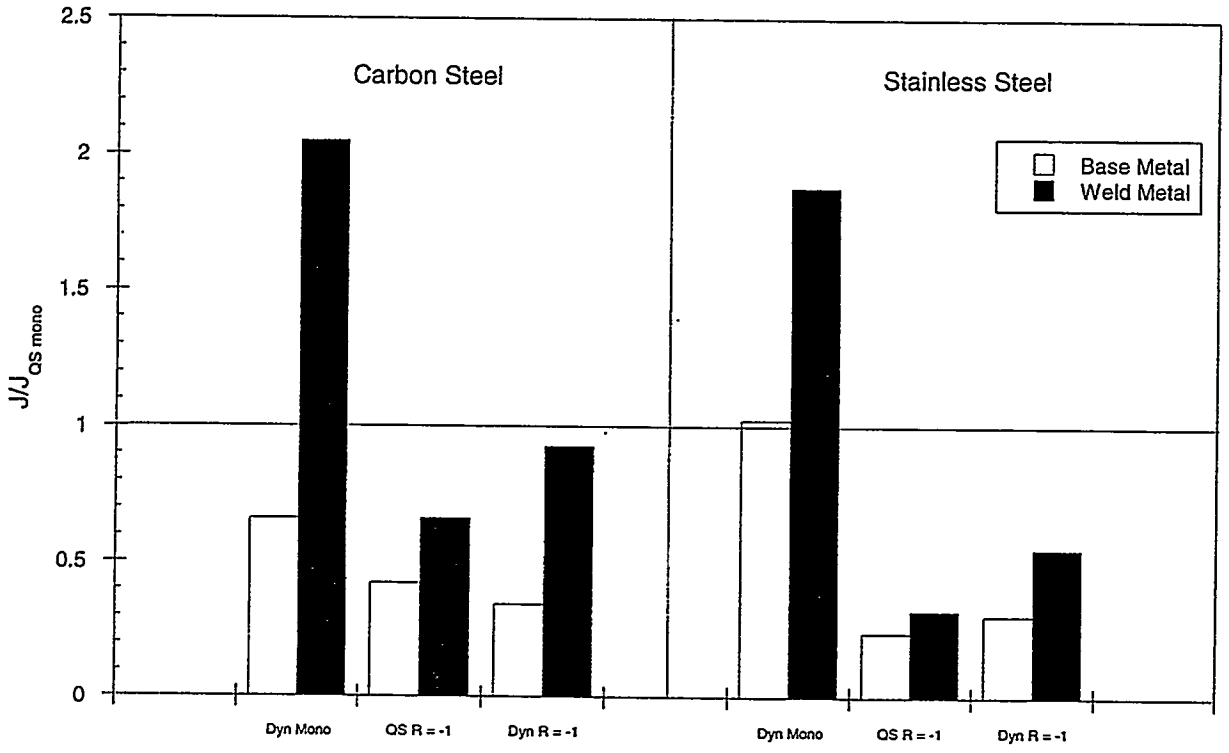

Figure 2.5 $J/J_{QS, mono}$ for carbon steel and stainless steel submerged-arc welds and base metals

Even though the cyclic (R = -1) and dynamic effects are not additive, a method for estimating the dynamic, cyclic resistance is proposed that multiplies the quasi-static, monotonic resistance ($J_{QS, mono}$) by the relative decrease in resistance due to both the cyclic (R = -1) and dynamic effects. Figure 2.6 shows the experimental J values at some crack extension for the dynamic, cyclic experiments ($J_{dyn, cyc}$) versus a calculated J using the quasi-static, monotonic resistance multiplied by a dynamic and cyclic correction factor $[J_{QS, mono}*(J_{dyn, mono}/J_{QS, mono})(J_{QS, cyc}/J_{QS, mono})]$. Note that all J values shown in Figure 2.6 are taken at a crack extension of 30 percent of the original ligament. Using the experimental cyclic (R = -1) and dynamic correction factors (the open symbols in Figure 2.6), the estimates closely matched the experimental dynamic, cyclic data, indicating that the dynamic and cyclic effects are multiplicative and no synergism exists.

The solid symbols in Figure 2.6 represent results calculated from the best-fit relationship between the load history effects and the material's yield-to-ultimate strength ratio. These results show that this estimate overpredicts the experimental dynamic, cyclic results. However, the results are encouraging, and with some refinement, a suitable criterion may be developed that can predict the resistance under dynamic, cyclic loading using the quasi-static, monotonic properties.

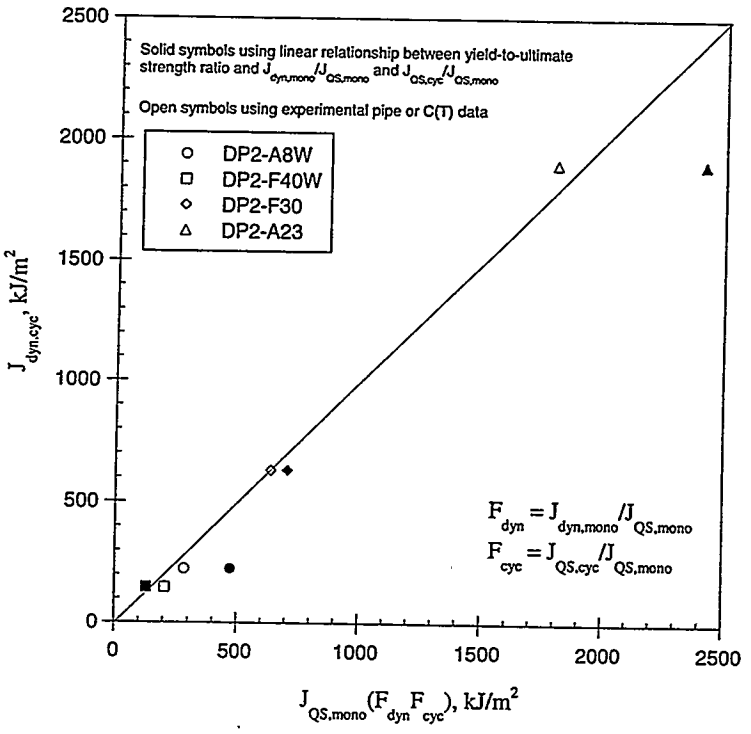

Figure 2.6 Experimental J versus calculated J for dynamic, cyclic (R = -1) experiments

2.2.2.3 Verification of Experimental Cyclic (R = -1) J-R Curve Calculations Using the Finite Element Method

In order verify the analysis procedure to calculate the J-R curve from the cyclic C(T) experiments, a series of two-dimensional finite element analyses was conducted. The point being addressed was the validity of using the upper envelope of the cyclic load-displacement curve with the ASTM E813/1152 J-R calculation procedure to get the cyclic J-R curve. These analyses were conducted under plane-stress and generalized plane-strain conditions using the classical isotropic and kinematic hardening laws. The ABAQUS finite element code was used in these analyses.* From these analyses, the kinematic hardening law produced results that closely match the tensile portion of the cyclic loading history, but severely underpredicted the compressive portion. On the other hand, the isotropic hardening (using both a linear fit and the actual stress-strain behavior) overpredicted both the tensile and compressive loads. A combined isotropic/kinematic hardening law may capture the cyclic load history trends better; however, these types of combined laws are not presently available in the ABAQUS code.

The J-integral value during the cyclic event was predicted from the plane-stress analyses. Figure 2.7 shows a comparison of the numerical J-R curve with the experimental data from a cyclic stainless steel specimen (Specimen A23-5c from Table 2.4). The crack initiated during the fifth loading cycle in this experiment.

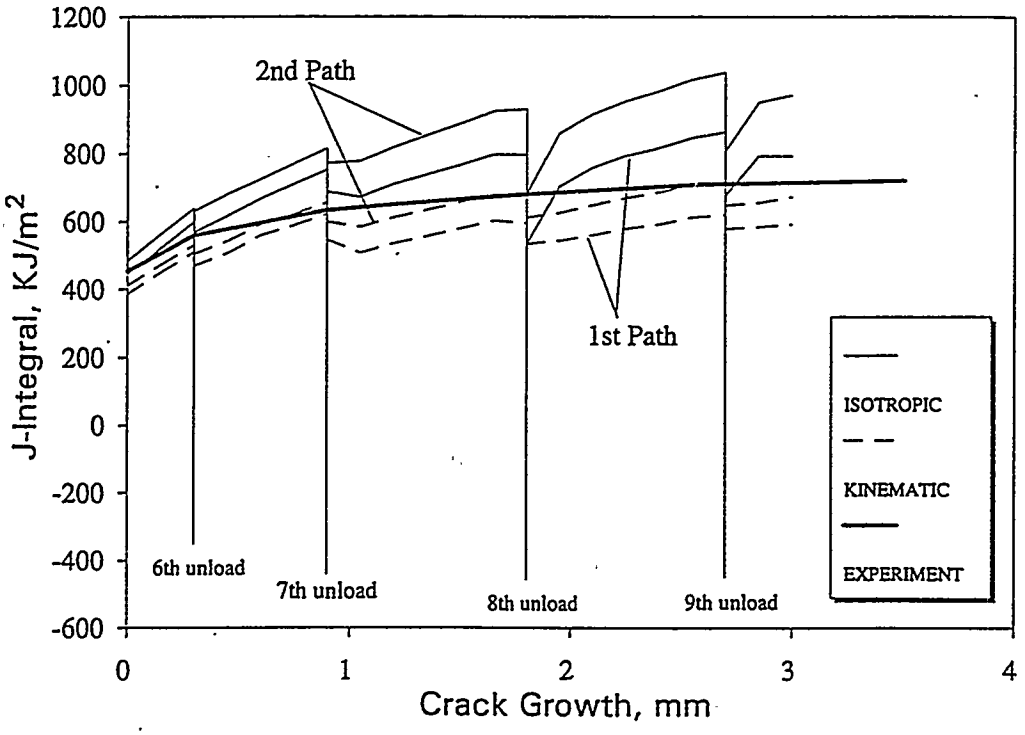

Figure 2.7 J-R curve comparison for a DP2-A23 stainless steel specimen tested at R = -1

* For details of these analyses, the reader is referred to NUREG/CR-6440.

after some crack extension as compared with the dynamic, monotonic experiment. These trends indicate that there is no interaction between the dynamic and cyclic effects on toughness for this material.

From Figure 2.9, the dynamic, monotonic resistance (A8II-20) for Pipe DP2-A8II was significantly higher than the quasi-static, monotonic resistance (A8II-17). This trend was similar to the trends for Pipe DP2-A8I. However, the J-R curve for the dynamic, monotonic specimen machined from Pipe DP2-A8II was still significantly lower than the J-R curve for the quasi-static monotonic specimen machined from Pipe DP2-A8I.

The quasi-static R = -0.3 specimen (A8II-21) had a slightly higher J_i value but no significant difference in the J-values during crack growth as compared with the quasi-static, monotonic specimen (A8II-17). Again, this trend is similar to what was observed for Pipe DP2-A8I. Both of the dynamic, R = -0.3 specimens (A8II-15 and A8II-16), showed a significant decease in toughness as compared with the quasi-static, monotonic (A8II-17) resistance. As discussed in Section 2.2.2.3, data from quasi-static, cyclic and dynamic, cyclic C(T) specimens tested at R = -1 suggested that there was no interaction between the dynamic and cyclic effects on toughness. In fact, a good estimation of experimental dynamic, cyclic (R = -1) toughness can be made by multiplying the percent change in toughness due to dynamic, monotonic and quasi-static, cyclic (R = -1) loading to the baseline quasi-static, monotonic resistance. However, this trend does not seem to be true for specimens tested at dynamic, R = -0.3 loading rates for material DP2-A8II. Since the dynamic, monotonic resistance showed an increase in toughness and the quasi-static R = -0.3 showed no change in toughness (after some crack growth) as compared with the quasi-static, monotonic resistance, the dynamic, R = -0.3 resistance would be slightly higher than the quasi-static, monotonic resistance if no interaction between the dynamic and cyclic effects existed. However, as shown in Figure 2.9, the dynamic, R = -0.3 J-R curves are considerably lower than the quasi-static, monotonic J-R curve.

The quasi-static, R = -1 specimen (A8II-18) had a significantly lower value of J at crack initiation as compared with the quasi-static, monotonic specimen (A8II-17). At a crack extension of 10 mm (0.39 inch) the J-value was 53 percent of the J-value for the quasi-static, monotonic specimen. Curiously, the resistance for the quasi-static R = -1 specimen was very similar to the resistance for the dynamic, R =-0.3 specimen. For this lot of material, even though there seemed to be some interaction between the cyclic and dynamic effects on toughness, the J-R curve from the quasi-static, R = -1 specimen seems to provide a reasonable lower bound. Note that even though no dynamic, R = -1 data exists, the typical seismic history has a more positive effective stress ratio than would be expected for fully-reversed loading.

SEN(T) Specimens. A series of single-edge-notched tensile [SENT(T)] specimens were conducted to determine the whether this geometry could be used to predict the surface-cracked pipe response of IPIRG-1 Experiment 1.3-3*. Monotonic and cyclic experiments were conducted, but only quasi-static loading rates were used. All SEN(T) specimens were machined from Pipe DP2-A8II. The experimental results showed that at a stress ratio of -1, the specimen experienced less plasticity than a similar specimen tested with monotonic loading. However, the was a minimal difference between the specimen tested at R = -0.3 and the one tested with monotonic loading, indicating that at R = -0.3, the effects of cyclic loads on the load-carrying capacity are minimal.

---

* A J-R curve calculated for Experiment 1.3-3 was considerably lower than a C(T) specimen J-R curve from the same material.

An estimate of the J-integral for this specimen geometry was made using two methods, i.e., the finite element method and the Ahmad J-estimation scheme method*. Even though the finite element method made good predictions of the experimental loads, the J values calculated were a factor of approximately 2 lower than the J values calculated from the Ahmad scheme for the monotonic experiments. This discrepancy is due to the fact that the Ahmad scheme may not be valid for high toughness materials.

If the J values calculated for the SEN(T) specimens from the finite element analyses are compared with the J values calculated for Experiment 1.3-3, an observation on the constraint of radially growing flaws can be made, see Figure 2.10.

For this geometry, the calculated J values are dependent on the depth of the surface flaw. The results show that the deeper the flaw, the lower the J values at crack initiation. Curiously, the J_i value for Experiment 1.3-3 (dynamic, cyclic with $a/t = 0.66$) was similar to the J_i value for Specimen SENT-6 (quasi-static, monotonic with $a/t = 0.72$). Even during crack growth, the J-R curve for Experiment 1.3-3 was similar to the J-R curve for Specimen SENT-6. Therefore, the SEN(T) specimen geometry seems to produce a good representation of the constraint in a SC pipe. However, no dynamic, cyclic SEN(T) specimen experiment was conducted for comparison purposes.

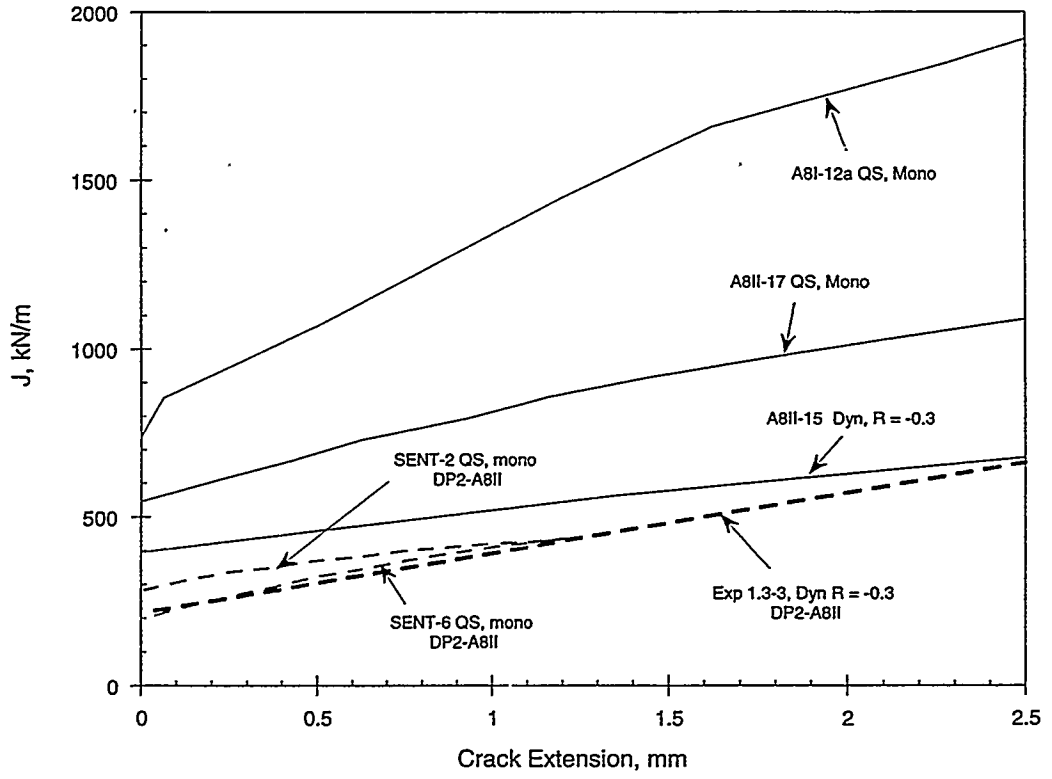

Figure 2.10 Several J-R curves for comparison with Experiment 1.3-3

* The reader is referred to NUREG/CR-6446.

2.2.3 Fractographic Results

Since the stress-strain fields ahead of a crack control the behavior of a cracked structure, it is important to fractographically study the area ahead of the crack tip as the damage is taking place. Because it is difficult to watch the material *in situ*, i.e., as the test is progressing, three specimens were tested on each base metal material evaluated. These specimens represent the possible damage forming portions of the cyclic process. The first specimen (A) was loaded to a displacement just beyond crack initiation and unloaded to zero load, see Figure 2.11. This test demonstrated the amount of damage ahead of a newly initiated crack in a simple monotonic test. The second specimen (B) was loaded to a displacement just past crack initiation,

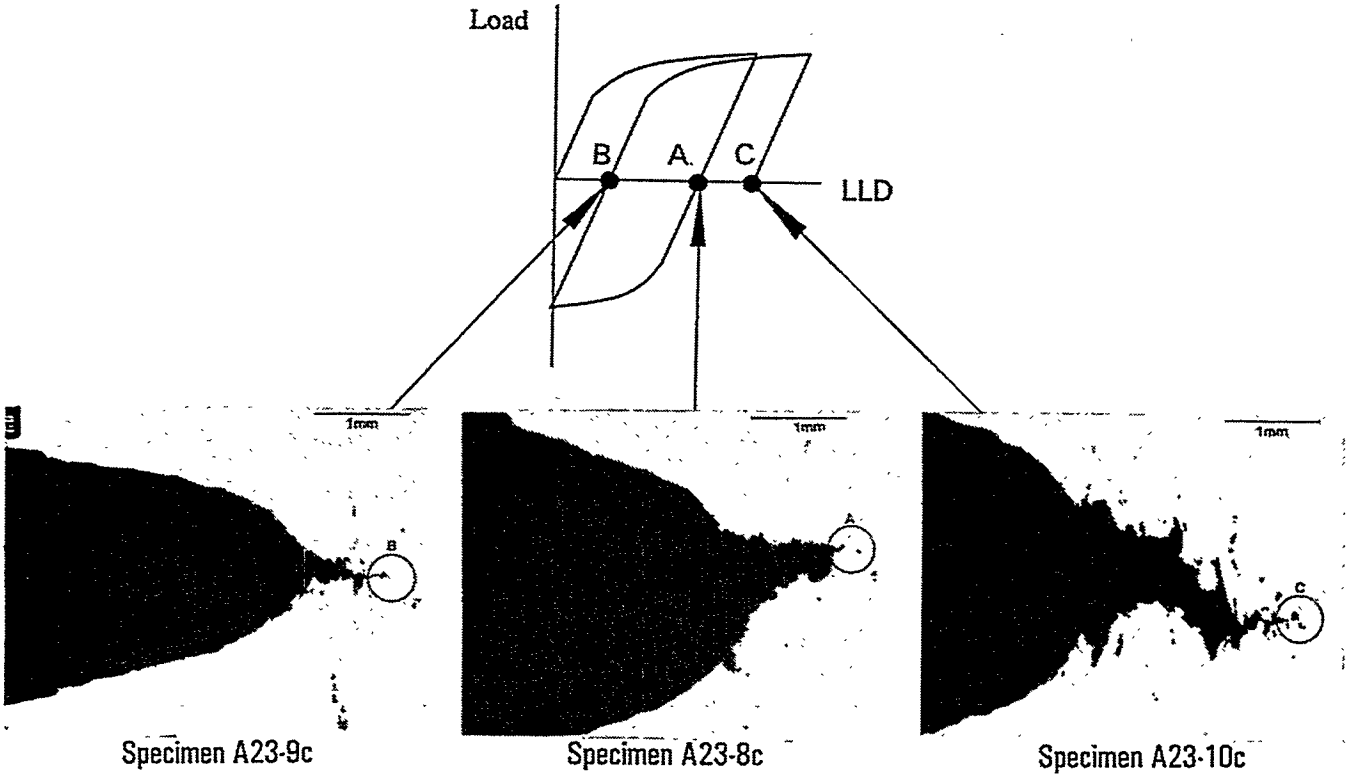

Figure 2.11 General view of three additional DP2-A23 stainless steel cyclic C(T) specimens

the load recorded, unloaded to a negative load equal to the recorded load, and reloaded to zero load. This test demonstrated the amount of damage present after one cycle of fully reversed plasticity. The third specimen (C) was loaded to a displacement just past crack initiation, the load recorded, unloaded to a negative load equal to the recorded load, reloaded to an additional displacement equal to 10 percent of the crack initiation displacement, and unloaded to zero load. This test showed the difference in the process zone after one complete reversed cycle with an additional amount of crack growth.

These additional DP2-A23 stainless steel cyclic C(T) specimens were sectioned at mid-thickness in order to view the cyclic damage near the crack tip. Figure 2.11 shows a general view of the three stainless steel specimens and their completion points along the load-displacement curve. There appears to be two main mechanisms present in the cyclic degradation process. First is crack-tip sharpening. Clearly, the crack tip for Specimen B is much sharper than the crack tip for Specimen A. It seems that the compressive plasticity sharpens the crack, thus raising the crack tip stress intensity and lowering the fracture resistance. This sharpening causes easier tearing during the next positive load cycle, as shown by the crack tip for Specimen C. Both the stainless and the carbon steels showed evidence of crack-tip sharpening. However, because of the more ductile nature of stainless steel, the increased amount of crack-tip blunting caused the sharpening to be less severe in the stainless steel specimens than in the carbon steel specimens.

Furthermore, it may take less compressive load to sharpen the crack tip for these lower toughness materials. Therefore, intermediate stress ratios could decrease the load-carrying capacity in the carbon steel, but have no effect on the stainless steel. In addition, since the crack will close until the initial crack faces transmit compressive loads, it is logical that there would be a limit to the amount the load and displacement are decreased by cyclic loading. This behavior was observed in the cyclic C(T) tests in this study. In the carbon steel base metal tested in this investigation, that limit seems to be at a stress ratio of -0.8. For this material, decreasing the stress ratio from -0.8 to -1 did not decrease the load-displacement curve any further.

The second important mechanism in the degradation process is void sharpening. In this case, only the carbon steel experienced substantial void sharpening. Sharp voids will enhance void coalescence and lower the apparent fracture toughness. The argument for this mechanism is similar to the one just made for the crack-tip sharpening; the higher the material's toughness, the larger the compressive load needed to promote void sharpening. Perhaps for compressive loading larger than that used in this investigation, void sharpening might occur in the stainless steel specimens. The crack tip and void sharpening work together in degrading the material's fracture resistance under cyclic loading.

2.3 References

2.1 Marschall, C. M., Landow, M. P., and Wilkowski, G. M., "Loading Rate Effects on Strength and Fracture Toughness of Pipe Steels Used in Task 1 of the IPIRG Program," NUREG/CR-6098, BMI-2175, October 1993.

2.2 Schwalbe, K. H. and Hellman, D., "Application of the Electric Potential Method to Crack Length Measurements Using Johnson's Formula," *Journal of Testing and Evaluation*, Vol. 9, No. 3, pp 218-221, 1981.

2.3 Scott, P., Kramer, G., Vieth, P., Francini, R., and Wilkowski, G., "The Effect of Dynamic and Cyclic Loading During Ductile Tearing on Circumferentially Cracked Pipe: Experimental Results," ASME PVP Vol. 280, pp 207-220, June 1994.

2.4 Dowling, N. E., and Bagley, J. A., "Fatigue Crack Growth During Gross Plasticity and The J-Integral," Mechanics of Crack Growth, ASTM STP 590, pp 82-103, 1976.

2.5 Wilkowski, G.M., Marschall, C.W., and Landow, M., "Extrapolation of C(T) Specimen J-R Curves for Use in Pipe Flaw Evaluations," ASTM STP 1074, pp 56-84, 1990.

3.0 FULL-SCALE PIPE EXPERIMENTS

During the course of the IPIRG-2 program, 6- and 16-inch nominal diameter pipe fracture experiments were conducted. Six 6-inch diameter pipe experiments were conducted. Four of these were concerned with determining whether pipe steels manufactured in accordance with the Japanese pipe specification STS410 are as sensitive to dynamic and cyclic loading effects as the carbon steel pipe steels previously tested by Battelle during the IPIRG-1 program (Ref. 3.1). The crack geometry for these experiments was a through-wall-crack (TWC), the same as evaluated in the IPIRG-1 Subtask 1.2 experiments. The fifth experiment was a cyclic through-wall-cracked pipe experiment conducted at a stress ratio of -0.6 and was designed as a comparison to R = 0 and R = -1 experiments conducted in IPIRG-1. The same 6-inch diameter A106 Grade B pipe material as used in the IPIRG-1 Subtask 1.2 experiments was used in this experiment. The final 6-inch diameter pipe test conducted as part of this effort was an experiment to evaluate the effectiveness of an internal bellows at sealing a pressurized through-wall-cracked pipe test specimen. The loading conditions for this experiment were combined internal pipe pressure and dynamic, monotonic four-point bending.

In addition to the 6-inch diameter pipe experiments, there were twelve 16-inch diameter pipe/elbow experiments conducted as part of this program. Six of these experiments involved cracks in straight pipe sections, two involved cracks at elbow-to-straight pipe girth welds, and four involved cracks in the extrados of 90-degree, long-radius elbows.

3.1 Experimental Procedures

All of the pipe experiments conducted as part of IPIRG-2 were conducted in accordance with the IPIRG-2 Quality Assurance document IPI2-PP-1. This document specified the procedures for the preparation of the test specimens, the set up of the experiments, the calibration of the instrumentation, and the conduct of the experiments. Associated with this document were detailed checklists which guided the engineers and technicians in fulfilling all of the necessary tasks associated with each of these activities.

3.2 6-Inch Nominal Diameter Through-Wall-Cracked Pipe Experiments

As part of the IPIRG-2 program, six 6-inch nominal diameter through-wall-cracked (TWC) pipe tests were conducted. Five of these experiments were unpressurized, elevated temperature four-point bend experiments that were conducted with monotonic and cyclic loading histories. The sixth was a combined pressure and dynamic, monotonic bend experiment. The five unpressurized experiments were conducted using the same fixtures used in the 6-inch nominal diameter TWC pipe tests conducted in IPIRG-1 (Ref. 3.1), see Figure 3.1. The loading history for the cyclic displacement-controlled experiments consisted of loading the specimen to a prescribed displacement, recording the peak load, and then loading the specimen in compression to the previous peak load value multiplied by the stress ratio. A BASIC program written for the IPIRG-1, Subtask 1.2 experiments (Ref. 3.1) was used to perform the calculations and output the displacement-time command signal. The TWC tests can be separated into two groups by material; Japanese STS410 carbon steel and A106 Grade B carbon steel.

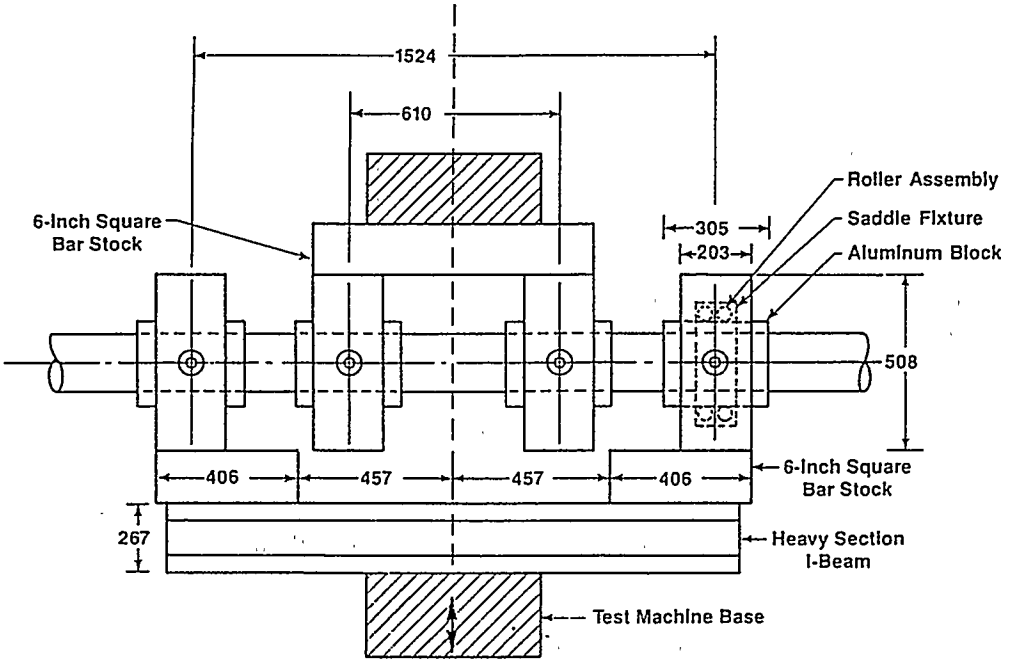

Note: All 4 saddle fixtures are identical to the detail.
All dimensions in millimeters.

Figure 3.1 Fixtures used in the 6-inch diameter, unpressurized, through-wall-cracked pipe experiments

3.2.1 Japanese STS410 TWC Pipe Experiments

This series of experiments was part of a larger program being conducted in Japan to develop a Japanese leak-before-break (LBB) criterion for carbon steel piping systems. The specific objective of this series of experiments was to ascertain whether Japanese STS410 carbon steel pipe is as sensitive to dynamic and cyclic loading effects as the carbon steel pipe steels previously tested at Battelle during the IPIRG-1 program. Table 3.1 shows the test matrix for these experiments. A detailed description of these experiments can be found in Reference 3.2.

A summary of the key results from these experiments is shown in Table 3.2. The maximum moment for the quasi-static, monotonic experiment (3.3-1) was approximately 10 percent higher than the maximum moment for the dynamic, monotonic experiment (4.2-1). This difference in load can be possibly attributed to a difference in crack growth angle. Note, the difference in crack section moment at crack initiation is not that significant. For Experiment 4.2-1, the crack grew at a 38-degree angle from the circumferential plane, while the crack in Experiment 3.3-1 grew at a 48-degree angle. This difference in angle causes a difference in the load-displacement response. Past studies (Ref. 3.3) have shown that as the angle from the circumferential plane is increased, the effective remaining ligament increases, and loads are increased. Comparing the behavior of the dynamic-monotonic (4.2-1) and dynamic-cyclic (4.2-2) base metal experiments, it can be seen that the maximum moment for the dynamic-cyclic experiment was only 7 percent lower than the maximum moment for the dynamic-monotonic experiment; however, the displacement at maximum moment for the dynamic-cyclic experiment was only approximately 30 percent

Table 3.1 Test matrix for Japanese STS410 TWC pipe experiments

	Base Metal Dynamic Monotonic	Base Metal Dynamic Cyclic R = -1	Weld Metal Dynamic Cyclic R = -1	Base Metal Quasi-static Monotonic
Experiment Number	4.2-1	4.2-2	4.2-3	3.3-1
Actual Pipe Outside Diameter	168.3 mm (6.625 inches)	165.6 mm (6.520 inches)	166.2 mm (6.545 inches)	166.0 mm (6.535 inches)
Actual Pipe Wall Thickness	14.5 mm (0.570 inches)	14.5 mm (0.571 inches)	14.4 mm (0.566 inches)	14.5 mm (0.569 inch)
Crack Location	Base Metal	Base Metal	Weld Metal	Base Metal
Through-Wall Crack Length	60 degrees	60 degrees	60 degrees	60 degrees
Test Temperature	300 C (572 F)	300 C (572 F)	300 C (572 F)	300 C (572 F)
Load History	Dynamic, Monotonic, Four-Point Bending	Dynamic, Cyclic (R = -1), Four-Point Bending	Dynamic, Cyclic (R = -1), Four-Point Bending	Quasi-static, Monotonic, Four-Point Bending
Target Loading Rate	25 mm/second (1 inch/sec)	25 mm/second (1 inch/sec)	25 mm/second (1 inch/sec)	0.07 mm/sec (0.003inch/sec)

Table 3.2 Summary of key results from Experiments 4.2-1, 4.2-2, 4.2-3, and 3.3-1

Experiment Number	4.2-1	4.2-2	4.2-3	3.3-1
Experiment Moment at Crack Initiation, kN-m	68.68	63.50	83.20	71.32
Experiment Maximum Moment, kN-m	84.08	78.44	87.98	92.76
Quasi-Static Yield Strength, MPa	221.0(1)	221.0(1)	516.0(2)	221.0(1)
Quasi-Static Ultimate Strength, MPa	493.0(1)	493.0(1)	693.0(2)	493.0(1)
Quasi-Static J at Crack Initiation, kN/m	378.6(1)	378.6(1)	760.9(2)	378.6(1)
Number of Cycles to Crack Initiation	N/A	8	13	N/A
Number of Cycles to Maximum Moment	N/A	14	13	N/A
Loading Rate	Dyn	Dyn	Dyn	QS
Load Ratio (Min/Max)	Mono	R = -1	R = -1	Mono
Load-Line Displacement Increments between Cycles, mm				
First Loading Block	N/A	1.6002	1.6002	N/A
Second Loading Block	N/A	0.8001	0.8001	N/A
Third Loading Block	N/A	3.2004	3.2004	N/A

(1) Base metal material data.
(2) Weld metal material data.

of the displacement at maximum moment for the dynamic, monotonic experiment. The fact that there was not much difference in load-carrying capacity between the quasi-static, monotonic and dynamic, monotonic experiments and the dynamic, cyclic and dynamic, monotonic experiments tend to indicate that while the Japanese STS410 pipe material may be affected somewhat by dynamic and cyclic loadings, the extent of the degradation due to these two mechanisms is probably less than what was observed previously for the A106 Grade B pipe material evaluated in the IPIRG-1, Subtask 1.2 experiments (Ref. 3.1).

Completing the discussion of the results from these pipe tests, it can be seen in Table 3.2 that the load-carrying capacity of the cracked weld specimen (Experiment 4.2-3) was approximately 12 percent higher than that for the corresponding (i.e., dynamic, monotonic) base metal experiment (Experiment 4.2-2). This is attributed to the higher strength and toughness of the weld when compared with the base metal material.

3.2.2 Intermediate Stress Ratio Experiment

In IPIRG-1 (Ref 3.1), a series of cyclic 6-inch nominal diameter TWC pipe tests were conducted on A106 Grade B carbon steel and TP304 stainless steel. These tests were conducted at stress ratios of 0 and -1. In order to explore the effects of a cyclic load history at an intermediate stress ratio, one additional TWC pipe test using the A106B pipe material was conducted as part of the IPIRG-2 program. This experiment was conducted with the same parameters as IPIRG-1 experiments, except the stress ratio was set at R = -0.6.

A summary of the key results for this experiment, along with the results from the applicable IPIRG-1 A106 Grade B TWC pipe experiments, are shown in Table 3.3.

Table 3.3 Experimental results for A106 Grade B 6-inch diameter TWC pipe experiments

Experiment Number	1.2-7	1.2-2	1.2-4	3.3-2
Experimental Moment at Crack Initiation, kN-m	37.08	27.26	34.56	31.81
Experimental Maximum Moment, kN-m	51.33	48.18	42.70	40.05
Load History	QS, mono	QS, cyclic	QS, cyclic	QS, cyclic
Load Ratio (Min/Max)	1	0	-1	-0.6
Outside Diameter, mm	167.6	167.6	167.6	167.8
Wall Thickness, mm	13.97	13.97	13.97	13.7
Total Percent TWC	36.0	36.0	36.0	36.9
Crack Growth Angle, degrees	40	46	45	32

In comparing the results from these tests, it is important to note that the angle from the circumferential plane at which the cracks grew was different for each of the experiments. Reference 3.3 suggests that most carbon steels will experience this type of out-of-plane crack growth because of the inherent anisotropy in the material. This particular heat of seamless pipe had inherent anisotropy due to the forming process. This anisotropy also causes a large scatter in the material properties. This variability is discussed in Reference 3.4.

As can be seen in Table 3.3, there is not much difference in the maximum load-carrying capacity between the quasi-static-monotonic and quasi-static cyclic (R = 0) experiments. Note, however, there is a significant difference in moment values at crack initiation for these two experiments. The reason for this difference is unclear at this time. There is also not much difference in the maximum load-carrying capacity between the R = -1 and R = -0.6 cyclic experiments, however, the maximum moments for the negative stress ratio experiments are 15 to 20 percent less than the maximum moment values for the R = 0 and monotonic experiments. These results suggest that there is some threshold stress ratio above which the effects of cyclic loadings can be ignored.

3.2.3 Dynamic, Monotonic, Pressurized Through-Wall-Cracked Pipe Experiment

A single dynamic, monotonic, pressurized through-wall-cracked pipe experiment was conducted in order to evaluate a potential sealing method for a pressurized through-wall-cracked 16-inch nominal diameter pipe system test specimen. The 6-inch nominal diameter test specimen was fabricated from a section of Schedule 80 A106 Grade B carbon steel pipe (DP2-F22). Due to the fact that the only purpose of this experiment was to evaluate a sealing method, limited instrumentation was attached to the specimen. However, due to the rather unique loading conditions for this experiment, it was decided after the fact to reduce and document the limited test data that were collected. Table 3.4 is a listing of the key results from this experiment.

Table 3.4 Key results for 6-inch diameter, dynamic, monotonic, pressurized through-wall-cracked pipe experiment

Expt. No.	Pipe Material	Outside Pipe Diameter, mm (inch)	Wall Thickness, mm (inch)	Test Temperature, C (F)	Test Pressure, MPa (psi)	θ/π	Loading Rate, mm/sec (inch/sec)	Moment at Crack Initiation, kN-m (in-kips)	Maximum Moment, kN-m (in-kips)
1-9	A106B	168.9 (6.650)	11.2 (0.440)	288 (550)	15.5 (2,250)	0.249	108 (4.24)	47.5 (420.4)	54.3 (480.6)

Figure 3.2 shows the test set up for Experiment 1-9. The outer load points were supported on rollers, while the inner load points were displaced downward. After a few small-amplitude cyclic loads, the load points were displaced 152 mm (6 inches) at a rate of 108 mm/sec (4.24 inch/sec). That loading failed to cause the sealing bellows to leak, so an additional 85 mm (3.35 inches) of displacement was applied whereupon the pipe severed into two pieces and after a very short delay, the bellows burst. The moment-rotation behavior of the crack is shown in Figure 3.3.

As a result of this test, the idea of using an internal bellow to seal a TWC was abandoned because of the unpredictable ability of the bellows to retain pressure. In a pipe-system test, a TWC seal would have to leak predictably to ensure that the facility would not be damaged by a DEGB.

3.2.4 Comparison of J-R Curves Between the IPIRG-1 and IPIRG-2 6-Inch Nominal Diameter, Unpressurized, TWC Pipe Experiments

J-R curves were calculated for the five unpressurized TWC experiments using an η-factor J-estimation scheme method (Refs. 3.5 and 3.6). The η-factor analysis, a simple method used in lieu of

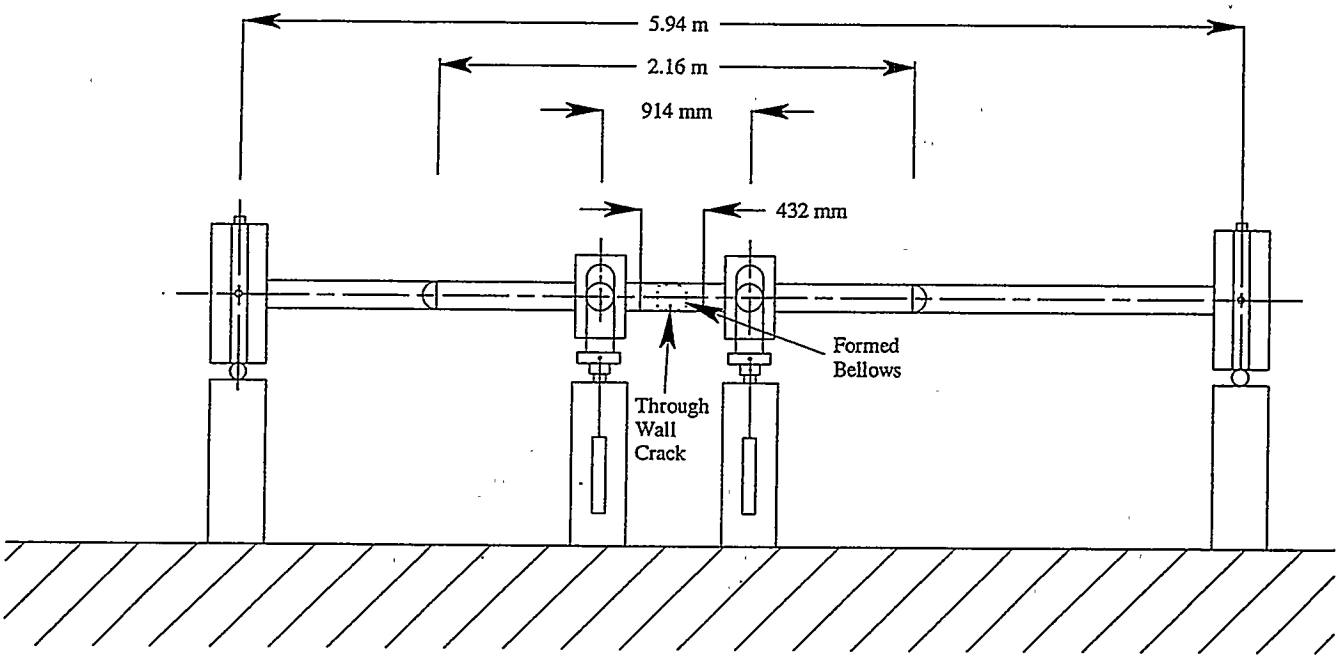

Figure 3.2 Experimental setup for Experiment 1-9

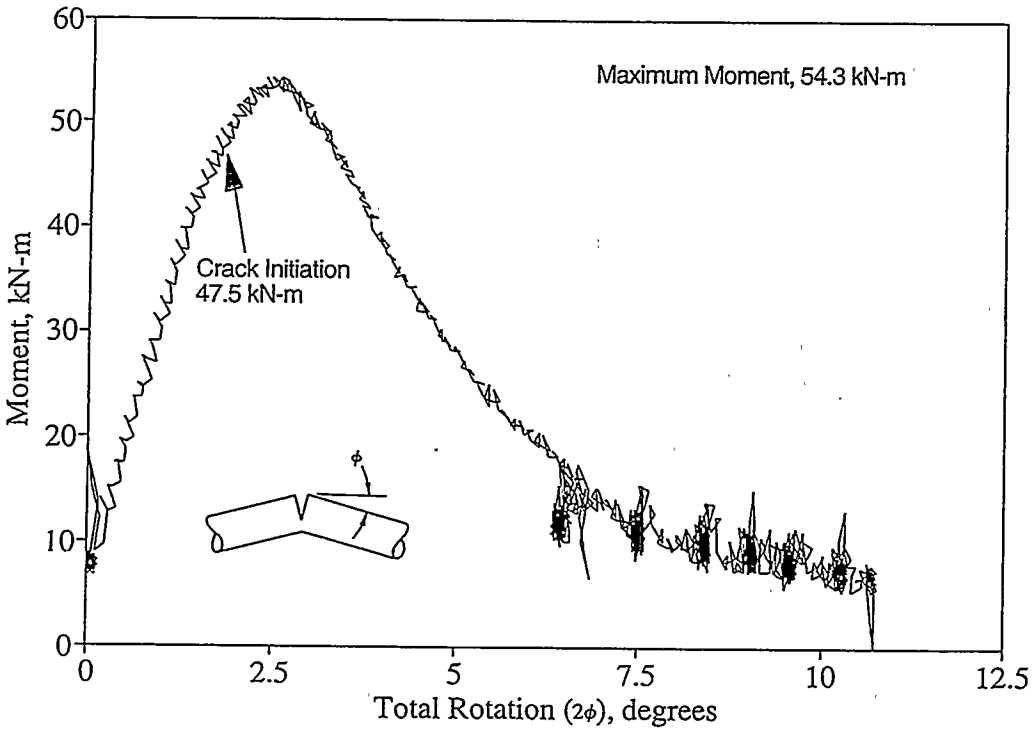

Figure 3.3 Moment-rotation response for Experiment 1-9

three-dimensional finite element analysis, is used to calculate the J-R curve from the experimental load-displacement, or moment-rotation, record. The energy absorbed during the test, i.e., the area under the moment-rotation or load-displacement curve, is proportional to the fracture resistance through a geometric term, i.e., the η-factor*.

Figure 3.4 shows the calculated J-R curves for the STS410 TWC pipe experiments. Also included in this figure are the J-R curves for several of the A106 Grade B pipe experiments conducted in IPIRG-1 (Ref. 3.7). This figure shows that the quasi-static (3.3-1) and dynamic, monotonic (4.2-1) STS410 experiments have approximately the same resistance until about 4 mm (0.16 inch) of crack extension. At this point, the

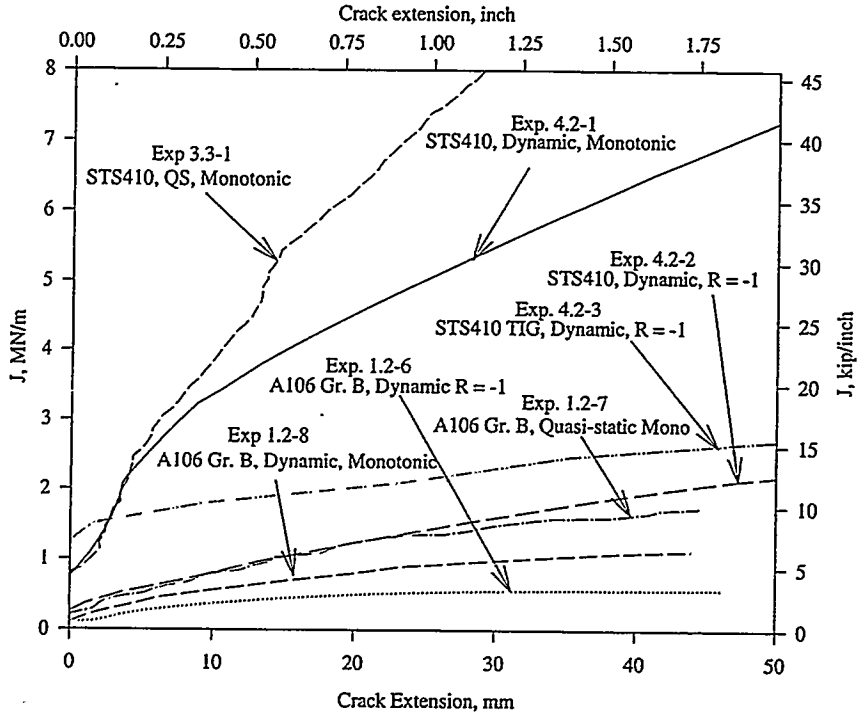

Figure 3.4 J-R curves for STS410 and A106 Grade B carbon steel TWC pipe experiments

quasi-static resistance became much higher than the dynamic resistance. A portion of this difference could be due to dynamic strain aging, but the major portion is probably due to differences in the crack extension angles. It is also of note that the value of J at crack initiation (J_i) for the pipe experiment with a crack in the weld (4.2-3) was quite a bit higher than the J_i values for the three base metal experiments. However, once the crack in the cyclic weld metal experiment (4.2-3) initiated, the J-R curve leveled off and tended to mirror the cyclic base metal experiment (4.2-2) J-R curve. This is not surprising in that once the crack in

* The computer code ETAFACTR was used in these analyses. This code was a refinement of an earlier version. The code refinement was done by Mr. Naoki Miura of CRIEPI while he was a visiting scientist at Battelle.

the weld metal experiment initiated, it turned out of the weld and grew in the base metal. This higher toughness for the weld metal, as well as the higher strength of the weld metal, when compared with the base metal, explains why the crack in the weld metal experiment would turn and grow out of the weld metal into the base metal. Also of note in Figure 3.4 is the fact that the J-R curves for the two dynamic, cyclic (R = -1) experiments (4.2-2 and 4.2-3) were both significantly below the J-R curves for the dynamic, monotonic, base-metal experiment (4.2-1). For this stress ratio (R = -1), this reduction in the J-R curve was expected. Comparing the J-R curves for Experiments 4.2-1 and 4.2-2 shows that at 30 mm (1.2 inches) of crack growth, the J value for the case when the pipe undergoes fully reversed loading is only 30 percent of the J value for the case of monotonic loading. Similarly, for the A106B material, the J value at the same amount of crack growth for the case when the pipe undergoes fully reversed loading is 50 percent of the J value for the case of monotonic loading. This suggests that the cyclic load history had a more significant effect on the crack growth portion of the STS410 experiments than the same history had on the A106 Grade B experiments.

Figure 3.5 shows the calculated J-R curve for Experiment 3.3-2, i.e., the intermediate stress ratio (R = -0.6) A106 Grade B experiment. Also included in this figure are the J-R curves for the monotonic

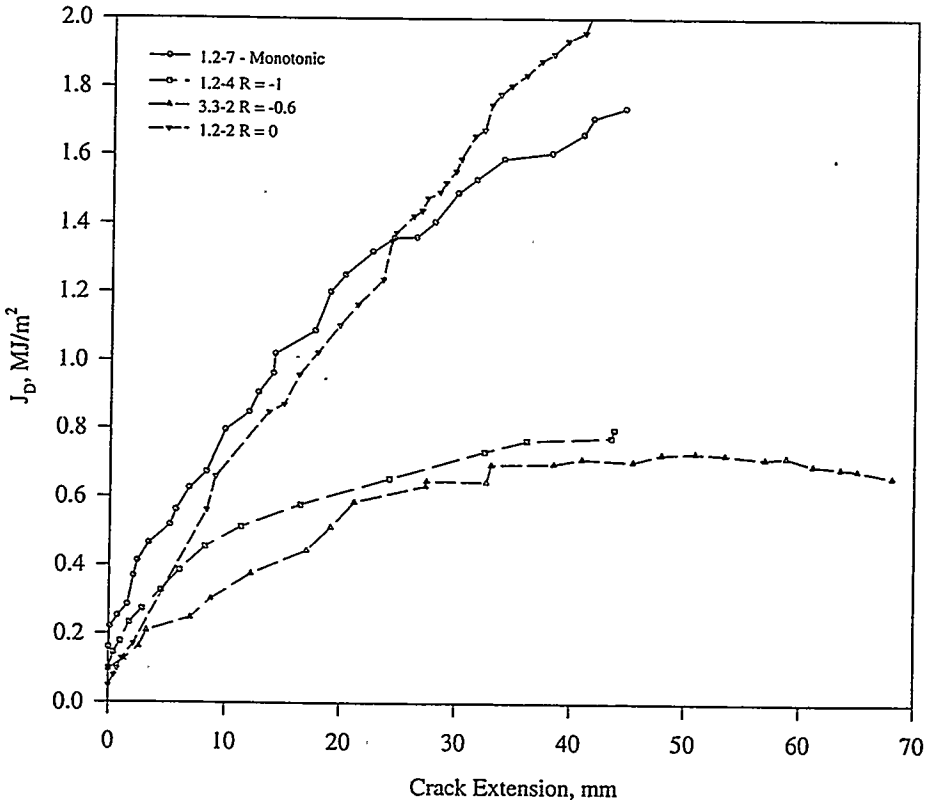

Figure 3.5 J-R curves for A106 Grade B carbon steel TWC pipe experiments

and cyclic (R = 0 and -1) A106B experiments from IPIRG-1. The J_i value calculated for Experiment 3.3-2 was almost identical to that calculated for the cyclic (R = -1) IPIRG-1 experiment. However, because of the differences in angled crack growth, the resistance for the R = -0.6 experiment appears to be slightly

lower than that for the R = -1 experiment. Both curves are significantly below the curve for the monotonic and R = 0 experiments.

3.3 16-Inch Nominal Diameter Pipe and Fitting Experiments

As part of the IPIRG-2 Program, twelve 16-inch diameter pipe experiments were conducted. Six of these experiments involved cracks in straight-pipe sections, two involved cracks in a girth weld at the junction of a straight-pipe section and a long-radius elbow, and four involved circumferential surface cracks along the extrados of a long radius elbow. Seven of the twelve 16-inch diameter experiments were dynamic pipe system experiments and five were quasi-static bend experiments. For comparison purposes, there are eight companion experiments conducted as part of the Degraded Piping (Ref. 3.8), IPIRG-1 (Ref. 3.9), and a Battelle/EPRI program (Ref. 3.10). Table 3.5 is a listing of the 16-inch diameter IPIRG-2 and companion experiments from the related programs.

3.3.1 Experimental Facilities

The quasi-static bend experiments were conducted using Battelle's large pipe bend facility at Battelle's West Jefferson, Ohio test site. For the straight pipe experiments, the test specimens were loaded in four-point bending, see Figure 3.6. For the quasi-static, elbow girth-weld experiment and the two quasi-static elbow experiments, the large pipe bend facility was modified to incorporate a curve test section, see Figure 3.7. For each quasi-static experiment, the applied loads were monotonically increasing displacements. In addition to the applied bending loads, the test specimens were typically pressurized to a pressurized water reactor (PWR) condition. The test specimens were loaded at a rate such that crack initiation typically occurred in 20 to 30 minutes.

The pipe system experiments were conducted in the IPIRG pipe loop experimental facility, see Figure 3.8. For use in IPIRG-2, the facility was essentially unchanged from IPIRG-1 except that two 190 liter (50 gallon) piston-type hydraulic accumulators were added to the servo-hydraulic system to accommodate the longer duration simulated seismic experiments and a restraint system was incorporated into the test specimen to control the pipe whip in the event of a double-ended guillotine break at the test flaw. Figure 3.9 is a schematic of the primary restraint system used for the IPIRG-2 straight pipe system experiments.

The IPIRG pipe loop facility is configured as an expansion loop with five long-radius elbows and approximately 30 meters (100 feet) of 16-inch diameter pipe. The 16-inch nominal diameter pipe size was selected early in the design process in IPIRG-1 because it permits assessment of a large range of possible failure modes. It was thought that higher toughness stainless steel test specimens would obtain fully plastic conditions representative of a limit-load type failure, while lower toughness carbon steel and weld test specimens would develop contained plasticity conditions representative of an elastic-plastic type failure. Testing lower toughness materials in 16-inch diameter pipe simulates conditions which may occur in larger diameter, higher toughness pipes typical of primary piping systems.

During the design process of the IPIRG-1 pipe loop facility, a number of design constraints had to be considered. For one, the test system had to be reusable. To minimize test costs, the test system had to be designed so that damage from each test was limited to a short distance around the crack location. It would have been cost prohibitive to replace major sections of the pipe loop after each experiment. To satisfy

Table 3.5 Listing of 16-inch diameter IPIRG-2 and companion experiments from related programs

Experiment No.	Program[1]	Material	Crack Geometry[2]	Crack Location	Loading History
EPRI 13S[3]	BCD/EPRI	TP304	SC	Pipe	QS, Mono.
1.3-3	IPIRG-1	TP304	SC	Pipe	Single Freq.
1-1	IPIRG-2	TP304	SC	Pipe	Sim. Seismic
4112-8[3]	DP^{3}II	A106B	SC	Pipe	QS, Mono.
1.3-2	IPIRG-1	A106B	SC	Pipe	Single Freq.
1-2	IPIRG-2	A106B	SC	Pipe	Sim. Seismic
4141-4	DP^{3}II	TP304 SAW	SC	Pipe	QS, Mono.
1.3-5	IPIRG-1	TP304 SAW	SC	Pipe	Single Freq.
1-6	IPIRG-2	TP304 SAW	SC	Pipe	QS, Mono.
1-5	IPIRG-2	TP304 SAW	SC	Pipe	Single Freq.
4141-8	DP^{3}II	A106B SAW	SC	Pipe	QS, Mono.
1.3-4	IPIRG-1	A106B SAW	SC	Pipe	Single Freq.
1-4	IPIRG-2	A106B SAW	SC	Elbow Girth Weld	QS, Mono.
1-3	IPIRG-2	A106B SAW	SC	Elbow Girth Weld	Single Freq.
2-2	IPIRG-2	A106B-90	SC	Elbow	QS, Mono.
2-1	IPIRG-2	A106B-90	SC	Elbow	Single Freq.
2-4	IPIRG-2	WP304L	SC	Elbow	QS, Mono.
2-3	IPIRG-2	WP304L	SC	Elbow	Single Freq.
1-8	IPIRG-2	A106B	TWC	Pipe	QS, Mono.
1-7	IPIRG-2	A106B	TWC	Pipe	Sim. Seismic

(1) BCD/EPRI (Ref. 3.10), DP^{3}II = Degraded Piping Program - Phase II (Ref. 3.8), IPIRG-1 (Ref. 3.9).
(2) SC = Surface crack; TWC = Through-wall crack.
(3) Unpressurized experiment, all other experiments pressurized to 15.5 MPa (2,250 psi) with the exception of 4141-4 which was pressurized to 11.0 MPa (1,600 psi).

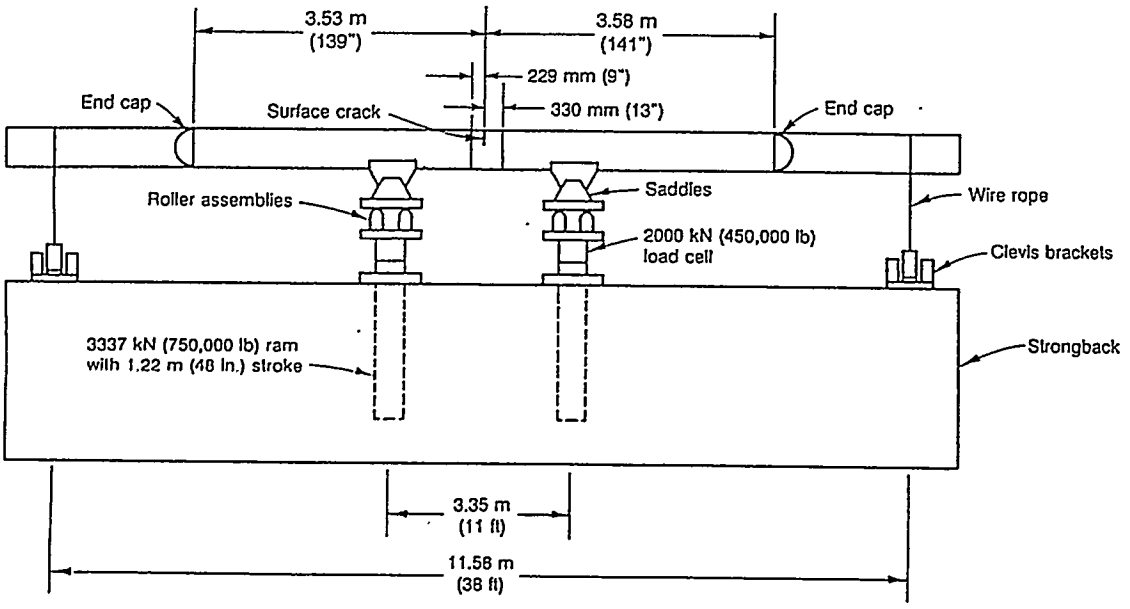

Figure 3.6 Quasi-static, monotonic pipe bend test fixture used for the 16-inch nominal diameter straight pipe experiments

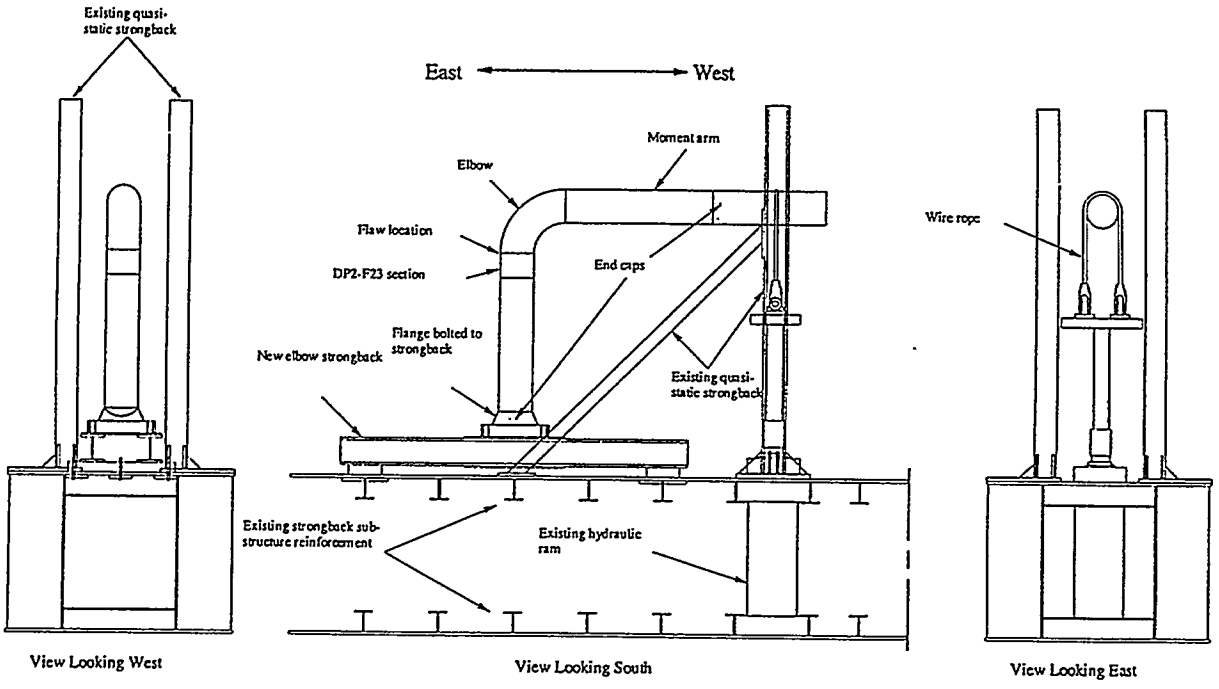

Figure 3.7 Quasi-static, monotonic, elbow test facility

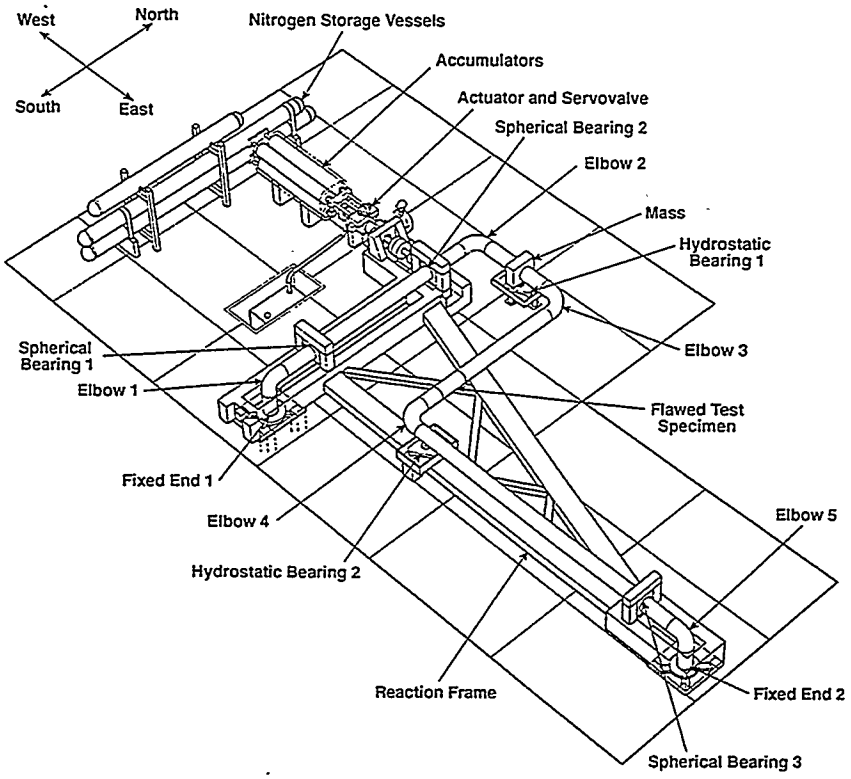

Figure 3.8 Artist's conception of the IPIRG pipe loop experimental facility

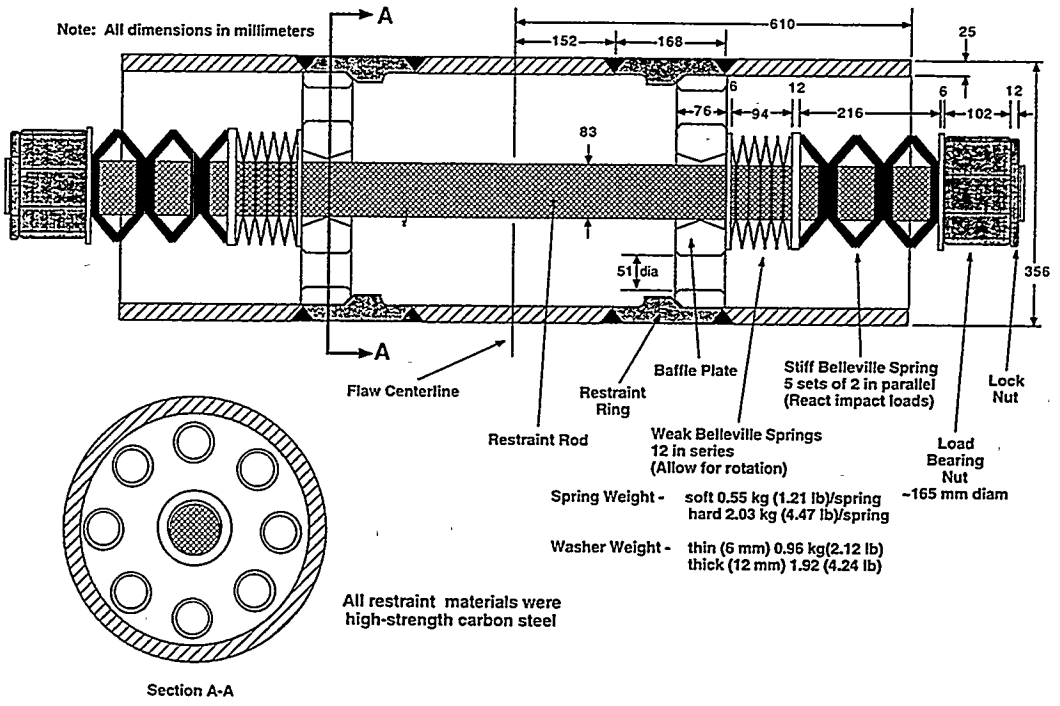

Figure 3.9 Schematic of primary restraint system used for the IPIRG-2 straight pipe-system experiments

this constraint, high strength pipe (ASTM A710 Grade A, Class 3) and elbow (WPHY65) materials were used in all of the loop but the test sections. While the use of these materials made it possible to limit plasticity to the cracked test section, their use removed an element of realism from the pipe loop design. A second constraint imposed was that the test system had to be amenable to mathematical modeling. Special care was taken to ensure that all aspects of the system, including the boundary conditions, could be simply described mathematically in a finite element analysis. In order to facilitate the mathematical description of the imposed boundary conditions, various specialized pieces of hardware, i.e., spherical bearings to represent the hangers and hydrostatic bearings to represent the vertical supports, were incorporated into the overall design. While this approach facilitated analyses of the experiments, it also had the effect of removing an element of realism from the pipe loop design. In addition, the satisfaction of these constraints, i.e., the use of high strength pipe and reduced friction boundary restraints, resulted in damping characteristics of the pipe loop being artificially low with respect to an actual plant piping systems.

Prior to the conduct of the first IPIRG-2 pipe system experiment, the performance and operation of the pipe loop facility were evaluated through a series of uncracked-pipe system experiments. The damping characteristics and first few natural frequencies of the pipe loop were measured. Table 3.6 shows a comparison of the experimentally measured damping values and first four natural frequencies for the

Table 3.6 Comparison of damping values and first four natural frequencies for the IPIRG-1 and IPIRG-2 pipe loop facilities

	Damping Value, percent	First Natural Frequency, Hz[1]	Second Natural Frequency, Hz[1]	Third Natural Frequency, Hz[1]	Fourth Natural Frequency, Hz[1]
IPIRG-1 Pipe Loop	0.50	4.43	7.5	13.35	19.5
IPIRG-2 Pipe Loop	0.45	4.5	8.5	14.2	19.2
ANSYS[2] Frequencies using nominal pipe wall thicknesses	NA	4.49	14.49	14.64	18.95
ANSYS[2] Frequencies using measured pipe wall thicknesses	NA	4.73	14.55	15.43	19.16

(1) Natural frequencies measured experimentally using actuator driven excitation with a bandwidth-limited random noise excitation signal at 15.5 MPa (2,250 psi) internal pipe pressure and 288 C (550 F) pipe temperature.
(2) From calculations conducted during IPIRG-2. These values are slightly different than the calculated values from IPIRG-1.

IPIRG-1 and IPIRG-2 test facilities. Also included in Table 3.6 are the calculated natural frequencies from ANSYS finite element analyses of the pipe loop. As can be seen in Table 3.6, the damping values and natural frequencies as measured in IPIRG-1 and IPIRG-2 are comparable.

7. A finite element model of the pipe system, including nonlinear representation of the cracks, was used to predict the response of the pipe system to the simulated seismic loading. The predicted response was the basis for Step 6.

Following these basic steps, a reasonably realistic seismic forcing function was developed. The forcing function included all of the essential elements of a true seismic event in a relatively simple fashion, without unnecessary complications. Further details of the design of this simulated seismic load history can be found in Reference 3.11.

Each of the simulated seismic experiments was conducted in two phases. For the first phase, the crack was loaded with a relatively low-level excitation representative of a safe shutdown earthquake (SSE). The amplitude of the SSE excitation was fixed using actual U.S. nuclear plant design stress values. It was expected that the SSE level of excitation would not cause the crack to extend and post-test examination of the data indicated that such was the case.

The second loading phase for the simulated seismic pipe system experiments involved application of a scaled-up amplitude version of the basic SSE excitation. To define the load level for this "Test" forcing function, nonlinear spring, cracked-pipe finite element analyses were used. In these analyses, the cracked section was modeled as a nonlinear moment-rotation spring. The amplitude of the forcing function was scaled to achieve predicted surface-crack penetration some time during the 20-second load history. The "Test" level excitation required to achieve surface-crack penetration for the carbon steel and stainless steel base metal experiments was 1.25 g for free field.

Figures 3.11 and 3.12 show the actuator displacement-time history for the "Normal plus SSE" and "Test" level excitations, respectively. The seismic functions lasted 20 seconds: 5 seconds of build up, 10 seconds of stationary signal, and 5 seconds of decay. Compared to the IPIRG-1 single-frequency forcing functions, the seismic functions are rich in frequency content and they show significant negative displacement excursions.

Figure 3.13 shows the response spectra for the simulated seismic load history. The damping values shown in this figure are representative of values for floor response spectra for nuclear power plants and are not equivalent to the damping associated with the IPIRG pipe loop. From Figure 3.13, it can be seen that the simulated seismic load history contains frequencies up to 40 Hz, with most of the large amplitude motions occurring in the 1 to 10 Hz range.

To assess whether the IPIRG-2 simulated seismic loading is representative of actual plant behavior, elastically-calculated stress data from some actual plant stress reports were compared with IPIRG crack location stresses. As can be seen in Figure 3.14, the stresses due to the SSE excitation agree very well with the calculated stresses from the actual plant piping systems. As should be expected, the calculated stresses due to the "Test" forcing function are quite a bit higher than the calculated stresses from the actual plant piping systems.

The key results (i.e., maximum moments) from the three simulated-seismic pipe-system experiments (1-1, 1-2, and 1-7) are shown in Table 3.7. Also included in Table 3.7 are the results from the companion quasi-static, monotonic four-point bend and companion single-frequency pipe system experiments from the related programs (Refs. 3.8, 3.9, and 3.10). For the stainless base metal experiments, the machined flaws were not fatigue precracked. For all other experiments, the flaws were fatigue precracked.

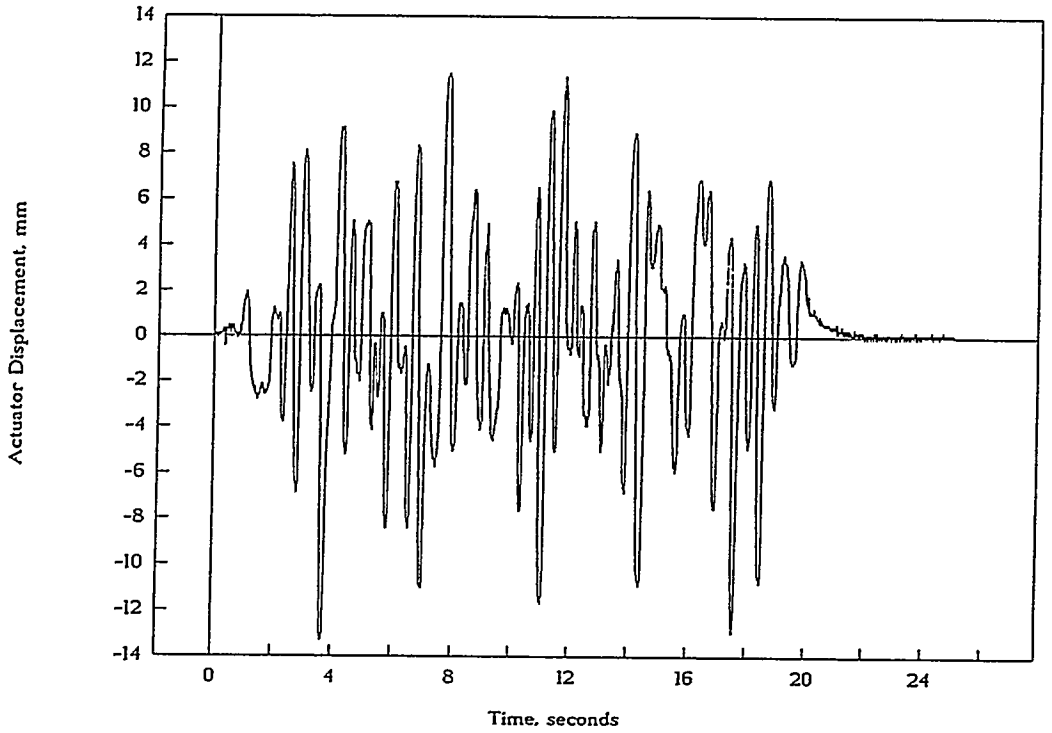

Figure 3.11 Actuator displacement-time history for the SSE forcing function

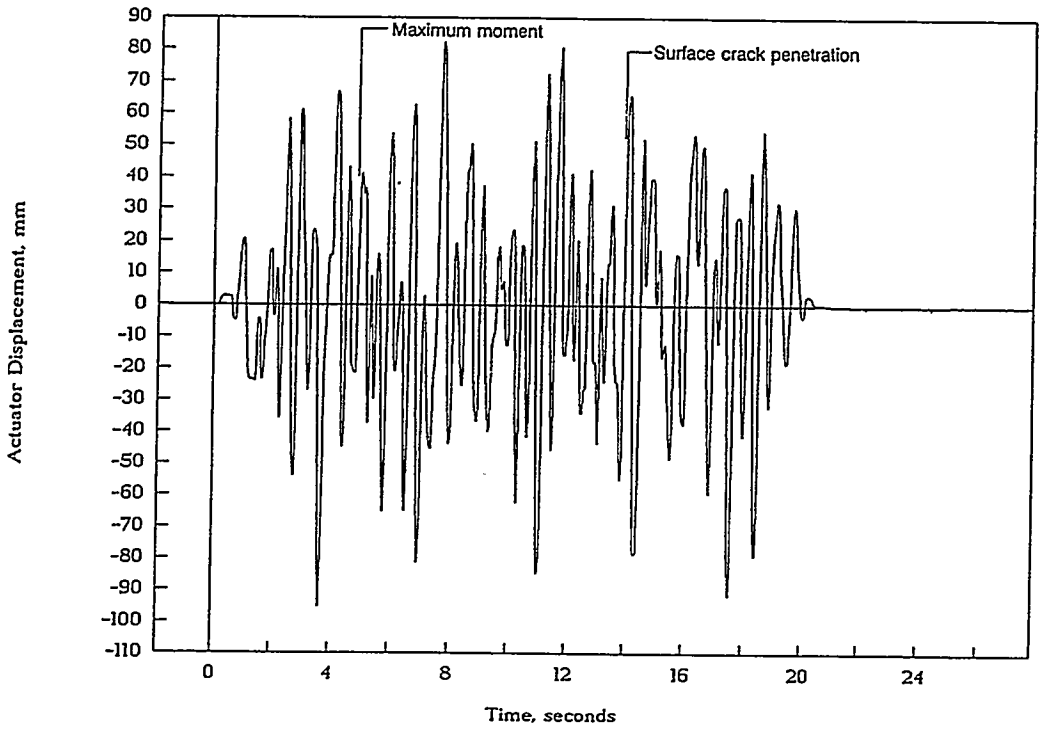

Figure 3.12 Actuator displacement-time history for the "Test" forcing function

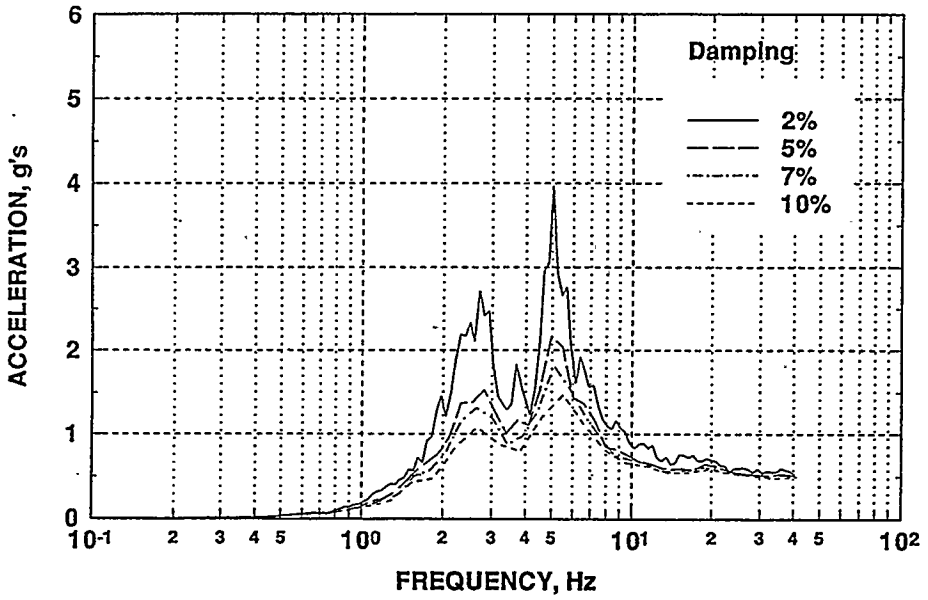

Figure 3.13 Response spectra of actuator motion for the simulated seismic load history

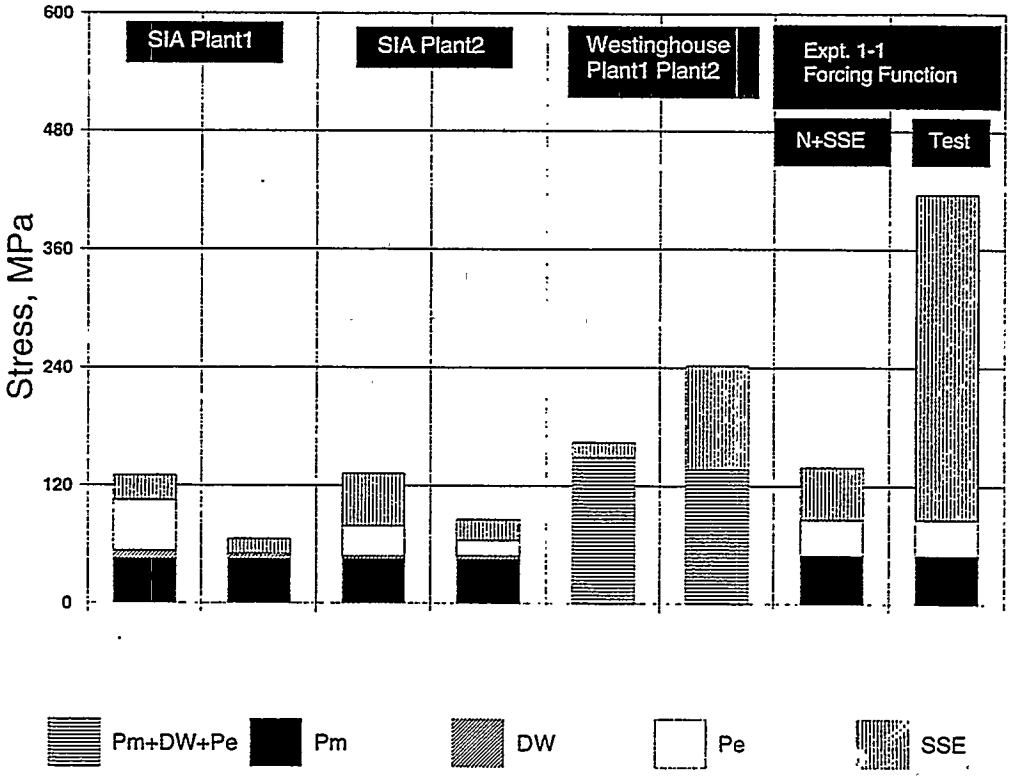

Figure 3.14 Comparison of the elastically-calculated stresses for actual plant piping systems to the crack section stresses for the IPIRG simulated seismic pipe-system experiments

Table 3.7 Key results from 16-inch diameter simulated seismic pipe-system experiments conducted as part of IPIRG-2 and companion experiments from IPIRG-2 and related programs (Refs. 3.8, 3.9, and 3.10)

Expt. No.	Pipe Material	Outside Pipe Diameter, mm (inch)	Wall Thickness, mm (inch)	Test Temperature, C (F)	Test Pressure, MPa (psi)	θ/π[1]	a/t	Maximum Moment, kN-m (in-kips)
1-1	TP304	417.1 (16.42)	25.5 (1.005)	288 (550)	15.5 (2,250)	0.527	0.628	597.7 (5,290)
EPRI 13S	TP304	413.5 (16.28)	28.3 (1.115)	22 (72)	0	0.58	0.66	1,260 (11,156)
1.3-3	TP304	415.8 (16.37)	26.2 (1.031)	288 (550)	15.5 (2,250)	0.552	0.66	425.9 (3,770)
1-2	A106B[2]	405.1 (15.95)	24.8 (0.977)	288 (550)	15.5 (2,250)	0.525	0.719	475.6 (4,210)
4112-8	A106B[2]	402.6 (15.85)	26.4 (1.04)	288 (550)	0	0.532	0.662	748.3 (6,623)
1.3-2	A106B[2]	403.9 (15.9)	25.7 (1.012)	288 (550)	15.5 (2,250)	0.525	0.727	341.2 (3,020)
1-7	A106B[3]	399.8 (15.74)	26.4 (1.039)	288 (550)	15.5 (2,250)	0.12	1.0	852 (7,540)
1-8	A106B[3]	399.3 (15.72)	26.2 (1.03)	288 (550)	15.5 (2,250)	0.12	1.0	1,038 (9,185)

(1) Based on total crack length.
(2) Pipe DP2-F29.
(3) Pipe DP2-F23.

Figures 3.15 through 3.17 compare the moment-rotation or moment-CMOD responses for the three simulated seismic pipe-system experiments with the applicable responses from the companion quasi-static, monotonic bend and single-frequency pipe-system experiments. Figure 3.15 is for the stainless steel base metal experiments, Figure 3.16 is for the carbon steel base metal experiments, and Figure 3.17 is for the short through-wall-cracked pipe experiments. (Note, for Figure 3.16, moment-CMOD response was shown instead of moment-rotation response because no valid rotation data exist for either of the carbon steel base metal pipe system experiments [1-1 and 1,3-2]).

As can be seen in Figure 3.15, the seismic load history for the stainless steel base metal experiment resulted in a cracked-section moment-rotation response which had significantly higher compressive moments than that for the single-frequency experiment. The effective stress ratio ($R_{effective}$) for this simulated-seismic experiment, accounting for the stress contribution due to the constant internal pipe pressure, was approximately -0.5, while for the single-frequency experiment, the effective stress ratio was

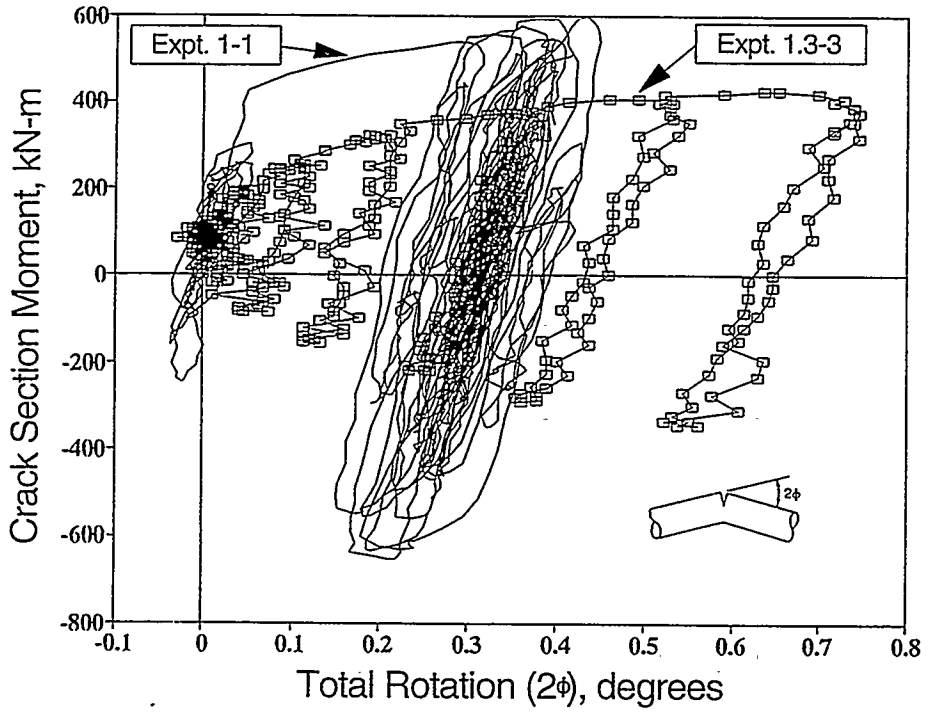

Figure 3.15 Comparison of the moment-rotation responses for the stainless steel, base-metal, simulated-seismic experiment (1-1) with the companion stainless steel, base-metal, single-frequency pipe-system experiment (1.3-3) from IPIRG-1 (Ref. 3.9)

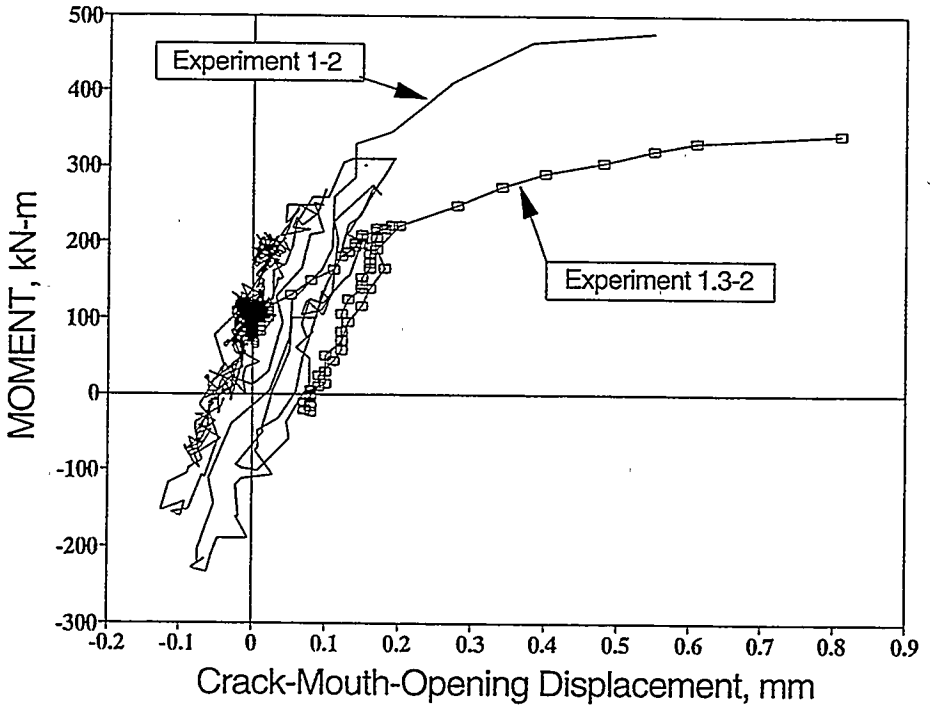

Figure 3.16 Comparison of the moment-CMOD responses for the carbon steel, base-metal, simulated-seismic experiment (1-2) and the companion carbon steel, base-metal, single-frequency, pipe-system experiment (1.3-2) from IPIRG-1 (Ref. 3.9)

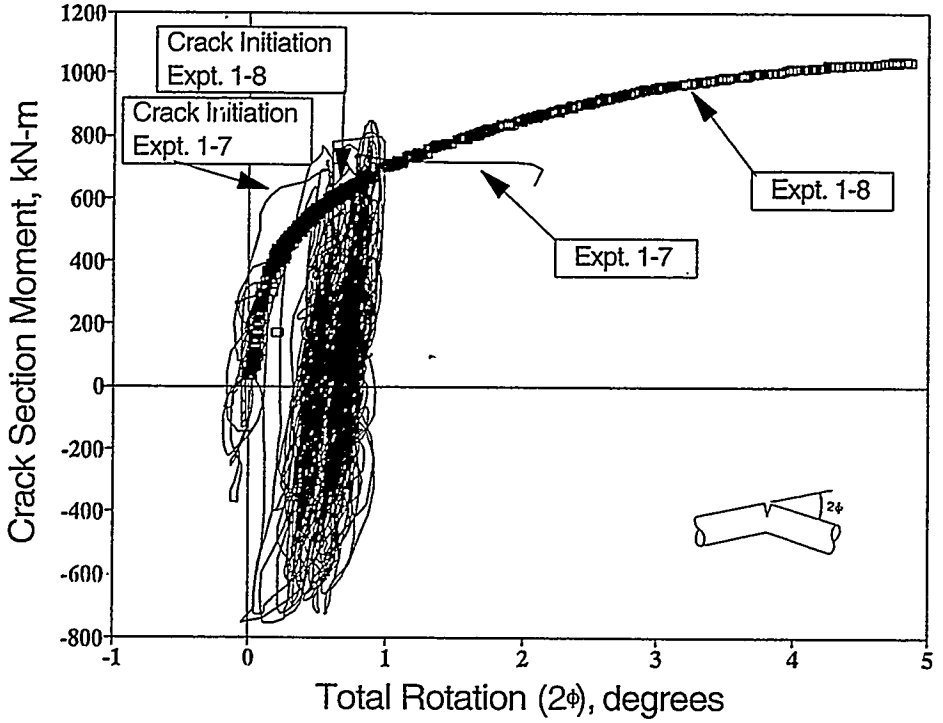

Figure 3.17 Comparison of the moment-rotation responses for the short-through-wall-cracked, simulated-seismic experiment (1-7) and the quasi-static, monotonic, four-point bend, short-through-wall-cracked pipe experiment (1-8)

approximately -0.2. Consequently, one might expect that the extent of cyclic damage for the simulated seismic experiment would be greater than that for the single-frequency pipe system experiment. However, closer examination of the moment-rotation responses for the two experiments indicates that the early load cycles prior to the first large amplitude cycle for the simulated seismic experiment were primarily elastic in nature. With the exception of one large amplitude cycle, there was little plasticity associated with any of these cycles. On the other hand, the relatively few cycles associated with the single-frequency experiment tended to exhibit a fair amount of plasticity. Thus, more cyclic plasticity damage was done in the single-frequency experiment than in the seismic experiment.

Figure 3.16 compares the moment-CMOD responses for the two carbon steel base metal pipe system experiments. Experiment 1-2 was a simulated-seismic experiment and Experiment 1.3-2 was a single-frequency experiment. Due to the relative severity (i.e., greater depth) of the crack in Experiment 1.3-2 when compared with Experiment 1-2, the crack in Experiment 1.3-2 broke through the pipe wall during the first cycle where plasticity occurred. Thus, it is difficult to make any statements about the effects of cyclic seismic loading on the flaw behavior for this carbon steel material, since this crack essentially failed under dynamic, monotonic loading. However, this test illustrated that the effective time to crack initiation could be as short as one quarter of the period of the first natural frequency, which is a guide for C(T) specimen testing times.

Figure 3.17 compares the moment-rotation responses for the short through-wall-cracked pipe system experiment (1-7) and the companion short through-wall-cracked quasi-static, monotonic four-point bend experiment (1-8). From Figure 3.17, it can be seen that the moment-rotation response for the quasi-static, monotonic, four-point bend experiment tends to follow the upper envelop of the moment-rotation response

for the pipe system experiment, at least up to the point of crack initiation. After crack initiation, the moment-rotation response for the quasi-static experiment (1-8) tends to lie above that for the pipe system experiment (1-7). This may be the result of the fact that the crack in Experiment 1-8 grew at a greater angle with respect to the circumferential plane than did the crack for Experiment 1-7. It has been shown previously (Ref. 3.3) that the greater the crack growth angle with respect to the circumferential plane, the higher the loads the cracked pipe can tolerate due to the fact that the effective remaining ligament is greater for the larger crack growth angle case. Alternatively, this discrepancy in the maximum loads for the two experiments may be an artifact of a problem with the experimental data for the quasi-static experiment after the point of crack initiation. Post-test examination of the patches used to seal the through-wall-cracked pipe experiments indicated that the patch in the quasi-static experiment appeared to have carried appreciable load, thus increasing the apparent load-carrying capacity of the flaw for this experiment. Caution is required, therefore, when evaluating maximum moments for Experiment 1-8.

3.3.3 Single-Frequency Pipe-System Experiments

Four single-frequency pipe-system experiments were conducted as part of IPIRG-2, a stainless steel weld short surface-cracked straight pipe-system experiment, an elbow-girth weld pipe-system experiment, and two cracked elbow pipe-system experiments. The single-frequency excitation used in each of these experiments was nominally the same. It was also nominally the same excitation used in the three stainless steel pipe system experiments from the IPIRG-1 program (Ref. 3.9). Figure 3.18 is a plot of the actuator displacement-time history used for the single-frequency excitation.

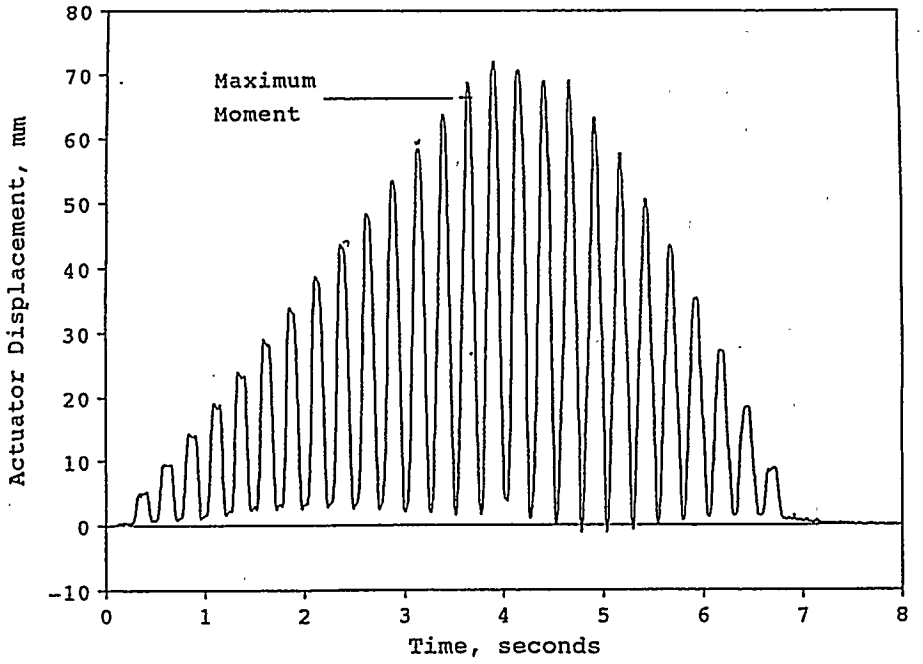

Figure 3.18 Actuator displacement versus time history for single-frequency pipe-system experiments

3.3.3.1 Straight Pipe and Elbow Girth Weld Experiments

The key results from the straight pipe and elbow girth weld single-frequency pipe system experiments, along with the key results from the companion experiments are shown in Table 3.8. The companion experiments for the stainless steel weld short surface-cracked pipe system experiment include two long surface-cracked pipe experiments from the Degraded Piping (Ref. 3.8) and IPIRG-1 (Ref. 3.9) programs as well as the companion, quasi-static, monotonic short surface-cracked pipe experiment conducted as part of this program. The companion experiments for the elbow girth weld pipe system experiment include two straight-pipe girth weld experiments, as well as the companion, quasi-static, monotonic, elbow girth weld experiment from this program. Flaws for all of the experiments were fatigue precracked.

Table 3.8 Key results from 16-inch diameter single-frequency pipe-system experiments conducted as part of IPIRG-2 and companion experiments from IPIRG-2 and related programs (Refs. 3.8, 3.9, and 3.10)

Expt. No.	Crack Location	Outside Pipe Diameter, mm (inch)	Wall[1] Thickness, mm (inch)	Test Temp., C (F)	Test Pressure, MPa (psi)	θ/π[2]	a/t[3]	Maximum Moment, kN-m (in-kips)
1-3	A106B SAW	406.7 (16.01)[4]	38.4 (1.511)	288 (550)	15.5 (2,250)	0.50	0.709	814.9 (7,213)
1-4	A106B SAW	406.9 (16.02)[4]	39.2 (1.543)	288 (550)	15.5 (2,250)	0.50	0.639	797.5 (7,059)
4141-8	A106B SAW	403.1 (15.87)	25.4 (0.999)[5]	288 (550)	15.5 (2,250)	0.50	0.67[5]	594.3 (5,260)
1.3-4	A106B SAW	402.6 (15.85)	29.1 (1.145)	288 (550)	15.5 (2,250)	0.535	0.678	618.0 (5,470)
1-5	TP304 SAW	415.3 (16.35)	28.1 (1.108)	288 (550)	15.5 (2,250)	0.267	0.442	776.2 (6,870)
1-6	TP304 SAW	412.8 (16.25)	28.4 (1.12)	288 (550)	15.5 (2,250)	0.27	0.620	697.0 (6,169)
4141-4	TP304 SAW	413.5 (16.28)	28.5 (1.124)	288 (550)	11.0 (1,600)	0.50	0.613	501.5 (4,439)
1.3-5	TP304 SAW	416.1 (16.38)	26.8 (1.055)	288 (550)	15.5 (2,250)	0.532	0.601	492.6 (4,360)

(1) Including weld crown height.
(2) Based on total crack length.
(3) Crack depth with respect to inside surface of pipe wall and thickness includes the height of the weld crown.
(4) Using pipe dimensions instead of elbow dimensions for elbow girth weld experiments.
(5) Thickness of pipe only since weld crown height was not documented.

Figures 3.19 and 3.20 show the moment-rotation response for the two single-frequency, stainless steel weld, straight-pipe and single-frequency, elbow girth weld, pipe-system experiments, respectively, as well as the moment-rotation response from the applicable companion experiments. Although direct

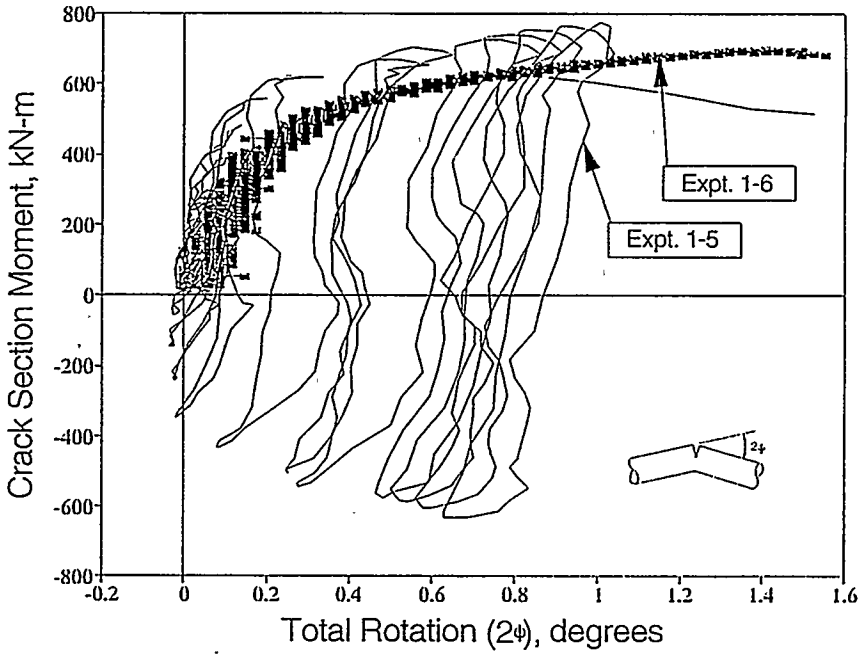

(a) Experiments 1-5 and 1-6

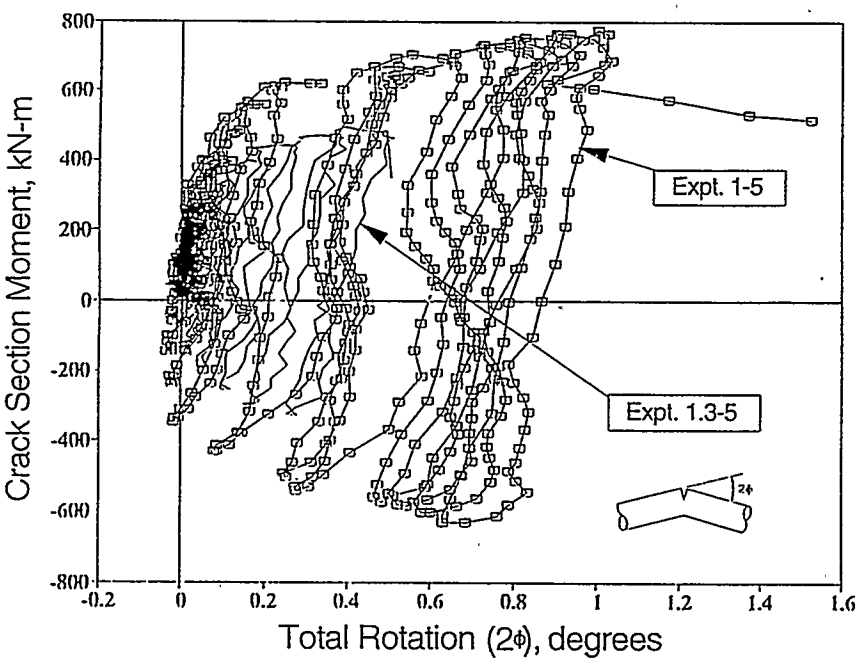

(b) Experiments 1-5 and 1.3-5

Figure 3.19 Comparison of the moment-rotation responses for the short-surface crack, stainless steel weld, single-frequency, pipe-system experiment conducted as part of IPIRG-2 (1-5) and the companion short surface crack, stainless steel weld, quasi-static, monotonic, pressure and four-point bend experiment from IPIRG-2 (1-6) and the companion long surface-crack, stainless steel weld, single-frequency, pipe-system experiment (1.3-5) from IPIRG-1 (Ref. 3.9)

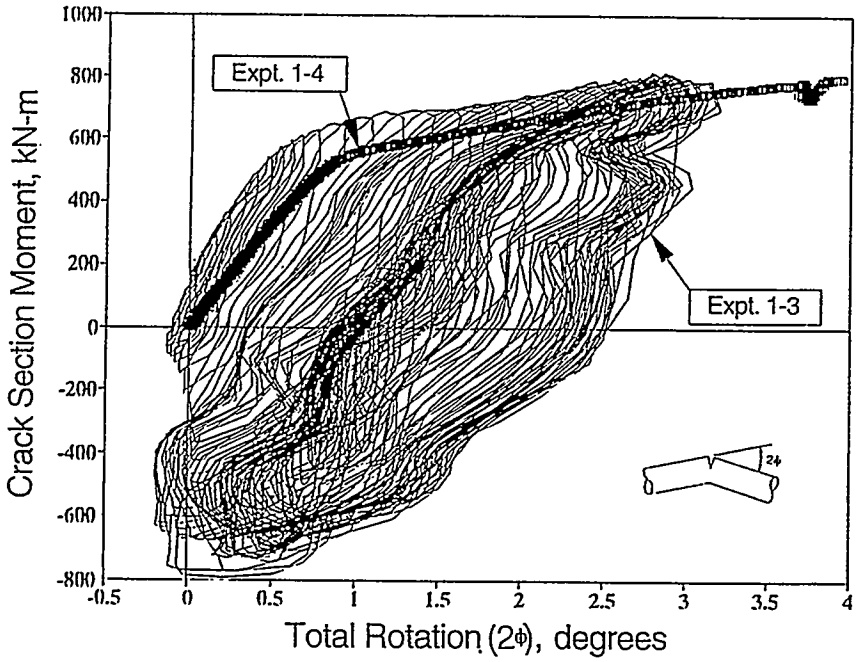

Figure 3.20 Comparison of the moment-rotation responses for the carbon steel, elbow girth weld single-frequency, pipe-system experiment conducted as part of IPIRG-2 (1-3) and the companion carbon steel elbow, girth weld, quasi-static, monotonic, pressure and bend experiment (1-4) from IPIRG-2

comparisons are limited by differences in actual crack sizes, some important general trends can be identified.

First, comparing the two curves in Figure 3.19a, it is clear that the tensile moment results from the short-surface-crack, stainless steel weld, pipe-system experiment (1-5), generally are consistent with the tensile moment results for the quasi-static, monotonic, short-surface-crack, stainless steel weld experiment (1-6).

Second, comparing moment-rotation responses for the long and short surface-cracked stainless steel weld pipe system experiments, Figure 3.19b, there are unexpected differences in the compressive-loading responses. Using the same nominal forcing function, one would expect a difference in response on the tension side, especially as the crack approaches maximum moment, due to crack size. On the compressive side, however, one would expect the response to be independent of crack size. In fact, however, the short surface crack negative moments are inexplicably larger than the moments for any of the other IPIRG single-frequency pipe system experiments, see Figure 3.21. Numerous attempts to model the anomalous behavior of Experiment 1-5 were unsuccessful, although there is a suspicion that the difference was caused by the DEGB restraint system.

Finally, in examining Figure 3.20, one can see that the moment-rotation response for the quasi-static bend elbow girth weld experiment (1-4) tends to follow the upper envelope of the moment-rotation response for the single-frequency pipe system elbow girth weld experiment (1-3), in spite of the very large number of cycles applied in Experiment 1-3.

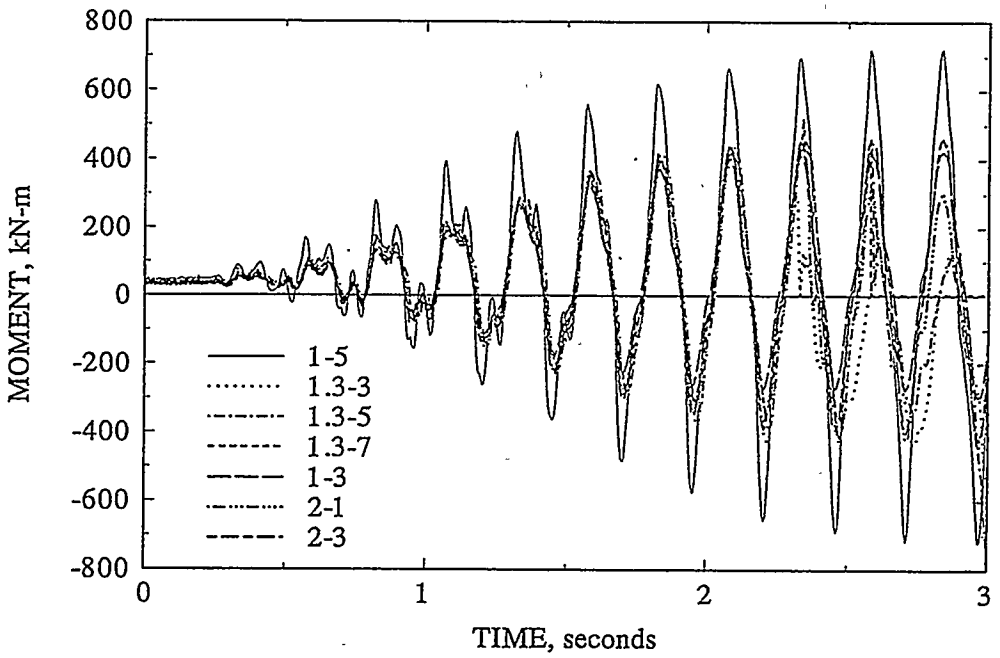

Figure 3.21 Moment-time response of the seven, single-frequency, pipe-system experiments from IPIRG-1 (Ref. 3.9) and IPIRG-2 which used the same single-frequency forcing function

3.3.3.2 Cracked Elbow Experiments

Table 3.9 shows the key results from the two cracked elbow single-frequency pipe system experiments, along with the key results from the two companion quasi-static, monotonic cracked elbow experiments. All four elbow experiments were performed on nominal 16-inch diameter long-radius 90-degree Schedule 100 seamless elbows. The circumferentially-oriented 180-degree internal surface cracks were located along the center of the elbow extrados. All elbows were tested in the "as received" condition (no machining of the outside or inside wall surface was performed to obtain a uniform wall thickness). Furthermore, the mechanically-induced notches were fatigue pre-cracked prior to testing.

A major difference between performing the elbow experiments compared to a similar straight-pipe experiment is that the location of maximum J is not at the crack centerline (i.e., at the midpoint of the elbow "extrados"), but at locations approximately ±45 degrees from the crack centerline. Therefore, considering local variations in the material behavior and in wall thickness, the exact region of crack initiation, or surface crack penetration is more difficult to determine.

Figure 3.22 shows the moment versus crack-mouth-opening displacement response for the carbon steel, single-frequency, pipe-system experiment and the companion quasi-static, monotonic, cracked-elbow experiment. The crack-mouth-opening displacement measurements were made using the transducer located 45-degrees from the flaw centerline (extrados) on the side where crack initiation and surface-crack penetration is believed to have first occurred. Crack-mouth-opening displacements are directly related to

Table 3.9 Key results from 16-inch nominal diameter, long-radius elbow, single-frequency, pipe-system and quasi-static, monotonic, pressure and bend companion experiments conducted as part of IPIRG-2

Expt. No.	Crack Location Material	Outside Diameter[1], mm (inch)	Wall Thickness[2], mm (inch)	Test Temperature, C (F)	Test Pressure, MPa (psi)	θ/π[3]	a/t[4]	Maximum Moment, kN-m (in-kips)
2-1	A106-90	409 (16.1)	32.1 (1.26)	288 (550)	15.5 (2,250)	0.49	0.84	579.8 (5,132)
2-2	A106-90	406 (16.0)	32.0 (1.26)	288 (550)	15.5 (2,250)	0.50	0.80	607.9 (5,380)
2-3	WP304L	409 (16.1)	33.2 (1.31)	288 (550)	15.5 (2,250)	0.50	0.73	728.5 (6,448)
2-4	WP304L	406 (16.0)	33.0 (1.30)	288 (550)	15.5 (2,250)	0.50	0.77	548.0 (4,850)

(1) Average of measurements taken from intrados-to-extrados and flank-to-flank.
(2) Average wall thickness measured at crack plane.
(3) Based on total crack length.
(4) Maximum crack depth with respect to local wall thickness.

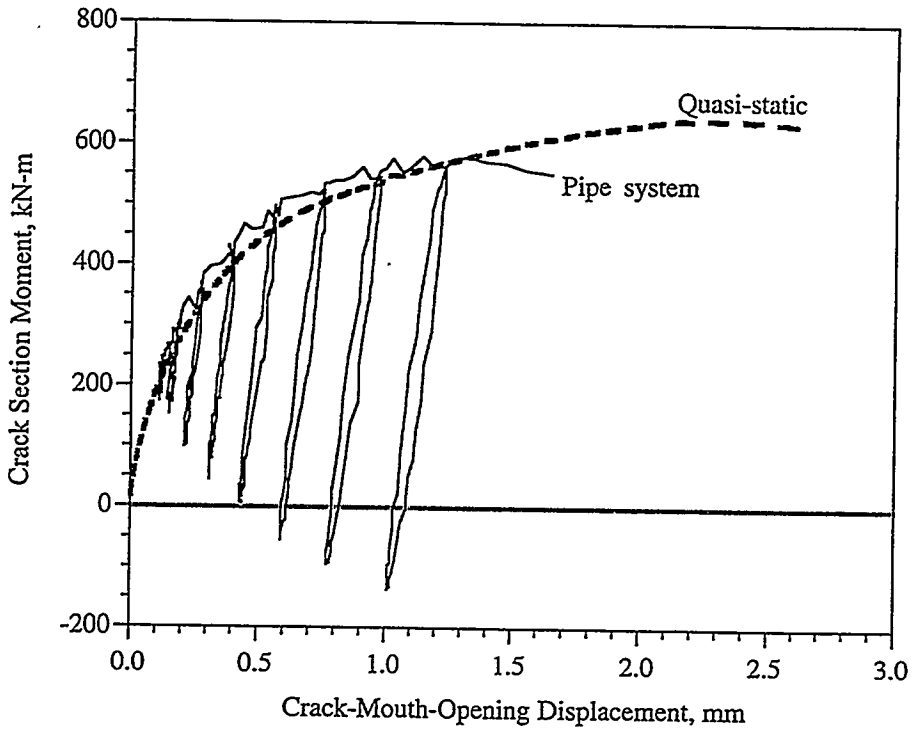

Figure 3.22 Moment versus crack-mouth-opening displacement for carbon steel elbow experiments

the global measurement of pipe rotation, but provide a measure of local crack response. Global measurements of the elbow response could be affected by wall thickness variations and ovalization of the elbow. Figure 3.23 shows similar data for the stainless steel elbow experiments. Note that the flaw depth (a/t) varied somewhat from experiment to experiment, and no adjustments of the data shown here has been performed here to account for this variability. Adjustments for crack depth will be accounted for when comparisons of this experimental data with straight pipe and elbow analysis predictions are made in Section 4.0.

The carbon steel elbows show similar response when comparing the quasi-static and pipe-system experiments. This is consistent with the toughness data developed for this elbow material under quasi-static and dynamic loading rates. However, for the stainless steel elbows, a substantial increase in crack-mouth-opening displacement at surface-crack penetration occurs for the pipe system experiment. This may be attributed to an increase in material toughness that occurs at dynamic loading rates.

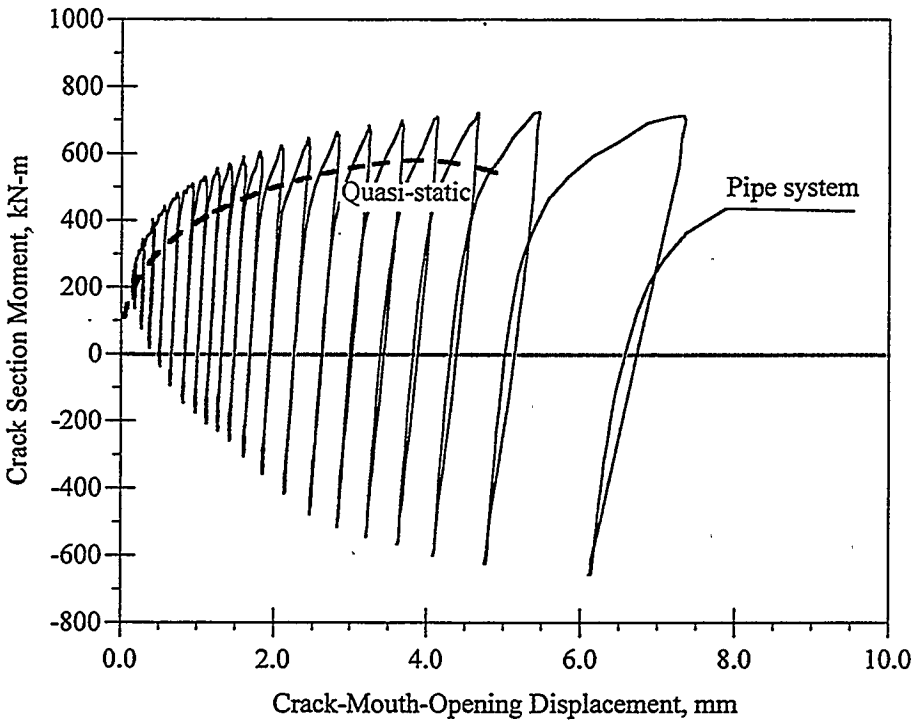

Figure 3.23 Moment versus crack-mouth-opening displacement for stainless steel elbow experiments

3.4 References

3.1 Scott, P., Kramer, G., Vieth, P., Francini, R., and Wilkowski, G., "The Effect of Dynamic and Cyclic Loading During Ductile Tearing on Circumferentially Cracked Pipe: Experimental Results," ASME PVP-Vol. 280, *Fatigue, Flaw Evaluation and Leak-Before-Break Assessments*, pp 207-220, June 1994.

3.2 Rudland, D. L., Scott, P. M., and Wilkowski, G. M., "The Effect of Cyclic and Dynamic Loads on Carbon Steel Pipe," NUREG/CR-6438, February 1996.

3.3 Mohan, R., Marschall, C., Krishnaswamy, P., Brust, F., Ghadiali, N., and Wilkowski, G., "Effects of Toughness Anisotropy and Combined Loading on Fracture Behavior of Ferritic Nuclear Pipe," NUREG/CR-6299, April 1995.

3.4 Marschall, C. W., Landow, M., and Wilkowski, G. M., "Loading Rate Effects on Strength and Fracture Toughness of Pipe Steels Used in Task 1 of the IPIRG Program," NUREG/CR-6098, October 1993.

3.5 Zahoor, A. and Kanninen, M. F., "A Plastic Fracture Mechanics Prediction for Fracture Instability in a Circumferentially Cracked Pipe in Bending - Part I. J-Integral Analysis," *Journal of Pressure Vessel Technology*, Vol. 103, pp 352-358, 1981.

3.6 Pan, J., Ahmad, J. A., Kanninen, M. F., and Popelar, C. H., "Applications of a Tearing Instability Analysis for Strain Hardening Materials to a Circumferentially Cracked Pipe in Bending," ASTM STP 833, pp 721-748, 1984.

3.7 Wilkowski, G., Kramer, G., Vieth, P., Francini, R., and Scott, P., "The Effect of Dynamic and Cyclic Loading During Ductile Tearing on Circumferentially Cracked Pipe: Analytical Results," ASME PVP-Vol 280, *Fatigue, Flaw Evaluation and Leak-Before-Break Assessments*, pp 221-239, June 1994.

3.8 Wilkowski, G. M., and others, "Degraded Piping Program - Phase II, Summary of Technical Results and Their Significance to Leak-Before-Break and In-Service Flaw Acceptance Criteria, March 1984 - January 1989," by Battelle Columbus Division, NUREG/CR-4082, Vol. 8, March 1989.

3.9 Scott, P., and others, "The IPIRG-1 Pipe System Fracture Tests: Experimental Results," ASME PVP Vol. 280, pp 135-151, June 1994.

3.10 Kanninen, M. F., and others, "Instability Predictions for Circumferentially Cracked Type 304 Stainless Steel Pipes Under Dynamic Loadings," Final Report on EPRI Project T118-2, by Battelle Columbus Laboratories, EPRI Report Number NP-2347, April 1982.

3.11 Olson, R., Scott, P., and Wilkowski, G., "Design of the IPIRG-2 Simulated Seismic Forcing Function," NUREG/CR-6439, February 1996.

4.0 ANALYSIS OF EXPERIMENTS

4.1 Fracture Analysis Prediction Methodologies

In this section of the report, the maximum experimental stresses from the IPIRG-2 pipe experiments, as well as the companion pipe experiments from the Degraded Piping (Ref. 4.1), IPIRG-1 (Refs. 4.2 and 4.3), and Battelle/EPRI (Ref. 4.4) programs, will be compared with analytical predictions from various fracture prediction analyses. The fracture analyses methods considered include:

Simple limit-load analyses such as the Net-Section-Collapse (NSC) analysis (Ref. 4.5),

Dimensionless-Plastic-Zone-Parameter (DPZP) analysis (Ref. 4.6),

Various J-estimation scheme analyses such as GE/EPRI (Ref. 4.7), LBB.NRC (Ref. 4.8), and LBB.ENG2 (Ref. 4.9) for through-wall-cracked pipe and SC.TNP1 (Ref. 4.10), SC.TNP2 (Ref. 4.11), SC.ENG1 (Ref. 4.11), and SC.ENG2 (Ref. 4.11) for surface-cracked pipe,

The ASME Section XI Appendix C approach for austenitic piping (Refs. 4.12 and 4.13), the ASME Section XI Appendix H approach for ferritic piping (Refs. 4.14 and 4.15) and the ASME Code Case N-494-3 approach (Refs. 4.16 and 4.17) for austenitic and ferritic piping, and

The R6 Revision 3 Option 1 method (Refs. 4.18 and 4.19).

Prior to comparing the experimental stresses at maximum load with the predictions, some of the key input parameters, i.e., flaw size definition and material property data, needed for these analyses are discussed. The various fracture prediction analysis methods are also discussed. Further details of each of the analysis methods can be found in the appropriate references.

4.1.1 "Intuitively Consistent" Flaw Size Definition

As part of this program, an "intuitively consistent" definition of flaw size for a circumferential surface-cracked pipe was defined as a crack with a length equal to the total crack length and a constant depth equal to the maximum crack depth, but reducing the experimentally applied bending stress by the cosine of the angle between the maximum crack depth location and the crack centerline location if the crack is not symmetric, i.e., the deepest part of the crack is off-centered*. Furthermore, if the experiment under consideration is an experiment for which the crack is in the center of a weld, then the wall thickness will be taken to be the wall thickness of the pipe plus the weld crown height (t_3 in Figure 4.1) and the surface-crack depth was the depth of the crack with respect to the inside surface of the pipe wall (a_1 in Figure 4.1). By using this "intuitively consistent" definition of flaw size in the subsequent fracture analyses, one will be

* For further details regarding the analyses which formed the basis for this finding, the reader is referred to the IPIRG-2, Task 1 Final Report, NUREG/CR-6389.

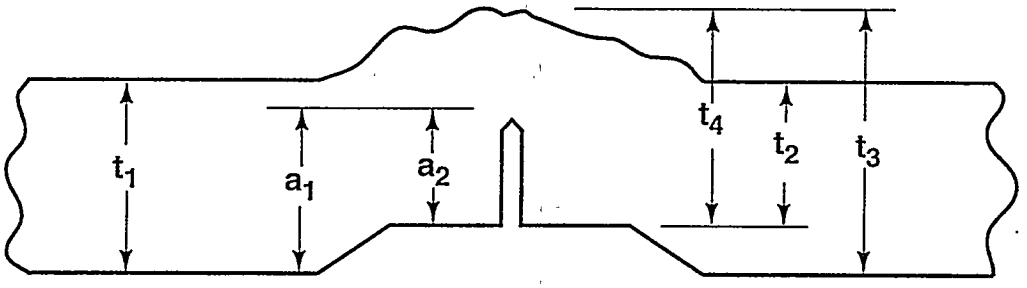

Figure 4.1 Nomenclature for weld crack geometry

able to make a more consistent comparison of fracture ratios (experimental/predicted loads) between experiments in order to better answer such questions as "What effect does seismic loading have on the fracture behavior, and what is the effect of long versus short crack lengths?"

The exception to this choice of crack size definition is the crack size definition used in the ASME analyses. When making predictions using the ASME analysis methods, the flaw size was assumed to be a constant depth flaw with the length being equal to the maximum crack length and the depth being equal to the maximum crack depth for the entire length of the crack. For cracks in welds, the wall thickness was taken to be the actual wall thickness of the pipe, excluding the weld crown, and minus any material removed by counterboring, t_2 in Figure 4.1. This definition appears to conform best with the specifications of Paragraph NB-3641.1 of Section III of the ASME Code. Following the spirit of this wall thickness definition, the crack depth definition was assumed to be the crack depth with respect to the surface of the counterbore, a_2 in Figure 4.1. For the through-wall-cracked experiments, the flaw size definition was the total crack length.

Two other aspects relative to flaw geometry definitions are noteworthy. First, some of the experiments analyzed in this report came from the Degraded Piping Program and the IPIRG-1 Program. In these programs, the flaw size definitions differed slightly, i.e., the flaw size did not include the weld crown, the maximum crack depth was used, typically the maximum flaw length was used, and the counterbore may or may not have been included in the thickness or crack depth measurements. These flaw size definitions affect the fracture predictions, hence there could be differences in the fracture predictions between these various reports.

The second point deals with the weld crown height. In all of the welded pipe fracture experiments, the weld crown was left intact and the flaw was machined in the center of the weld from the inside surface. In real plant piping, the weld crown may be removed by grinding for UT inspection. Hence, the accuracy of surface-flaw evaluation of girth welds in service depends on whether the weld crown height should be included in the analysis. This problem is discussed in Section 7 of this report.

4.1.2 Material Property Data Used in the Fracture Analyses

A question addressed in a number of tasks in the IPIRG-2 program was what is the most appropriate material property data to use in a pipe fracture analysis? It was shown that using quasi-static tensile and quasi-static J-R curve data in the analyses of the quasi-statically loaded pipe experiments and quasi-static tensile data and dynamic J-R curve data in the analyses of the dynamic experiments resulted in the most consistent predictions of the maximum experimental stresses when compared with the analyses of the pipe fracture experiments from Reference 4.11*. In addition, it was shown that cyclic J-R curve data are oftentimes needed to properly analyze some of the larger diameter cyclically loaded pipe experiments. In addition, there appears to be a threshold effective stress ratio value above which the effects of cyclic loading are negligible, and hence the cyclic J-R curve is approximately equal to the monotonic J-R curve. This threshold value of $R_{effective}$ appears to be material dependent. Further discussion, based on the results from Task 3 of this program, as to what is the most appropriate material property data to use in a pipe fracture analyses, is provided in Section 4.1.4 of this report.

4.1.2.1 Tensile Data

For the limit-load (i.e., Net-Section-Collapse) or modified limit-load (i.e., Dimensionless-Plastic-Zone-Parameter) analyses, the tensile property required is the flow stress of the material. The flow stress for these analyses has been defined as the average of the yield and ultimate strengths at the test temperature under consideration.

For the ASME Section XI Code approaches, i.e., IWB-3640 and Appendix C for austenitic steels and IWB-3650 and Appendix H for ferritic steels, the flow stress has been defined as $3S_m$ and $2.4S_m$, respectively, per Section XI procedures. The ASME Code Design Stress Intensity (S_m) has been defined to be either the S_m values from Table 2A of Part D of Section II of the 1995 Edition of the ASME Code, i.e., S_m(Code), or in the spirit of the Code using the criteria specified in Article 2110 of Appendix III of Section III Division 1 of the 1989 Edition of the ASME Code, i.e., S_m(Actual). The S_m(Code) definition provides a direct comparison of the experiments to the ASME Code procedures. The S_m(Actual) definition was used to evaluate the technical basis of the Code flaw evaluation procedures and is an attempt to analyze the pipe experiments as if the pipes used had the minimum properties defined in Section II of the ASME Code. In this manner, it was possible to account for the fact that the pipes tested in this program frequently had higher strength values than the Code specified values. The term S_m(Actual) was calculated using the actual quasi-static tensile properties of the pipes tested adhering to the spirit of Article 2110 of Appendix III of Section III Division 1 of the 1989 Edition of the Code, as the lowest of:

* For further details regarding the analyses which formed the basis for this finding, the reader is referred to the IPIRG-2 Task 1 and Task 3 Final Reports, NUREG/CR-6389 and NUREG/CR-6440, respectively.

(1) One-third of the actual room temperature ultimate tensile strength (for both ferritic and austenitic pipes)

(2) One-third of the actual ultimate tensile strength at the pipe test temperature (for both ferritic and austenitic pipes)

(3) Two-thirds of the actual yield strength at room temperature (for both ferritic and austenitic pipes)

(4) Two-thirds of the actual yield strength at the pipe test temperature (for ferritic pipes), or 90 percent of the actual yield strength at the pipe test temperature (for austenitic pipes).

For the J-estimation schemes considered, i.e., SC.TNP1, SC.TNP2, SC.ENG1, and SC.ENG2, for the surface-cracked pipe experiments, and GE/EPRI, LBB.NRC, and LBB.ENG2, for the through-wall-cracked pipe experiments, the material stress-strain curve was needed for the analyses. This stress-strain behavior was modeled using a Ramberg-Osgood relationship, see Equation 4-1.

$$(\epsilon/\epsilon_o) = \sigma/\sigma_o + \alpha(\sigma/\sigma_o)^n \qquad (4\text{-}1)$$

where,

σ = stress
σ_o = reference stress, i.e., the yield strength (σ_y) for the analyses conducted as part of this effort
ϵ = strain
ϵ_o = reference strain (σ_y/E)
α = Ramberg-Osgood parameter
n = strain-hardening exponent
E = elastic modulus

The Ramberg-Osgood equation was fit to the engineering stress-strain curve data in the range of 0.1 percent strain to the strain corresponding to 80 percent of the ultimate strength. The fit of the stress-strain data to the Ramberg-Osgood equation was made using a Battelle-written computer program, ROFIT. Table 4.1 shows the tensile properties of the pipe materials used in the IPIRG-2 and companion experiments conducted as part of related programs (Refs. 4.1, 4.2, 4.3, and 4.4).

4.1.2.2 J-R Curve Data

The J-R curves used in these analyses were based on both the deformation theory (J_D) and modified J (J_M) J-resistance curves. If not specified, the J_D-R curves were used. For the surface-cracked pipe experiments, differences in predictions between using J_M-R and J_D-R curves are insignificant due to the fact that there is only a small amount of crack growth prior to maximum load.

Table 4.1 Tensile properties of pipe materials used in IPIRG-2 and companion pipe experiments

Material Ident.	Material Grade	Applicable Pipe Experiments	Quasi-static Data					Tensile Spec. No.	Dynamic Data					Tensile Spec. No.	S_m (Code), MPa	S_m (Actual), MPa
			σ_y, MPa	σ_u, MPa	ϵ_o[1]	α	n		σ_y, MPa	σ_u, MPa	ϵ_o[1]	α	n			
DP2-A8	TP304	1-1, 1.3-3, 1-5, 1-6, 4141-4, 1.3-5	171	456	0.000936	5.34	4.17	A8-40	200	429	0.00102	6.98	5.04	A8-103	117	152
DP2-A8[2]	TP304	EPRI 13S	295	743	0.00162	3.93	5.07	A8-35	ND[3]	ND	ND	ND	ND	NA[4]	138	197
DP2-F29	A106B	1-2, 4112-8, 1.3-2, 4141-8, 1.3-4	241	618	0.00127	2.19	3.39	F29-5	234	443	0.00123	5.98	4.06	F29-102	125	160
IP2-FE17	A106B	1-3, 1-4, 2-1, 2-2	215	446	0.001114	3.92	3.70	FE17T2	249	387	0.00127	5.00	6.24	FE17-HT3	125	143
IP2-AE1	WP304L	2-3, 2-4	200	408	0.00102	14.79	3.98	AE1-T3	ND	ND	ND	ND	ND	NA	99.3	136
DP2-F23	A106B	1-3, 1-4, 1-7, 1-8	223	514	0.001154	2.37	4.03	F23-3t	ND	ND	ND	ND	ND	NA	125	148
DP2-F22	A106B	1-9	259	588	0.00136	2.76	3.56	F22t1	328	526	0.00173	12.1	3.41	F22B	125	173
DP2-F30	A106B	3.3-2, 1.2-2, 1.2-4, 1.2-7, 1.2-8	294	599	0.00152	1.97	5.37	F30-104	250	562	0.001319	2.02	4.25	F30-101	125	196
									356	479	0.001878	2.23	11.2	F30-107	125	196
DP2-A23	TP304	1.2-5	139	400	0.00076	11.2	3.56	A23-105	NA	NA	NA	NA	NA	NA	117	125
IPF13	STS410	4.2-1, 4.2-2, 4.2-3, 3.3-1	216	493	0.001138	3.20	3.72	IPF13-T1	180	413	0.000949	5.93	3.79	IPF13-T4	NA	144
									224	423	0.001181	1.95	7.28	IPF13-T6		

(1) $\epsilon_o = \sigma_o/E$, where $\sigma_o = \sigma_y$.
(2) Room temperature data; all other data shown for 288 C (550 F) tensile tests.
(3) ND = not determined.
(4) NA = not applicable.

The J-R curves typically used were for monotonically loaded L-C oriented C(T) specimens. However, where available, cyclic J-R curves were also used in selected analyses. Table 4.2 presents the extrapolated J-R curve constants for the test specimen materials. Included in Table 4.2, are the applicable constants, i.e., C_3 and m, from Equation 4-2 for each material and loading condition. Where available, Table 4.2 also includes the applicable constants for the cyclic J-R curves. In addition, Table 4.2 includes the specimen numbers on which the extrapolated J-R curve constants are based.

$$J = J_i + C_3(\Delta a/r)^m \qquad (4\text{-}2)$$

where r has a value of 1.0 in the same units as Δa, so that C_3 has the same units as J.

4.1.3 Description of Fracture Prediction Analysis Methods

The predictive circumferentially cracked-pipe fracture analyses to which the experimental data were compared include:

- the Net-Section-Collapse analysis (Ref. 4.5),
- the Dimensionless-Plastic-Zone-Parameter (DPZP) analysis (Ref. 4.6), and
- various J-estimation scheme methods such as the GE/EPRI (Ref. 4.7), LBB.NRC (Ref. 4.8), and LBB.ENG2 (Ref. 4.9) for through-wall-cracked pipe and SC.TNP1 (Ref. 4.10), SC.TNP2 (Ref. 4.11), SC.ENG1 (Ref. 4.11), and SC.ENG2 (Ref. 4.11) for surface-cracked pipe.

Note, the various failure avoidance criteria, i.e., the ASME Section XI and R6 approaches, will be discussed in Section 4.1.4.

4.1.3.1 Net-Section-Collapse Analysis

The original Net-Section-Collapse (NSC) analysis method was included in this comparative analysis because it is the analysis method which forms the basis for the circumferential flaw evaluation procedures in Section XI of the ASME Code, i.e., IWB-3640 and Appendix C for austenitic piping and IWB-3650 and Appendix H for ferritic piping. (Note, Kurihara [Ref. 4.20] empirically modified the basic approach to account for perceived inaccuracies in the original NSC method for very deep cracks. Comparisons between the Kurihara modified version of the Net-Section-Collapse analysis and the experimental data are not included herein. However, the Kurihara modified Net-Section-Collapse equations are used in the SC.ENG2 method whereas the original Net-Section-Collapse equation are used in the SC.ENG1 method.) The original NSC analysis is a simple limit-load analysis and as such assumes maximum moment/stress occurs when the pipe section containing the crack becomes fully plastic, and that there is insignificant crack growth from crack initiation to maximum load. This occurs when the toughness of the material is sufficiently high, and hence the failure is governed by the strength of the material (i.e., the flow stress or collapse stress). The flow stress is a hypothetical term that is approximated as a value between the yield and ultimate strengths of the material so the analysis can be simplified for a perfectly plastic material, see Figure 4.2. This assumption that the net-section stress reaches a fully-plastic condition is satisfied for smaller diameter pipes with reasonable toughness values and larger diameter pipes made from high

Table 4.2 Extrapolated J_D-R curve constants[1] for the pipe materials used in the IPIRG-2 and companion pipe experiments

Material Ident.	Material Grade	Applicable Pipe Experiments	Stress Ratio (R)	δ_{cr}/δ_i	Quasi-static Data[1]			Spec No.	Dynamic Data[1]			Spec. No.
					J_i, kJ/m²	C_J, kJ/m²	m		J_i, kJ/m²	C_J, kJ/m²	m	
Monotonic Data												
DP2-A8I	TP304	1-1	1.0	N/A	854	452	0.769	A8-12a	1,302	510	0.739	A8-9a
DP2-A8II	TP304	1.3-3	1.0	N/A	546	300	0.615	A8II-17	815	336	0.612	A8II-20
DP2-A8 [2]	TP304	EPRI 13S	1.0	N/A	2,277	1,292	0.502	(2)	ND[3]	ND	ND	NA[4]
DP2-F29	A106B	1-2, 4112-8, 1.3-2	1.0	N/A	149	92.6	0.470	F29-18	68.3	67.1	0.622	F29-9
DP2-F29W	SAW	4141-8, 1.3-4	1.0	N/A	82.0	78.9	0.630	F29W-12	118	123	0.618	F29W-9
DP2-F55W	SAW	1-3, 1-4	1.0	N/A	65.4	53.3	0.554	F55W-2	913	132	0.484	F55W-3
DP2-A8W	SAW	1-5, 1-6, 4141-4, 1.3-5	1.0	N/A	55	153	0.576	A8W-110	140	209	0.704	A8W-107
DP2-F23	A106B	1-7, 1-8	1.0	N/A	74.3	120	0.698	F23-1	94.9	124	0.604	F23-3
DP2-F22	A106B	1-9	1.0	N/A	77.1	120	0.566	F22-3	43.6	67.5	0.359	F22-2
IP2-FE17	A106B	2-1, 2-2, 1-3, 1-4	1.0	N/A	533	298	0.624	FE17-3	373	314	0.676	FE17-1
IP2-AE1	WP304L	2-3, 2-4	1.0	N/A	106.2	211	0.487	AE1-5	1377	217	0.510	AE1-2
IP-F13	STS410	4.2-1, 4.2-2, 4.2-3, 3.3-1	1.0	N/A	389	276	0.631	IPF13-1	507	225	0.675	IPF13-5
Cyclic Data												
DP2-A8	TP304	1-1	-0.3	0.1	952	571	0.462	A8-13	1.297	395	0.76	A8I-22
DP2-A8	TP304	1-1	-1.0	0.1	356	283	0.432	A8-14	ND	ND	ND	ND
DP2-A8II	TP304	1.3-3	-0.3	0.1	652	261	0.643	A8II-21	395	154	0.721	A8II-15
DP2-A8II	TP304	1.3-3	-1.0	0.1	313	140	0.708	A8II-18	ND	ND	ND	ND
DP2-A8W	SAW	1-5, 1-6	-0.6	0.1	46.4	72.3	0.750	A8W-103c	60.2	88.8	0.641	A8W-108c
DP2-A8W	SAW	4141-4, 1.3.5	-1.0	0.1	39.3	38.0	0.614	A8W-101c	33.6	78.5	0.675	A8W-107c
DP2-F40W	SAW	4141-8, 1.3-4,	-0.6	0.1	47.3	32.6	0.694	F40W-7	33.4	71.2	0.501	F40W-13c
DP2-F40W	SAW	1-3, 1-4	-1.0	0.1	30.1	44.4	0.384	F40W-5	38.6	59.6	0.402	F40W-10c
DP2-A23	TP304	N/A	1	N/A	1124	145	0.652	A23-2c	ND	ND	ND	ND
DP2-A23	TP304		0	0.1	1150	98.8	0.455	A23-4c	ND	ND	ND	ND
DP2-A23	TP304		0	0.1	862	400	0.287	A23-21c	ND	ND	ND	ND
DP2-A23	TP304		0	0.2	1014	353	0.258	A23-6c	ND	ND	ND	ND
DP2-A23	TP304		0	0.025	1405	296	0.689	A23-11c	ND	ND	ND	ND
DP2-A23	TP304		0	0.025	938	208	0.613	A23-22c	ND	ND	ND	ND
DP2-A23	TP304		-1	0.1	455	176	0.379	A23-5c	ND	ND	ND	ND
DP2-A23	TP304		-1	0.1	254	145	0.644	A23-20c	ND	ND	ND	ND
DP2-A23	TP304		-1	0.2	344	96.1	0.789	A23-7c	ND	ND	ND	ND
DP2-F30	A106B	N/A	-1	0.025	158	150	0.990	A23-12c	ND	ND	ND	ND
DP2-F30	A106B		1	N/A	98.3	124	0.510	F30-1c	ND	ND	ND	ND
DP2-F30	A106B		0	0.1	94.2	97.7	0.701	F30-2c	ND	ND	ND	ND
DP2-F30	A106B		0	0.1	75.5	25.7	0.666	F30-6c	ND	ND	ND	ND
DP2-F30	A106B		-1	0.1	63.2	37.1	0.512	F30-3c	ND	ND	ND	ND
DP2-F30	A106B		-1	0.1	106	112	0.654	F30-7c	ND	ND	ND	ND

(1) $J = J_i + C_J (\Delta a/r)^m$, where r = 1.0 in same units as Δa.
(2) Average fit for Specimens A8a-1, A8a-2, and A8a-3.
(3) ND = not determined.
(4) N/A = not applicable.

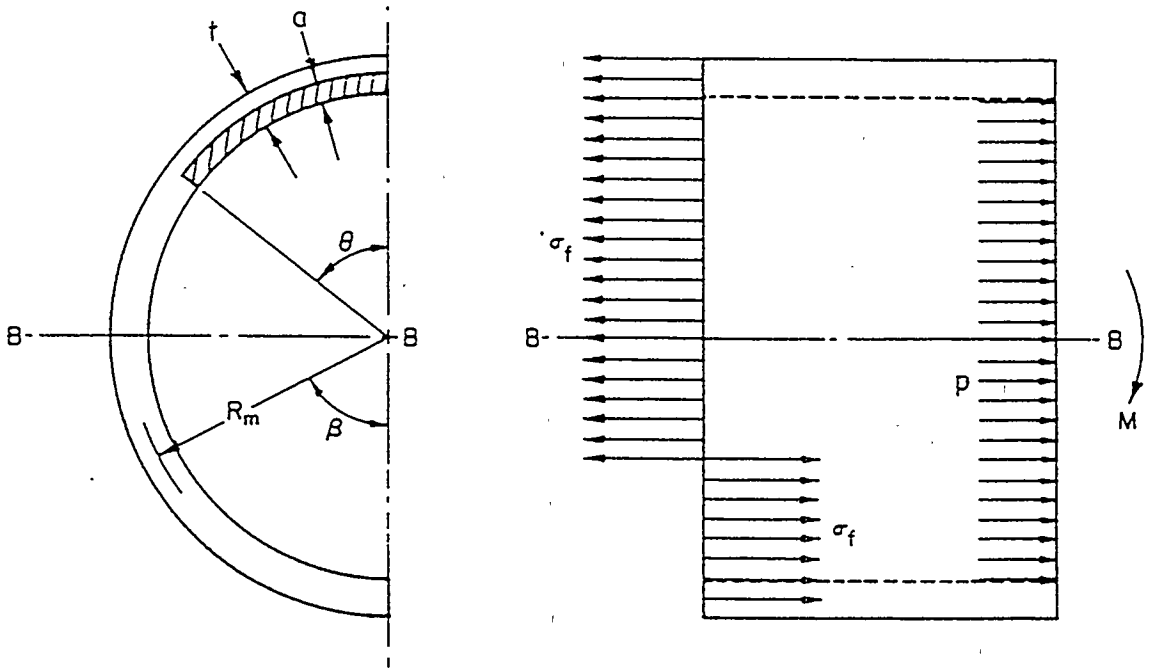

Figure 4.2 Nomenclature and assumed stress distribution for the Net-Section-Collapse analysis

toughness materials, i.e., stainless steel. However, for lower toughness ferritic pipes, especially larger diameter ferritic pipes, the assumption of fully-plastic conditions is not necessarily satisfied. For these larger diameter, lower toughness pipes, contained plasticity conditions often exist, and the resultant failure stresses are typically below those predicted by the Net-Section-Collapse analysis.

4.1.3.2 Dimensionless-Plastic-Zone-Parameter Analysis

As part of the Degraded Piping program (Ref. 4.1), a semi-empirical limit-load screening analysis method was developed which allows one to make an assessment of whether or not the assumptions embodied in the Net-Section-Collapse analysis, i.e., fully-plastic conditions, are satisfied. This analysis was then extended as part of Reference 4.6 such that the failure stresses for these contained plasticity experiments could be predicted. As part of this analysis method, the ratio of the predicted failure stress-to-the Net-Section-Collapse predicted failure stress was found to be a function of a dimensionless-plastic-zone-size parameter. This dimensionless-plastic-zone-size parameter is the ratio of the plastic-zone size to the remaining tensile ligament of the cracked pipe, i.e., the distance from the crack centerline for surface-cracked pipe or the crack tip for through-wall-cracked pipe to the neutral bending axis, see Figure 4.3. This dimensionless-plastic-zone-size parameter is proportional to the toughness of the material and inversely proportional to the pipe diameter and flow stress of the material. Equation 4-3 is a simplification of this dimensionless plastic-zone parameter, where the crack length effects were eliminated.

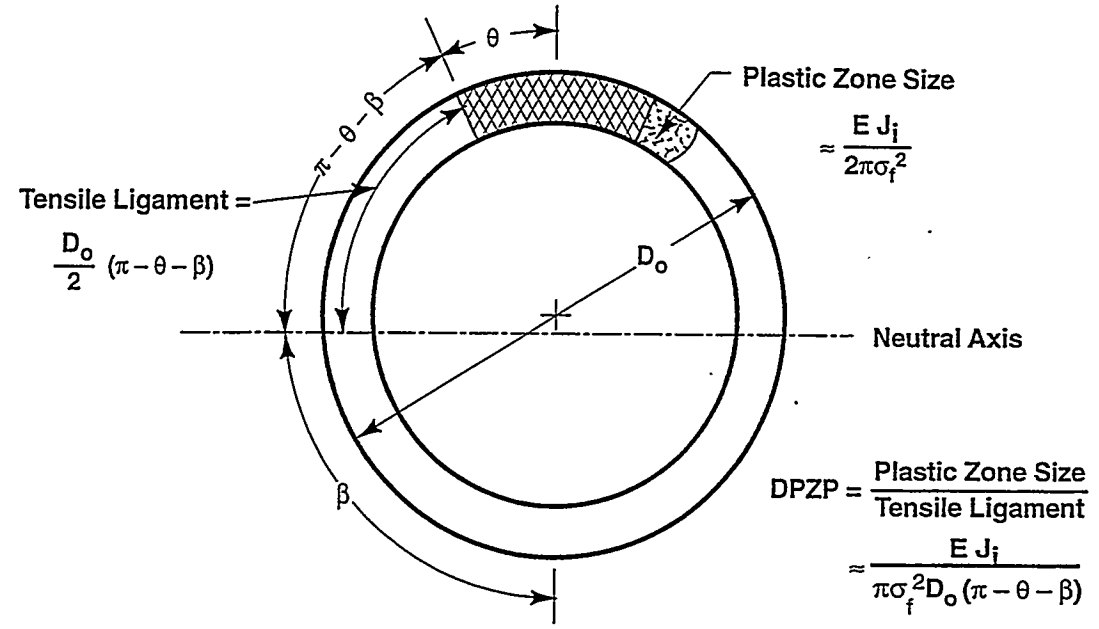

(a) Through-Wall Crack

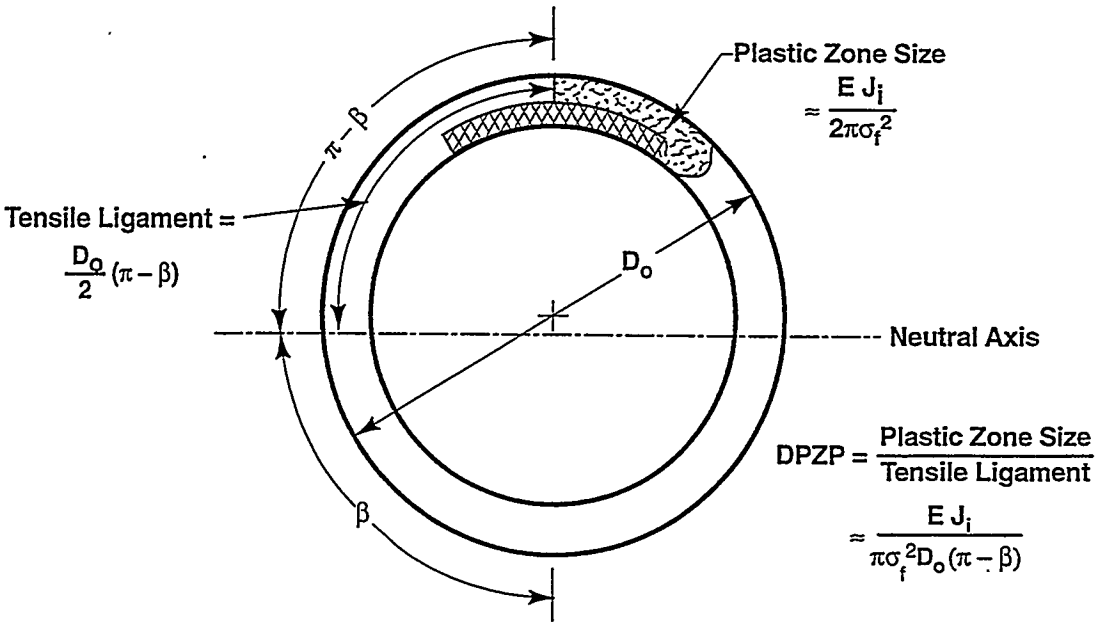

(b) Surface Crack

Figure 4.3 Nomenclature and key parameter definitions for Dimensionless-Plastic-Zone-Parameter analysis

$$DPZP = 2EJ_i/(\pi^2 D_m \sigma_f^2) \quad (4\text{-}3)$$

where

DPZP = Simplified dimensionless-plastic-zone-parameter
E = Elastic modulus
J_i = Value of J at crack initiation from a C(T) specimen test
D_m = Mean pipe diameter
σ_f = Flow stress, average of the yield and ultimate strengths

As part of References 4.6 and 4.11, "best-fit" curves were made from the experimental data relating the ratio of the experimental failure stress-to-the Net-Section-Collapse stress and the simplified Dimensionless-Plastic-Zone-Parameter (DPZP), see Figure 4.4. Separate curve fits were made for surface-cracked and through-wall-cracked pipe experiments, see Equation 4-4.

$$P/P_{NSC} = \frac{2}{\pi} \text{Arccos}(e^{-C_1[DPZP]}) \quad (4\text{-}4)$$

where

P = DPZP predicted failure stress
P_{NSC} = Net-Section-Collapse failure stress
C_1 = Empirically derived constant

For surface-cracked pipe, the "best-fit" empirically derived constant (C_1) was found to be 34. For through-wall-cracked pipe, the "best-fit" empirically derived constant, was found to be 18.3*, see Figure 4.4. These new C_1 values tend to increase the DPZP predicted maximum stresses in the EPFM range.

* The "best-fit" curve for the through-wall-cracked pipe data were recently updated based on the data in the CIRCUMCK pipe fracture database (Ref. 4.21). The previously published curve fit constant "C_1" for the through-wall-cracked pipe data was 4.6 and for surface-cracked pipe, the constant was 21.8. The updated curve fits will be published in the 1996 ASME PVP proceedings.

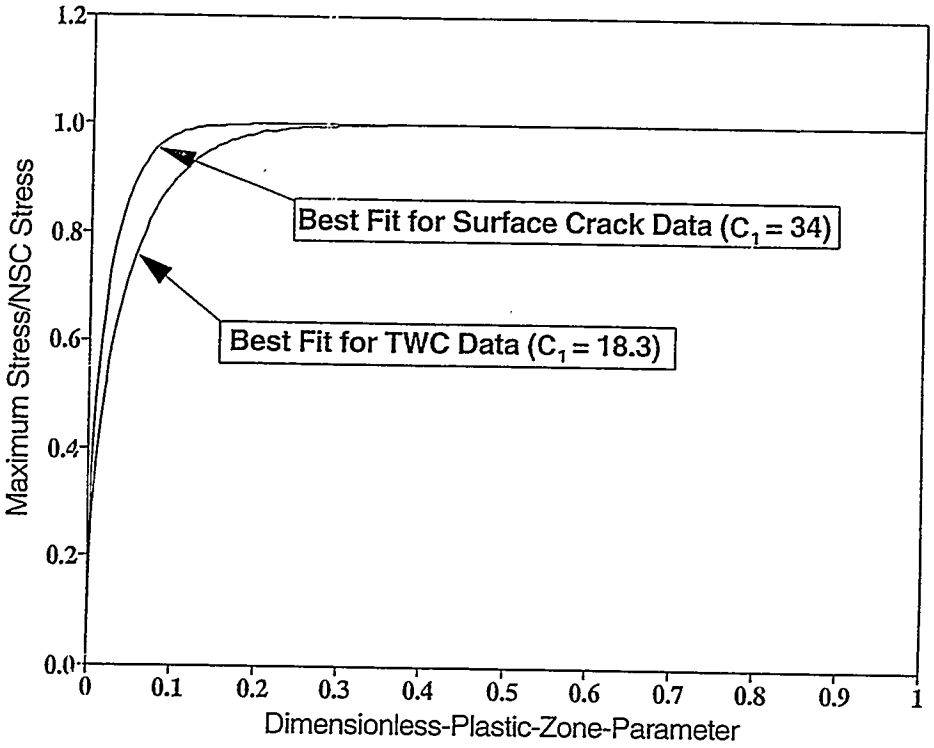

Figure 4.4 Ratio of experimental failure stress to Net-Section-Collapse predicted failure stress as a function of the Dimensionless-Plastic-Zone-Parameter (DPZP)

Knowing the value of J at crack initiation (J_i) from a C(T) specimen test and the flow stress of the material, the dimensionless-plastic-zone-parameter (DPZP) can be calculated. Knowing the pipe and flaw dimensions and the flow stress, the Net-Section-Collapse stress can be calculated. Knowing these quantities, the DPZP predicted stress can be calculated using Equation 4-4. This method was found to be very accurate for predicting the maximum experimental stresses, especially for surface-cracked pipe (Ref. 4.11).

4.1.3.3 GE/EPRI J-Estimation Scheme Method for Through-Wall-Cracked Pipe

The original GE/EPRI method is based on a compilation of finite-element solutions for circumferentially through-wall-cracked (TWC) pipes using deformation theory of plasticity. These solutions are catalogued in References 4.7, 4.22, and 4.23 for various geometric and material parameters. For TWC pipes subjected to pure bending, the J-integral is calculated by breaking it down into its elastic and plastic components. The elastic and plastic components of J are given in References 4.7, 4.22, and 4.23 as

$$J_e = f_1(\theta/\pi, R_m/t) M^2/E \tag{4-5}$$

$$J_p = \alpha \sigma_o \epsilon_o R_m \theta (1-\theta/\pi) h_1(\theta/\pi, R_m/t, n)(M/M_o)^{n+1} \tag{4-6}$$

where the elastic f_1 and plastic h_1 functions are influence functions calculated from finite element results and tabulated in References 4.7, 4.22, and 4.23. M_o is the limit-moment of a through-wall-cracked pipe under pure bending.

As part of the Short Cracks in Piping and Piping Welds program (Ref. 4.24), a number of improvements were made to the GE/EPRI method. Specifically, finite element solutions were compiled to improve the f-, V-, and h-functions for Ramberg-Osgood strain-hardening exponents (n) of 1, 2, 3, 4, 5, and 10 for both the case of short and long cracks. In addition, for the short TWC case, the effect of combined tension and bending was considered. This method was included in this comparative analysis because it tends to be the most widely used of all of the through-wall-cracked pipe J-estimation schemes.

4.1.3.4 LBB.NRC J-Estimation Scheme for Through-Wall-Cracked Pipe

The LBB.NRC method (Ref. 4.8) for circumferentially TWC pipe subjected to bending was developed primarily for use by the U.S. NRC staff as a means to evaluate Leak-Before-Break submittals by the nuclear industry. It is based on earlier work by Paris and Tada in NUREG/CR-3464 (Ref. 4.25) with modifications developed by the NRC staff to account for the strain-hardening characteristics of typical nuclear power plant piping materials.

4.1.3.5 LBB.ENG2 J-Estimation Scheme for Through-Wall-Cracked Pipe

The LBB.ENG2 method was originally developed by Brust and Gilles during the Degraded Piping program (Refs. 4.9, 4.26, and 4.27) to compute the energy release rates for TWC pipes subjected to bending loads. It involves an equivalence criterion incorporating a reduced thickness analogy for simulating the system compliance due to the presence of a through-wall crack in a pipe.

The elastic and plastic components of J (J_e and J_p) are given in Equations 4-7 and 4-8 below:

$$J_e = K_I^2/E \tag{4-7}$$

$$J_p = \{\alpha/(E\sigma_o^{n-1})\}\{\pi R_m/(2[n+1])\}H_B(n,\theta)L_B(n,\theta)I_B(\theta)\{M/\pi R_m^2 t\}^{n+1} \tag{4-8}$$

where $H_B(n,\theta)$ and $L_B(n,\theta)$ are conveniently defined elementary functions with explicit forms available in References 4.9, 4.26, and 4.27.

As part of the Short Cracks in Piping and Piping Welds program (Ref. 4.24), this method was extended to consider the case of a TWC pipe subjected to combined tensile and bending loading conditions. The method is similar to the case of pure bending and is also based on deformation plasticity, Ramberg-Osgood constitutive model, and an equivalence criterion incorporating a reduced thickness analogy for simulating the cracked-pipe compliance. Further details of this method regarding energy release rates due to combined bending and tension can be obtained from Reference 4.28.

4.1.3.6 SC.TNP1 and SC.TNP2 J-Estimation Scheme Analyses for Surface-Cracked Pipe

The SC.TNP analysis method for finite length surface cracks was first developed as part of the Degraded Piping program (Ref. 4.10). The SC.TNP methodology uses a length parameter, L, which is the distance from the crack plane to the plane for which the stresses in the pipe wall can be assumed to be equal to that in the uncracked pipe. Since a clear definition of this length parameter is elusive, the parameter was initially chosen to be approximately equal to the thickness of the pipe wall (Ref. 4.10). This original definition of L (i.e., L = t) was used in the original version of SC.TNP, i.e., SC.TNP1. As part of the Short Cracks in Piping and Piping Welds program (Ref. 4.11), the effect of changing this length parameter, L, was examined. As part of that effort, it was shown that predictions of J using SC.TNP agreed well with finite element results when L was chosen to be between 2t and 3t for a strain-hardening exponent (n) value of 3, whereas L needs to be closer to 9t for the case of n = 10. This finding demonstrated the influence of the strain-hardening level of the material on the choice of L. Based on the dependence of the SC.TNP predictions on the length parameter, L, it appeared that the SC.TNP method could be modified by incorporating the dependence of L on the hardening exponent. For the modified version of SC.TNP, i.e., SC.TNP2, this length parameter is defined as (n-1)t, where t is the wall thickness of the pipe and n is the strain-hardening exponent of the material.

In Reference 4.11, it was shown that the modified version of SC.TNP, i.e., SC.TNP2, results in more accurate predictions of J when compared with finite element results. However, as part of this same reference, it was shown that the original version of SC.TNP, i.e., SC.TNP1, results in more accurate predictions of the maximum experimental stresses when compared with experimental data. This apparent discrepancy has been attributed to the fact that the original version of SC.TNP, i.e., SC.TNP1, tends to underpredict the crack-driving force (J) for a given applied bending moment, but that this underprediction is offset by the fact that the crack growth resistance (J_R) for a surface crack growing radially through the pipe wall is being underpredicted by a J-R curve established from L-C oriented C(T) specimens, i.e., there are constraint and anisotropy factors that make the surface-cracked pipe behave tougher than that from the C(T) specimen, see Reference 4.11.

4.1.3.7 SC.ENG1 and SC.ENG2 J-Estimation Scheme Analyses for Surface-Cracked-Pipe

As part of the U.S. NRC's Short Cracks in Piping and Piping Welds program (Ref. 4.11), a new surface-cracked pipe J-estimation scheme was developed. This method predicted the energy release rates for surface-cracked pipes subjected to remote bending loads. This method of analysis involves determining the moment-rotation behavior based on; (1) classical deformation theory of plasticity, (2) a constitutive law characterized by the Ramberg-Osgood model, and (3) an equivalence criterion incorporating a reduced thickness analogy for simulating the system compliance due to the presence of a part-through surface crack in a pipe. This reduced thickness analogy, see Figure 4.5, was first developed for through-wall-cracked pipe for the LBB.ENG2 (Ref. 4.9) analysis method. The SC.ENG method is general in the sense that it may be applied in the complete range between elastic and fully plastic conditions. Since it is based on J-tearing theory, it is subject to the usual limitations imposed upon this theory, e.g., proportional loading, etc. It also has the implication that the crack growth must be small, although in practice, J-tearing methodology is used far beyond the limits of its theoretical validity with acceptable results (Ref. 4.29). Furthermore, the extent of surface-crack growth in piping is often relatively small.

As indicated in the derivation of the SC.ENG method in Reference 4.11, the evaluation of the plastic component of J (J_p) requires determination of the terms H(a/t) and dH(a/t)/d(a/t). According to the

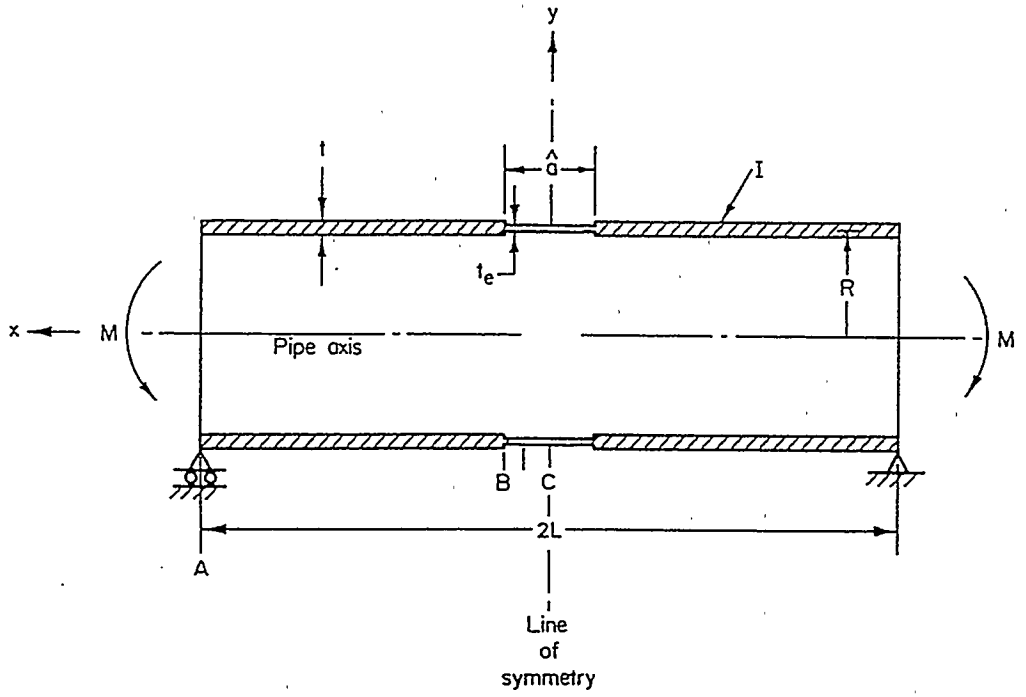

Figure 4.5 Reduced thickness analogy for SC.ENG1 and SC.ENG2 analysis methods

definition of H(a/t) in this derivation, this also requires estimating the equivalent thickness, t_e, for the uncracked pipe, see Figure 4.5. In the equivalence method proposed in Reference 4.11, t_e can be determined by forcing the Net-Section-Collapse moment of the equivalent uncracked pipe to be equal to the Net-Section-Collapse moment of the actual cracked pipe. For an uncracked pipe with reduced thickness, t_e, the Net-Section-Collapse moment, M_L^d, is

$$M_L^d = 4\sigma_f R_m^2 t_e \tag{4-9}$$

where σ_f is the flow or collapse stress of the material and R_m is the mean radius of the pipe. In determining the Net-Section-Collapse moment, M_L^c, for circumferentially surface-cracked pipe, several solutions are available in the literature. In Reference 4.11, two such equations, based on the original Net-Section-Collapse criterion (Ref. 4.5) and the Kurihara modification (Ref. 4.20) to the Net-Section-Collapse criterion, are used to determine H(a/t) and its derivative for the evaluation of J_p. Accordingly, the expressions of J_p based on H(a/t) and dH(a/t)/d(a/t) obtained from the original Net-Section-Collapse equations and the Kurihara modification to the Net-Section-Collapse equations are referred to as SC.ENG1 and SC.ENG2, respectively.

Further details of each of these fracture prediction methods can be found in the appropriate references.

4.1.4 Description of Failure Avoidance Criteria

The failure avoidance criteria to which the experimental data were compared include:

- The ASME Section XI Appendix C criteria for austenitic piping (Refs. 4.12 and 4.13), the ASME Section XI Appendix H criteria for ferritic piping (Refs. 4.14 and 4.15), and the ASME Code Case N-494-3 approach (Refs. 4.16 and 4.17), and
- The R6 Revision 3 Option 1 method (Refs. 4.18 and 4.19).

The methods described previously Section 4.1.3 were all fracture prediction methodologies typically used to give reasonably accurate predictions of the actual failure stresses. In the following sections, the R6 Revision 3 Option 1 approach and three pipe flaw evaluation methodologies embodied in Section XI of the ASME Code, i.e., IWB-3640 and Appendix C for austenitic piping, IWB-3650 and Appendix H for ferritic piping, and Code Case N-494-3 for austenitic and ferritic piping* are described. These methods are intended to be failure avoidance criteria rather than accurate predictive tools, and, hence, should consistently underpredict the experimental results. Note, to facilitate the comparative analysis between the experimental data and the ASME Section XI procedures, a value of 1.0 has been used throughout for the applied safety factors. There are no explicit safety factors in the R6 method.

4.1.4.1 ASME Section XI IWB-3640 and Appendix C Flaw Evaluation Criteria for Austenitic Piping

The technical basis for the ASME Section XI IWB-3640 and Appendix C flaw evaluation criteria for austenitic piping is the Net-Section-Collapse criterion (Ref. 4.5). However, there are three distinct differences between the Appendix C and the NSC criteria.

(1) The flow stress definition in the Appendix C criteria is defined as 3 times the design stress intensity factor (S_m) as defined in Section II Part D of the ASME Code rather than the average of the measured yield and ultimate strengths as used in the NSC analyses discussed above. As discussed previously, the flow stress defined as $3S_m$ was based on an S_m from material property data following the procedures specified in Article 2110 of Appendix III Section III Division 1 of the 1989 edition of the ASME code, i.e., S_m (Actual), as well as the code values in Section II, Part D, i.e., S_m(Code).

(2) For some classes of piping, the exact thick-wall solution is used to calculate the bending stresses for uncracked pipe.

(3) A Z-factor is introduced in the analyses to account for cracks in lower toughness flux welds in predicting the maximum allowable stresses of these cracked welds.

* The Code Case N-494-3 criteria for austenitic piping was approved by ASME Section XI Working Group on Pipe Flaw Evaluation at the March 1996 meeting in Charlotte, North Carolina.

4.1.4.2 ASME Section XI IWB-3650 and Appendix H Flaw Evaluation Criteria for Ferritic Piping

The ASME Section XI Appendix H flaw evaluation criteria for ferritic piping (Refs. 4.14 and 4.15) is fundamentally different than the Appendix C criteria for austenitic piping in that the Appendix H criteria incorporates a screening criterion to establish the failure mechanism of the flawed pipe (i.e., linear-elastic, elastic-plastic, or limit-load) depending on the strength and fracture toughness of the cracked pipe material. For lower toughness ferritic pipes and their associated weldments, Appendix H incorporates a stress multiplier (i.e., Z-factor) into the elastic-plastic analysis to account for the crack being in a lower-toughness material. This Z-factor approach is similar to that used for the austenitic criteria in Appendix C for the case of cracks in lower toughness austenitic flux welds, i.e., submerged-arc and shielded-metal-arc welds.

4.1.4.3 ASME Code Case N-494-3 Approach

The Code Case N-494-3 approach (Refs. 4.16 and 4.17) is similar to the R6 method (discussed next) in that it involves a Failure Assessment Diagram (FAD). It is based on deformation plasticity and uses some of the GE/EPRI functions to specify the bounding failure assessment diagram for surface-cracked pipe. This method is essentially the same as the EPFM approach used in the GE/EPRI J-estimation scheme. While safety factors may be specified externally in this method, it suffers from the same limitations as those for the R6 approach, namely that rotations and/or displacements are not predicted. The shape of the FAD curve is material and geometry dependent. This method is currently being incorporated into the ASME Section XI Flaw Evaluation Procedures by using a lower bound FAD curve shape (Ref. 4.16) with R/t limits to ensure it is bounding.

4.1.4.4 R6 Revision 3 Option 1 Method

This approach for evaluating the integrity of flawed structures made of strain-hardening materials was originally developed by the Central Electric Generating Board (CEGB) in the United Kingdom (Refs. 4.18 and 4.19). The basic method involves a diagram of the toughness ratio (K_r) versus the load ratio (L_r) as shown in Figure 4.6. The value of K_r for a flawed structure is the ratio of the linear-elastic stress intensity factors (K_I) to the material toughness (K_{Ic}). The value of L_r is the ratio of the nominal stress in the component to the yield stress of the material. If the point (L_r, K_r) falls within the failure assessment diagram, shown in Figure 4.6, then the structure is deemed to be safe. If the assessment point (L_r, K_r) falls outside the failure assessment diagram, the structure is not necessarily unsafe, but should be evaluated using some other evaluation method, e.g., R6 Option 2 or 3.

This method has some inherent safety factors incorporated into the Failure Assessment Diagram (FAD), $K_r = f(L_r)$, and hence, the predicted failure loads should never be lower than the experimental values. The ratio of the distance from the origin to the FAD through the assessment point (L_r, K_r) to the distance from the origin to the assessment point (L_r, K_r) in Figure 4.6 is indicative of the margin. Note, the moment-rotation behavior of the cracked pipe cannot be predicted using this method as is possible using some of the J-estimation scheme analysis methods.

Further details of each of these failure avoidance methods can be found in the appropriate references.

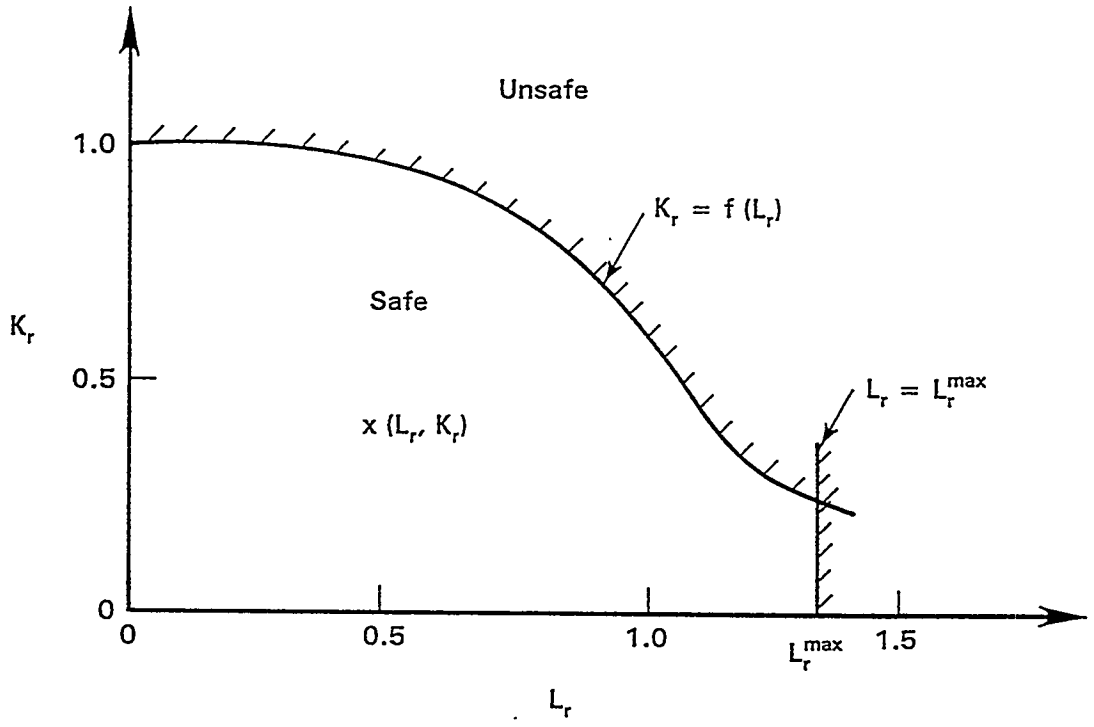

Figure 4.6 Failure assessment diagram (FAD) for R6 Revision 3 Option 1 analysis method

4.1.5 Elbow Fracture Mechanics Analyses

During the course of the IPIRG-2 program, J-estimation schemes were developed for the case of an axial surface crack along the flank (side) of an elbow and for the case of a circumferential surface crack centered along the extrados of the elbow (Ref. 4.30). These J-estimation schemes were developed in the spirit of the GE/EPRI scheme where elastic and plastic contributions to J were used to develop influence functions (f_1 and h_1-functions) from a matrix of line-spring/shell element FEM analyses.

The IPIRG-2 analyses were for combined hoop stress, axial stress, and bending loads, where the axial load corresponded to a pressure stress equal to an average S_m value for typical carbon and stainless steel elbow materials. The elbows were 90-degree long radius elbows in all cases.

The ABAQUS computer code was used with thick-shell elements and line-spring elements to simulate the crack. Selected analyses were checked against 3D brick analyses and very good agreement was found prior to conducting the matrix of line-spring FEM analyses.

The following sections briefly explain the development of the J-estimation schemes for the elbow surface cracks. Reference 4.30 gives an in-depth discussion of these developments. Additionally, later in this report, a simplified procedure for elbow cracks based on these elbow J-estimation schemes and straight-pipe J-estimation schemes is presented and compared to experimental results.

4.1.5.1 Analysis for Circumferential Surface Crack Along an Elbow Extrados

For the case of the circumferential surface crack along the elbow extrados, the loading was hoop and axial stress from pressure loads, and in-plane bending in the closing direction. The following parameters were included in the matrix of FEM analyses:

- R_m/t of 5, 10, and 20
- a/t of 0.3, 0.5, and 0.75
- n values of 1 (elastic), 3, 5, and 10
- a circumferential crack length of 50 percent of the circumference.

In addition to the 3D validation analyses, this gave 36 line-spring FEM analyses in this matrix. Elastic f_1-function values were determined as well as fully plastic h_1-function values. The h_1-function values depend on the selection of the reference moment. Two reference moment solutions were used to determine the h_1-function values. The first method (called SC.ELB1) used the straight-pipe circumferential surface flaw Net-Section-Collapse solution for the reference moment. The second method (called SC.ELB2) was in the spirit of other GE/EPRI reference moment equations, where the reference moment came from the cracked pipe section area (see Reference 4.30 for further details). Of these two reference moment solutions, it was found that the GE/EPRI reference moment solution (SC.ELB2) gave h_1 functions that were smoother for interpolation purposes, and hence is recommended.

4.1.5.2 Analysis for Axial Surface Cracks Along the Flank of an Elbow

For the case of the axial surface crack along the elbow flank (side), the loading was hoop and axial stress from pressure loads, and in-plane bending in the opening direction. The following parameters, similar to those in the axial flaw analysis, were included in the matrix of FEM analyses:

- R_m/t of 5, 10, and 20
- a/t of 0.3, 0.5, and 0.75
- n values of 1 (elastic), 3, 5, and 10
- a crack length of 30 degrees of the 90-degree elbow.

This gave 72 FEM analyses in this matrix. Elastic f_1-function values were determined as well as fully plastic h_1-function values for the internal pressure as well as the combined pressure and bending cases. The h_1-function values depend on the selection of the reference moment. In this case, the straight pipe axial flaw limit-load solution was used for the reference moment. The resulting J-estimation scheme was called SC.ELB3.

4.1.5.3 The IP2ELBOW Code and Sample Calculations

The resulting J-estimation schemes were programed into a computer code called IP2ELBOW. This computer code used the NRCPIPE user interface in a Windows format. Figure 4.7 shows a comparison of J versus moment curves calculated for the sample case of a crack in a TP304 stainless steel elbow and straight pipe. The thickness, diameter, crack size, and material properties were the same in all the analyses. The circumferentially surface-cracked straight-pipe solution used for reference purposes was the SC.TNP2 analysis, which was found in Reference 4.31 to agree well with line-spring FEM analyses J-moment

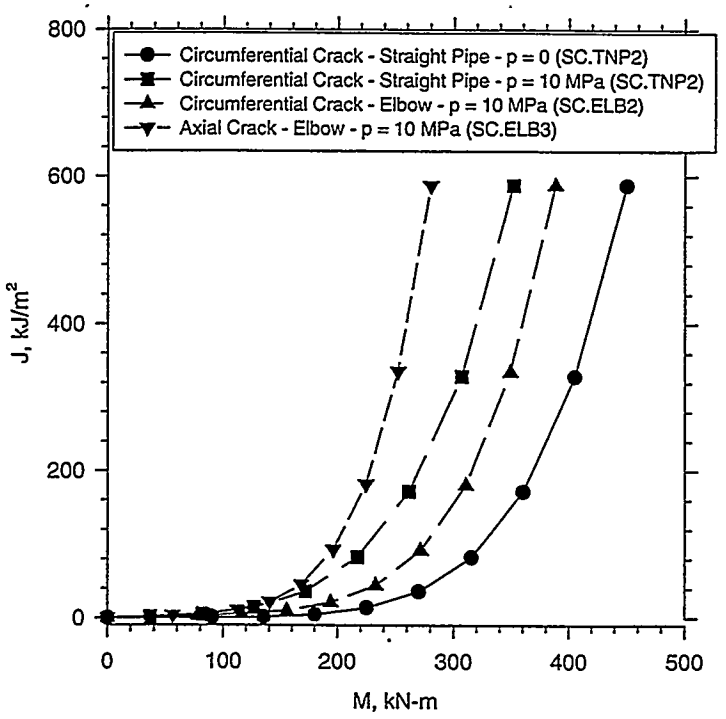

(a) $R_m/t = 10$

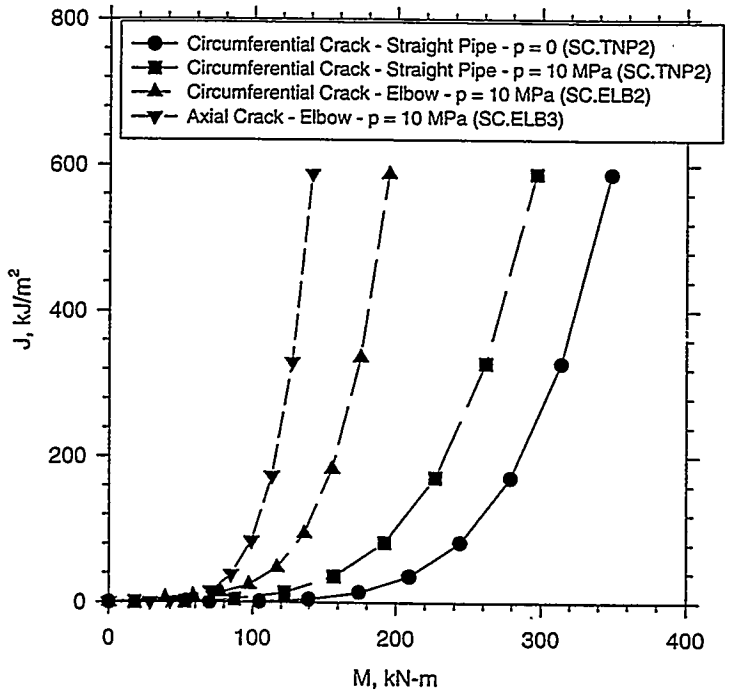

(b) $R_m/t = 20$

Figure 4.7 Variation of J with applied bending moment for axially and circumferentially cracked elbows and circumferentially cracked straight pipe

curves. Results for R_m/t cases of 10 and 20 are shown in Figure 4.7. Note that the crack-driving force (J) is much higher for the axially flawed elbow case for the same applied moments than any other case. Also for the R_m/t case of 10, the circumferential surface crack in the elbow and straight pipe solutions are about the same, but at the R_m/t of 20 case, the J values for the elbow become significantly larger than for the straight pipe.

4.2 6-Inch Nominal Diameter Through-Wall-Cracked Pipe Moment Predictions

This section presents the results from a series of analyses of the 6-inch nominal diameter through-wall-cracked (TWC) pipe experiments from this program and the IPIRG-1 program (Ref. 4.3). There were three separate sets of analyses conducted. The first set of TWC analyses were aimed at assessing the appropriateness of using either quasi-static or dynamic material properties in making predictions for dynamically-loaded pipe experiments. A series of analyses, using both quasi-static and dynamic stress-strain and fracture toughness properties, was conducted in making this assessment, as well as in some sensitivity studies examining failure loads versus pipe diameter. The second was a set of analyses of the Japanese STS410 carbon steel pipe experiments discussed in Reference 4.30. These analyses used quasi-static stress-strain and J-R curve data for predicting the maximum moments from the monotonic and cyclic pipe experiments, which were conducted at quasi-static and dynamic loading rates. The third set of analyses presented are aimed at determining whether cyclic J-R curves should be used in predicting cyclic pipe response. The cyclic J-R curves discussed in Section 2 of this report were used in predicting the IPIRG-1, Subtask 1.2, TWC cyclic pipe moment response (Ref. 4.3), and in some sensitivity studies examining failure loads versus pipe diameter.

4.2.1 Prediction of Dynamic TWC Pipe Response Using Dynamic Material Properties

In order to make accurate dynamic pipe predictions, both the appropriate stress-strain curve and J-R curve need to be used in the analyses. This section discusses a series of analyses aimed at making a determination as to what is the appropriate stress-strain and J-R curve to use in a pipe fracture analysis.

4.2.1.1 Determination of Appropriate Stress-Strain Curve to be Used in Dynamic Pipe Fracture Analyses

The current practice in dynamic pipe fracture analyses is to determine the peak uncracked pipe dynamic loads, and use them in a fracture analysis. Usually, quasi-static material properties are used in the fracture analyses. As shown in this report, loading rates typical of seismic events can cause the strength and toughness of nuclear piping materials to change.

In making a dynamic pipe fracture prediction, one can conduct either a finite element analysis or use a simple closed-form pipe fracture solution. In most industrial applications, the simple pipe fracture analyses will be used since it is cheaper and easier to use than a detailed finite element analysis.

Closed-form fracture solutions consist of either limit-load analyses, simple fracture analyses, or more detailed J-estimation schemes. For the limit-load analyses, such as the NSC analysis (Ref. 4.5) the yield and ultimate strength values are required. For the simple fracture analyses like the Battelle DPZP method

(Ref. 4.6) the yield, ultimate strengths and J_i values are needed. For the R6 Revision 3 Option 1 approach (Refs. 4.18 and 4.19), the yield, ultimate, and J-R curves are needed. For the J-estimation schemes, the appropriate stress-strain and J-R curves are needed.

The determination of the loading rate for the J-R curve is relatively simple. This is because large amplitude dynamic loads will occur near the first natural frequency of the pipe-system of interest. Hence, the J-R curve specimen should be tested so that the time to reach crack initiation corresponds to one quarter of the period of the first natural frequency.

The determination of what strain-rate should be used in the tensile test is more complicated. The strain rates in a cracked structure differ throughout the structure. Hence, in a pipe fracture analysis, an effective strain rate for the cracked pipe must be determined. Because of the difficulty in incorporating dynamic strain aging into constitutive laws for FEM analyses, it was easier, and perhaps more convincing to determine this point experimentally.

This experimental investigation involved two aspects. First, a particular carbon steel pipe was found that had the same toughness in quasi-static and dynamic C(T) tests, but the quasi-static and dynamic stress-strain curves were different. A dynamic pipe test on this material (Japanese carbon steel, STS410) was available through Reference 4.32. Consequently, an identical quasi-static pipe experiment was conducted for relative comparisons.

The second aspect of this investigation was to compare existing quasi-static and dynamic C(T) specimen results. If identical specimens are compared, then the shapes of the load-displacement curves up to crack initiation will show if there are differences in the strain-hardening exponent, and hence confirm if there are differences in the stress-strain behavior in these specimens between quasi-static and dynamic loading. Since a larger percentage of a C(T) specimen experiences plasticity than a cracked pipe (unless there is a very small crack in the pipe), the C(T) specimen results may show larger effects of loading rate on the effective strain-hardening exponent than a pipe experiment.

Figure 4.8 shows the experimental load-displacement curves for the STS410 quasi-static and dynamic TWC pipe experiments. Since these pipe tests had cracks that grew at different angles from the circumferential plane (48 degrees for Experiment 3.3-1 and 38 degrees for Experiment 4.2-1), the data only up to crack initiation should be considered. As shown in Figure 4.8, the quasi-static-load and the dynamic-load experiments had approximately the same load-displacement record up to the point of crack initiation. The dynamic-load experiment showed a slightly higher yield point, which is typical of dynamic tests.

After some crack growth, the quasi-static test had a higher load-displacement record than the dynamic test. This is attributed to angled crack growth. Previous work on this phenomenon (Ref. 4.33) suggests that as the crack growth becomes more axial, the area under the moment-rotation curve increases, thus increasing the apparent resistance. Since the crack in the quasi-static experiment grew at an angle about 10 degrees more than the dynamic experiment, it would be expected to have a higher load-displacement record. These differences may be due to slight material property variations as noted in Reference 4.33.

Figure 4.9 shows the load-displacement record for the quasi-static- and dynamic-load C(T) experiments from the same pipe material. Interestingly, the quasi-static test and the dynamic test with crack initiation in 0.2 seconds show the same trend as was seen in the pipe test comparisons. This result indicates that even though the strain rate at the crack tip in both a C(T) and pipe experiment may be high, the effective

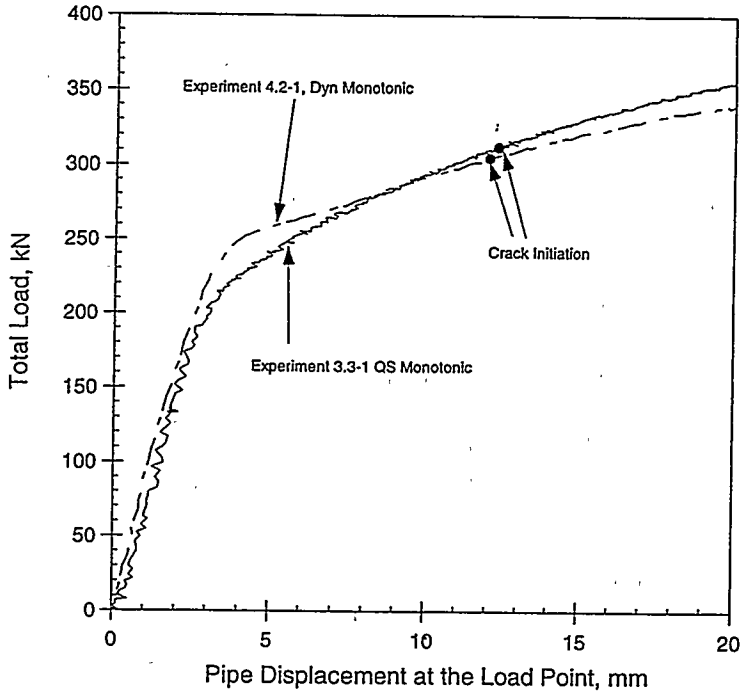

Figure 4.8 Load versus pipe displacement at the load point for Experiments 4.2-1 and 3.3-1

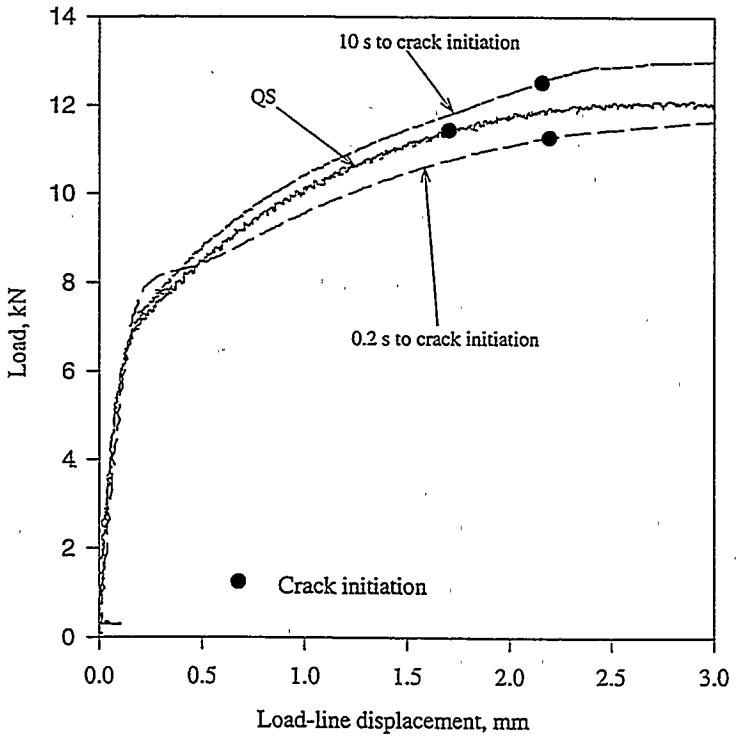

Figure 4.9 Load versus load-line displacement for STS410 C(T) specimen tests

strain rate is similar to quasi-static strain rates. Figure 4.8 indicates that the load-displacement behavior of these pipe experiments are similar up to the point of crack initiation whether the loading rate is quasi-static or dynamic. Therefore, the results show that it is appropriate to use quasi-static stress-strain properties in making dynamic moment predictions. Since there was concern that this conclusion is applicable only to this material, available data from C(T) tests for other ferritic pipe materials were also examined.

Existing C(T) specimen data were examined for Pipes DP2-F30 and DP2-F29. Both of these pipes were highly susceptible to dynamic strain aging as evident by stress-strain curve and J-R curve differences from quasi-static to dynamic rates. Figure 4.10 shows the load-displacement records for the quasi-static and dynamic C(T) tests. Even though the initiation toughness values are different at the different loading rates, the load-displacement records are similar up to the point of crack initiation. From this evaluation, it can be concluded that the quasi-static stress-strain curve appears to be sufficient for fracture predictions at rates investigated in this program.

4.2.1.2 Assessment of Appropriate J-R Curve to be Used in Dynamic Pipe Fracture Analyses

In the prior section, it was shown that using the quasi-static stress-strain curve was sufficient for cracked pipe fracture analyses. In this section, several dynamic pipe tests are analyzed to determine if the quasi-static J-R curve is sufficient or if the dynamic J-R curve is needed. The following TWC pipe tests were considered in this analyses since they were dynamically loaded without cyclic effects.

(1) IPIRG-1 Experiment 1.2-8, on a 6-inch nominal diameter A106 Grade B carbon steel pipe containing a through-wall crack that was tested under dynamic 4-point bending. The material properties for this pipe showed a decrease in strength and toughness with increasing strain rate. Also several crack jumps occurred in both the pipe test and quasi-static C(T) tests.

(2) IPIRG-2 Experiment 4.2-1, on a 6-inch nominal diameter STS410 Japanese carbon steel pipe containing a through-wall crack and tested under dynamic 4-point bending. The material properties for this pipe showed a decrease in strength but no significant change in toughness with increasing strain rate.

(3) IPIRG-2 Experiment 1-9, on another 6-inch nominal diameter A106 Grade B carbon steel pipe containing a through-wall crack and tested under dynamic 4-point bending and internal pipe pressure. The material properties for this pipe showed a decrease in both strength and toughness with increasing strain rate.

Each of the pipe tests were analyzed using the pipe, quasi-static C(T), and dynamic C(T) J-R curves as well as the quasi-static, 1/sec, and 10/sec stress-strain curves, when available. However, only the results using the quasi-static stress-strain curve are presented since it has been shown in Section 4.2.3.1 that this is the appropriate stress-strain curve to use in a dynamic analyses. These analyses were conducted using the NRCPIPE computer code, Version 1.4g. The through-wall-cracked pipe analyses were conducted using the through-wall-cracked pipe J-estimation schemes described in Section 4.1

Tables 4.3, 4.4, and 4.5 show the maximum moment/stress predictions using both the J_D-R and J_M-R curves for Experiments 1.2-8, 4.2-1, and 1-9, respectively. Since Experiments 1-9 was a combined pressure and bend experiment, the moment values were converted to longitudinal stress in order to take into account the axial stress due to internal pipe pressure. Since this version of the J-estimation scheme

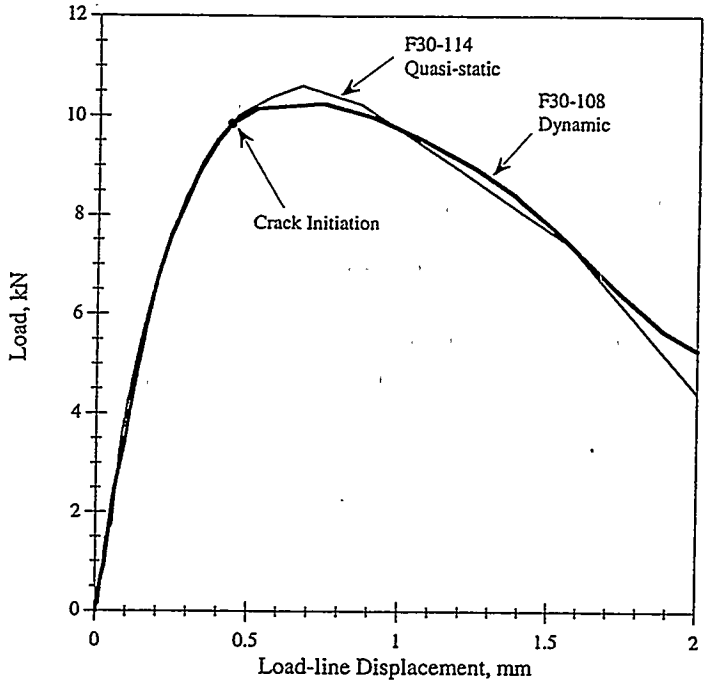

(a) DP2-F30

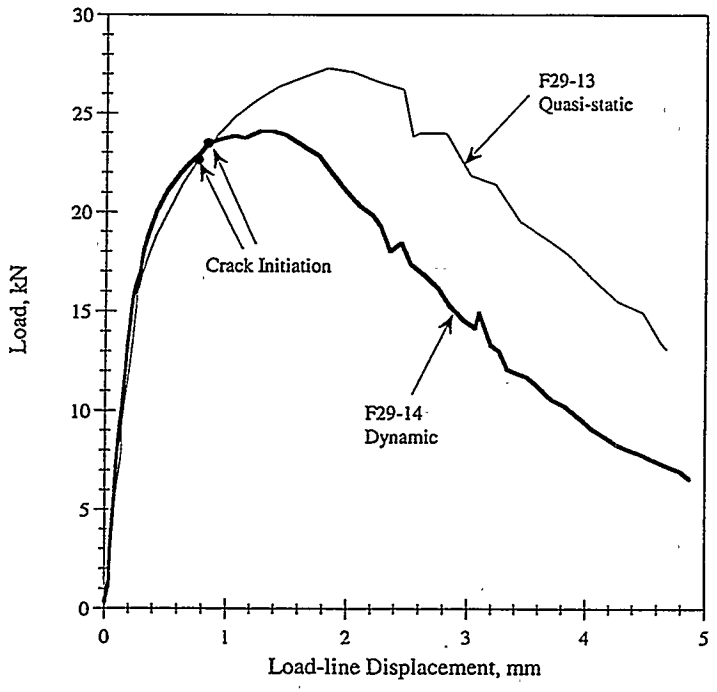

(b) DP2-F29

Figure 4.10 Quasi-static and dynamic load versus displacement records for carbon steel C(T) specimens

Table 4.3 Maximum moment ratios for Experiment 1.2-8

		Experimental-to-Predicted Moment Ratios								
	J-R curve	GE/EPRI		LBB.NRC		LBB.ENG2		R6		NSC
J-R Curve	Type	Initiation	Maximum	Initiation	Maximum	Initiation	Maximum	Initiation	Maximum	Maximum
Pipe Exp 1.2-8	JD	1.153	1.123	0.873	0.860	0.957	1.005	1.104	1.233	0.759
Pipe Exp 1.2-8	JM	1.153	1.118	0.873	0.859	0.957	1.002	1.104	1.230	0.759
QS C(T) F30-112	JD	1.329	1.215	1.025	0.912	1.087	1.075	1.255	1.282	0.759
QS C(T) F30-112	JM	1.329	1.055	1.025	0.846	1.087	0.969	1.255	1.212	0.759
Dyn C(T) F30-110	JD	1.501	1.246	1.176	0.935	1.220	1.107	1.417	1.316	0.759
Dyn C(T) F30-110	JM	1.501	1.199	1.176	0.913	1.220	1.081	1.417	1.300	0.759

Table 4.4 Maximum moment ratios for Experiment 4.2-1

		Experimental-to-Predicted Moment Ratios								
	J-R curve	GE/EPRI		LBB.NRC		LBB.ENG2		R6		NSC
J-R Curve	Type	Initiation	Maximum	Initiation	Maximum	Initiation	Maximum	Initiation	Maximum	Maximum
Pipe Exp 4.2-1	JD	0.906	0.889	0.826	0.986	0.819	0.829	1.042	1.081	0.966
Pipe Exp 4.2-1	JM	0.906	0.888	0.826	0.986	0.819	0.828	1.042	1.080	0.966
QS C(T) IPF13-1	JD	1.057	1.058	0.907	1.020	0.953	0.982	1.123	1.287	0.966
QS C(T) IPF13-1	JM	1.057	0.936	0.907	0.999	0.953	0.888	1.123	1.151	0.966
Dyn C(T) IPF13-5	JD	0.993	1.057	0.870	1.016	0.895	0.979	1.090	1.280	0.966
Dyn C(T) IPF13-5	JM	0.993	0.955	0.870	0.997	0.895	0.903	1.090	1.175	0.966

Table 4.5 Maximum longitudinal stress ratios for Experiment 1-9

		Experimental-to-Predicted Longitudinal Stress Ratios								
	J-R Curve	GE/EPRI		LBB.NRC		LBB.ENG2		R6		NSC
J-R Curve	Type	Initiation	Maximum	Initiation	Maximum	Initiation	Maximum	Initiation	Maximum	Maximum
Pipe Exp 1-9	JD	1.246	1.387	1.069	1.181	1.153	1.207	1.338	1.496	0.945
Pipe Exp 1-9	JM	1.246	1.386	1.069	1.180	1.153	1.203	1.338	1.496	0.945
QS C(T) F22-3	JD	1.964	1.473	1.727	1.271	1.850	1.342	1.675	1.622	0.945
QS C(T) F22-3	JM	1.964	1.360	1.727	1.159	1.849	1.150	1.675	1.587	0.945
Dyn C(T) F22-2	JD	2.298	1.791	2.136	1.491	2.246	1.613	1.900	1.760	0.945
Dyn C(T) F22-2	JM	2.298	1.585	2.136	1.308	2.246	1.366	1.900	1.702	0.945

computer code (Version 1.4g) did not account for the effects of pressure on the moment, the EPFM maximum moments were adjusted using the following relationships:

$$M_{Pred}^{B+T} = M_{Pred}^{B} - \Delta M_{NSC} \quad (4\text{-}10)$$

$$\Delta M_{NSC} = \left(M_{NSC}^{B}\right) - \left(M_{NSC}^{B+T}\right) \quad (4\text{-}11)$$

The subscript NSC refers to the moment calculated by the Net-Section-Collapse analysis, the subscript "Pred" is for the J-estimation scheme prediction, and the superscripts are for bending (B) and tension (T).

The differences in predictions when using J-R curves from the quasi-static C(T) specimen tests and the dynamic C(T) specimen tests were small for Experiments 1.2-8 (Pipe number DP2-F30, A106B material) and Experiment 4.2-1 (Pipe number IP-F13, STS410 material.) The difference was much more significant for Experiment 1-9. This is a result of the more pronounced reduction in the J-R curve for the pipe in Experiment 1-9 (Pipe number DP2-F22, A106 Grade B) when compared with the reduction in J-R curves for pipe materials DP2-F30 (Experiment 1.2-8) and IP-F13 (Experiment 4.2-1), see Figure 4.11.

4.2.1.3 Sensitivity Analyses for Dynamic Loading

To assess the effect of pipe diameter on the maximum moment for dynamically loaded pipe, a series of J-estimation scheme analyses was conducted. For these analyses, the LBB.ENG2 method was chosen since it was more accurate in predicting maximum loads than the other analysis methods. The carbon steel materials tested in this investigation fall into two categories:

1. Stress-strain curve and J-R curve lowered by increasing the strain rate (Pipes DP2-F30, DP2-F22, and DP2-F29).

2. Stress-strain curve lowered but J-R curve unaffected by increasing the strain rate (Pipe IP-F13).

In order to fully assess the effect of pipe diameter, an analysis using each of the material types is required. However, for the IP-F13 material, since the J-R curve is not affected by an increasing strain rate, and the quasi-static stress-strain properties are appropriate to use in predicting the dynamic pipe response, the effect of diameter on the maximum moment of a dynamically loaded pipe would be the same as the effect of diameter on a quasi-statically loaded pipe. Therefore, only an analysis using a material whose J-R curve was lowered by increasing the strain rate was performed. A 36.6 percent TWC with a pipe having an $R_m/t = 5.7$ was used in these analyses.

Figure 4.12 shows the results of these sensitivity analyses. Figure 4.12 shows the normalized maximum moment predictions versus pipe diameter for the 6-inch nominal diameter A106 Grade B (DP2-F30) pipe.

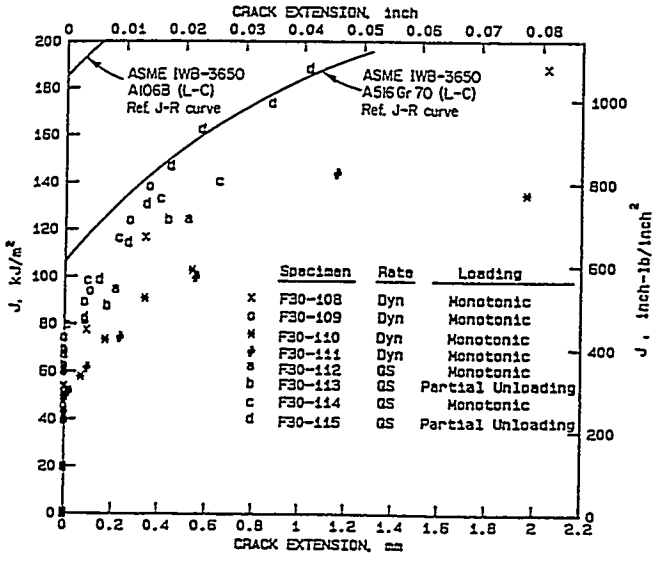

(a) DP2-F30

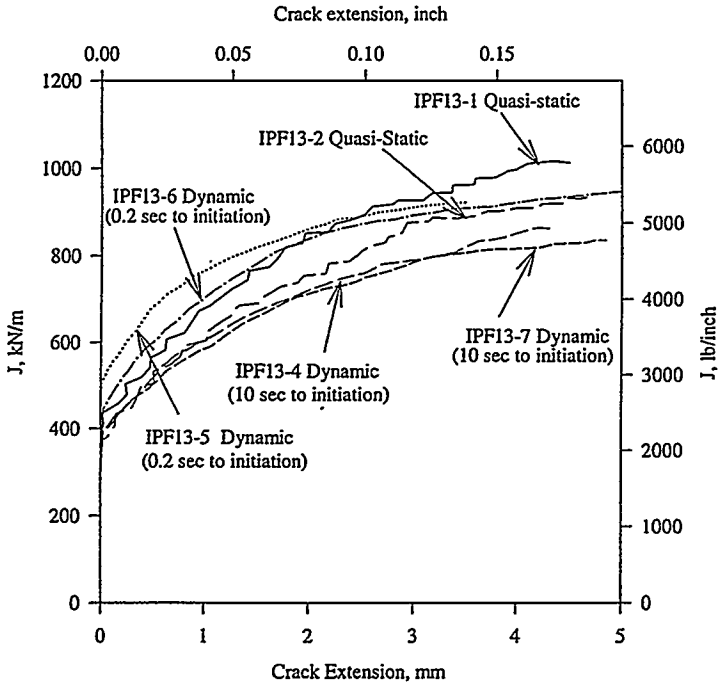

(b) IP-F13

Figure 4.11 Comparison of quasi-static and dynamic J-R curves for C(T) specimens removed from pipe materials DP2-F30 (Experiment 1.2-8), IP-F13 (Experiment 4.2-1), and DP2-F22 (Experiment 1-9)

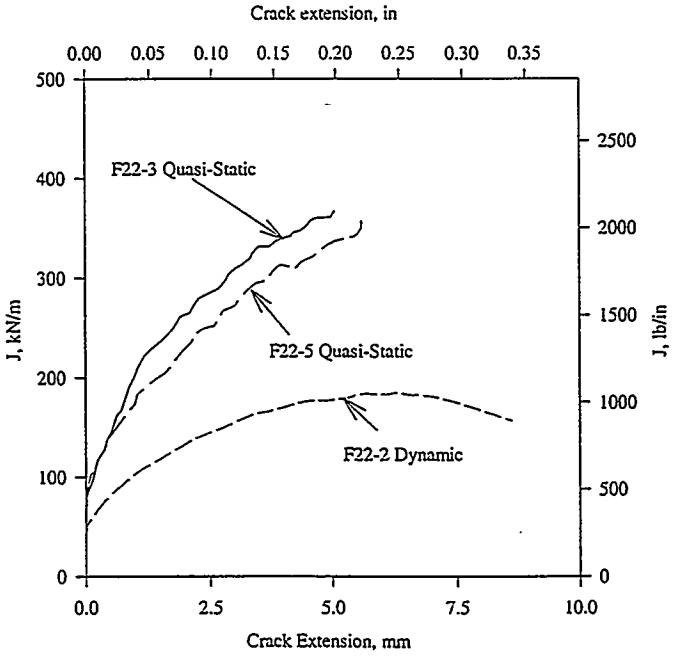

(c) DP2-F22

Figure 4.11 (Continued)

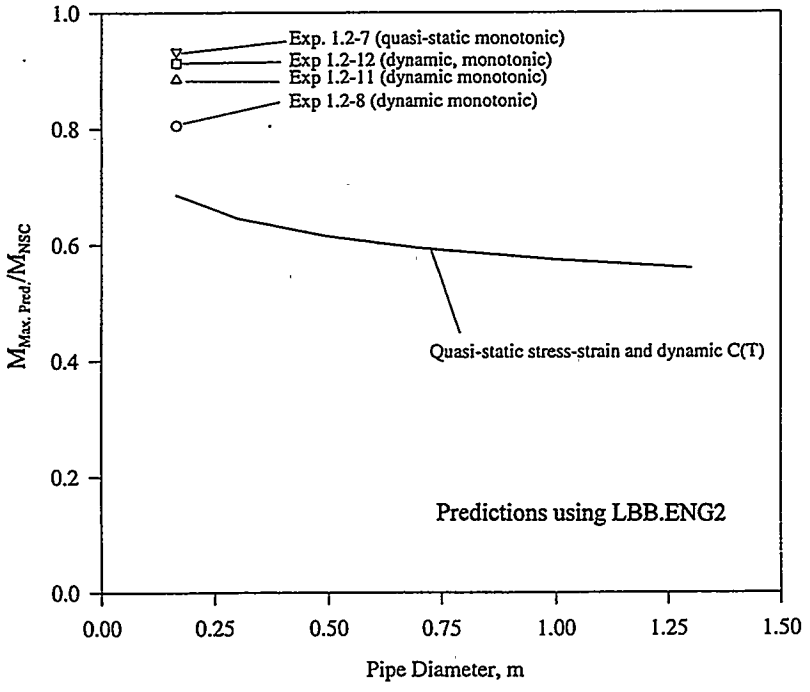

Figure 4.12 Normalized dynamic-maximum-moment predictions versus pipe diameter for carbon steel TWC pipe

Also included on this figure are the normalized maximum moments for each of the pipe experiments. All moment values on this figure have been normalized with respect to the moments the Net-Section Collapse analysis predicted. The trends shown for the initiation moment are also present in the maximum moment predictions, but are less severe in the latter. For a pipe whose diameter is 1.25 m (49.2 inches), the normalized maximum moment predicted is approximately 80 percent of the normalized maximum moment for the 0.152 m (6 inch) diameter pipe.

4.2.2 Maximum Moment Predictions for Japanese STS410 Carbon Steel Pipe

Comparisons were made between the maximum experimental moments and the maximum predicted moments using the Net-Section-Collapse, Dimensionless-Plastic-Zone-Parameter, GE/EPRI, LBB.ENG2, and R6 Revision 3 Option 1 methods. The details of these estimation schemes can be found in Section 4.1. The predictions were made with the aid of a Battelle-written computer code, NRCPIPE, Version 1.4g. (Note, subsequent calculations for unpressurized through-wall-cracked pipe were made using NRCPIPE, Version 2.0 and no differences were found.) The GE/EPRI method used in this analysis was the original GE/EPRI method, with the plastic-zone correction in the elastic term. The results of those comparisons are shown in Table 4.6.

In examining Table 4.6, the NSC, DPZP, GE/EPRI, and LBB.ENG2 methods overpredicted the maximum moment for Experiments 4.2-1 and 4.2-2 by as much as 15 percent. The NSC and DPZP methods underpredicted the Experiment 4.2-3 maximum moment by about 4 percent. All analysis methods underpredicted the maximum moment for Experiment 3.3-1, from 4 percent for the LBB.ENG2 method to 38 percent for the R6 Revision 3 Option 1 analysis. The fracture ratios (experimental/predicted loads) for the R6 Revision 3 Option 1 analysis are slightly higher than the others, indicative of the fact that the R6 Revision 3 Option 1 method is more of a failure avoidance criteria, with some built-in conservatisms, than a true fracture prediction analysis method like the other analysis methods considered. It can also be seen that the Net-Section-Collapse and Dimensionless-Plastic-Zone-Parameter analyses both had the exact same fracture ratios for all four experiments. This is the result of the fact that the toughness of this carbon steel pipe material (STS410) was great enough, and the pipe diameter was small enough, 6 inches, that fully plastic conditions were easily satisfied such that the pipes should have failed under limit-load conditions.

This was not the case for the A106B pipe material evaluated in IPIRG-1 (Ref. 4.34). The toughness of that 6-inch nominal diameter pipe was low enough such that the Dimensionless-Plastic-Zone-Parameter analysis predicted maximum moments were 92 percent of the Net-Section-Collapse predicted maximum moments, i.e., it was just barely in the EPFM region.

Also of note from Table 4.6 is the fact that for each of the analysis methods, the fracture ratios (i.e., experimental/predicted moment) at maximum moment for the dynamic, cyclic, base metal experiment (4.2-2) were only about 5 percent less than the fracture ratios at maximum moment for the dynamic, monotonic, base metal experiment (4.2-1). Conversely, in Reference 4.31 it was shown that the fracture ratios at maximum moment, for each of the analysis methods for the IPIRG-1 Subtask 1.2 dynamic, cyclic experiment (1.2-6) were about 20 percent less than the average fracture ratio for the three IPIRG-1 Subtask 1.2 dynamic, monotonic experiments (1.2-8, 1.2-11, and 1.2-12). This tends to suggest that the Japanese STS410 material evaluated in this program may not be as sensitive to cyclic loading effects as the A106 Grade B material evaluated in IPIRG-1 (Ref. 4.34).

Table 4.6 Comparison of maximum experimental moments with Net-Section-Collapse, DPZP, GE/EPRI, LBB.ENG2, and R6 predictions for the 6-inch nominal diameter STS410 through-wall-cracked pipe experiments

Expt. No.	Maximum Experimental Moment, kN-m	Load History	Experimental/Predicted Maximum Moments[1]				
			NSC	DPZP	GE/EPRI	LBB.ENG2	R6
4.2-1	84.1	Dyn, Mono	0.961	0.961	0.935	0.888	1.151
4.2-2	77.3	Dyn, R = -1	0.928	0.928	0.884	0.844	1.095
4.2-3[2]	87.9	Dyn, R = -1	1.039	1.039	0.968	0.914	1.186
3.3-1	92.8	QS, Mono	1.093	1.093	1.136	1.043	1.383

(1) Quasi-static material properties were used in these analyses.
(2) Crack in a TIG weld, and grew into the base metal shortly after initiation.

4.2.3 Cyclic TWC Pipe Moment Predictions Using Cyclic J-R Curves

The results for the cyclic TWC J-estimation scheme moment predictions are discussed below. The results are presented as a ratio of the experimental-to-predicted moments. Three different combinations of J-R curves were used in these analyses. First, the cyclic J-R curves calculated from the C(T) experiments were used to predict the cyclic pipe response. For example, when predicting the moment response of the IPIRG-1, quasi-static, cyclic (R = -1), stainless steel, TWC experiment (1.2-5), each of the stainless steel cyclic C(T) experiments with a stress ratio of -1 were used. In addition, the η-factor calculated J-R curves from the pipe experiments were also used to predict the experimental pipe response. Finally, the monotonic C(T) specimen J-R curves were used to predict the cyclic TWC pipe response. Quasi-static, monotonic, stress-strain properties were used in all of these analyses*.

4.2.3.1 Stainless Steel Base Metal Maximum Moment Predictions

The experimental-to-predicted maximum moment predictions for the stainless steel base metal pipe experiments are shown in Table 4.7. The NSC predictions in all cases were close to the experimental

* The quasi-static, monotonic, maximum moment predictions presented in Sections 4.2.3.1 and 4.2.3.2 differ slightly from those presented in the IPIRG-1 program (Ref. 4.34) since non-sidegrooved C(T) specimen results, generated in Task 3 of this program, were used in the analyses conducted in this program and not the standard sidegrooved C(T) results that were used in the IPIRG-1 analyses.

Table 4.7 Predictions of stainless steel, cyclic, TWC pipe response using a variety of J-R curves

J-R Curve Specimen #	Specimen Load History	Displacement Increment	Experimental-to-Predicted Moment Ratios						
			GE/EPRI		LBB.ENG2		LBB.NRC		NSC
			Initiation	Maximum	Initiation	Maximum	Initiation	Maximum	Maximum
Analysis of Monotonic Pipe Experiment 4131-5 (Initiation Moment = 29.72 kN-m, Maximum Moment = 37.74 kN-m)									
4131-5	Pipe, Monotonic	N/A	1.391	1.443	1.295	1.379	0.995	1.156	1.099
A23-2c	C(T) Monotonic	N/A	1.223	1.532	1.142	1.434	0.911	1.153	1.099
Analysis of R = 0 Pipe Experiment 1.2-3 (Initiation Moment = 28.98 kN-m, Maximum Moment = 34.60 kN-m)									
1.2-3	Pipe, R = 0	0.1[1]	1.202	1.315	1.115	1.246	0.887	1.033	0.972
A23-2c	C(T) Monotonic	N/A	1.193	1.404	1.113	1.315	0.889	1.057	0.972
A23-4c	C(T), R = 0	0.1	1.084	1.291	0.997	1.191	0.819	0.977	0.972
A23-6c	C(T), R = 0	0.2	1.115	1.251	1.008	1.155	0.834	0.961	0.972
A23-11c	C(T), R = 0	0.025	1.035	1.198	0.953	1.110	0.796	0.943	0.972
A23-21c	C(T), R = 0	0.1	1.089	1.500	0.996	1.398	0.771	1.097	0.972
A23-22c	C(T), R = 0	0.025	1.035	1.198	0.953	1.110	0.796	0.943	0.972
Analysis of R = -1 Pipe Experiment 1.2-5 (Initiation Moment = 22.00 kN-m, Maximum Moment = 32.99 kN-m)									
1.2-5	Pipe R = -1	0.1[1]	1.164	1.469	1.064	1.369	0.818	1.060	0.871
A23-2c	C(T) Monotonic	N/A	0.906	1.339	0.845	1.254	0.675	1.008	0.871
A23-5c	C(T), R = -1	0.1	1.019	1.430	0.934	1.319	0.729	1.036	0.871
A23-7c	C(T), R = -1	0.2	1.089	1.500	0.996	1.398	0.771	1.097	0.871
A23-12c	C(T), R = -1	0.025	1.226	1.580	1.118	1.493	0.857	1.123	0.871
A23-20c	C(T), R = -1	0.1	1.170	1.487	1.068	1.392	0.822	1.071	0.871

(1) Displacement increment changed after maximum load exceeded.

moments. This is typical for smaller diameter, higher toughness pipes. The GE/EPRI and LBB.ENG2 methods greatly underpredicted the experimental moments in all cases, while the LBB.NRC method gave results that were close to the experimental moments.

In examining the predictions for these stainless steel TWC pipe experiments, it is clear that the degree of accuracy of the predictions is not a function of which J-R curve is used. This is probably due to the fact that this is a small diameter pipe, and it doesn't take much toughness to reach limit-load conditions. For example, using the LBB.NRC method to analyze Experiment 1.2-5 (R = -1) gave a variation of 12 percent between maximum moment predictions using the different J-R curves. Using the monotonic J-R curve (highest curve) with this estimation scheme, gave a moment ratio of 1.008, while using the R = -1, δ_{cyc}/δ_i=0.025*, C(T) specimen J-R curve (lowest curve) gave a moment ratio of 1.123. Since experimental scatter in the maximum loads for identical pipe tests can be as large as 10 percent, the difference between these predictions is considered insignificant for these stainless steel experiments.

4.2.3.2 Carbon Steel Base Metal Maximum Moment Predictions

Table 4.8 shows the ratio of experimental-to-predicted maximum moment values for the carbon steel base pipe experiments. In all cases, the NSC analysis overpredicted the maximum moment for these carbon steel experiments. This trend was expected since this material had a lower toughness and elastic-plastic fracture mechanics (EPFM) will govern over collapse.

Unlike the stainless steel experiments, the accuracy of the predictions was slightly influenced by the J-R curve used. Using the cyclic C(T) specimen (R = -1) J-R curves resulted in much lower predictions (approximately 25 percent) than when the monotonic C(T) specimen J-R curve or the TWC cyclic pipe J-R curve were used. If the monotonic J-R curve was used with the LBB.NRC method for the R = -1 pipe test, the maximum loads were overpredicted by about 20 percent. Using the R = -1 C(T) specimen J-R curve gave an accurate prediction.

4.2.3.3 Cyclic-Load Sensitivity Analysis

To assess the effect of pipe diameter on the maximum moments for cyclically loaded pipe, a series of J-estimation scheme analyses was conducted. For these analyses, the LBB.ENG2 method was chosen since it is typically more accurate than the other analysis schemes in predicting the maximum moment results of quasi-static, monotonic pipe experiments.

Stainless Steel Results

For these analyses, a 38 percent through-wall crack with an R_m/t = 5.5 was used. The maximum loads were normalized by the Net-Section-Collapse analysis, using the average of the yield and ultimate strengths as the flow stress. The effect of pipe diameter on the normalized maximum moment at various

* δ_{cyc}/δ_i is the incremental cyclic plastic displacement divided by the displacement to reach crack initiation in a monotonic test. The inverse of this ratio is the number of cycles to reach the displacement at crack initiation in the cyclic test. The cyclic displacement is synonymous to ratcheting for uncracked pipe. The ratio of 0.025 corresponds to 40 cycles.

Table 4.8 Predictions of carbon steel, cyclic, TWC pipe response using a variety of J-R curves

J-R Curve Specimen #	Specimen Load History	Displacement Increment	Experimental-to-Predicted Moment Ratios						
			GE/EPRI		LBB.ENG2		LBB.NRC		NSC
			Initiation	Maximum	Initiation	Maximum	Initiation	Maximum	Maximum
Analysis of Monotonic Pipe Experiment 1.2-7 (Initiation Moment = 37.08 kN-m, Maximum Moment = 51.33 kN-m)									
1.2-7	Pipe, Monotonic	N/A	1.128	1.224	0.944	1.092	0.839	0.938	0.844
F30-1c	C(T), Monotonic	N/A	1.314	1.330	1.079	1.168	0.992	0.992	0.844
Analysis of R = 0 Pipe Experiment 1.2-2 (Initiation Moment = 27.26 kN-m, Maximum Moment = 48.18 kN-m)									
1.2-2	Pipe, R = 0	0.1(1)	1.243	1.174	1.002	1.058	0.968	0.918	0.793
F30-1c	C(T), Monotonic	N/A	0.966	1.249	0.793	1.097	0.729	0.931	0.793
F30-2c	C(T), R = 0	0.1	0.981	1.218	0.803	1.084	0.741	0.919	0.793
F30-7c	C(T), R = 0	0.1	0.942	1.195	0.775	1.064	0.708	0.906	0.793
Analysis of R = -1 Pipe Experiment 1.2-4 (Initiation Moment = 34.57 kN-m, Maximum Moment = 42.70 kN-m)									
1.2-4	Pipe, R = -1	0.1(1)	1.223	1.114	1.003	0.987	0.922	0.834	0.702
F30-1c	C(T), Monotonic	N/A	1.225	1.107	1.005	0.972	0.924	0.825	0.702
F30-3c	C(T), R = -1	0.1	1.434	1.423	1.160	1.205	1.103	1.052	0.702
F30-6c	C(T), R = -1	0.1	1.343	1.408	1.092	1.199	1.025	1.038	0.702

(1) Displacement increment changed after maximum load exceeded.

stress ratios can be seen in Figure 4.13. These calculations show that as the pipe diameter is increased the normalized maximum moment at all stress ratios is decreased. Interestingly, the amount of decrease among the various stress ratios seems to be constant. Whether the pipe diameter is 0.1 m (3.94 inches) or 1m (39.4 inches), the R = -1 case shows a 20 percent decrease as compared with the R = 0 case.

Carbon Steel Results

The same analysis procedures were used for the carbon steel analyses as were used for the stainless steel analyses. A 36.6 percent through-wall crack with an $R_m/t = 5.7$ was used in these analyses. The effect of stress ratio on the normalized maximum moment as a function of the pipe diameter is shown in Figure 4.14. This figure shows that the load-carrying capacity of the carbon steel is more affected by intermediate stress ratios than is the stainless steel. It also shows that the decrease in load-carrying capacity in the carbon steel is greater at large diameters than at small diameters. For the R = -1 case there is a 20 percent decrease in maximum load for a 0.17m (6.69 inch) diameter pipe, while there is a 27 percent decrease in maximum load for a 1.3m (51.2 inch) diameter pipe.

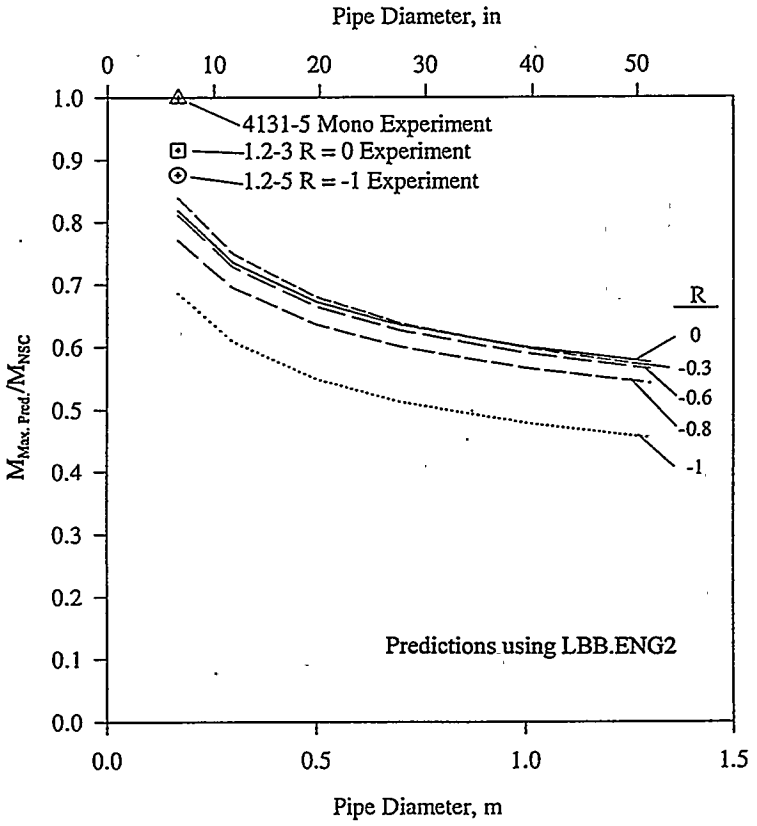

Figure 4.13 Normalized maximum moment predictions versus pipe diameter for stainless steel TWC pipe

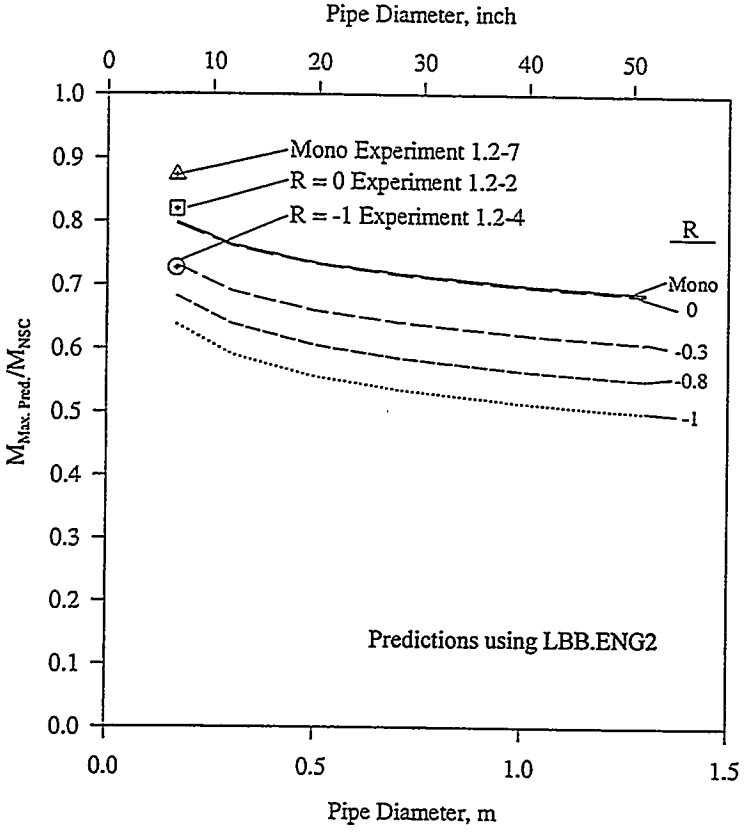

Figure 4.14 Normalized maximum moment predictions versus pipe diameter for carbon steel TWC pipe

4.3 16-Inch Nominal Diameter Straight Pipe Maximum Stress Predictions

In this section, the experimental data for the 16-inch nominal diameter straight pipe experiments are compared with the maximum stress predictions using the various fracture prediction analysis methods described in Section 4.1.3. In the next section, similar comparisons are made using the failure avoidance criteria described in Section 4.1.4.

4.3.1 Simulated-Seismic, Surface-Cracked Pipe Experiments

Two simulated seismic surface-cracked pipe-system experiments were conducted as part of Task 1, i.e., Experiments 1-1 and 1-2. The cracks for Experiments 1-1 and 1-2 were internal circumferential surface cracks located in sections of 16-inch nominal diameter, Schedule 100, TP304 stainless steel pipe (DP2-A8) and A106 Grade B carbon steel pipe (DP2-F29), respectively.

In calculating the fracture ratios for these experiments (i.e., the ratio of experimental-to-predicted stress*, the required bending stress terms were calculated by converting the bending moments (experimental and predicted) to bending stresses through a simple strength of materials formulation (i.e., Mc/I) where c is the outside pipe radius and I equals $0.0491\left(D_o^4 - D_i^4\right)$, where D_o is the outside pipe diameter and D_i is the inside pipe diameter. The membrane stress term was calculated using the simple thin-wall Barlow equation but with the outside diameter as per Section III of the ASME Code ($pD_o/4t$).

Table 4.9 presents the results of the fracture ratio calculations for the two simulated-seismic, pipe-system experiments and the four companion four-point bend and single-frequency pipe-system experiments using the definition of flaw size as discussed in Section 4.1.1. During the analyses of these experiments, quasi-static, monotonic stress-strain curves were used throughout. Furthermore, quasi-static, monotonic J-R curves were used to analyze the quasi-static four-point-bend experiments and dynamic, monotonic J-R curves were used to analyze the pipe-system experiments. In addition, dynamic, cyclic (R = -0.3) J-R curve data were used to analyze the two stainless steel base metal pipe-system experiments. No dynamic, cyclic J-R curve data exist for the carbon steel material evaluated in these experiments, however, since the pipe-system experiments on this material involve failure before cyclic plasticity occurred at the crack, the dynamic, monotonic J-R curve is appropriate to use.

As can be seen in Table 4.9, the fracture ratios for the single-frequency pipe-system experiments are less than the fracture ratios for the simulated-seismic pipe-system experiments. To understand this, the factors that affect cyclic degradation were examined closer. The first factor generally considered is the applied stress ratio. It was found that the effective stress ratios ($R_{effective}$) for the simulated seismic experiments were more negative than the effective stress ratios for the companion single-frequency experiments for both materials, see Table 4.9. Yet, when the crack-section moments were plotted against the crack-mouth-opening displacements for the various experiments, it was found that the cycles prior to maximum load for the simulated-seismic experiments were primarily elastic, see Figure 4.15. In contrast, the cycles prior to maximum moment for the single-frequency experiments exhibited a significant amount of plasticity that gradually built up cycle by cycle until the maximum load was reached. This was especially true for the stainless steel, base-metal, single-frequency, pipe-system experiment, see Figure 4.16. The fact that the cycles prior to maximum moment were essentially elastic for the simulated-seismic experiments implies that these experiments could probably be analyzed much in the same manner as one would analyze a dynamic monotonic pipe experiment. Hence, the cyclic incremental plastic displacement (δ_{cyc}) was very large in the seismic test. If some other simulated seismic forcing function had been used, with a more gradual buildup of large amplitude cycles (i.e., a smaller δ_{cyc}/δ_i), then more cyclic degradation would have occurred during these simulated seismic experiments.

In reviewing Table 4.9, it can also be seen that for the case of the Net-Section-Collapse analysis, that the fracture ratios for the two carbon steel pipe-system experiments are significantly less (up to 25 percent less) than the fracture ratio for the companion, quasi-static, experiment. In the analyses represented in Table 4.9, quasi-static tensile properties were used throughout. For the other analysis methods, the agreement between the fracture ratios for the quasi-static experiment and the two that included the dynamic toughness pipe-system experiments was better. The lower NSC fracture ratios for the dynamic carbon steel

* Including bending and membrane stress components.

Table 4.9 Results of fracture ratio calculations for the two simulated-seismic, surface-cracked, pipe-system experiments (1-1 and 1-2) plus two companion quasi-static, four-point bend (4112-8 and EPRI 13S) and two companion single-frequency, pipe-system experiments (1.3-2 and 1.3-3)

Experiment Number	Material	Load History	Pressure, MPa	Effective Stress Ratio (R)[1]	Fracture Ratios[2]					
					NSC	DPZP	SC.TNP1	SC.TNP2	SC.ENG1	SC.ENG2
Using Monotonic J-R Curve Data										
4112-8	A106B	QS Bend	0	1.0	0.894	0.935	1.021	1.310	1.362	1.567
1.3-2	A106B	Single Freq.	15.5	0.3	0.709	0.876	0.903	1.182	1.325	1.617
1-2[3]	A106B	Sim. Seismic	15.5	-0.1	0.801	0.991	1.018	1.333	1.485	1.801
EPRI 13S[4]	TP304	QS Bend	0	1.0	1.144	1.144	1.008	1.316	1.324	1.522
1.3-3	TP304	Single Freq.	15.5	-0.2	0.975	0.975	0.890	1.165	1.155	1.342
1-1	TP304	Sim. Seismic	15.5	-0.5	1.156	1.156	0.999	1.291	1.222	1.403
Using Dynamic, Cyclic (R = -0.3) J-R Curve Data										
1.3-3	TP304	Single Freq.	15.5	-0.2	0.975	0.975	1.036	ND[5]	ND	ND
1-1	TP304	Sim. Seismic	15.5	-0.5	1.156	1.156	1.011	ND	ND	ND

(1) $R_{effective} = \left(\sigma_{B_{min}} + \sigma_m\right) / \left(\sigma_{B_{max}} + \sigma_m\right)$

(2) Fracture ratio = $\left(\sigma_{B_{expt.}} + \sigma_m\right) / \left(\sigma_{B_{analysis}} + \sigma_m\right)$

(3) Fracture ratio for Experiment 1-2 has been adjusted to account for the deepest part of the crack not being at the crack centerline where the stress was the highest, i.e., fracture ratio = $\left(\sigma_{B_{expt.}} \cos(\psi) + \sigma_m\right) / \left(\sigma_{B_{analysis}} + \sigma_m\right)$ where $\psi = 33$ degrees.

(4) Analyzed using an average fit of the J-R curves for Specimens A8a-1, A8a-2, and A8a-3.

(5) ND = Not determined.

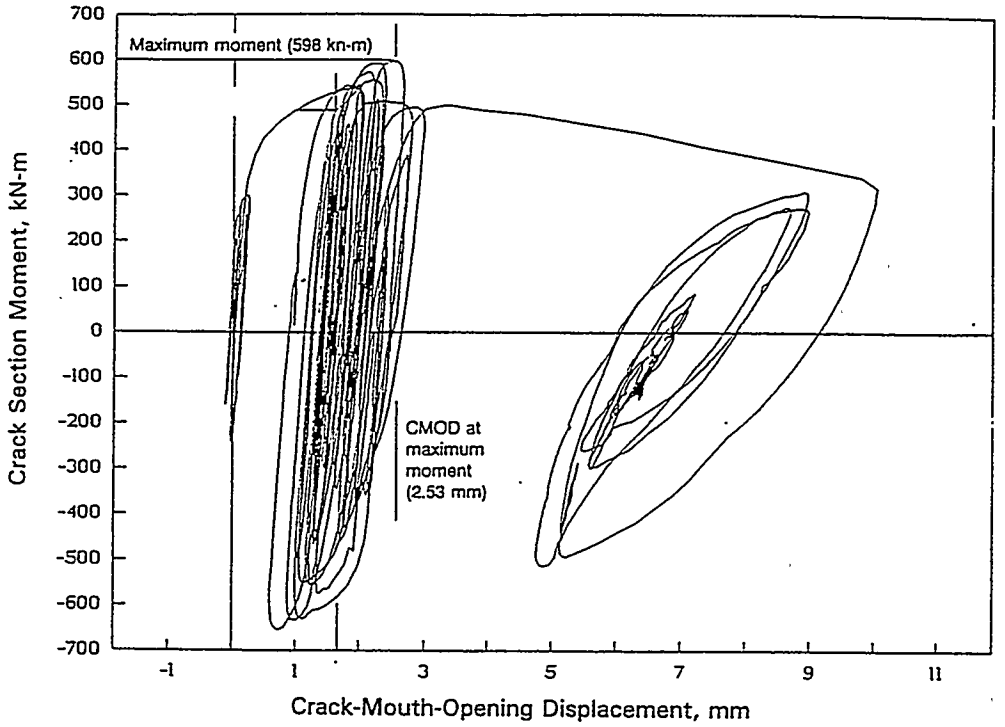

Figure 4.15 Moment-CMOD response for stainless steel, base metal, simulated-seismic, pipe-system experiment (1-1)

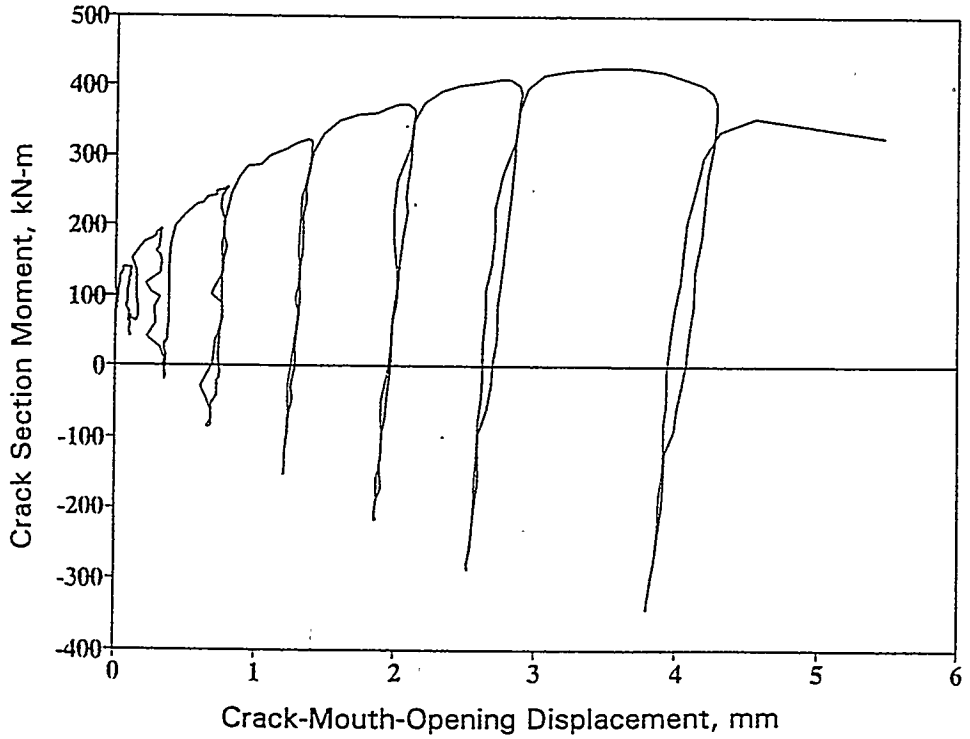

Figure 4.16 Moment-CMOD response for stainless steel, base metal, single-frequency, pipe-system experiment (1.3-3) from IPIRG-1 (Ref. 4.2)

experiments are probably attributed to the fact that the Net-Section-Collapse analysis is a limit-load analysis and, as such, does not consider the dynamic toughness of the material in the analysis.

Finally, of note from Table 4.9 is the fact that the use of the quasi-static, cyclic (R=-0.3), C(T) specimen J-R curve data has little impact on the fracture ratios for the two stainless steel base metal pipe-system experiments. This is because there was not a significant difference between the monotonic and the R = -0.3 cyclic J-R curves for this material which was used in these analyses.

4.3.2 Elbow Girth Weld Pipe Experiments

Two experiments with internal circumferential surface cracks in a girth weld joining a section of 16-inch nominal diameter straight pipe to a 16-inch diameter, Schedule 100, long-radius 90-degree elbow were conducted as part the IPIRG-2 program, i.e., Experiments 1-3 and 1-4. For these two experiments, both the elbows and straight pipe sections were fabricated from A106 Grade B pipe. The weld procedure used for these experiments was a C-Mn-Mo-Ni submerged-arc weld (SAW) procedure developed by Babcock and Wilcox (B&W) and fabricated by the United McGill Corporation in Columbus, Ohio. This was the same weld procedure used in the companion quasi-static, four-point bend and single-frequency, pipe-system, straight pipe-to-pipe girth weld experiments conducted as part of the Degraded Piping (Ref. 4.1) and IPIRG-1 (Ref. 4.2) programs, respectively.

Figure 4.17 shows a comparison of the weld cross-section geometry for the straight pipe-to-pipe girth welds tested in the companion experiments and the pipe-to-elbow girth welds tested in these IPIRG-2 experiments. As discussed in Section 4.1.1, when considering cracks in welds, the "intuitively correct" crack depth is referenced to the inside pipe surface (a_1), and not the counterbore surface, and the pipe wall thickness is the wall thickness of the pipe plus the weld crown height (t_3), see Figure 4.1. In analyzing these elbow girth weld experiments, there is the further complication that the inside surfaces of the pipes and elbows do not match up. For the elbow girth weld experiments, the inside surfaces of the straight pipe sections were machined such that the resultant wall thicknesses of the straight pipes were the same as the average wall thicknesses of the test elbows. However, since the outside diameters of the elbows were slightly larger than the outside diameters of the straight pipe sections, the inside diameters did not match, see Figure 4.17. As a result, fracture prediction analyses were conducted using both the straight pipe and elbow dimensions in the analyses. For both cases, the crack depths were referenced to the inside surface of the pipe or elbow and the wall thicknesses included the relative height of the weld crown. In addition, for the case where the straight pipe dimensions were used in the analyses, the stress-strain curve for the straight pipe material was used, and for the case where the elbow dimensions were used, the elbow stress-strain curve was used. The results of those analyses are shown in Table 4.10.

As can be seen in Table 4.10, the fracture ratios (experiment/predicted maximum stresses) for the straight pipe experiments agree closely with those for the elbow girth weld experiments, especially for the case when the straight pipe dimensions and the straight pipe stress-strain curve were used in the analyses. For instance, when the SC.TNP1 analysis method was used, the fracture ratios for the two elbow girth weld and two straight pipe weld experiments all agreed within 5 percent of each other. This finding suggests that straight pipe analyses can be used to predict the behavior of surface cracks located in elbow-to-straight pipe girth welds. This is significant since it implies that special analysis procedures for the case of surface cracks in elbow-to-straight pipe girth welds need not be developed. One can simply use the surface-cracked straight pipe analyses previously developed and verified (Refs. 4.1 and 4.11).

Table 4.10 Results of fracture ratio calculations for the two elbow girth weld experiments plus the companion straight pipe girth weld experiments

Experiment No.	Material	Weld Configuration	Load History	Effective[1] Stress Ratio	Pressure, MPa	Fracture Ratios[2] NSC	DPZP	SC.TNP1	SC.TNP2	SC.ENG1	SC.ENG2
Elbow Girth Weld Experiments Using Straight Pipe Dimensions and Stress-Strain Curve and Monotonic J-R Curve Data											
1-3	A106B SAW	Elbow Girth Weld	Single Freq.	-0.55	15.5	0.802	0.863	0.887	1.154	1.210	1.480
1-4	A106B SAW	Elbow Girth Weld	QS Bend	-1.0	15.5	0.679	0.783	0.882	1.131	1.156	1.326
Elbow Girth Weld Experiments Using Elbow Dimensions and Stress-Strain Curve and Monotonic J-R Curve Data											
1-3	A106B SAW	Elbow Girth Weld	Single Freq.	-0.55	15.5	0.857	0.896	0.956	1.225	1.262	1.494
1-4	A106B SAW	Elbow Girth Weld	QS Bend	1.0	15.5	0.818	0.903	1.058	1.341	1.357	1.546
Straight Pipe Experiments Analyzed Using Monotonic J-R Curve Data											
4141-8	A106B SAW	Straight Pipe Weld	QS Bend	1.0	15.5	0.696	0.817	0.923	1.164	1.157	1.295
1.3-4	A106B SAW	Straight Pipe Weld	Single Freq.	-0.15	15.5	0.754	0.816	0.902	1.143	1.149	1.282
Pipe System Experiments Analyzed Using Dynamic, Cyclic (R = -0.6) J-R Curve Data											
1-3[3]	A106B SAW	Elbow Girth Weld	Single Freq.	-0.55	15.5	0.802	1.137	1.029	1.339	1.443	1.756
1.3-4	A106B SAW	Straight Pipe Weld	Single Freq.	-0.15	15.5	0.754	1.197	1.080	1.369	1.418	1.575

(1) $R_{effective} = (\sigma_{B_{min}} + \sigma_m)/(\sigma_{B_{max}} + \sigma_m)$.

(2) The fracture ratios for Experiments 1-3 and 1-4 have been adjusted to account for the crack being off-center, i.e., fracture ratio = $(\sigma_{B_{expt.}}\cos(\psi)+\sigma_m)/(\sigma_{B_{analysis}}+\sigma_m)$ where $\psi = 43$ degrees.

(3) Analyzed using straight pipe dimensions and stress-strain curve.

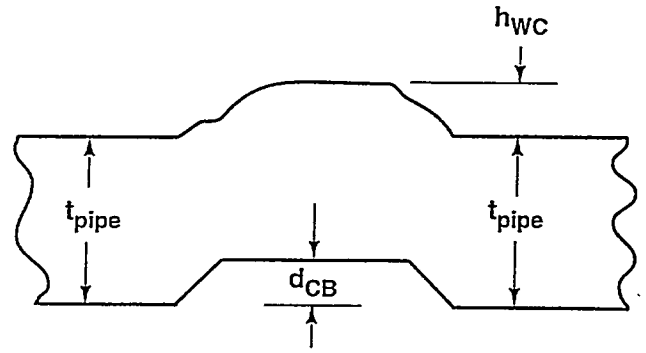

Straight pipe-to-straight pipe weld

h_{WC} = Weld Crown Height
d_{CB} = Counterbore Depth

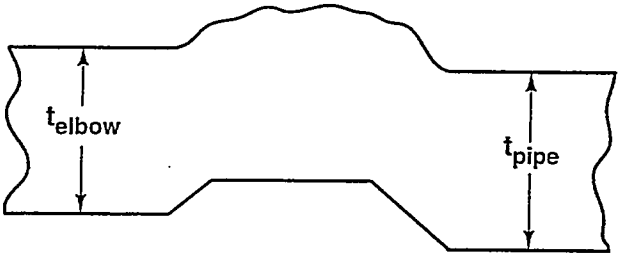

Figure 4.17 Comparison of weld cross-section geometry for straight pipe-to-pipe and elbow-to-straight pipe girth welds

The dynamic, cyclic (R = -0.6) C(T) specimen J-R curve data were used in the analyses of the two dynamic, cyclic pipe-system experiments. The IPIRG-1 experiment had an R-ratio of -0.15 and the IPIRG-2 experiment had an R-ratio of -0.55. Hence, the second pipe-system test had a similar R-ratio to the C(T) specimen tested. No C(T) data with more positive R-ratios were developed.

From the analysis results in Table 4.10, it can be seen that the predictions using the dynamic, cyclic (R = -0.6), C(T) specimen, J-R curve data improved the accuracy of the analyses. However, the relative agreement between the quasi-static, monotonic four-point bend experimental results and the dynamic, cyclic, pipe-system experiments gets much worse. The use of the cyclic J-R curves raised the fracture ratios (i.e., lowered the predictions) by approximately 30-45 percent when using the DPZP analysis and 10-20 percent when using the SC.TNP1 analysis. This finding suggests that the use of cyclic C(T) specimen data for the analysis of cyclicly-loaded pipe-system experiments improved the accuracy of the pipe-system test predictions, but the quasi-static test loads were significantly below the predicted values. This observation comes about from using the weld crown in the flaw size definitions, which is discussed further in the Discussion Section.

4.3.3 Short Surface-Cracked Pipe Experiments

Two pipe experiments with relatively short (25 percent of the pipe circumference) internal circumferential surface cracks in stainless steel pipe-to-pipe girth welds were conducted as part the IPIRG-2 program, i.e., Experiments 1-5 and 1-6. The weld procedure used in fabricating the test welds for these two short surface-cracked pipe experiments was the same submerged-arc weld (SAW) procedure used previously in two long crack (50 percent of the pipe circumference) pipe experiments conducted as part of the Degraded Piping (Ref. 4.1) and IPIRG-1 (Ref. 4.2) programs, i.e., Experiments 4141-4 and 1.3-5, respectively. The weld procedure was originally supplied to Battelle by General Electric (GE) as part of the Degraded Piping Program (Ref. 4.1).

The results of the fracture ratio (experimental/predicted maximum stresses) calculations for the two short and two long surface-cracked pipe experiments for the six analysis methods considered are shown in Table 4.11. As can be seen in Table 4.11, when using monotonic J-R curve data in these analyses, the results for the quasi-static bend short surface crack experiment (Experiment 1-6) agree very closely with the results from both of the long surface crack experiments (Experiments 4141-4 and 1.3-5). As can be seen in Table 4.11, the agreement in fracture ratios between these three experiments is typically within 5 to 7 percent of each other, well within the experimental scatter band typically observed for this type of experiment. However, the calculated fracture ratios for the various analysis methods for the short surface-cracked pipe-system experiment (Experiment 1-5) are up to 30 percent less than the fracture ratios for the other three stainless steel weld experiments. This finding has been attributed to the fact that the cyclic damage for short surface-cracked pipe-system experiment was probably greater than the cyclic damage for the long surface-cracked pipe-system experiment or the two quasi-static monotonic experiments. Figure 4.18 shows

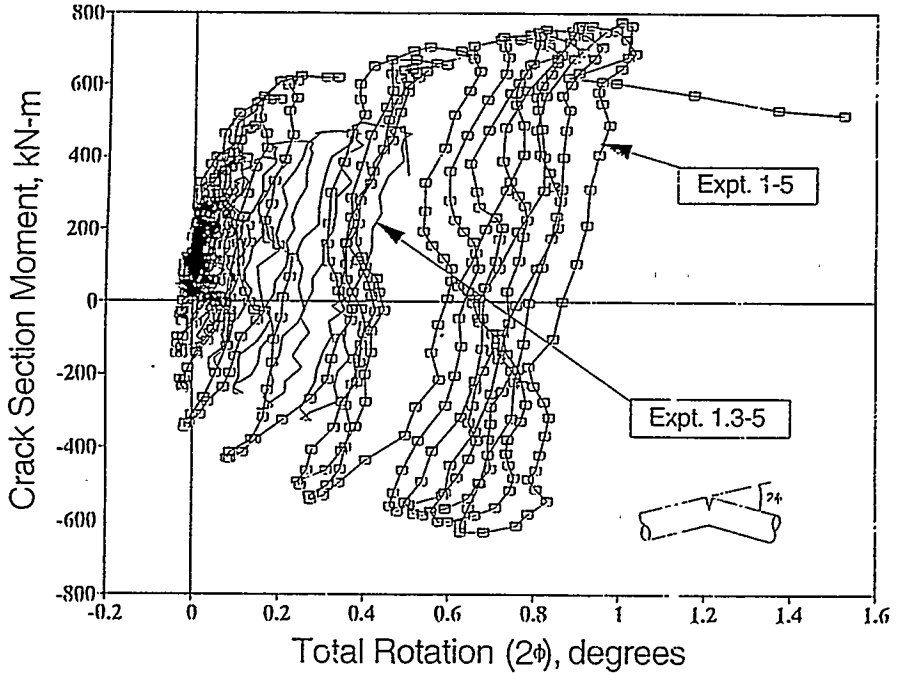

Figure 4.18 Moment-rotation response for the stainless steel weld short surface-cracked pipe-system experiment (1-5) and the stainless steel weld long surface-cracked pipe-system experiment (1.3-5) from IPIRG-1 (Ref. 4.2)

Table 4.11 Results of fracture ratio calculations for the two short surface-cracked pipe experiments plus the companion long surface-cracked pipe experiments

Expt. No.	Material	Load History	Pressure, MPa	Effective Stress Ratio[1]	a/t[2]	θ/π[3]	Fracture Ratios[4]					
							NSC	DPZP	SC.TNP1	SC.TNP2	SC.ENG1	SC.ENG2
Using Monotonic J-R Curve Data												
1-6	TP304 SAW	QS Bend	15.5	1.0	0.620	0.270	0.844	0.955	1.117	1.431	1.319	1.677
4141-4	TP304 SAW	QS Bend	11.0	1.0	0.613	0.50	0.801	0.906	1.082	1.396	1.340	1.555
1-5	TP304 SAW	Single Freq.	15.5	-0.5	0.442	0.267	0.815	0.822	0.981	1.217	1.029	1.166
1.3-5	TP304 SAW	Single Freq.	15.5	-0.2	0.601	0.532	0.917	0.924	1.111	1.441	1.389	1.585
Using Dynamic, Cyclic (R = -0.6) J-R Curve Data												
1-5	TP304 SAW	Single Freq.	15.5	-0.5	0.442	0.267	0.815	0.905	1.160	1.423	1.216	1.365
1.3-5	TP304 SAW	Single Freq.	15.5	-0.2	0.601	0.532	0.917	1.019	1.321	1.711	1.662	1.889

(1) $R_{effective} = \left(\sigma_{B_{min}} + \sigma_m\right) / \left(\sigma_{B_{Max}} + \sigma_m\right)$.

(2) Using "intuitively consistent" definition (a_1/t_3; see Figure 4.1).

(3) Using total crack length.

(4) Fracture ratio = $\left(\sigma_{B_{expt}} + \sigma_{B_m}\right) / \left(\sigma_{B_{analysis}} + \sigma_m\right)$.

plots of the moment-rotation behavior for both the short and long surface-cracked pipe-system experiments. As can be seen in Figure 4.11, the magnitude of the compressive moments for the short surface-cracked pipe-system experiment is approximately twice that for the long surface-cracked pipe-system experiment due to a change in test boundary conditions.

As was the case for Tables 4.9 and 4.10, Table 4.11 also includes comparisons of the experimental data with the maximum stress predictions for these stainless steel weld experiments when cyclic J-R curve data were used in the analyses. The use of the cyclic J-R curves raised the fracture ratios by approximately 5 to 10 percent when using the DPZP analysis method, which only considers the value of J at crack initiation (J_i), and 15 to 25 percent when using the different J-estimation scheme analysis methods which use the full J-R curve.

In comparing the fracture ratios for when cyclic and monotonic J-R curve data were used in the analyses of these stainless steel weld experiments, it can be seen that if the dynamic, cyclic (R = -0.6) J-R curve for this weld were used in the analyses of Experiment 1-5, which experienced larger compressive moments ($R_{effective}$ = -0.5) than those for Experiment 1.3-5 ($R_{effective}$ = -0.2), then the calculated fracture ratios for Experiment 1-5 agree very closely with the calculated fracture ratios for the other three stainless steel weld experiments when monotonic J-R curve data were used in the analyses of these three experiments. Thus, it appears cyclic J-R curve data are needed to properly analyze an experiment like Experiment 1-5. It also appears that for Experiment 1.3-5, which had an effective stress ratio of -0.2, reasonably accurate predictions were made using the monotonic J-R curve data instead of cyclic (R = -0.6) J-R curve data. Due to a limited amount of weld metal, cyclic J-R curves at more positive stress ratios were not generated. Thus, it appears that there is a threshold value of $R_{effective}$ above which it is not necessary, or appropriate, to consider the effects of cyclic loading on the toughness of the material. However, when comparing the results from Tables 4.10 for the carbon steel SAW experiments and Table 4.11 for the stainless steel SAW experiments, it appears that this threshold value of $R_{effective}$ may be material dependent. This material dependent effect on the threshold R-ratio was found to occur in the cyclic C(T) results on TP304 and A106 Grade B base metals, see Section 2.2.2.

The overall results of the analyses represented by Table 4.11 tend to indicate that the analysis methods previously developed and validated for the case of long surface cracks work equally well for the case of a relatively short surface crack, if the effects of cyclic loading can be properly accounted for. This conclusion is supported by the findings of Reference 4.11.

4.3.4 Short Through-Wall-Cracked Pipe Experiments

Two short through-wall-cracked pipe experiments were conducted as part of the IPIRG-2 program. The through-wall-cracks were located in the base metal of a 16-inch nominal diameter carbon steel pipe with a wall thickness equal to Schedule 100 specifications. The crack lengths for both these experiments were 12 percent of the pipe circumference. Experiment 1-7 was a simulated-seismic, pipe-system experiment using a slightly increased amplitude version of the forcing function used in the seismic-loaded surface-cracked pipe experiments. Experiment 1-8 was a quasi-static, monotonic, four-point bending experiment. In both cases the test pipe specimens were pressurized with subcooled water to a test pressure of 15.5 MPa (2,250 psi) at 288 C (550 F). The internal pipe pressure for these two experiments was sealed with an external patch, see Figure 4.19.

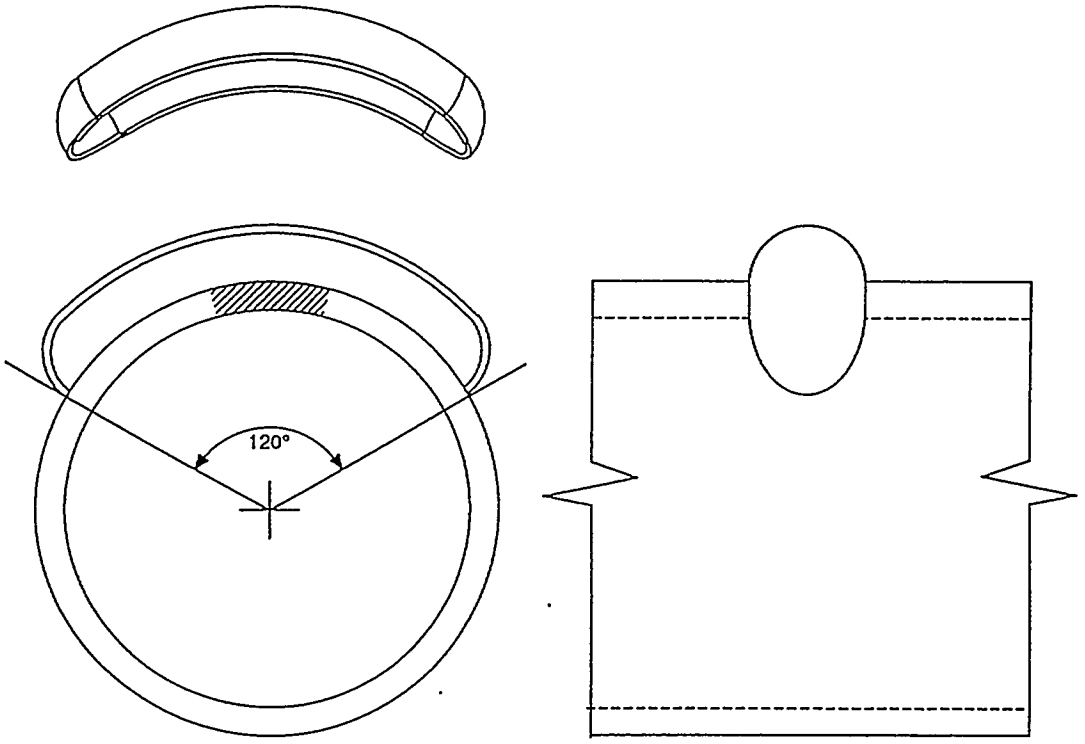

Figure 4.19 Schematic of patch used to seal the two combined pressure and bend through-wall-cracked pipe experiments

The results of the fracture ratio calculations (experimental/predicted maximum stresses) for these two experiments are shown in Table 4.12. The quasi-static stress-strain curve and J-R curve were used in these calculations. As can be seen in Table 4.12, the fracture ratios for the simulated-seismic experiment (Experiment 1-7) are approximately 15 percent less than the corresponding fracture ratios for the companion quasi-static experiment (Experiment 1-8). The lower load-carrying capacity for the simulated-seismic experiment could be attributed to cyclic loading effects. As can be seen in Figure 4.20, which is the moment versus crack-mouth-opening-displacement (CMOD) response for this experiment, there were a number of large amplitude plastic cycles prior to the attainment of maximum moment for this experiment. In addition, the magnitude of the compressive moment values is approximately the same as the magnitude of the tensile component of the moment values which with the pressure stress gave an stress ratio of -0.55. The combined result of these large amplitude plastic cycles and the large compressive moments creates a situation in which significant cyclic damage could occur.

Another possible explanation for the observed reduction in load-carrying capacity for the pipe-system experiment is dynamic loading rate effects. However, dynamic loading rates did not appear to have a large impact on either the stress-strain or J-R curves for this material (DP2-F23). At dynamic rates the yield strength increased slightly when compared with the quasi-static values, and the ultimate strength decreased approximately the same amount. Consequently, the flow stress, when defined as the average of the yield

Table 4.12 Results of fracture ratio calculations for the two 16-inch diameter through-wall-cracked pipe experiments conducted as part of IPIRG-2 Task 1

Experiment No.	Material	Load History	Pressure, MPa	θ/π	Fracture Ratios[1]				
					NSC	DPZP	GE/EPRI	LBB.NRC	LBB.ENG2
1-7	A106B	Sim. Seismic	15.5	0.12	0.869	1.066	1.247	1.153	1.106
1-8	A106B	QS Bend	15.5	0.12	1.039	1.375	1.436	1.333	1.268

(1) Fracture ratio = $(\sigma_{B_{expt.}} + \sigma_m)/(\sigma_{B_{analysis}} + \sigma_m)$. Quasi-static stress-strain curve and J-R curve used in the analyses. The dynamic J-R curve was similar to the quasi-static J-R curve.

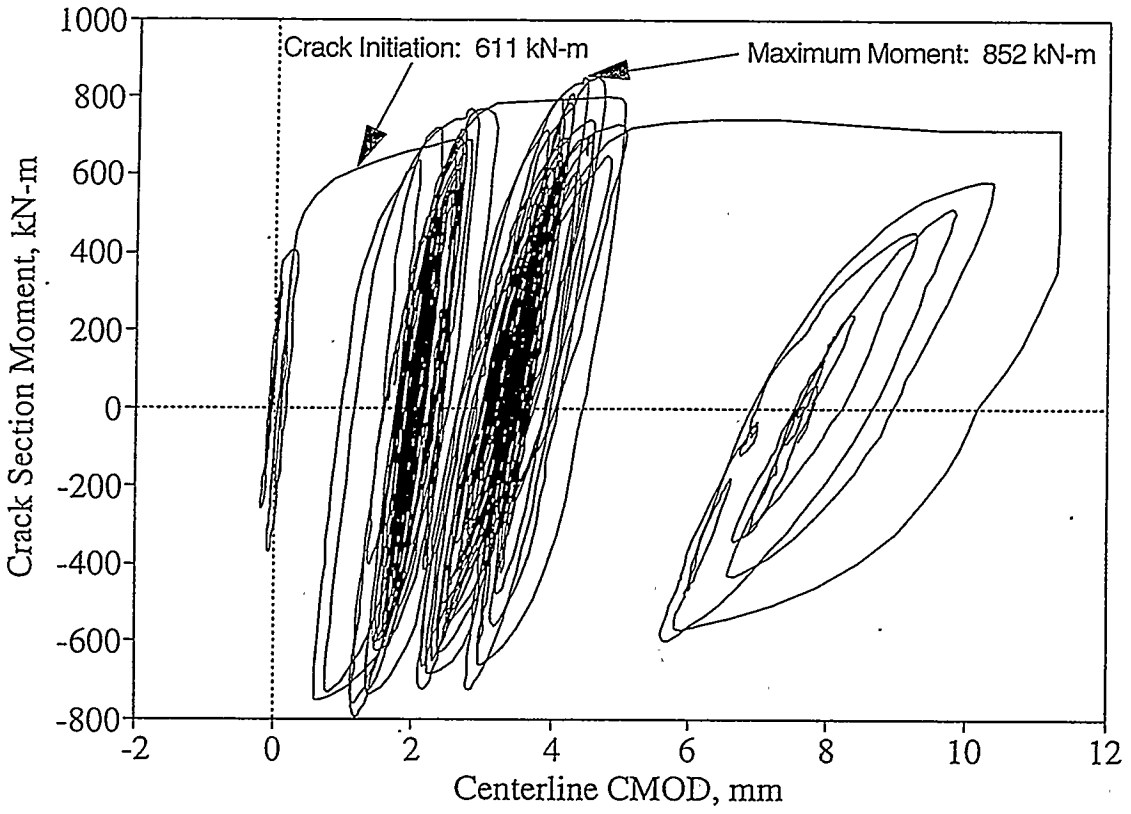

Figure 4.20 Moment-CMOD response for the short through-wall-cracked pipe-system experiment (1-7)

and ultimate strengths, would be virtually unchanged as a result of this increase in strain rate. Similarly, there was not a dramatic change in the J-R curves between the quasi-static and dynamic loading rate C(T) specimen tests for this material. As can be seen in Figure 4.21, the J-R curves for the quasi-static C(T) specimen tests are only slightly higher than the J-R curves for the dynamic C(T) specimen tests.

One of the more significant observable differences between these two experiments was that the crack grew at a 60 to 65 degree angle in the quasi-static experiment versus 30 to 35 degrees in the dynamic pipe-system experiment, see Figure 4.22. Past experience with helical crack growth in ferritic pipe steels is documented in Reference 4.33. From past data on a series of tests on small diameter pipes, it was found that the greater the angle of the crack growth, the flatter the moment-rotation curve after maximum load was reached, see Figure 4.23. That is, with more axial growth, the moment-rotation (or moment-CMOD) curve is higher. With the 16-inch diameter pipe, crack initiation was well before maximum load, and the angled crack growth occurred immediately. Hence, the moment-CMOD curve would be expected to be higher once the crack initiated and grew with a large angle. This behavior occurred in these tests, see Figure 4.20.

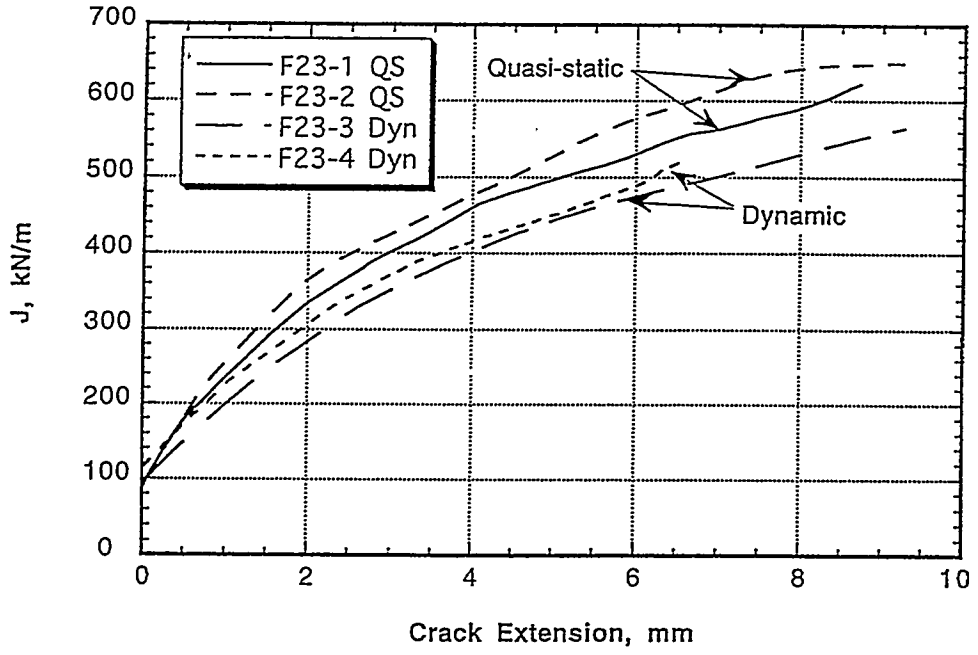

Figure 4.21 Quasi-static, monotonic and dynamic, monotonic J-R curves for A106 Grade B carbon steel pipe material (DP2-F23) used in the two short through-wall-cracked pipe experiments

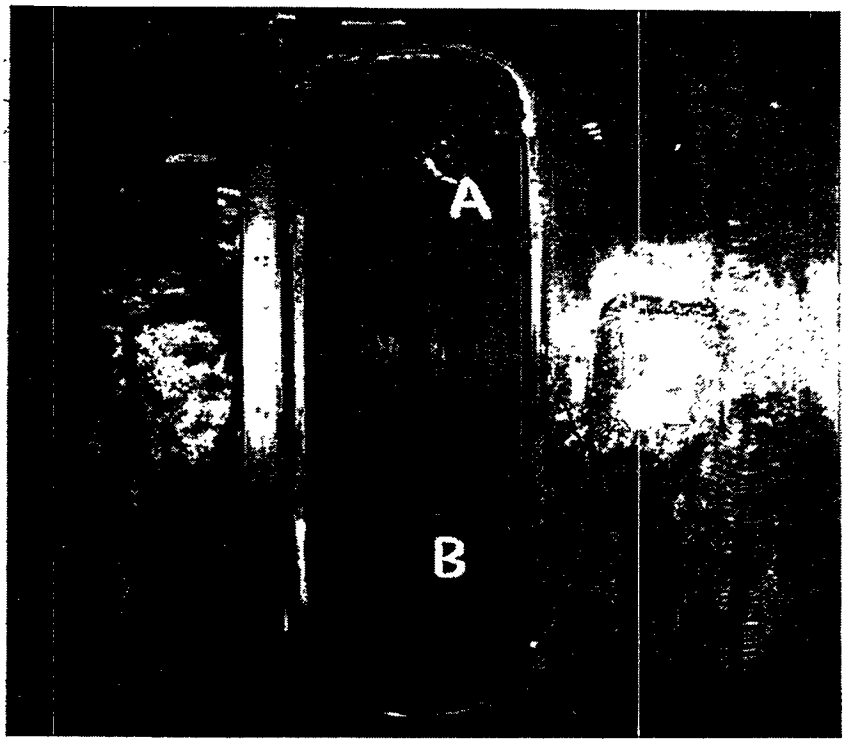

(a) Experiment 1-7

(b) Experiment 1-8

Figure 4.22 Photographs showing differences in angled crack growth in TWC pipe experiments

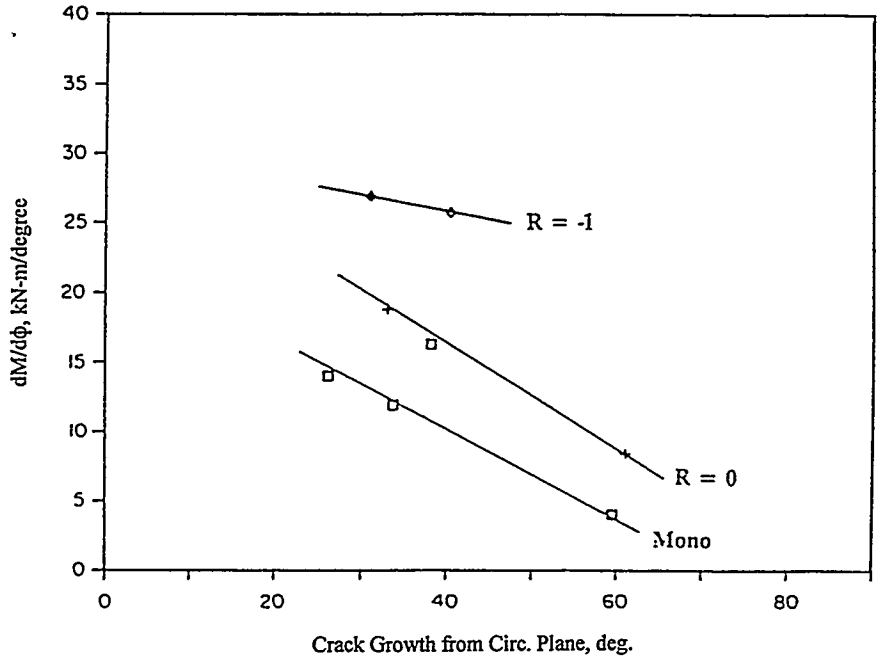

(a) IPIRG-1 Subtask 1.2 6-inch Schedule 120 A106 Grade B experimental results

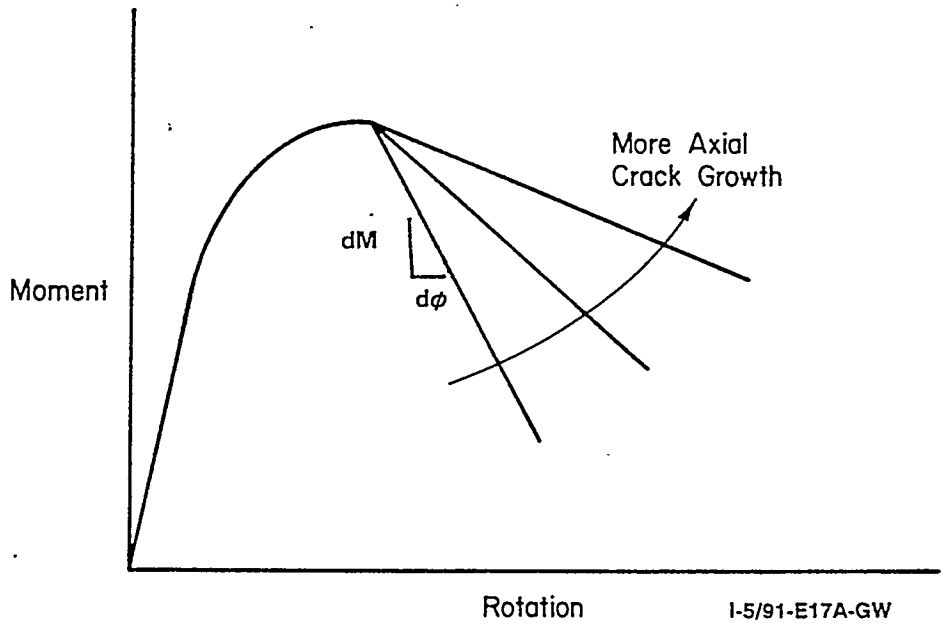

(b) Schematic showing increase in dm/dϕ with more axial crack growth

Figure 4.23 Effect of angled crack growth on moment-rotation response

Another noteworthy point is that in Figure 4.20 the quasi-static test had an apparently lower yield moment and then strain hardened more. This may have been due to dynamic effects on the stress-strain curve, which has not been as noticeable in the other data developed in this program, see discussion in Section 4.2.1. An observation from a video of an IPIRG-1 TWC pipe experiment with angled crack growth, was that the plastic zone prior to crack initiation could also be seen to form at an angle. Hence, the shape of the load-displacement curve prior to crack initiation may also be affected in these anisotropic materials. Reference 4.33 gives a detailed investigation on this effect. Finally, it should be noted, that the angled crack growth although an unusual behavior, is helpful in resisting fracture under tension and bending loads. The fracture behavior of such pipes under torsional loading, may not be as beneficial. Fortunately, primary nuclear plant piping systems have low torsional stresses.

A final aspect considered was the effect of the patch. Nonlinear FEM analyses were conducted in designing the external bellows patch, see Figure 4.24*. For the CMOD values in the two experiments,

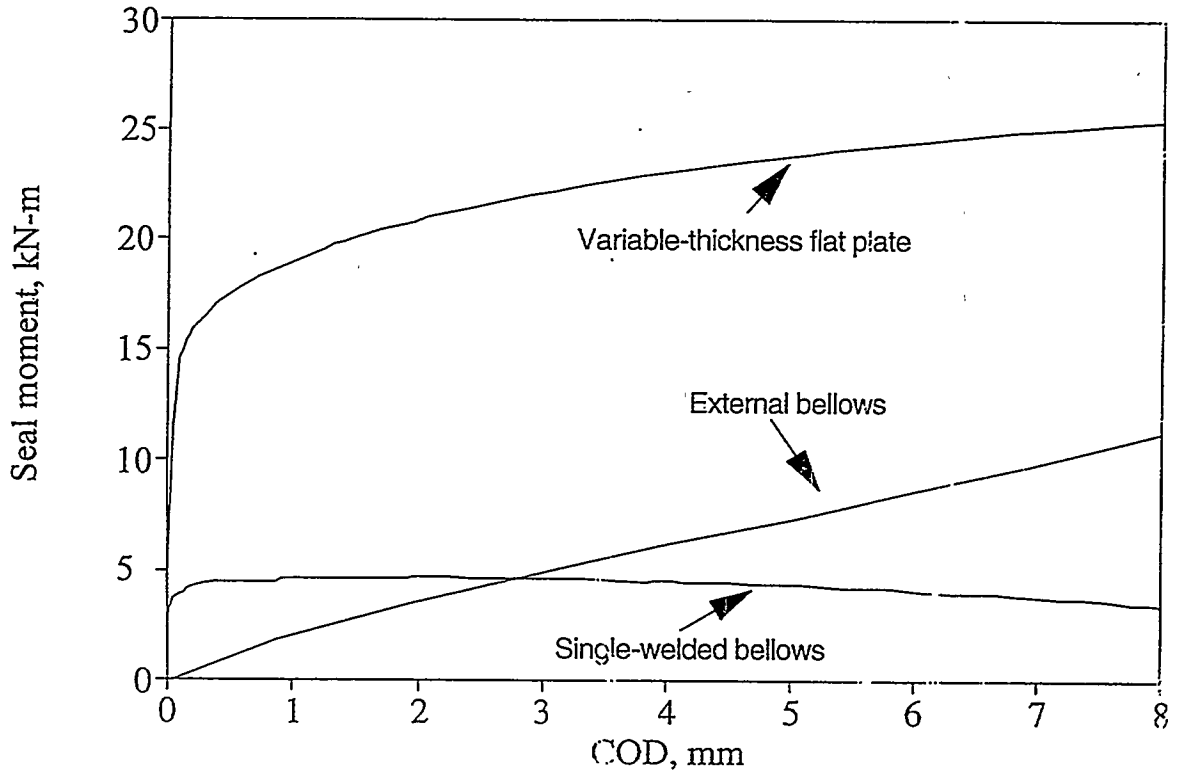

Figure 4.24 Calculated moment across the crack due to the presence of the curved plate seal

* From NUREG/CR-6389, Section 4.4.1

see Figure 4.20, the patch would have caused an extra resisting moment of 7 kN-m in the quasi-static test at it's maximum load than for the pipe-system experiment at its maximum load. The higher resisting moment in the quasi-static tests from the patch was estimated to be roughly 1.5 to 3 percent of the difference in the maximum loads. Hence, the effect of the patch on the loads at crack initiation and at maximum load were insignificant. The flattening of the patch in the quasi-static test, as noted in Section 3, and development of significantly more restraining moment across the crack should only have occurred once the maximum load was exceeded considerably.

4.4 Comparison of Maximum Stress Predictions from Failure Avoidance Criteria with Experimental Data for 16-Inch Diameter Straight Pipe Experiments

In this section, comparisons of maximum stress predictions are made with two failure avoidance criteria, i.e., the ASME Section XI and R6 approaches described in Section 4.1.4. For both of these criteria, two different approaches to define a "fracture ratio" have been considered. In the first approach (Approach 1), the experimental stresses are compared with the ASME and R6 predicted stresses without applied safety factors. Basically, this approach evaluates the flaw capacity source equations, but it ignores the prediction of the crack-driving force, i.e., the piping stress analysis and its associated safety factors and inherent inaccuracies. The second approach (Approach 2) considers not only the "allowable stresses" but also the calculated "applied stresses". Thus, Approach 2 provides an assessment of the complete flaw evaluation procedures, including all implicit or explicit safety factors.

To perform an Approach 1 assessment, the stresses at the flaw at the maximum applied load condition, the post-test measured flaw geometry, and code-specified material properties are required. For the Approach 2 analysis, all of the Approach 1 information plus the results of an elastic stress analysis are required. Given a prescription of the analysis equations, the "fracture ratio" is calculated as the applied stress divided by the predicted allowable stress typically at the maximum moment.

4.4.1 Approach 1 Fracture Ratios

As indicated, Approach 1 is an evaluation of the source equations for flaw capacity. That is, the maximum experimentally applied bending plus pressure stress is compared with the maximum predicted flaw bending plus pressure stress capacity using no factors of safety. Table 4.13 presents the Approach 1 fracture ratios for the IPIRG-2 straight pipe experiments and the companion experiments from the related programs (Refs. 4.1, 4.2, and 4.4) for both the ASME Section XI and R6 Revision 3 Option 1 methods. The crack shape/size assumed in these analyses was the idealized constant depth crack shape, with the crack depth equal to the crack depth at the deepest location along the crack front ($a=a_{max}$) and the crack length equal to the total crack length. For both the ASME Section XI and R6 analyses of the weld crack experiments, the crack depth (a) and the wall thickness (t) are referenced with respect to the counterbore surface, i.e., $a=a_2$ and $t=t_2$, see Figure 4.1, per the specifications of Paragraph NB-3641.1 of Section III of the ASME Code. For both the Section XI and R6 analyses, the presence of the weld crown was ignored. For the ASME Appendices C and H analyses, the flow stress was based on both S_m(Code) and S_m(Actual). The S_m(Actual) definition accounts for material variability and essentially evaluates every pipe experiment as if the test pipe had the same strength properties as those defined in Table 2A of Part D of Section II of the Code. For the ASME Code Case N-494-3 and R6 approaches, the flow stress was based on actual material data. As can be seen in Table 4.13, the Appendix H criteria for ferritic pipes results in higher

Table 4.13 Comparison of maximum experimental stresses for IPIRG-2 straight pipe surface-cracked pipe experiments and companion experiments with maximum stress predictions from ASME Section XI and R6 Revision 3 Option 1

					Fracture Ratios[1]							
					Appendix C		Appendix H		Code[5] Case	Code [6] Case		
Expt. No.	Material	Load History	a/t[2,3]	θ/π[4]	S_m(Code)	S_m(Actual)	S_m(Code)	S_m(Actual)	N-494-3	N-494-3	R6[5]	R6[6]
EPRI 13S[7]	TP304	QS Bend	0.660	0.580	1.533	1.074	NA	NA	1.319	1.319	1.377	1.377
1.3-3	TP304	Single Freq.	0.660	0.552	0.977	0.728	NA	NA	1.182	1.182	1.570	1.490
1-1	TP304	Sim. Seismic	0.628	0.527	1.154	0.865	NA	NA	1.326	1.326	1.722	1.634
4112-8	A106B	QS Bend	0.662	0.532	NA	NA	2.007	1.565	1.554	1.554	1.504	1.504
1.3-2	A106B	Single Freq.	0.727	0.525	NA	NA	1.785	1.329	1.107	1.250	1.268	1.347
1-2	A106B	Sim. Seismic	0.719	0.525	NA	NA	2.293	1.704	1.418	1.613	1.632	1.729
1-3[8]	A106B SAW	Single Freq.	0.766	0.50	NA	NA	3.746	3.053	2.671	2.000	2.780	2.675
1-4[8]	A106B SAW	QS Bend	0.677	0.50	NA	NA	3.042	2.520	2.328	2.328	2.313	2.313
4141-8	A106B SAW	QS Bend	0.670	0.50	NA	NA	2.478	1.871	1.642	1.642	1.704	1.704
1.3-4	A106B SAW	Single Freq.	0.692	0.535	NA	NA	2.863	2.141	1.834	1.630	1.935	1.875
1-5	TP304 SAW	Single Freq.	0.427	0.267	1.397	1.078	NA	NA	1.663	1.511	1.672	1.594
1-6	TP304 SAW	QS Bend	0.649	0.27	1.486	1.139	NA	NA	1.819	1.819	1.889	1.889
4141-4	TP304 SAW	QS Bend	0.633	0.50	1.405	1.066	NA	NA	1.501	1.501	1.780	1.780
1.3-5	TP304 SAW	Single Freq.	0.574	0.532	1.489	1.116	NA	NA	1.646	1.485	2.003	1.929

(1) Fracture ratio $=(\sigma_{B_{expt.}}+\sigma_m)/(\sigma_{B_{analysis}}+\sigma_m)$.
(2) $a = a_{max}$.
(3) For weld tests the wall thickness "t" is the wall thickness of the pipe less the counterbore depth and excluding the weld crown height, i.e., t_2 in Figure 5.16, and the crack depth "a" is the crack depth with respect to the inside surface of the counterbore, i.e., a_2 in Figure 5.16.
(4) θ = maximum value on inside surface.
(5) Using actual quasi-static yield and ultimate strength values, and quasi-static, monotonic, J-R curves in analyzing all experiments.
(6) Using actual quasi-static yield and ultimate strength values, and quasi-static, monotonic, J-R curves in analyzing the quasi-static experiments and dynamic, monotonic, J-R curves in analyzing the dynamic, pipe-system experiments.
(7) Room temperature test; all other tests conducted at 288 C (550 F).
(8) Elbow girth weld experiment; using straight pipe dimensions in analysis.

fracture ratios (greater underpredictions of the experimental stresses) than the Appendix C criteria for austenitic pipes. This finding has been reported previously (Refs. 4.2 and 4.11). An explanation for this finding will be provided in the Discussion Section (Section 7.0) of this report.

It is also of note from Table 4.13 that the fracture ratios for the four stainless steel weld experiments were greater than 1.0 regardless of whether the flow stress was based on S_m(Code) or S_m(Actual). As noted earlier, the predicted moments/stresses for these stainless steel weld experiments were calculated assuming that the wall thickness "t" was the wall thickness of the pipe less the counterbore depth (and excluding the weld crown height), i.e., t_2 in Figure 4.1, and the crack depth "a" was the depth of the crack with respect to the inside surface of the counterbore, i.e., a_2 in Figure 4.1. This set of assumptions seems to be most closely aligned with the spirit of the ASME Code in that Paragraph NB-3641.1 of Section III specifies that "the wall thickness 't' is the specified or actual wall thickness of the pipe minus material removed by counterboring, among other things". If one were to define the wall thickness as the actual wall thickness (less the weld crown height), i.e., t_1 in Figure 4.1, and the depth of the crack was referenced with respect to the inside surface of the pipe, i.e., a_1 in Figure 4.1, then the calculated fracture ratios for these stainless steel weld experiments are somewhat less than those shown in Table 4.13.

Furthermore of note from Table 4.13 is the fact that the fracture ratios for the ASME Code Case N-494-3 approach for austenitic and ferritic steels and the R6 Option 1 Revision 3 approach are comparable. For these analyses, the same material property data and same crack size definition were used for both the R6 and ASME Code Case N-494-3 assessments. Both of these methods (N-494-3 and R6) are based on predictions using a Failure Assessment Diagram (FAD) approach. For both methods the calculated fracture ratios range from approximately 1.1 to 2.0 for the straight pipe experiments and 2.3 to 2.8 for the elbow girth weld experiments. The reason why the fracture ratios for the elbow girth weld experiments are so much greater than the fracture ratios for the straight pipe experiments probably has to do with the assumed wall thicknesses and crack depths for the two elbow girth weld experiments. The actual wall thicknesses of the straight pipe sections and elbows for these two experiments were approximately 33.5 mm (1.32 inches) while the assumed wall thickness for these code-type analyses were in the range of 26.0 to 27.1 mm (1.02 to 1.07 inches) due to the significant counterbores associated with these girth welds.

4.4.2 Approach 2 Fracture Ratios

The Approach 2 fracture ratios consider not only the source equations for the flaw capacity, but also the underlying piping stress analysis and the factors of safety applied to various stress components.

To calculate the Approach 2 fracture ratios, a linear elastic stress analysis is required. For these experiments four components of stress exist: thermal, inertial, seismic anchor motion-induced (SAM), and pressure-induced membrane stresses. Dead-weight loads, out-of-plane bending, and torsional stresses were insignificant. Typically, the various stress components were calculated as follows:

- The thermal and pressure stresses come from the stress state at time=0 from an elastic stress analysis
- The SAM stress comes from a static anchor motion, displacement-loaded elastic stress analysis

- The inertial stress is the total dynamic stress less the SAM stress.

The predicted stresses are combined according to specified rules to find the code-prescribed total applied stress. Where specified, factors of safety are applied to various stress components or stress components are ignored altogether to reflect the perceived propensity of the stress to cause crack growth. (For instance, in ASME Section XI, Appendix C, thermal expansion stresses are ignored for stainless steel base metal flaws thus suggesting that the Code authors did not believe that thermal expansion stresses contribute to the crack propagation process.) In a similar manner, the flaw capacity source equations, with specified safety factors, can be manipulated to find an expression for the total allowable stress. The ratio of the total applied stress to the total allowable stress is the fracture ratio.

In concept, the calculations are simple to perform, however, for some of the IPIRG-2 pipe-system experiments, the validity of the pipe system elastic stress analysis results is questionable. Because using the questionable linear elastic analysis results would compromise the usefulness of the fracture ratios, it was decided to not report any Approach 2 fracture ratio results in this report.

The difficulties encountered with the pipe system elastic stress analysis were for experiments that included the DEGB restraint system. In these experiments, the predicted moment-time response of the pipe-system, even using the most sophisticated nonlinear spring-cracked pipe analysis, did not agree with the experimental results, even for the first few seconds of the experiment when the crack would not have had any perceptible effect on the system response. Because the analysis could not be made to match the elastic portion of the response, the boundary conditions in the analysis were deemed suspect. Although the pipe system elastic analysis for the experiments without the DEGB restraint appear to be "correct", it was felt that to be consistent, an "all or none" philosophy should be followed for reporting Approach 2 fracture ratios.

To try to circumvent the problem with the pipe system elastic stress analyses, an attempt was made to try to use the experimental data to predict what the elastic response would be. These efforts included trying to directly use the experimental maximum moment and extrapolating the linear portions of the experimental displacement-moment plots. These efforts were either completely futile or the resulting fracture ratios were nonsensical (some were actually negative).

For consistency with what was done in IPIRG-1 (Ref. 4.35), it was desirable to present Approach 2 fracture ratios. However, it was deemed essential to use a consistent approach to doing the calculations. The position that was adopted was to abandon reporting Approach 2 fracture ratios, since it was deemed technically prudent to avoid reporting fracture ratios that may give a false sense of security, or alarm, about the failure avoidance criteria.

4.5 16-Inch Diameter Elbow Maximum Stress Predictions

Two, single-frequency, pipe-system experiments were conducted on cracked elbows as part of Task 2, i.e., Experiment 2-1 and 2-3. The cracks for Experiments 2-1 and 2-3 were internal circumferential surface cracks located at the extrados of 16-inch nominal diameter, Schedule 100, long-radius 90-degree seamless elbows. The elbows for Experiments 2-1 and 2-3 were fabricated from A106 Grade B carbon steel and TP304L stainless steel material, respectively. In addition to the elbow system experiments, quasi-static,

monotonic, elbow companion experiments were conducted for both elbow materials, i.e., Experiments 2-2 and 2-4.

A main objective of Task 2 was to assess the applicability of existing straight pipe fracture analyses for predicting failure stresses of cracked elbows. To accomplish this, experimental data were compared with the maximum stress predictions using the various straight pipe fracture prediction analysis methods described in Section 4.1.3, and the elbow fracture analysis prediction methods developed as part of Task 2 of this program (Ref. 4.30). Fracture ratio calculations were performed for the four elbow experiments by calculating the ratio of the experimental stress (bending stress plus membrane stress due to internal pipe pressure) to the predicted stress (bending plus membrane). The bending stress was calculated from the experimental and predicted moment values using the flexural stress formulation Mc/I, where I equals $0.0491\left(D_o^4-D_i^4\right)$. The membrane stress was calculated using the simple thin-wall Barlow equation with the outside diameter as per Section III of the ASME Code ($pD_o/4t$). These formulations assume circular cross-sections and a constant wall thickness, neither of which occurred for these elbows. However, because the objective was to assess the applicability of straight pipe analysis techniques, no adjustments were made to the analysis predictions for variations in wall thickness or out-of-roundness.

Table 4.14 shows the results of the fracture ratio calculations (experimental/predicted maximum stresses) for the two single-frequency elbow experiments and the two companion, quasi-static, monotonic bend, elbow experiments. Local crack depths (a) and local wall thicknesses (t) corresponding to the locations of maximum a/t along the crack length were used in the analyses. Quasi-static stress-strain properties were used in the analysis of all experiments. For the most part, quasi-static J-R curves were used in the analysis of the quasi-static experiments (2-2 and 2-4), while dynamic J-R curves were used to analyze the dynamic, cyclic elbow system experiments (2-1 and 2-3). The one exception is that for the R6 analysis, quasi-static J-R curves were used in the analysis of the pipe-system experiments in addition to analyzing them using dynamic J-R curve data. As discussed in Section 4.1.2, this combination of material property data has been demonstrated to give the best correlation for the straight pipe analyses. This same correlation was shown to be valid for the elbow predictions, see in Table 4.14. Comparing these elbow fracture ratios with fracture ratios for straight pipe experiments loaded in combined bending and pressure shows that the elbow data fall within the established scatter bands associated with the straight pipe experiments (Ref. 4.11) for the SC.TNP1 and ASME methods. Except for Experiment 2-2, there is good agreement for the R6 analysis, with the Experiment 2-2 ratio falling slightly above the expected scatter band (mean plus one standard deviation) from Reference 4.11. For the NSC and DPZP analysis, the average fracture ratios for the elbow experiments are 43 and 26 percent, respectively, higher than the corresponding straight pipe mean fracture ratios. The reason is not clear as to why the NSC analysis consistently predicts higher fracture ratios for these elbow experiments. However, the fact that the DPZP analysis consistently predicts higher fracture ratios for the elbow experiments than previously observed for the straight pipe experiments is probably a carry over of the inaccuracy associated with the NSC analysis since the DPZP predictions are based on the NSC predictions.

The two new J-estimation schemes for elbows (SC.ELB1 and SC.ELB2) included in Table 4.14 were developed for the case of an internal circumferential surface crack along the extrados of an elbow (Ref. 4.30), see Section 4.1.5. The difference between the two methods is in the definition of the limit moment, M_o. The SC.ELB1 method uses the NSC moment equation for its reference moment while the SC.ELB2 method uses a reference moment solution from the GE/EPRI analysis method. Both methods consider internal pressure and in-plane bending as the loading mechanisms. As can be seen in Table 4.14, the accuracy of the SC.ELB2 method is very comparable to that for the SC.TNP1 straight pipe method for all

Table 4.14 Fracture ratios for Task 2 elbow experiments

Experiment Number	Material	Loading Condition	SC.ELB1[1] (Elbow)	SC.ELB2[1] (Elbow)	NSC[1] (Straight)	SC.TNP1[1] (Straight)	DPZP[1] (Straight)	R6[1] (Straight)	R6[2] (Straight)	ASME[1] App. C (Straight)	ASME[1] App. II (Straight)
2-1	A106-B Carbon Steel	Pipe System	0.94	1.18	1.37	1.23	1.38	1.80	1.79	NA[3]	2.36
2-2	A106-B Carbon Steel	Quasi-static	0.94	1.14	1.33	1.15	1.33	1.92	1.92	NA	2.26
2-3	TP304L Stainless Steel	Pipe System	1.22	1.22	1.37	1.21	1.37	1.54	1.61	1.35	NA
2-4	TP304L Stainless Steel	Quasi-static	1.06	1.12	1.20	1.12	1.21	1.42	1.42	1.20	NA

Comparison of experimental maximum moment with analytical predictions for combined bending and pressure load cases for straight pipe (Ref. 4.11)		NSC (Straight)	SC.TNP1 (Straight)	DPZP (Straight)	R6 (Straight)	R6 (Straight)	ASME App. C (Straight)	ASME App. H (Straight)
	Average	0.92	1.10	1.05	1.43	ND[4]	1.16	2.14
	Std. Dev.	0.12	0.15	0.13	0.40	ND	0.19	0.29

(1) Using quasi-static stress-strain data for the analysis of all the experiments and quasi-static J-R curve data for the analysis of the quasi-static experiments and dynamic J-R curve data for the analysis of the dynamic, pipe-system experiments.
(2) Using quasi-static stress-strain data and quasi-static J-R curve data for the analysis of all experiments.
(3) Not applicable.
(4) Not determined.

four experiments considered. The accuracy of the SC.ELB1 method is comparable to that of the SC.ELB2 and SC.TNP1 methods for the two stainless steel elbow experiments, however, this method (SC.ELB1) overpredicted the experimental stresses for the two carbon steel elbow experiments.

4.5.1 Development of a Simplified Failure Avoidance Analysis Procedure for Cracks in Fittings

Even though a number of variables (flaw depth, R_m/t ratios, and strain-hardening exponents) were considered during the development of the J-estimation schemes for cracked elbows in Reference 4.33, these analyses are applicable to only one flaw length, in-plane bending, and long radius 90-degree elbows. Unfortunately, since there is such a large number of other variables which must be considered when analyzing cracked fittings, the development of a general solution for all pipe fittings and loading combinations becomes a formidable task. The lack of detailed solutions for a wider variety of problems, in combination with the desire to have a codifiable approach, led to the development of a simplified solution that could be used as a failure avoidance criterion. The development of this criterion and its validation with the limited experimental database is discussed in the next section. Note the term "failure avoidance criterion" is used since it is recognized that this may not be the most accurate solution that could be developed, but it should be conservative considering its developmental assumptions. It should be emphasized that this is an initial development effort that gives promising results for the cases examined; however, the procedure is obviously not sufficiently validated for codification at this time.

The basic concept behind this approach involved the use of the ASME B_2 or C_2 stress indices as stress multipliers on straight pipe flaw evaluation solutions. The B_2 index is a stress multiplier for the bending stress in a fitting relative to the bending stress in a straight pipe for limit-load analyses from a design stress viewpoint. (Note that in design stress analyses, limit-load conditions are different than limit-load conditions for cracked pipe. The design stress limit-load definition usually refers to a condition when a pipe fitting experiences a limited amount of global plastic bending. The design stress limit moment corresponds to a moment where an uncracked pipe/fitting test record or nonlinear analysis moment-displacement curve intercepts an elastic slope with twice the actual elastic compliance, see Figure 4.25. The pipe fracture limit load occurs when the maximum load of a cracked structure is reached, and the material is tough enough that there is no crack growth prior to reaching maximum load.)

Following the desire to develop a simple failure avoidance analysis that could be readily codified, the following general steps were followed:

(1) Applied J versus moment curves were generated for the same size flaw in a straight pipe and a comparable fitting. These calculations were done for a stationary crack, i.e., no crack growth was considered in the analyses. In particular, the calculations were done for flaws in elbows relative to straight pipes. The absolute values of the flaw lengths and depths were kept the same. The calculations were done for combined pressure and bending, with the pressure levels being the same.

(2) For these calculations, the ratio of the moment for a straight pipe to the moment for an elbow at the same value of applied J was determined. This moment ratio was virtually independent of the applied J level for J_{Ic} values of typical nuclear piping steels.

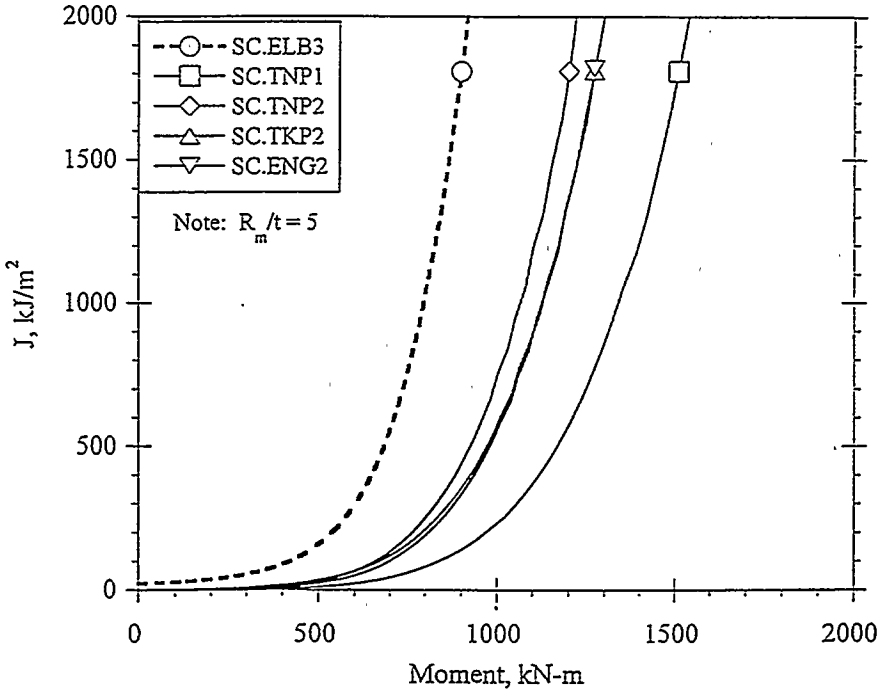

(a) $R_m/t = 5$

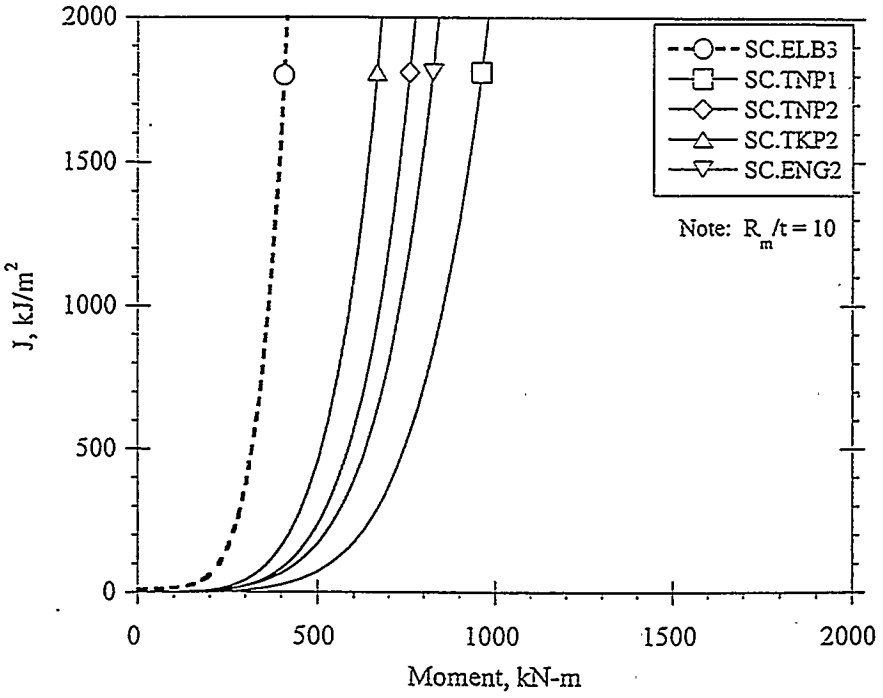

(b) $R_m/t = 10$

Figure 4.26 Comparison of applied J versus moment for the axially-cracked SC.ELB3 elbow analysis and four straight pipe analyses (SC.TNP1, SC.TNP2, SC.ENG1, and SC.ENG2)

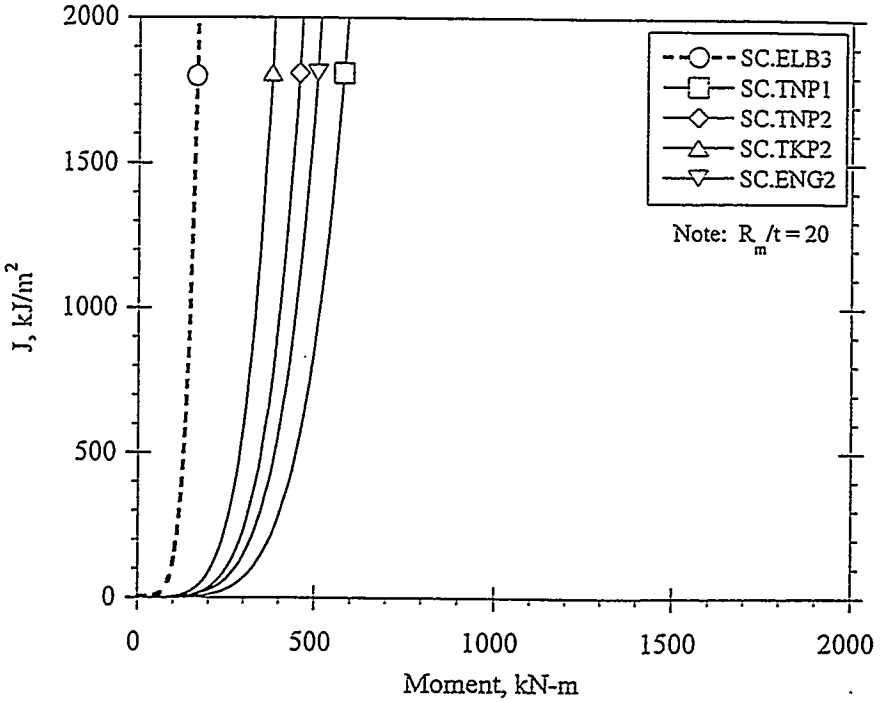

(c) $R_m/t = 20$

Figure 4.26 (Continued)

Only the SC.TNP1 and SC.TNP2 analyses were used in the following comparisons. (The NRCPIPES code Version 3.0 was used for the straight pipe analyses, and IP2ELBOW code Version 1.0 was used for the elbow analyses.)

The next step was to construct the ratio of the moments for the straight pipe to those for the elbow at the same J values, i.e., $(M^{pipe}/M^{elbow})|_J$. The variation of this ratio with applied J is illustrated in Figure 4.27. A key aspect is that after some plasticity occurs this moment ratio becomes a constant.

In the elastic range, it can be seen that there are different trends for the three R_m/t cases. These different trends in the transition from the elastic to plastic behavior with different R_m/t values are due to the inaccuracy of the straight pipe elastic f-function that is generally used.

Finally, in Figure 4.27 it should be noted that the plastic part of J dominates the moment ratio for $J_{applied}$ values of generally greater than 100 kJ/m^2 (570 in-lb/in^2) which bounds the toughness range of typical nuclear piping materials, except perhaps some aged CF8M steels.

The next step was to compare these moment ratios with the stress indices for the elbows. Since the elbow was under bending, we used the B_2 and C_2 indices. The B_2 index is for primary bending stresses to avoid failure by collapse (using the design stress analysis definition of limit load). The C_2 stress index is for primary and secondary bending stresses also to avoid collapse. It should be noted that these stress indices essentially give stress multipliers for the location in the piping product where the stresses are the highest. For the case of an elbow under bending, the stresses are the highest along the flank of the elbow normal to the axial direction, i.e., the flaw location for this evaluation. Equations 4-12 and 4-13 give the B_2 and C_2 stress indices, respectively. These equations came from Section III, Article NB-3683.7 of the ASME Boiler and Pressure Vessel Code.

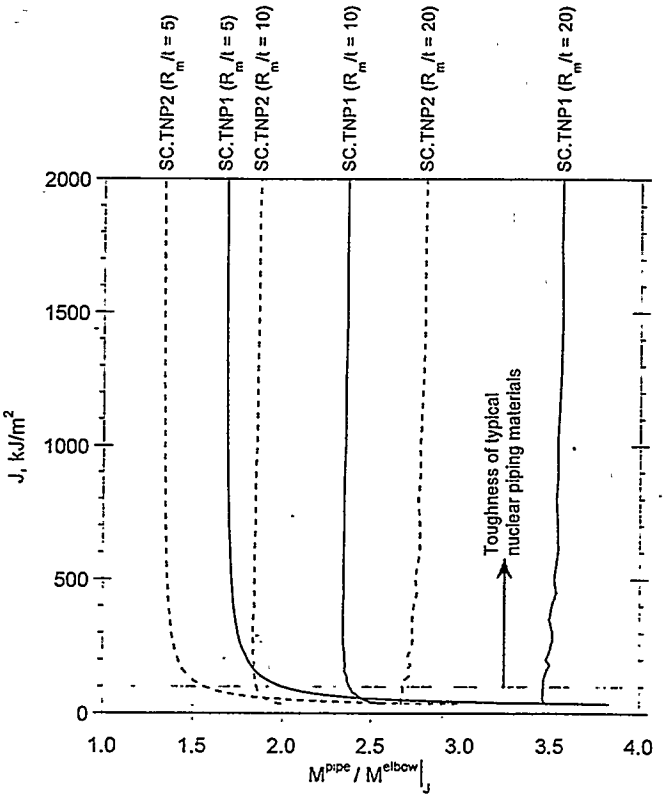

Figure 4.27 The applied J as a function of the ratio of moments for the straight pipe to moments for an axial-flank-cracked elbow

$$B_2 = 1.3/h^{2/3} \tag{4-12}$$

with B_2 not less than 1.0, and

$$C_2 = 1.95/h^{2/3} \tag{4-13}$$

with C_2 not less than 1.5, and

$$h = tR_{el}/R_m^{\,2} \tag{4-14}$$

These equations assume the elbows have a perfectly circular cross-section, which was a condition in the development of the SC.ELB3 J-estimation scheme.

Figure 4.28 shows a comparison of the $(M^{pipe}/M^{elbow})|_J$ values with the B_2 and C_2 stress indices. Several aspects need to be pointed out in this figure.

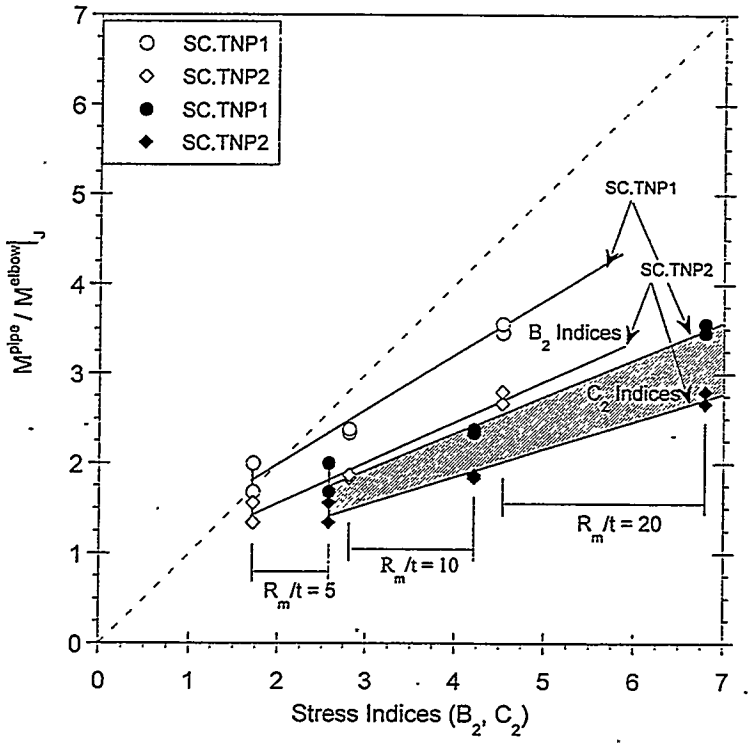

Figure 4.28 Ratio of the moments for the straight pipe to moments for an axial-flank-cracked elbow as a function of the stress indices B_2 and C_2

- First and most importantly, the linear scatter bands show that the stress indices are greater than $(M^{pipe}/M^{elbow})|_J$ values, hence using the straight pipe solution with the stress indices will underpredict the moment-carrying capacity of the flawed elbow at the same $J_{applied}$ value in the straight pipe.

- Secondly, it can be seen that there is a linear trend of the B_2 or C_2 stress indices with $(M^{pipe}/M^{elbow})|_J$ values, and that using the B_2 indices gives a closer agreement to the 1:1 line.

- Thirdly, for each of the scatter bands, the upper bound occurred when using the SC.TNP1 straight pipe analyses, and the lower bound to the scatter band occurred when using the SCTNP2 straight pipe analyses. (Using the SC.TNP1 analysis gives closer agreement to the 1:1 line.),

- Finally, the range of scatter in the moment ratio for J values of 100 to 2,000 kJ/m^2 (570 to 11,430 in-lb/in^2) is reflected by the symbols with the lines between them, or the touching symbols of the same type.

To further validate the use of this failure avoidance approach, comparisons were made with experimental data. Although there are limited experimental results for axial, flank, surface cracks in elbows where there is good documentation of all of the pertinent variables, there are a few experiments sufficiently documented. One such experiment was an elbow experiment conducted by Electricité de France (EDF) (Ref. 4.36). The experimental conditions for this experiment are given in Table 4.16. Although this was a long-radius elbow experiment and the strain-hardening exponent (n) is similar to that used in developing Figure 4.28, some key differences between this experiment and the conditions in the analyses used to develop Figure 4.28 were:

Table 4.16 Parameters in EDF axial, flank, surface-cracked, elbow Experiment Y6135

Variable	Experimental Data
Diameter, mm (inch)	580 (22.8)
Thickness, mm (inch)	44.0 (1.73)
R_m/t	6.6
Crack length, mm (inch)	210 (8.27)
Flaw depth-to-thickness (a/t)	0.26
Yield and reference stress, $\sigma_y=\sigma_o$, MPa (ksi)	321 (46.6)
Ultimate strength, MPa (ksi)	743 (107.8)
Strain-hardening exponent (n)	4.062
Elastic modulus(1), GPa (ksi)	188.8 (27,400)
J_{Ic}, kJ/m^2 (in-lb/in^2)	56 (320)
Internal pressure, MPa (psi)	15.5 (2,250)
Moment at crack initiation, kN-m (in-kips)	2,250 (19,900)

(1) Reference strain in Ramberg-Osgood analyses equal to reference stress divided by elastic modulus.

(1) the crack length was slightly shorter, 26.7 degrees around the circumference versus 30 degrees in the analyses for Figure 4.28,

(2) the crack depth was much shallower, a/t of 0.24 versus 0.5 for the analyses used to create Figure 4.28, and

(3) the toughness was 56 kJ/m^2 (320 in-lb/in^2) which is lower than the 100 kJ/m^2 (570 in-lb/in^2) lower bound used in creating Figure 4.28.

Calculations were made with the SC.TNP1 and SCTNP2 straight pipe analysis methods to get the M^{pipe} value at crack initiation, and the experimental moment at crack initiation was used for the M^{elbow} value. The experimental moment ratio values along with the failure avoidance criterion are shown in Figure 4.29. Considering the large differences in material properties and flaw sizes, the agreement is remarkably good. This evaluation shows that this methodology is promising for the case of an axial surface crack in an elbow.

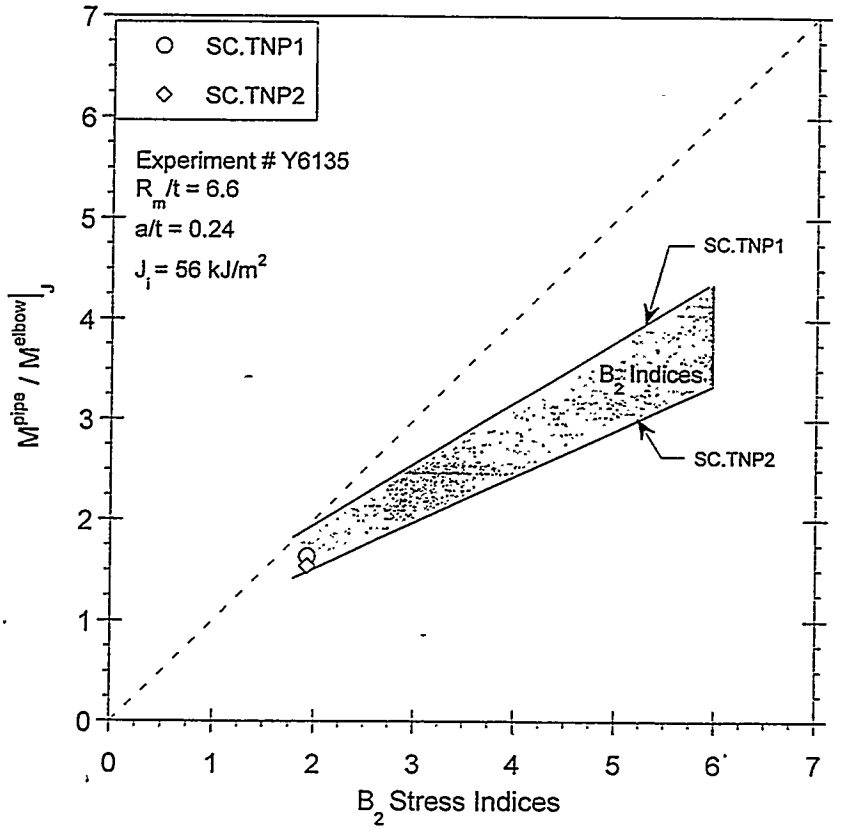

Figure 4.29 Ratio of the moments for the straight pipe to moments for an axial-flank-cracked elbow as a function of the stress indices B_2 and C_2 with the experimental data for EDF Experiment Y6135 shown for comparison

4.5.1.2 Circumferential Surface Crack Centered on the Extrados of an Elbow

The development of the failure avoidance criterion for a circumferential crack centered along the extrados of an elbow, is parallel to that for the elbow axial crack. Some noteworthy differences are:

(1) For the circumferential crack in the elbow, the peak J value is at 45 degrees from the center of the crack, whereas for a straight pipe, the peak J value is at the center of the crack. These differences are accounted for in the J-estimation schemes used.

(2) The B_2 and C_2 indices are stress multipliers for the location corresponding to the flank (side or crown) of the elbow, however the peak driving force for the crack does not occur at this location. Hence, it is logical to expect that the stress indices would be less sensitive to the moment ratios at constant J values than were the moment ratios derived for the axial flank surface crack case.

SC.ENG1, and SC.ENG2)

ANALYSIS OF EXPERIMENTS Section 4

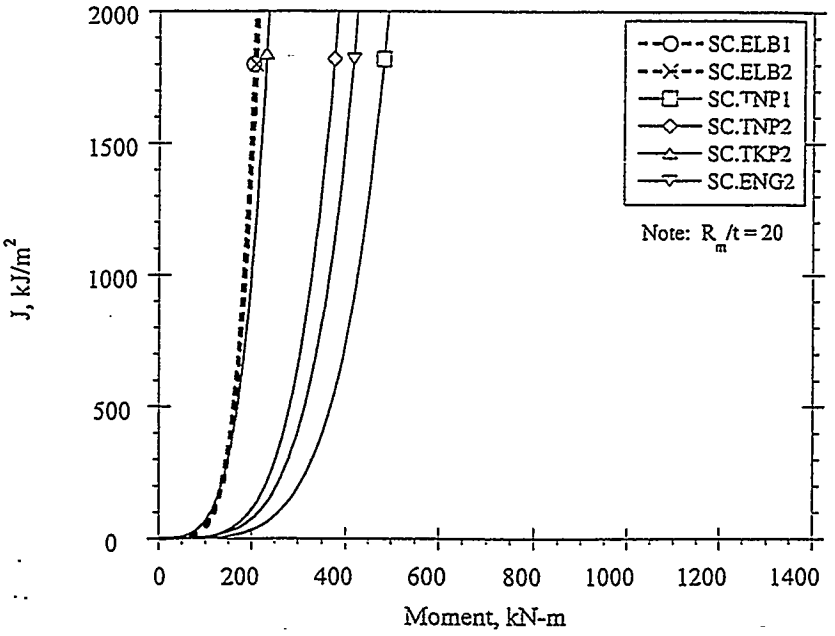

(c) $R_m/t = 20$

Figure 4.30 (Continued)

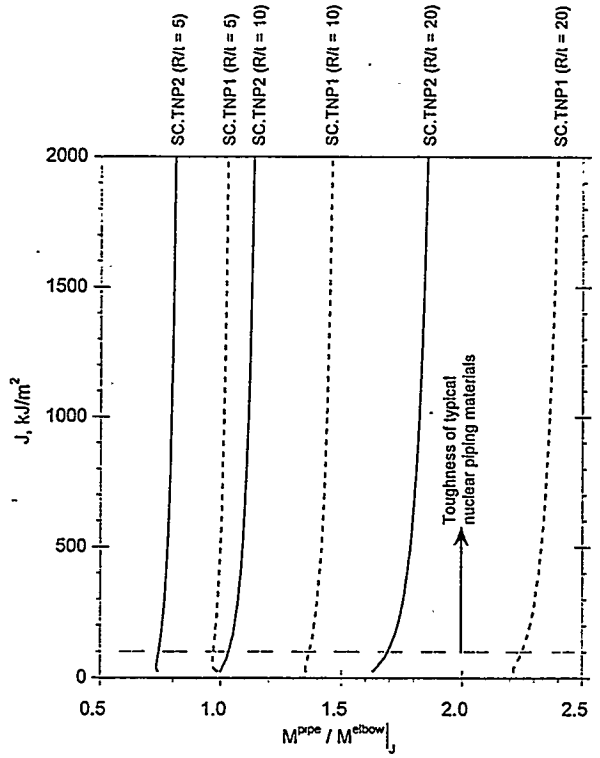

(a) Using the SC.ELB1 analysis

Figure 4.31 The applied J as a function of the ratio of moments for the straight pipe to moments for a circumferentially cracked elbow

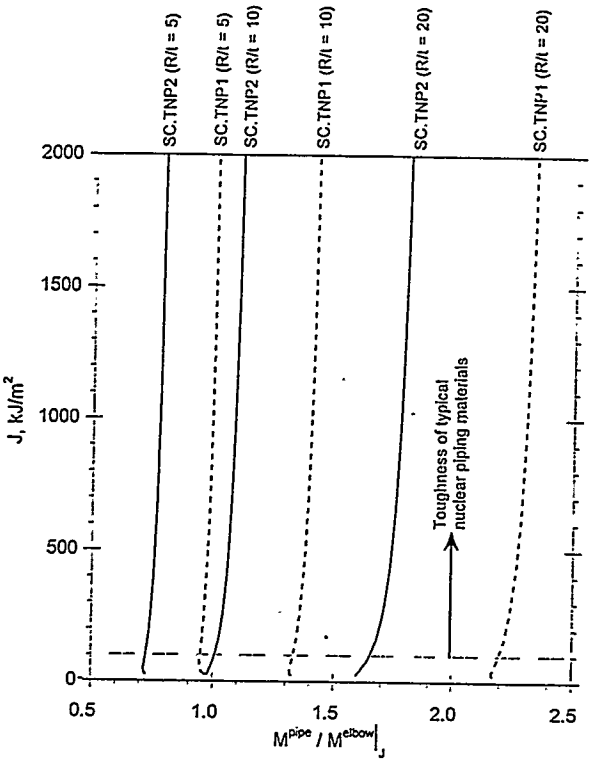

(b) Using the SC.ELB2 analysis

Figure 4.31 (Continued)

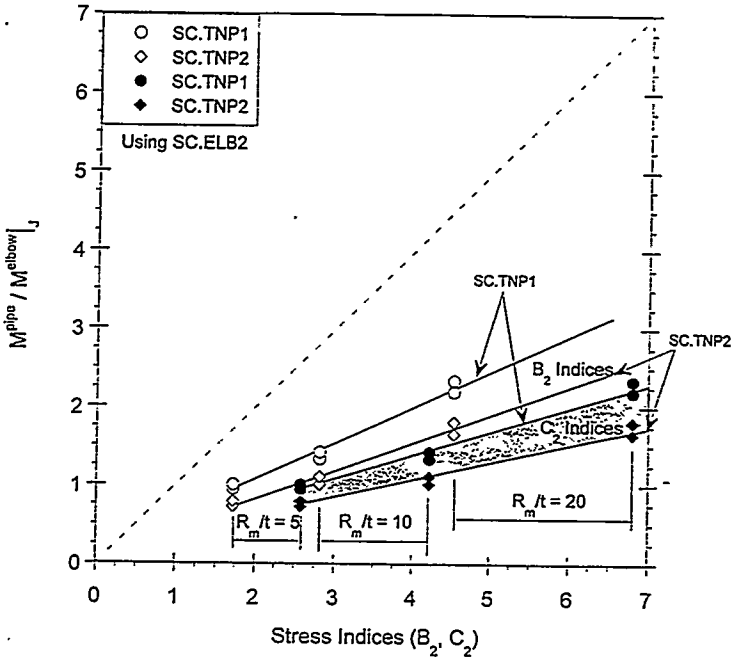

(a) Using the SC.ELB1 analysis

Figure 4.32 Ratio of the moments for the straight pipe to moments for a circumferentially cracked elbow as a function of the stress indices B_2 and C_2

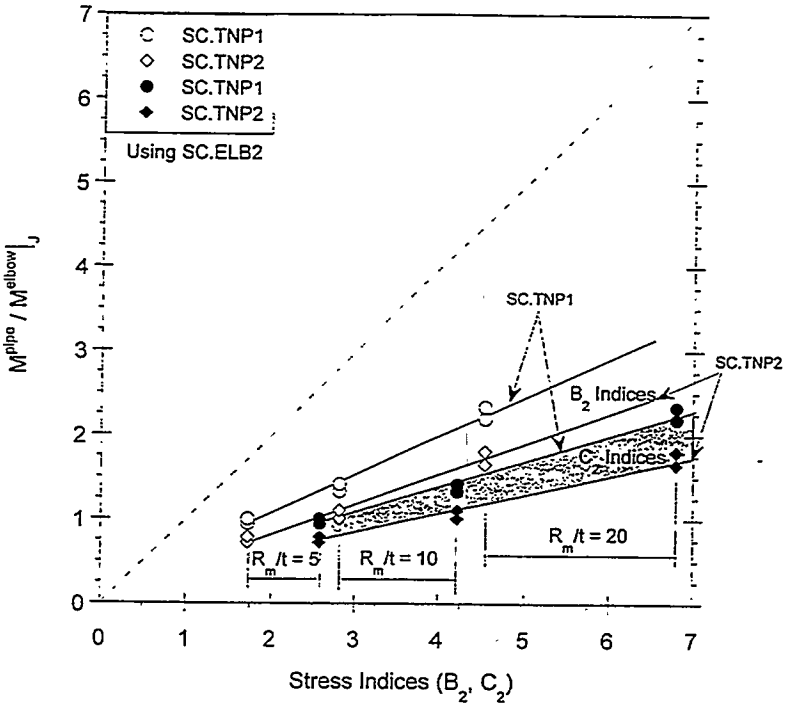

(b) Using the SC.ELB2 analysis

Figure 4.32 (Continued)

To further validate the use of this failure avoidance approach for circumferential elbow cracks, it was desirable to compare this approach with the IPIRG-2 elbow experimental data discussed earlier in this report. The experimental conditions used in the analyses are given in Table 4.17. There were four experiments conducted, two on A106-90 (Grade B) elbows and two on stainless steel WP304L elbows.

For each material, a companion quasi-static bend and a pipe-system experiment were conducted. These experimental conditions were close to the same assumptions used in the analyses to develop the "elbow circumferential flaw failure avoidance" curve. The differences between these experiments and the analyses used to develop Figures 4.32a and 4.32b were:

(1) The crack depths for the experiments were deeper than those used in the development of the analyses shown in Figures 4.32a and 4.32b.

(2) The elbows in these experiments started with some known out-of-roundness. This out-of-roundness was not accounted for in the B_2 value since in reality this value may not be known. (The French cast elbow tests discussed in the axial elbow tests had no significant out-of-roundness.)

Table 4.17 Parameters in IPIRG-2 circumferential, extrados, surface-crack, elbow experiments

Variable	Experimental Values			
IPIRG-2 Experiment Number	2-1	2-2	2-3	2-4
Material	A106 B	A106 B	WP304L	WP304L
Diameter, mm (inch)	409 (16.1)	406 (16.0)	409 (16.1)	406 (16.0)
Thickness, mm (inch)	32.1 (1.263)	32.0 (1.26)	33.2 (1.31)	33.0 (1.30)
R_m/t	5.9	5.8	5.7	5.7
Crack length, mm (inch)	531 (20.9)	537 (21.1)	536 (21.1)	534 (21.0)
Flaw depth-to-thickness (a/t)	0.84	0.80	0.73	0.77
Yield and reference stress, $\sigma_y = \sigma_o$, MPa (ksi)	208 (30.2)	208 (30.2)	200 (29.0)	200 (29.0)
Ultimate strength, MPa (ksi)	450 (65.2)	450 (65.2)	408 (59.2)	408 (59.2)
Strain-hardening exponent (n)	4.421	4.421	3.981	3.981
Elastic modulus(1), GPa (ksi)	196.5 (28,500)	196.5 (28,500)	182.7 (26,500)	182.7 (26,500)
J_{Ic}, kJ/m^2 (in-lb/in^2)	373 (2,130)	402 (2,300)	1,380 (7,860)	1,060 (6,065)
Internal pressure, MPa (psi)	15.5 (2,250)	15.5 (2,250)	15.5 (2,250)	15.5 (2,250)
Moment at crack initiation, kN-m (in-kips)	562 (4,970)	593 (5,250)	601 (5,320)	536 (4,745)

(1) Reference strain in Ramberg-Osgood analyses equal to reference stress divided by the elastic modulus.

(3) The stainless steel elbow had a much lower strain-hardening exponent than used in creating Figures 4.32a and 4.32b, but the toughness was much higher than the 100 kJ/m^2 (570 kJ/m^2) lower-bound limit used in creating Figures 4.32a and 4.32b. (The carbon steel elbow had the same strain-hardening exponent as used in creating Figures 4.32a and 4.32b, and the toughness was above the 100 kJ/m^2 (570 kJ/m^2) lower-bound limit used.)

Calculations were made with the SC.TNP1 and SCTNP2 straight pipe analysis methods and with the SC.ELB2 surface-cracked elbow method to get the M^{pipe} values at crack initiation, and the experimental moments at crack initiation were used for the M^{elbow} values. The experimental moment ratio values are shown in Figure 4.33 in comparison to the scatter band from the analyses predictions and the 1:1 failure

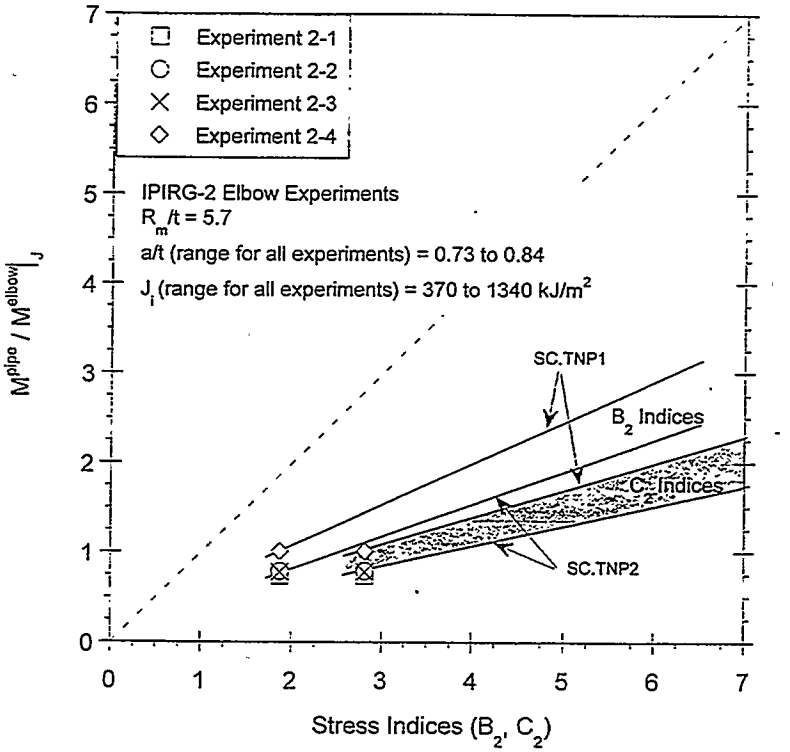

Figure 4.33 Ratios of moments for the straight pipe to moments for a circumferentially cracked elbow as a function of the stress indices B_2 with the IPIRG-2 elbow experimental data shown for comparison

avoidance criteria. As in the axial elbow crack case, the agreement is remarkably good with the calculated scatter bands, however, in this case there is more conservatism if the 1:1 line is assumed in the failure avoidance criterion.

4.6 References

4.1 Wilkowski, G. M., and others, "Degraded Piping Program - Phase II, Summary of Technical Results and Their Significance to Leak-Before-Break and In-Service Flaw Acceptance Criteria," March 1984 - January 1989, NUREG/CR-4082, Vol. 8, March 1989.

4.2 Scott, P., and others, "The IPIRG-1 Pipe-System Fracture Tests: Experimental Results," PVP Vol. 280, pp 135-151, June 1994.

4.3 Scott, P., and others, "The Effect of Dynamic and Cyclic Loading During Ductile Tearing on Circumferentially Cracked Pipe: Experimental Results," PVP Vol. 280, pp 207-220, June 1994.

4.4 Kanninen, M. F., and others, "Instability Predictions for Circumferentially Cracked Type 304 Stainless Steel Pipes Under Dynamic Loadings," EPRI Report NP-2347, April 1982.

4.5 Kanninen, M. F., and others, "Mechanical Fracture Predictions for Sensitized Stainless Steel Piping with Circumferential Cracks," Final Report, EPRI NP-192, September 1976.

4.6 Wilkowski, G. M., and Scott, P. M., "A Statistical Based Circumferentially Cracked Pipe Fracture Mechanics Analysis for Design or Code Implementation," *Nuclear Engineering and Design*, Vol. 111, pp 173-187, 1989.

4.7 Kumar, V., German, M., and Shih, C., "An Engineering Approach for Elastic-Plastic Fracture Analysis," EPRI Report NP-1931, July 1981.

4.8 Klecker, R., Brust, F., and Wilkowski, G., "NRC Leak-Before-Break (LBB.NRC) Analysis Method for Circumferentially Through-Wall-Cracked Pipe Under Axial Plus Bending Loads," NUREG/CR-4572, May 1986.

4.9 Brust, F. W., "Approximate Methods for Fracture Analyses of Through-Wall Cracked Pipes," NUREG/CR-4853, February 1987.

4.10 Scott, P., and Ahmad, J., "Experimental and Analytical Assessment of Circumferentially Surface-Cracked Pipes Under Bending," NUREG/CR-4872, April 1987.

4.11 Krishnaswamy, P., and others, "Fracture Behavior of Short Circumferentially Surface-Cracked Pipe," NUREG/CR-6298, November 1995.

4.12 ASME Boiler and Pressure Vessel Code, Section XI, Appendix C, 1995 Edition, July 1995.

4.13 "Evaluation of Flaws in Austenitic Steel Piping," (Technical basis document for ASME IWB-3640 analysis procedures), prepared by Section XI Task Group for Piping Flaw Evaluation, EPRI Report NP-4690-SR, April 1986.

4.14 ASME Boiler and Pressure Vessel Code, Section XI, Appendix H, 1995 Edition, July 1995.

4.15 "Evaluation of Flaws in Ferritic Piping," EPRI Report NP-6045, prepared by Novetech Corporation, October 1988.

4.16 ASME Boiler and Pressure Vessel Code, Code Case N-494-2, 1992 Edition, Supplement No. 8, July 1992.

4.17 Bloom, J. M., and Malik, S. N., "A Procedure for the Assessment of Integrity of Structures Containing Defects," EPRI Report NP-2431, June 1982.

4.18 Milne, I., Ainsworth, R. A., Dowling, A. R., and Stewart, A. T., "Assessment of the Integrity of Structures Containing Defects," CEGB Report R/H/R6 - Revision 3, 1986.

4.19 Milne, I., Ainsworth, R. A., Dowling, A. R., and Stewart, A. T., "Background to and Validation of CEGB Report R/H/R6 - Revision 3," January 1987.

4.20 Kurihara, R., Ueda, S., and Sturm, D., "Estimation of the Ductile Unstable Fracture of Pipe with a Circumferential Surface Crack Subjected to Bending," *Nuclear Engineering and Design*, Vol. 106, pp 265-273, 1988.

4.21 Wilkowski, G. M., and others, "Short Cracks in Piping and Piping Welds - Seventh Program Report: March 1993 - December 1994," NUREG/CR-4599, Vol. 4, No. 1, January 1995.

4.22 Kumar, V., and others, "Advances in Elastic-Plastic Analysis," EPRI Final Report NP-3607, August 1984.

4.23 Brust, F., Rahman, S., and Ghadiali, N., "Elastic-Plastic Analysis of Small Cracks in Tubes," Proceedings of the 11th International Conference on Offshore Mechanics and Arctic Engineering, Calgary, Alberta, Canada, June 1992.

4.24 Brust, F. W., and others, "Assessment of Short Through-Wall Circumferential Cracks in Pipes," NUREG/CR-6235, April 1995.

4.25 Paris, P. C., and Tada, H., "The Application of Fracture Proof Design Methods Using Tearing Instability Theory to Nuclear Piping Postulating Circumferential Through-Wall Cracks," NUREG/CR-3464, September 1983.

4.26 Gilles, P., and Brust, F., "Approximate Fracture Methods for Pipes - Part I: Theory," *Nuclear Engineering and Design*, Vol. 127, pp 1-27, 1991.

4.27 Gilles, P., Chao, K. S., and Brust, F., "Approximate Fracture Methods for Pipes - Part II: Applications," *Nuclear Engineering and Design*, Vol. 127, pp 13-31, 1991.

4.28 Brust, F. W., and Gilles, P., "Approximate Methods for Fracture Analysis of Tubular Members Subjected to Combined Tensile and Bending Loads," ASME, *Journal of Offshore Mechanics and Arctic Engineering*, Vol. 116, pp 221-227, November 1994.

4.29 Kanninen, M., and Popelar, C., *Advanced Fracture Mechanics*, Oxford University Press, New York, 1985.

4.30 Mohan, R., Brust, F. W., and Ghadiali, N., "Development of a J-Estimation Scheme for Internal Circumferential and Axial Surface Cracks in Elbows," NUREG/CR-6445, June 1996.

4.31 Krishnaswamy, P., and others, "Fracture Behavior of Short Circumferential Surface-Cracked Pipe," NUREG/CR-6298, BMI-2183, November, 1995.

4.32 Rudland, D. L., Scott, P. M., and Wilkowski, G. M., "The Effect of Cyclic and Dynamic Loads on Carbon Steel Pipe," NUREG/CR-6438, February 1996.

4.33 Mohan, R., Marschall, C., Krishnaswamy, P., Brust, F., Ghadiali, N., and Wilkowski, G., "Effects of Toughness Anisotropy and Combined Loading on Fracture Behavior of Ferritic Nuclear Pipe," NUREG/CR-6299, April 1995.

4.34 Wilkowski, G. M., and others, "The Effect of Dynamic and Cyclic Loading During Ductile Tearing on Circumferentially Cracked Pipe: Analytical Results," PVP Vol. 280, pp 221-239, June 1994.

4.35 Scott, P., Olson, R., and Wilkowski, G., "The IPIRG-1 Pipe-system Fracture Tests: Analytical Results," PVP Vol. 280, pp 153-163, June 1994.

4.36 LeDelliou, P., Semete, P., and Ignaccolo, J., "Fracture Mechanics Analysis of Cast Duplex Stainless Steel Elbows Containing a Surface Crack," 1996 ASME PVP Conference, *Fatigue and Fracture - 1996*, Vol. MF-1, July 1996.

5.0 ADDITIONAL TECHNICAL DEVELOPMENTS AND ANALYSES

This section of the report describes efforts undertaken to address issues supporting the scope of the main program. Topics discussed are:

- Development and improvements of computer codes,
- Development and improvements of databases,
- Uncertainty analyses, and
- Comparison of pretest ultrasonic examination of test flaws with post-test measurements.

5.1 Development and Improvement of Computer Codes

During the course of the IPIRG-2 program, several computer codes were improved or developed. These computer codes were:

- NRCPIPE - Version 3.0 for Windows,
- NRCPIPES - Version 3.0 for Windows,
- IP2ELBOW - Version 1.0 for Windows, and
- SQUIRT - Version 2.4 for DOS.

A brief description of the codes and the work that was done on them is provided below.

5.1.1 NRCPIPE - Version 3.0 for Windows

The NRCPIPE code conducts limit-load and elastic-plastic fracture analyses for circumferentially through-wall-cracked pipe. This code was originally developed as a DOS-based program during the Degraded Piping Program - Phase II, (Ref. 5.1) and was improved during the NRC's Short Cracks in Piping and Piping Welds program (Ref. 5.2). The work in the Short Cracks in Piping and Piping Welds program involved making several technical and user-interface changes to the DOS version (Version 2.0). This version, Version 2.0, is available through the Energy Science and Technology Software Center (P.O. Box 1020, Oak Ridge, TN 37831). The effort in the IPIRG-2 program consisted of porting the program to the Windows environment and making some minor technical improvements.

The analysis procedures currently in NRCPIPE include:

- The original Net-Section-Collapse (limit-load) analysis (Ref. 5.3),
- The Battelle Dimensionless Plastic-Zone Parameter (DPZP) analysis (Ref. 5.4),

- The R6 Revision 3 Option 1 analysis (Ref. 5.5),
- The GE/EPRI method with the following options:
  - Original GE/EPRI method with the plastic-zone correction in the elastic term (Ref. 5.6),
  - The GE/EPRI method without the plastic-zone correction in the elastic term (Ref. 5.7),
  - The Zahoor-modified GE/EPRI method with a modification on α in the J_p term (Ref. 5.8), and
  - The original GE/EPRI method with Battelle-revised F and h function values (Ref. 5.9),
- The LBB.NRC method (Ref. 5.10),
- The Battelle LBB.ENG2 method (Ref. 5.7), and
- The Battelle LBB.GE method (Ref. 5.7).

Improvements made to the NRCPIPE code as part of the IPIRG-2 program include the following:

- The code was put into a Windows 3.1 format. This makes the code easier to use, i.e., input changes can now readily be made for sensitivity studies. Also, help commands and instructions from the manual were implemented in the user interface.
- Several technical changes were made:
  - In the R6, Revision 3, Option 1 method, the cut-off stress ratio can now be calculated with new options. The past options were: (1) to use the cut-off stress ratio recommendations in the R6 manual (i.e., 1.25 for mild steel welds or 1.8 for austenitic steels), (2) to use the ratio of the flow stress to yield strength (flow stress = average of yield and ultimate strengths), or (3) any user-defined option. The new cut-off stress ratio option is to use the ratio of the Net-Section-Collapse stress using the flow strength to the Net-Section-Collapse stress using yield stress. This new option makes the limit-load results from the R6 method agree with the Net-Section-Collapse analysis for the case of combined loading. In the new version, the user-defined cut-off stress ratio option has been eliminated.
  - In the Original GE/EPRI method, the plastic-zone correction term now automatically uses yield strength, whereas in the past, this was an option for the user.

The new version is called NRCPIPE Version 3.0 for Windows.

5.1.2 NRCPIPES - Version 3.0 for Windows

The NRCPIPES code conducts limit-load and elastic-plastic fracture analyses for circumferentially surface-cracked pipe. It was originally developed during the Degraded Piping Program - Phase II (Ref. 5.11) for

use on a VAX computer, and was improved during the NRC's Short Cracks in Piping and Piping Welds program (Ref. 5.12) and made into a DOS-based PC program. The present effort involved porting the program to the Windows environment and making some minor technical improvements. Version 2.0a, the DOS version, is available through the Energy Science and Technology Software Center (P.O. Box 1020, Oak Ridge, TN 37831).

There are few analysis methods available for predicting loads and displacements for finite-length circumferential surface-cracked pipes. The analysis procedures in NRCPIPES are:

- The original Net-Section-Collapse (limit load) analysis (Ref. 5.3),
- The Battelle Dimensionless Plastic-Zone Parameter (DPZP) analysis (Ref. 5.4),
- The R6 Revision 3 Option 1 analysis (Ref. 5.5),
- ASME Section XI pipe flaw evaluation procedures (1995 edition),
  - Section XI Appendix C for austenitic pipe (including changes on a/t limits and use of actual pipe diameter in the Z-factor austenitic weld calculations, approved as of March 1996, but not published at that time),
  - Section XI Appendix H for ferritic pipe,
  - Code Case N-494-2 analysis method for ferritic pipe, as well as the austenitic pipe flaw evaluation criteria accepted at the March 1996 Section XI meeting, but not published at that time (to be Code Case N-494-3),
- The Battelle SC.TNP1 and SC.TNP2 analyses (Ref. 5.12),
- The Battelle SC.TKP1 and SC.TKP2 analyses (Ref. 5.12), and
- The Battelle SC.ENG1 and SC.ENG2 analyses (Ref. 5.12).

During the IPIRG-2 program, the following improvements were made to the NRCPIPES code:

- The code was put into a Windows 3.1 format. This makes the code more user friendly, e.g., input changes can readily be made for sensitivity studies. Help commands and instructions from the manual were implemented in the user interface.
- Technical changes include the following:
  - In the R6, Revision 3, Option 1 method, the cut-off stress ratio can now be calculated with a new option. In the past, the options were: (1) to use the cut-off stress ratio recommendations in the R6 manual (i.e., 1.25 for mild steel welds or 1.8 for austenitic steels), (2) to use the ratio of the flow stress to yield strength (flow stress = average of yield and ultimate strengths), or (3) any user-defined option. The new cut-off stress ratio option is to use the ratio of the Net-Section-Collapse stress using the flow stress to the

Net-Section-Collapse stress using the yield strength. This new option makes the limit-load results from the R6 method agree with the Net-Section-Collapse analysis for the case of combined loading. The user-defined cut-off stress ratio option has been eliminated.

- The new a/t limits and pipe diameter limits in the Z-factor equation approved in March 1996 were included.

- The austenitic pipe criteria for Code Case N-494-3 were included.

The latest version of NRCPIPES is called NRCPIPES Version 3.0 for Windows.

5.1.3 IP2ELBOW - Version 1.0 for Windows

The IP2ELBOW program is a J-estimation scheme for predicting surface-crack behavior for elbows that was written as a result of analytical developments from the IPIRG-2 program. These efforts are described in Section 4.5 of this report and in Reference 5.13. The analysis method developed is applicable to both axial and circumferential surface cracks in elbows under in-plane bending (elbow bent in closing mode).

The IP2ELBOW methodology follows the pattern of the GE/EPRI estimation scheme, in which elastic F-functions and fully plastic h-functions were developed to predict cracked pipe response. The elbow F- and h-functions were implemented in the Windows version of NRCPIPES. Hence, the user interface features of NRCPIPE, NRCPIPES, and IP2ELBOW are all similar.

Development of J-estimation schemes for cracked elbows is quite a new pipe fracture effort. As a consequence, IP2ELBOW is limited in scope. The technical limitations for the code are as follows:

- It is for elbows where the R_m/t ratio of the attached straight pipe is from 5 to 20.

- The elbows have a bend radius of 1.5 times the pipe diameter.

- The elbows are loaded in pure bending or combined pressure and bending with the restriction that the hoop stress be at the ASME Code S_m magnitude. (This is typical for U.S. plants, but probably is inconsistent with German and Japanese use of high-strength carbon steels.)

- The elbows are loaded by in-plane bending in the closing mode.

- For the circumferential surface crack case, the crack is centered on the extrados, and is on the inside surface. Solutions are limited to a crack length of half of the elbow circumference.

- For the axial surface crack case, the crack is along the flank (side) of the elbow, and is on the inside surface. Solutions are limited to a crack length of 30 degrees.

- Solutions for both circumferential and axial cracks were developed for a/t values of 0.25 to 0.75 and strain-hardening values of 1 to 10.

The current revision of the IP2ELBOW computer program is called Version 1.0 for Windows.

5.1.4 SQUIRT - Version 2.4 for DOS

The SQUIRT code is a leak-rate analysis code used for leak-before-break (LBB) analyses. It was originally developed during the IPIRG-1 program (Ref. 5.14.) as a DOS program and was improved during the NRC's Short Cracks in Piping and Piping Welds program (Ref. 5.15). At the completion of the Short Cracks in Piping and Piping Welds program, the code was made available through the Energy Science and Technology Software Center (P.O. Box 1020, Oak Ridge, TN 37831) as Version 2.3. Further improvements to the DOS version to bring it to Version 2.4 were made in the IPIRG-2 program.

There are several modules to SQUIRT. These modules are:

- SQUIRT1, which performs crack-opening displacement analyses for a circumferential through-wall crack in a pipe under pressure and bending loading.
- SQUIRT2, which performs leak-rate calculations for a given crack-opening shape and thermal-hydraulic conditions.
- SQUIRT3, which performs leak-rate predictions for a pipe with a given flaw size, thermal-hydraulic condition, and pressure loading for various bending loads up to the maximum load.
- SQUIRT4, which performs the first step in an LBB analysis, i.e., it calculates the crack size, when the leak rate is given for a pipe with a specific size, pressure and bending loads, and thermal hydraulic condition.

Improvements made to the new version of SQUIRT (Version 2.4) include the following:

- Instructions for data input more clearly note limitations of the code:
  - SQUIRT was originally written for two-phase flow through a crack and subsequently a single-phase all-liquid flow model for very large cracks was added. Because of the large crack limitation for the single-phase flow mode, the transition from single-phase liquid flow to two-phase flow leak-rates is not smooth. A warning message in this transition region is now printed with the output.
  - All of the crack flow models basically use the Henry-Fauske two-phase flow model with the Von Karman friction factor equation, but perhaps with different constants in the Von Karman equation, i.e., the Nikuradse or John et al. constants. Because this is an empirical equation, it is not applicable for all conditions. In particular, the validity of the friction factor equation is questionable when the crack-opening displacement (COD) approaches the value of the surface roughness. The SQUIRT code (Version 2.4) now prints out a warning message when the user is getting results outside the range of validation for the friction factor equation. The SQUIRT2 module displays this warning message and gives the user several options for redefining the roughness, friction factor, etc. The SQUIRT3 and SQUIRT4 modules, being iterative in nature, display the warning at each iteration and also at the end of the iterations, but do not allow the user to change any values during iterations. Improvements to the SQUIRT code in the tight crack region are suggested in Reference 5.15

where the roughness and number of turns become dependent on the COD. However, this COD-dependent crack morphology model is not incorporated into Version 2.4 of SQUIRT. (See discussion in Section 5.3.1.2 of this report.)

- The default values of surface roughness and number of turns were changed in SQUIRT Version 2.4. The Version 2.3 default values were not based on service experience and were input merely for a sample calculation. The Version 2.4 values are significantly different from the Version 2.3 default values. The Version 2.4 default values come from average values of statistical evaluations of cracks removed from service (Ref. 5.15). Service cracks are typically much rougher than fatigue cracks grown in air, and hence, there is a large difference in the calculated leak-rate values from an IGSCC or corrosion-fatigue crack than a fatigue crack grown in air.

- The manual for Version 2.4 was changed so that the example figures clearly indicate that the experimental crack morphology values from specific experiments were used to calculate the leak-rate values, not the new default crack morphology values. A sensitivity study showing the change in leak rate caused when different crack morphology default values are used (SQUIRT Version 2.3 and 2.4 and PICEP Version 4.0) is given in Section 5.3.1.1 of this report.

5.1.5 QA of Computer Programs

None of the software packages discussed above were written in accordance with nuclear QA requirements. Rather, the codes are research tools developed for Battelle internal use that eventually were distributed to the NRC and IPIRG TAG members. Although none of the codes have been through a rigorous nuclear QA, they have been compared with other similar codes or experimental data, which is an acceptable QA procedure. NRCPIPE has been compared to numerous pipe experiments during the last nine years, has been used in round-robin calculations, has been compared against spreadsheet results from separate programs, has been checked against hand calculations in ASME Section XI Pipe Flaw Evaluation Working Group analysis efforts, and has been used in thousands of sensitivity calculations. The experience with NRCPIPES has been similar to the experience with NRCPIPE, except that it has only been in use for five years. IP2ELBOW is a new program and so there is less user experience when compared with the NRCPIPE and NRCPIPES codes. It has been compared with the IPIRG-2 elbow experiments and an EDF axial crack elbow experiment, and has been used for a few sensitivity studies. The QA on SQUIRT has consisted of comparisons with experimental data (using experimentally measured crack morphology parameters and not the default values), comparison with other leak rate codes, and a favorable comparison with a coding of the SQUIRT equations by VTT Energy in Finland*.

In general, Battelle has high confidence that the equations implemented in the NRCPIPE, NRCPIPES, and SQUIRT codes are as defined in the manuals, reference papers, and background reports. Analyses with these programs have been shown to give good predictions when compared with experimental data. Because it is so new, the IP2ELBOW code results should be checked with some hand calculations if the analysis is for plant applications.

---

* Miettnen, J., and others, "A Thermal Hydraulic Modelling for Leak-Before-Break Applications," PVP Vol. 323, Fatigue and Fracture - 1996 - Vol. 1, pp 233-240, 1996.

5.2 Development and Improvements of Databases

A number of pipe fracture databases were either made available to the fracture community, created, or improved during the course of this program. These databases are:

- AXIALCK,
- CIRCUMCK,
- ELBOWCK,
- TEECK, and
- PIFRAC.

The first four of these databases deal with full-scale pipe and fitting experimental fracture data, and are in spreadsheet format, i.e., Lotus® 1-2-3. The PIFRAC database contains pipe and fitting material property data and is in dBase III software format.

5.2.1 AXIALCK

AXIALCK Version 1.0 was created during the Short Cracks in Piping and Piping Welds program (Ref. 5.2). It contains burst test results on axially cracked pipe experiments from Battelle, MPA (Ref. 5.16), and General Electric (Ref. 5.17). There are about 250 pipe experiments in AXIALCK, but there is a large amount of data in the literature that could be added to it. In the IPIRG-2 program, AXIALCK was made available to the IPIRG members and some additional General Electric data were added.

5.2.2 CIRCUMCK

CIRCUMCK Version 2.2 was created during the Short Cracks in Piping and Piping Welds program (Ref. 5.2). It contains circumferentially cracked pipe experimental data for loading to maximum load for about 700 pipe experiments from tests conducted throughout the world.

CIRCUMCK Version 3.0 is an update to Version 2.2 that includes the following additions and corrections:

- The IPIRG-2 pipe test data were added.
- Recent cyclic pipe experiments conducted in Japan were added (Ref. 5.18).
- Recent MPA pipe experiments on TP347 stainless steel pipe were added (Ref. 5.19).
- Some small diameter repair groove data from a prior Battelle program were added (Ref. 5.20).

- The material property data from Version 2.2 were found to have some errors, and these errors were corrected. The test specimens used in determining the Ramberg-Osgood or J-R curve equation constants were documented in the database for traceability.

5.2.3 ELBOWCK

The ELBOWCK database was created as part of Task 2 of the IPIRG-2 program. This is a database of elbow fracture experiments. It contains 76 experiments conducted in the U.S., France, and Germany. There are both circumferential and axial crack experiments in this database. The four IPIRG-2 elbow fracture experiments are included.

5.2.4 TEECK

The TEECK database was created as part of Task 2 of the IPIRG-2 program. This is a database of tee fracture experiments found in the literature from the United States, Germany, and the Czech Republic. It contains 18 experiments conducted in the U.S. No tee experiments were conducted in the IPIRG-2 program.

Because of the additional geometry parameters needed to describe a tee experiment when compared with an elbow or straight pipe experiment, descriptions of the tee geometry and flaw are most conveniently given in graphical form. As a consequence, a contemporary spreadsheet with embedded graphics capabilities must be used to take full advantage of TEECK.

5.2.5 PIFRAC

The PIFRAC database was originally created by Materials Engineering Associates (MEA) for the U.S. NRC to document the material properties of commonly used nuclear piping materials (Ref. 5.21). The original version was written for a mainframe computer, and Version 2.0 was a PC-based version in dBase III+ software.

Version 3.0 was an update by Battelle made during the Short Cracks in Piping and Piping Welds program (Ref. 5.2). This version involved making QA improvements to Version 2.0, and expanding the database to triple the size.

Version 3.1 was an update by Battelle made during the IPIRG-2 program. This version contains the following additions.

- Additional IPIRG-2 data were added.
- Data from a research program conducted at Battelle on Inconel 600 base metal and welds were added.

The database now contains:

- Chemical compositions on most of the materials tested,

- Charpy data on many of the materials tested,
- 835 tensile test stress-strain curves,
- 863 J-R curves including the raw load-displacement-crack growth data and specimen geometry so that J-R curves can be recalculated should some new fracture parameter standard be created in the future,
- Information on the product form and specimen orientations, and
- Cross references for the data and product information.

5.2.6 QA OF DATABASES

5.2.6.1 QA of Pipe and Fitting Fracture Databases

None of the pipe fracture databases developed in this and other NRC pipe fracture programs, were written to the standards of nuclear QA requirements. In spite of this, the data are considered to be of high quality because of the following reasons:

1. The data from outside of Battelle were entered by Battelle and QA'ed by the organization that conducted the experiments. The level of QA is noted in the spreadsheet.
2. The Battelle data were cross-checked against the experimental test records.
3. References for each experiment are given for traceability.
4. The data have been used in numerous analyses at Battelle and in IPIRG round-robin calculations.
5. The data have been used in numerous analyses by ASME Section XI committee members.

For the data developed at Battelle, confidence in the experimental data comes from several considerations:

1. Good laboratory calibration practices were used.
2. Careful analog-to-digital conversion processes were used.
3. Details are documented in Battelle Laboratory Record Books that are controlled by Battelle Records Management Office.
4. The original files of the engineer who conducted the experiment are kept in a central file location.
5. The Battelle Laboratory Record Book number is given in each NRC/IPIRG/DP^{3}II/Short Cracks program Data Record Book for traceability.

6. Duplicate experiments, in some cases on different test machines, giving the same results are available for some test conditions.

7. Duplicate experiments, conducted at different laboratories, (e.g., EDF and DTRC) that give the same results are available for some test conditions.

8. Good agreement was found in comparisons with similar data from other organizations.

9. The data have been reviewed periodically to assess consistency and accuracy.

10. Corrections/clarifications, additions, and deletions to the data from 8 years of use have been issued.

Thus, while the data were not generated under a rigorous QA program, these considerations give confidence that the data are reliable.

5.2.6.2 QA of the PIFRAC Material Property Database

For PIFRAC, there are two QA issues: (1) the quality of the raw data, and (2) how well these data were entered in the database.

For the data developed at Battelle, the data are considered to be of high quality because of:

1. Good laboratory calibration practice.

2. Careful analog-to-digital conversion of the data.

3. Participation and good agreement in ASTM testing round robins.

4. Favorable results from calculational round robins for J-R curves with other labs for a given data file, see Section 3 of NUREG/CR-4082, Volume 4.

5. Good experience in a tensile testing round robin at elevated temperatures with other NRC contractors, see Section 3 of NUREG/CR-4082, Volume 4.

6. Use of duplicate or triplicate specimens for most materials.

7. Details documented in Battelle Laboratory Record Books that are controlled by Battelle Records Management Office.

8. The original personal files of the engineer for the tests are kept in a central file location.

9. Comparisons with similar data from other organizations showing that the data sets are in agreement.

10. Periodic review and reassessment of the data.

11. Corrections/clarifications, additions, and deletions to the Degraded Piping Program data from 8 years of use have been issued and any material property data corrections have been implemented in PIFRAC.

12. Plots of load-displacement and J-Δa curves have been made for all tests and examined for discontinuities and unusual features.

Thus, while the data were not generated under a rigorous QA program, these considerations give confidence that the data are reliable.

For files from the PIFRAC Version 2.0 database, some errors were discovered while doing a thorough QA. The reliability of these data have been enhanced by the following actions:

1. Obtaining the original MEA digital files and making corrections to these data.

2. Making plots of the stress-strain curves and load-displacement and J-R curves to examine the data for anomalous points. Some tests were eliminated from Version 2.0 of the database because of uncertainties in the data.

3. For archival purposes, the hard copy graphs are now stored at Battelle.

For files from outside sources, the following checks and actions were taken:

1. Including a reference source (technical paper or report) for each data set, so that the original data developers can be contacted if there are questions.

2. Only including J-R curve data that had complete information (specimen dimensions, load-displacement-crack growth files) so that the J-R curve can be recalculated (data with only J-Δa data were not included).

3. Data were screened by making plots of J-Δa and load-displacement curves.

4. For digitized data from hard copies, the data were compared with the original hard copy curves to make sure the data made sense.

As a result of the actions taken, the data from Battelle are as good as prudent laboratory practice permits. For data developed outside of Battelle, the quality of the data is as good as the QA done by the organization that submitted the data.

5.3 Uncertainty Analyses

During the NRC's International Piping Integrity Research Group Programs (Ref. 5.22), Short Cracks in Piping and Piping Welds Program (Ref. 5.2), and Degraded Piping Program (Ref. 5.1), the potential variability of numerous technical issues that could affect leak-before-break (LBB) and in-service flaw evaluation criteria was identified as an unresolved technical issue. To determine the significance of these

factors, several deterministic and probabilistic calculations were undertaken as part of the IPIRG-2 program, Ref. 5.23.

The deterministic calculations involved the following:

(a) Evaluation of the change in load-carrying capacity of through-wall-cracked pipe (for LBB) and surface-cracked pipes (for in-service flaw evaluation criteria) due to the effects of dynamic and cyclic loading on toughness,

(b) Sensitivity study of leakage flaw sizes to different default crack leak-rate morphology parameters,

(c) Assessment of the effects of off-centered cracks during leakage on the maximum load-carrying capacity for LBB evaluations,

(d) Determination of the effect of restraint of pressure-induced bending in a piping system on LBB, and

(e) Evaluation of the effect of weld residual stresses on LBB analysis.

Probabilistic analyses were performed on the following parameters for LBB applications:

(f) Magnitude of normal operating stresses,

(g) Magnitude of normal plus safe-shutdown earthquake (N+SSE) stresses,

(h) Off-centered leaking cracks,

(i) Restraint of pressure-induced bending,

(j) Dynamic and cyclic load effects on toughness and resulting pipe fracture analyses, and

(k) Weld residual stresses.

Additional probabilistic analyses were conduced for in-service flaw evaluation. The effects of the following parameters on the probability distribution of failure loads were determined:

(l) Statistical variation of material properties using fixed flaw sizes for baseline calculations,

(m) Same as Item (l) but with dynamic and cyclic load effects on material toughness, and

(n) Same as Item (l) but with uncertainty in crack depth measurements.

The following summarizes the specific objectives and results of the studies, and presents conclusions from both the deterministic and probabilistic analyses. These results are organized by the technical aspect being evaluated. In most cases there are both deterministic and probabilistic results. The deterministic analyses were conducted independently of the probabilistic analysis, which offered the opportunity to validate conclusions from each of these studies. At the end of this discussion, the relative significance of these

various technical issues are ranked. A detailed description of how these analyses were performed and the results can be found in Reference 5.23.

5.3.1 Uncertainty Analyses Relative to LBB

5.3.1.1 Evaluation of Different Crack Morphology Default Values

The objective in this effort was to assess any differences in default crack morphology parameters between PICEP Version 4.0, SQUIRT Version 2.3, and SQUIRT Version 2.4. This evaluation was done only in a deterministic manner. The SQUIRT Version 2.3 default values were typical values from an experiment, but no special attempt was made to define these values (Ref. 5.14). The basis of the PICEP (Ref. 5.24) default values is not known. The SQUIRT Version 2.4 default crack morphology parameters are the mean values from statistical evaluation of cracks removed from service as documented in Reference 5.25. The crack morphology parameters in these analyses are the surface roughness and the number of turns per unit of thickness. Cracks resulting from both IGSCC and corrosion-fatigue mechanisms were considered.

The calculated crack lengths for a given leak rate using both SQUIRT versions and PICEP Version 4.0 default crack morphology parameters for IGSCC cracks were very close. However, it should be noted that the default values are mean values and there is a high statistical variability for IGSCC crack morphology parameters. This is due to the fact that typical wrought stainless steel piping products will have grain sizes of 3 to 6*. Using ASTM Standard E112 to convert grain size numbers to physical dimensions gives a range of grain sizes that vary by a factor of 2.77 in average "diameter". Consequently, roughness and number of turns will vary proportionally to this change in grain size for an IGSCC.

The calculated crack lengths for a given leak rate using the corrosion-fatigue crack default parameters had a larger difference, see Figure 5.1. These resulted in a 16 to 40 percent larger crack length, for the 18.9 liters per minute (5 gpm) leak, when using SQUIRT 2.3 default parameters compared with PICEP or SQUIRT 2.4. The new SQUIRT Version 2.4 statistical default values resulted in crack lengths of 4 to 12 percent larger values than crack lengths calculated using the PICEP default values at the 18.9 liters per minute (5 gpm) leak rate. All of these differences were less for the 1.89 lpm (0.5 gpm) leak.

5.3.1.2 Evaluation of COD-Dependent and Independent Crack Morphology Models for Tight Crack Leak-Rate Analyses

The objective of this analysis was to assess the effect of using a COD-dependent crack morphology model (Ref. 5.25) to alleviate problems in leak-rate calculations for tight cracks. This analysis was only conducted in a deterministic manner.

One of the major concerns with tight cracks comes from limitations on the friction factor equations used in all leak-rate codes. Experimental data exist over a limited range for these friction factor equations, and extrapolating them to lower crack-opening values was found to give erroneous numerical solutions. In fact, at low COD values a critical term in the friction-factor equation becomes negative which contributes to the calculated leak-rate going to zero and then increasing again with even smaller COD values, see Figure 5.2. The COD-dependant crack morphology model circumvents the friction-factor problem by

* Information from Dr. H. Mehta of GE Nuclear Energy Operations.

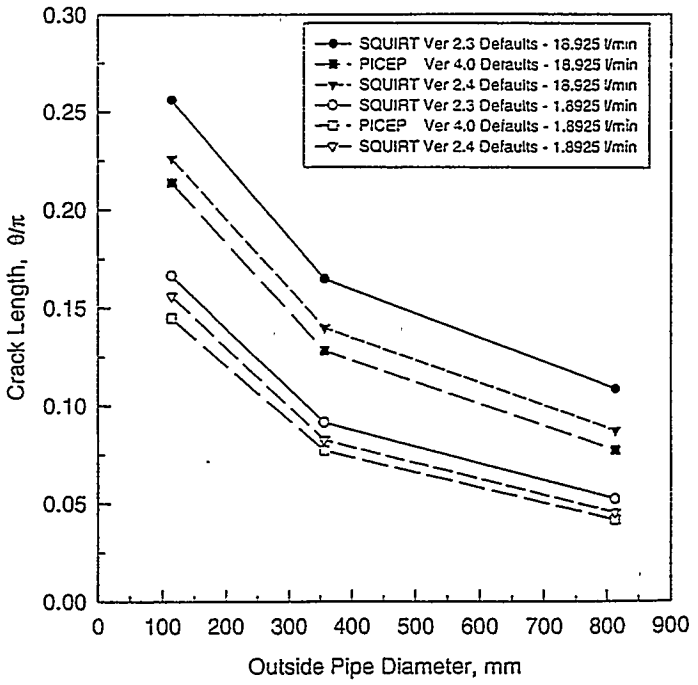

Figure 5.1 Comparison of calculated crack lengths for a given leak rate for various default crack morphology parameters (corrosion-fatigue crack using the SQUIRT2 program)

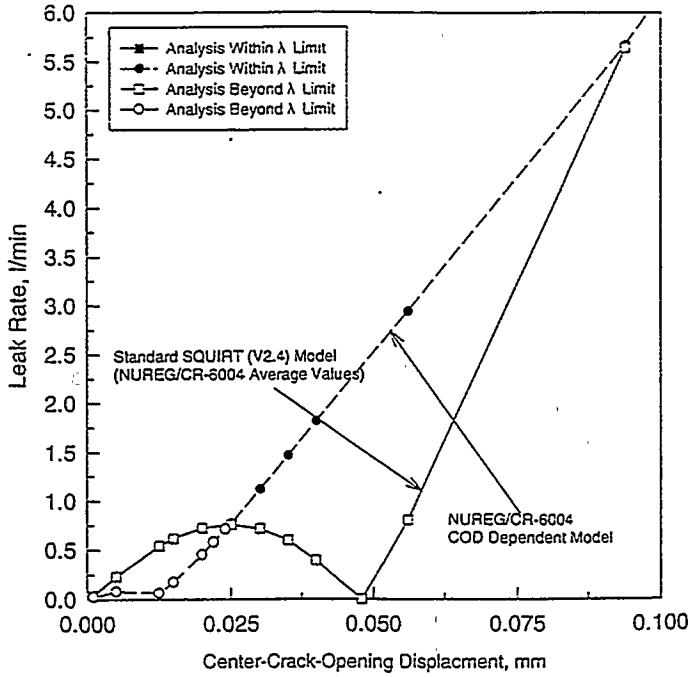

Figure 5.2 Comparison of calculated leak rates between current SQUIRT Version 2.4 and NUREG/CR-6004 COD dependant crack morphology models (small leak rates)

increasing the number of turns in the flow path and reducing the surface roughness, i.e., the local roughness is that of a grain boundary for an IGSCC. By doing this, it was found that the COD-dependent crack-morphology model gave leak rates which could be a factor of four below the standard COD-independent crack-morphology models when the friction factor equation lower limit was reached.

For the case studied, the improved model was the same as the standard model for leak rates greater than 7.56 lpm (2 gpm), had some improvement for leak rates from 4.5 to 3.5 lpm (0.93 to 1.2 gpm), and was significantly different for leak rates less than 3.5 lpm (0.93 gpm). These leak rates are within the range of leak rates of interest for LBB analyses, but without the safety factor of 10 used in the NRC SRP 3.6.3 (Ref. 5.26). If deterministic calculations are made with the safety factor of 10 on leak rates for LBB analyses, then the current COD-independent models and the COD-dependent model give the same result. If the safety factor is not used in the analyses (i.e., in probabilistic analyses), or much lower leak rates are of interest, then the new COD-dependent crack-morphology model should be used in the leak-rate analyses.

5.3.1.3 Changes of Normal Operating and N+SSE Stress Levels on Failure Probability

LBB analyses could be conducted with either a conservative deterministic analysis, or with a probabilistic analysis. Deterministic LBB analyses typically involve a two-step calculation. First, a flaw size corresponding to a given leak rate (with some safety factor on the leak rate) is determined at the normal operating stresses. The second step is that flaw size is used to calculate if the flaw is stable at the expected SSE loads. In this second step, safety factors may be applied to either the leaking crack length or the SSE loads, and the worst case material properties are used.

There are many variables in an LBB analysis, and these all have some statistical variation. To assess this variability on the likelihood of a failure, probabilistic analyses were conducted. The term conditional probability of failure (CPOF) is frequently used in probabilistic work and means two things. First, there are some important conditions or assumptions in the analysis. For example, in the calculations conducted in this report, it was assumed that an SSE load would occur with a probability of 1.0. The probability of an SSE event occurring is a site-specific probability, which could be multiplied times our CPOF value to "decondition" the analysis. Another condition is that the leakage at a given rate would occur and be detected with a probability of 1.0. Subcritical crack growth analyses could be conducted to determine the probability of a leaking crack occurring, and the reliability of the leak-detection system could be determined. Again, this probability times our CPOF would further decondition the analyses. In reality, all probability analyses are conditional or have some inherent assumptions in the deterministic analyses or analysis logic.

The second important aspect of the term CPOF is the meaning of the word failure. The failure criterion in this probabilistic analysis is normal plus SSE stresses equaling or exceeding the maximum load-carrying capacity of the through-wall-cracked pipe. This is consistent with the U.S. NRC LBB analysis procedures. In actuality, if some of these stresses are secondary stresses, it is possible that the cracked pipe may not experience a double-ended guillotine break failure, i.e., there will only be a large leak. Also if the stresses are dynamic and cyclic, the crack may start to grow, but the cyclic loads may decrease fast enough to arrest unstable crack growth. Additionally, the analyses use elastic uncracked pipe stress values, where the presence of the crack and plasticity from the crack may truncate the magnitude of the seismic moments. All of these considerations could be used to refine the deterministic "failure" analyses and hence to further "decondition" the CPOF values in the analyses. This would make the CPOF values more realistic.

Unfortunately, such improvements make the probabilistic model much more complicated than could be undertaken within the scope of this analysis.

With the above limitations on the conditions and definitions of "failure" in mind, the objective of this study was to expand the original probabilistic results from Reference 5.25 to a larger range of normal operating stresses as well as a larger range of N+SSE stresses. This was only a probabilistic study, where the safety factors on leak rate, crack length, and SSE loads are not used. Additionally, these CPOF values are used as baseline values for additional probabilistic analyses where the importance of other technical issues are evaluated in this report.

From the results of the probabilistic analysis of ten different PWR and BWR piping systems, it was found that the normal operating stresses have a more profound effect on the conditional probability of failure than the level of the SSE stresses in the LBB analyses. Any uncertainty in the normal operating stresses can lead to large variations in the predicted conditional probability of failure, see Figure 5.3 for a sample case. As shown in Figure 5.3, the change in the failure probabilities for normal operating stresses from 0.25 to 1.0 of Service Level A limits is 6 to 9 orders of magnitude (depending on the leak rate).

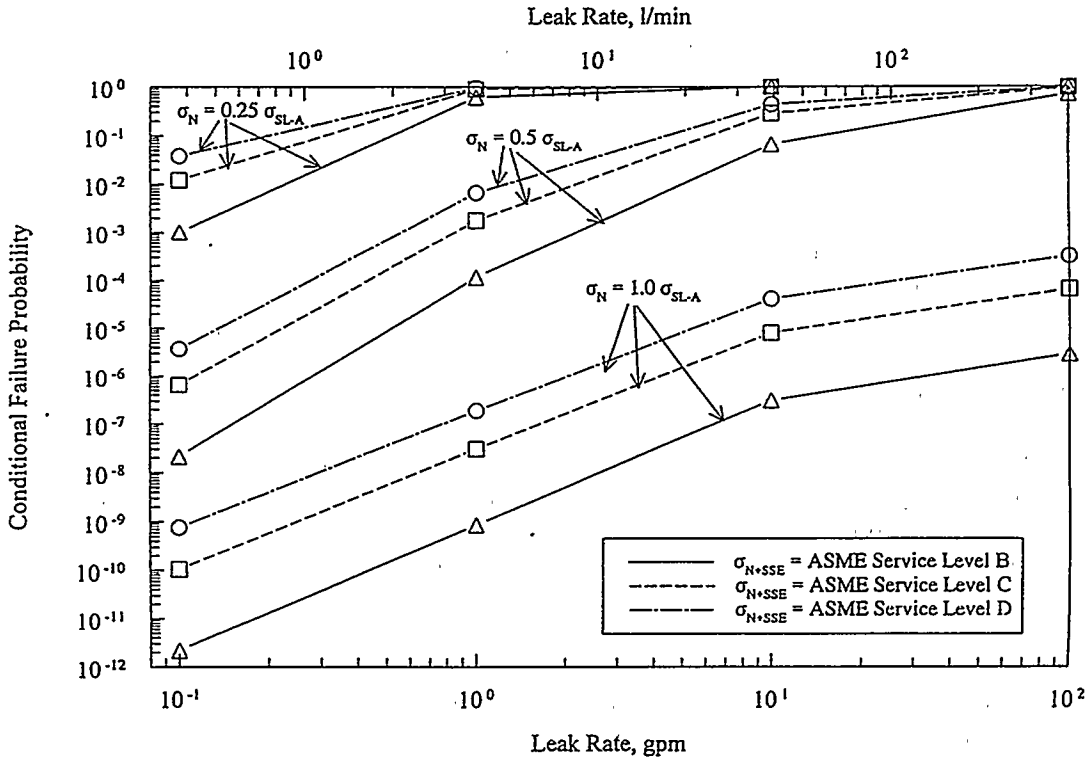

Figure 5.3 Conditional failure probability for a crack in a SAW in a 28-inch nominal diameter Schedule 80 TP304 stainless steel pipe for various combinations of normal operating and N+SSE stresses

For a fixed normal operating stress, any increase in the N+SSE stress above the ASME Service Level B maximum limits to ASME Service Levels C or D maximum limits will also increase the conditional probability of failure, but these changes in the conditional probability of failure were much smaller (up to 3 orders of magnitude change) than changes due to the normal operating stresses, also illustrated in Figure 5.3.

One major implication from this work is that the requirement for conducting an LBB analysis may need to be reconsidered. For instance, NRC SRP 3.6.3 for LBB analyses (Ref. 5.26) requires the plant operator to "Identify the location(s) at which the highest stresses coincident with the poorest material properties occur..." It was shown that the conditional failure probabilities are the highest when the normal operating stresses are low, and that a location with lower N+SSE stresses and low normal operating stresses would have a higher failure probability than a location with higher normal operating stresses and higher N+SSE stresses. Hence, the LBB criterion needs to be more specific on what stresses are the highest, i.e., either the normal operating stresses or normal plus SSE stresses. The technical basis document for SRP 3.6.3 was NUREG-1061, Volume 3, where it was specifically noted that the location with the highest N+SSE stresses should be used. Using the lowest normal operating stresses would give the greatest failure probability, but this is not physically correct. Since a crack is more likely to occur with high normal operating stresses, one logical choice is to select the locations with the highest normal operating stresses for LBB analyses.

5.3.1.4 Dynamic and Cyclic Load History Effects on Load-Carrying Capacity of Through-Wall-Cracked Pipe for LBB Fracture Analyses

The objective of this effort was to assess the significance of toughness changes due to cyclic and dynamic load effects on LBB fracture load predictions. These dynamic and cyclic effects have been found to affect the toughness of nuclear piping steels in the IPIRG programs (Ref. 5.22). Deterministic and probabilistic analyses were conducted for this technical issue.

From the deterministic through-wall-cracked pipe analyses, the results show that the predicted effects of cyclic loading using both the LBB.NRC (Ref. 5.10) and GE/EPRI (Ref. 5.6) J-estimation schemes are more severe than the existing through-wall-cracked cyclic-loaded pipe test data indicate, see Figure 5.4. Additionally, it was found that the Z-factor approach in SRP 3.6.3 (Ref. 5.26) would under predict the maximum loads if the flaw size effects are taken into account in a detailed EPFM analysis, particularly for pipe diameters larger than 254 mm (10 inches).

The results of the probability analyses show that the conditional failure probability will increase when the dynamic and cyclic loading effects are included via correction factors on the fracture toughness. The magnitude of their resultant effect will, however, depend on the values of correction factors, which in turn are strongly dependent on the quasi-static yield-to-ultimate strength ratio. Based on the results of analyses of some specific pipes, dynamic and cyclic load histories can affect the prediction of the conditional failure probability for both austenitic and ferritic pipes. Analyses were not conducted for welds, where there may actually be an improvement in the toughness due to the combined effects of dynamic and cyclic loading.

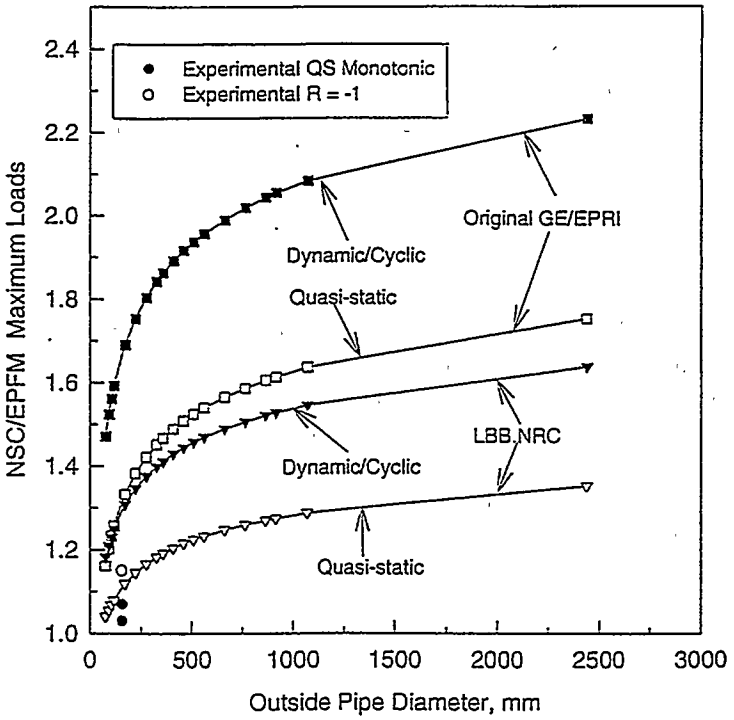

Figure 5.4 Ratio of NSC to EPFM maximum loads (Z-factor) when keeping the circumferential TWC length equal to 30 percent of the circumference for stainless steel base metal pipe and varying the toughness to account for quasi-static and dynamic/cyclic effects

The probabilistic results are consistent with the deterministic calculations, but the existing experimental data suggest the LBB.NRC and GE/EPRI EPFM analyses over predict the detrimental effects of cyclic and dynamic loading for through-wall-cracked pipes.

5.3.1.5 Evaluation of the Effect of Off-Centered Cracks for LBB Evaluations

The objective of this investigation was to assess the effect of having a leaking crack off the center of the bending plane at normal operating conditions, but centered on the bending plane for N+SSE loading. Reference 5.15 gives some prior results. These analyses were conducted in both deterministic and probabilistic evaluations.

The deterministic calculations for the effects of off-centered cracks during leakage of 3.8 liters per minute (1 gpm) on the maximum load-carrying capacity for LBB evaluations showed that there was not a very large difference in the crack lengths between on-centered and off-centered cracks for a given leak rate until the center of the crack was more than 50 degrees off the center of the bending plane.

Further deterministic analyses of the change in the maximum load-carrying capacity relative to the centered leaking crack case showed that the maximum load capacity of the off-centered crack (under normal operating conditions) was less than 10 percent lower than the centered crack maximum load when the middle of the off-centered crack was less than 50-degrees off the bending plane, see Figure 5.5. This 10 percent difference is considered insignificant.

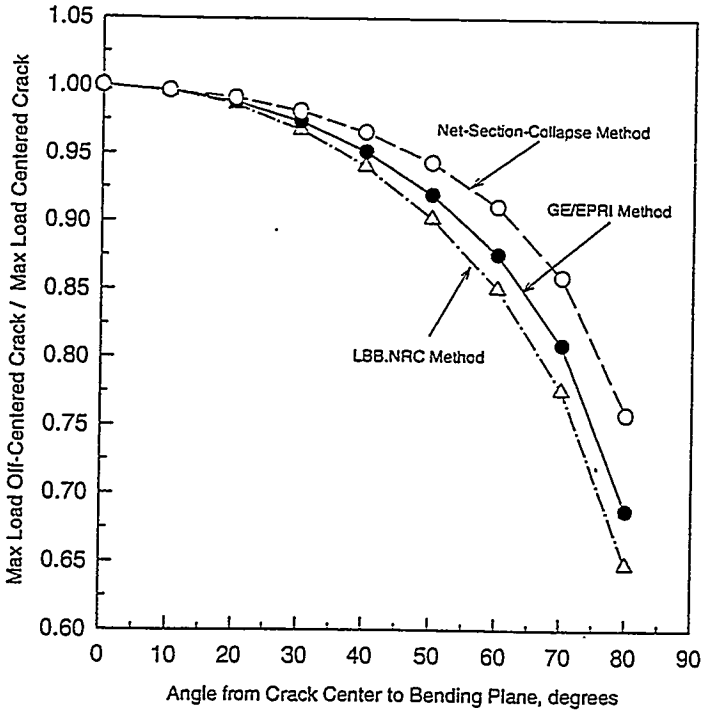

Figure 5.5 Comparison of maximum loads for 3.785 lpm (1 gpm) leaking cracks that were off-centered during leakage but centered during N+SSE loading versus angle from center of off-centered crack to the bending plane

From the probabilistic analysis, it was found that if the center of the crack is allowed to vary randomly by ±90 degrees, then the conditional failure probability increased moderately, see Figure 5.6. The change in the conditional probabilities of failure due to the cracks being centered or off centered was roughly equal to the failure probability change of a centered crack experiencing Service Level D stresses rather than Service Level B stresses. This can be seen by comparing Figures 5.3 and 5.6. The random crack locations with the center being offset more than 50 degrees caused the change in the conditional failure probabilities.

5.3.1.6 Evaluation of the Effect of Restraint of Pressure Induced Bending on LBB Evaluations

The objective of this evaluation was to assess the effect of the restraint of induced bending from axial stresses in a pipe system. Typical fracture mechanics analyses assume that the ends of a pipe under pressure loading are free to rotate. However, in a pipe system, the attached piping restrains this rotation. This restraint of pipe rotation at the crack plane has two effects. First, it increases the maximum load-carrying capacity (Ref. 5.27). Second, it reduces the crack-opening displacement for leak-rate analyses (Ref. 5.15). Figure 5.7 illustrates the results for elastic finite element analyses where the restraint of the pressure induced bending on the COD was determined as a function of the distance from the crack plane to the restraint location. These two restraint effects (leak rate versus failure load changes) compete when conducting an LBB analysis.

Both deterministic and probabilistic analyses were conducted to assess the impact of the restraint of pressure-induced bending. In this analysis, it was assumed that a crack was close to a nozzle, and the restraint distance was equal to one pipe diameter, i.e., the normalized restraint length was 1.0 in Figure 5.7.

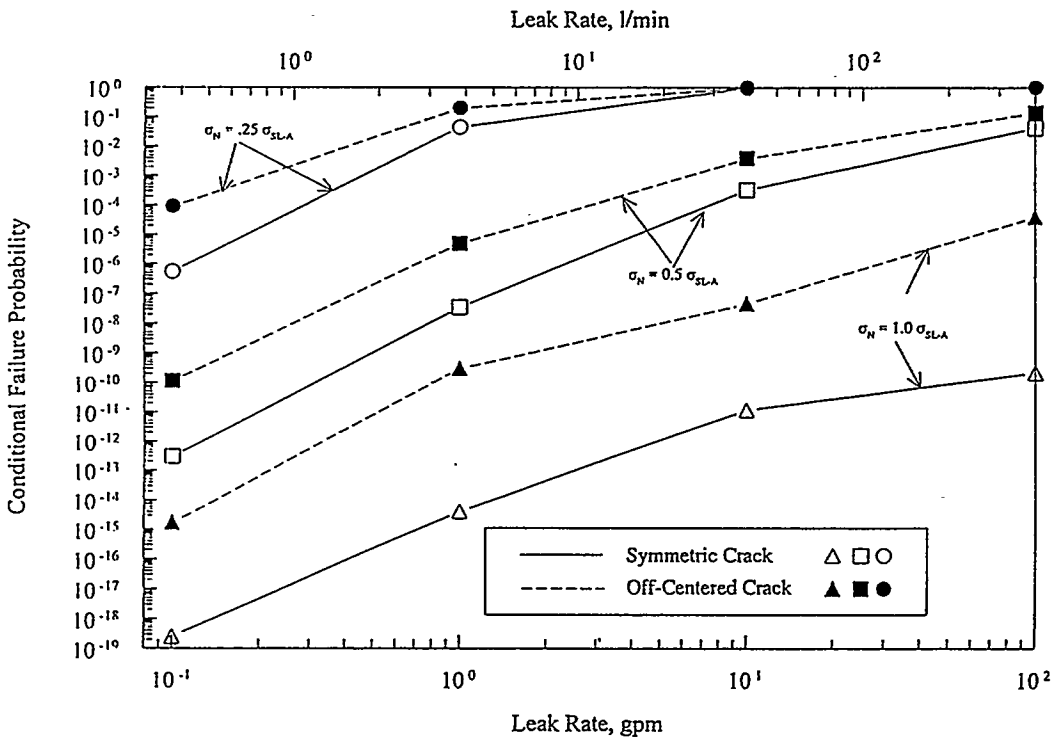

Figure 5.6 Conditional failure probability for a crack in the base metal of a 28-inch nominal diameter Schedule 80 TP304 stainless steel pipe for various crack orientations (off-centered cracks)

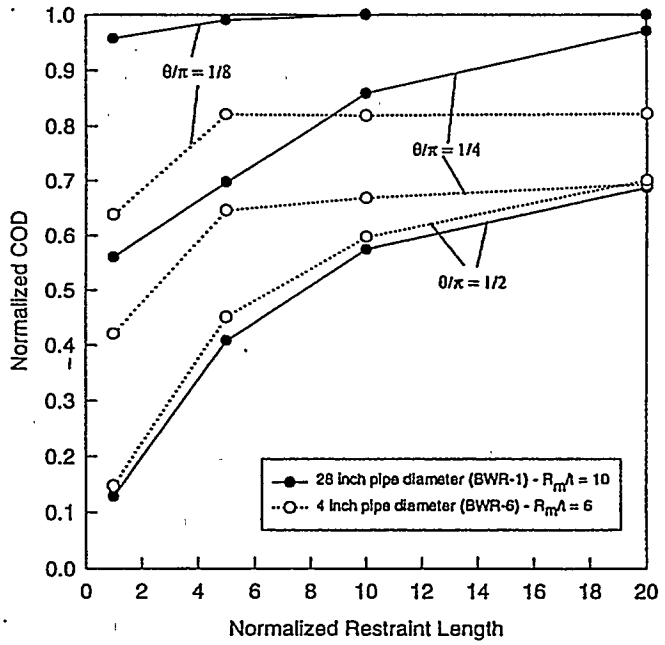

Figure 5.7 Effects of restrained bending from axial loading on COD normalized by the unrestrained COD

Furthermore, these calculations were made for a constant leak rate and at the same normal operating stresses. Hence, the crack length is much shorter in the large diameter pipe case.

The deterministic results showed that the effect on maximum load was insignificant for large-diameter pipe, i.e., shorter crack lengths. However, for small-diameter pipe, the effect was tremendous, i.e., the maximum load under the restrained conditions dropped to 11 percent of the unrestrained maximum load. This comes about because: (1) the short crack length in the large diameter pipe made both the restraint effects on the COD and the restraint effect in increasing the maximum loads negligible, and (2) for the small-diameter pipe, the effect of restraint on the COD made the leaking crack length very large, but the higher load-carrying capacity for the restraint of pressure induced bending loads offered little compensation for the large crack size. This result is significant in regard to application of LBB to smaller diameter pipe. The trend for other intermediate pipe sizes should be examined.

The probabilistic calculations involved only a large-diameter pipe analysis. These results showed that due to the increase in the failure load, the estimated conditional failure probability for a restrained condition was actually slightly lower. This is consistent with the deterministic calculations. Probabilistic calculations for the small-diameter pipe case were not conducted.

5.3.1.7 Evaluation of the Effect of Residual Stresses on Leak-Rate Analyses for LBB

The objective of this analysis was to assess the effect of weld residual stresses on leak-rate analyses for LBB evaluations. Deterministic and probabilistic analyses were conducted on this topic.

Past work (Ref. 5.28) on as-welded pipe and solution-annealed welds with identical cracks showed that solution annealing to eliminate residual stresses did not improve the load-carrying capacity, and in fact, the solution annealing lowered the fracture loads (probably because the strength of the weld metal was lowered by the solution annealing). Hence, this past work showed that residual stresses in a low toughness stainless steel SAW did not affect the maximum load-carrying capacity. For the present investigation, only the effects of residual stresses on the leaking crack at low normal operating stress levels were considered. Results from this program, including work by Brickstad and Moberg of SAQ in Sweden for an IPIRG-2 round-robin problem (Ref. 5.29), and other concurrent efforts by Dong at Battelle (Ref. 5.30) are summarized.

The deterministic results of the effects of weld residual stresses on LBB showed that weld residual stresses can significantly affect the leak rate for pipes welded with tension-compression residual stress fields through the thickness. This is more likely to occur with thinner pipe and hence smaller diameter pipe, see Figure 5.8. The most significant effect on leak rate seemed to be from the effective shortening of the crack length due to the crack-face rotations pinching off the crack opening at the ends of the flaw. An effective countermeasure to this would be to stress-relieve the welds or hydro test to a high enough stress level to reduce the residual stress fields. Either of these countermeasures would help to mitigate subcritical crack growth as well, but the high-pressure hydro testing would not lower the weld metal strength giving the pipe a higher load-carrying capacity for fracture resistance.

The probabilistic results accounted for residual stresses only by the rotation of the crack faces. The effect of pinching off of the crack opening at the ends of the crack was neglected until the center of the crack was also closed by the residual stress rotation of the crack faces. The results showed significant effects when

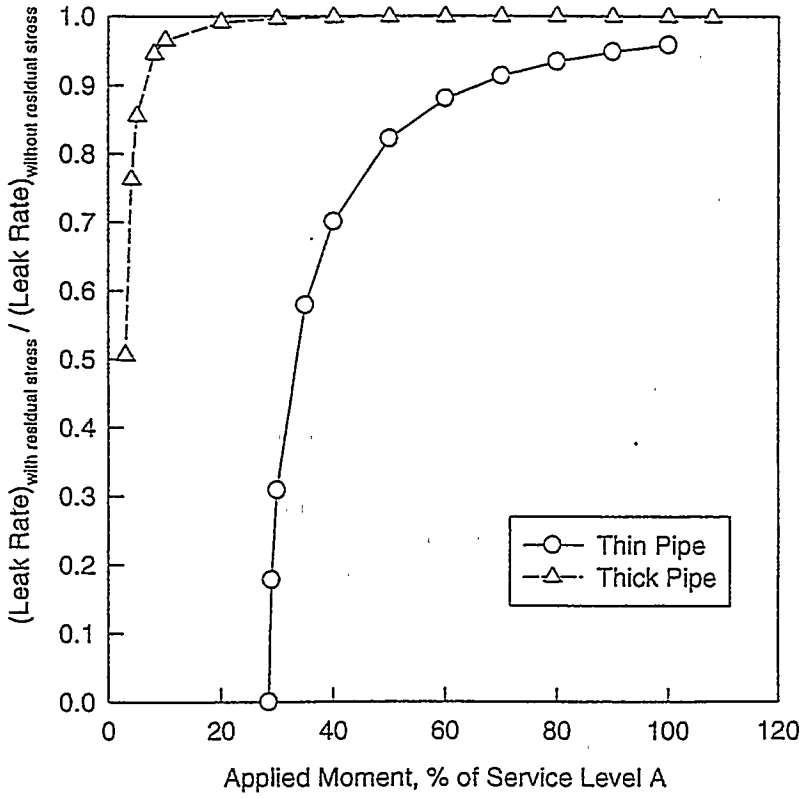

Figure 5.8 Ratio of leak rates, with and without residual stresses, as a function of applied loads

the crack opening was completely pinched off for the thinner pipe case, but negligible effects of just having the crack faces rotate. Accounting for the crack being pinched off at the ends would change the probabilistic results.

In summary, the residual stress effects were negligible for the thick pipe case, but were highly significant for the thin (less than 25 mm [1 inch] thick) case. Cases between the thin-wall and thick-wall pipes were not addressed in this limited study.

5.3.2 Uncertainty Analyses Relative to In-Service Flaw Evaluations

5.3.2.1 Dynamic and Cyclic Loads History Effects on Load-Carrying Capacity of Surface-Cracked Pipe for In-Service Flaw Evaluations

The objective of this effort was to assess the significance of toughness changes due to cyclic and dynamic load effects (Ref. 5.23) on surface-cracked pipe predictions for in-service flaw evaluation. Deterministic and probabilistic analyses were independently conducted on this technical aspect.

The results of the deterministic calculations for TP304 stainless steel base metal are shown in Figure 5.9. In this figure, the limit load is normalized by the EPFM load. The normalized limit load is plotted as a function of pipe diameter. The EPFM analysis in this case was the SC.TNP1 analysis which has been found to be the most accurate method for predicting experimental maximum loads. This normalized load ratio is equivalent to the ASME Z-factor.

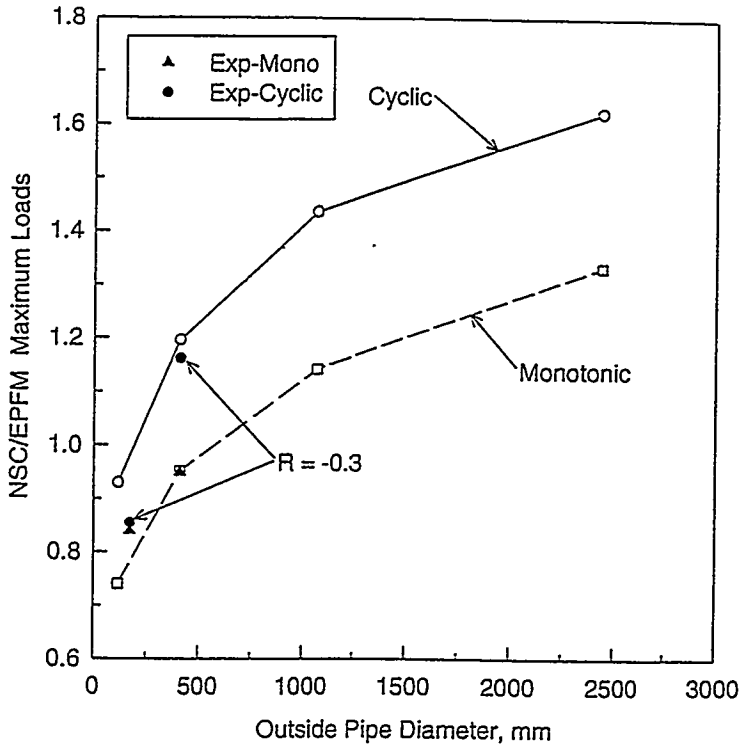

Figure 5.9 Ratio of NSC to EPFM maximum loads (Z-factor) for surface-cracked TP304 stainless steel pipe ($R_m/t = 10$) showing the effect of quasi-static and dynamic/cyclic toughness and comparisons with experimental data

The results showed that the EPFM load-carrying capacity for surface cracks can be reduced by 20 to 30 percent for stainless steel pipes under cyclic dynamic loading compared with quasi-static monotonic loading. The analyses support the conclusion that failure is essentially a limit-load failure for stainless steel base metal pipes of typical size for nuclear plants in the absence of cyclic/dynamic loading effects on toughness. However, for the cyclic/dynamic loading case, failure loads dropped below the limit load. This calculated effect was validated with experimental results, see Figure 5.9.

The importance of this finding is that an EPFM analysis (i.e., a Z-factor) for stainless steel pipes under N+SSE loading may be needed, but not for normal operating or OBE conditions where the cyclic loads are small. The change in load-carrying capacity under cyclic/dynamic loading is significant for N+SSE loads where the applied safety factor is 1.39, and hence a reduction of 20 to 30 percent in load-carrying capacity erodes that margin considerably.

The probabilistic results were first evaluated by comparing mean loads with and without the effects of cyclic/dynamic loading on the toughness. These results suggest that the effect of cyclic/dynamic loading on the maximum loads was to reduce the maximum loads by about 4 to 10 percent for A516 Grade 70 and TP304 cases, respectively. Interestingly, from the separate deterministic analysis conducted on the TP304 stainless steel pipe with the same pipe diameter, a reduction in maximum loads of about 20 percent was observed. This appears to be an inconsistency between the deterministic and probabilistic results, so the initial inputs were examined closer. The deterministic analyses used a stainless steel pipe that had a lower yield-to-ultimate strength ratio than the average statistical value used in the probabilistic analysis.

Hence, the dynamic/cyclic toughness correction was lower in the deterministic analyses than the mean values from the probabilistic analyses. Thus, the apparent inconsistency can be explained.

To improve such probabilistic analysis in the future, the yield-to-ultimate strength ratios need to be statistically determined (with the proper cross-correlation coefficients) and then used to determine a statistical toughness correction due to cyclic and dynamic effects, rather than keeping the toughness correction as a constant.

Results from the deterministic and probabilistic analyses show that the effect of the yield-to-ultimate strength ratio is an important parameter in determining the corrections to the toughness and the subsequent effects on the load-carrying capacity.

Finally, from the probabilistic analysis, the coefficient of variance (COV), which is the ratio of the standard deviation to the mean, did not change much with the dynamic/cyclic loading effects. The COV values may have changed more if, rather than using a constant dynamic/cyclic correction factor on the toughness, the correction factor was statistically varied with the yield-to-ultimate strength.

5.3.2.2 Effect of Uncertainty in UT Flaw Sizing for In-Service Flaw Evaluations

This analysis was conducted to assess the sensitivity of UT flaw sizing variability on the maximum-load capacity of circumferentially surface-cracked pipe. The UT flaw sizing variability data came from 1989 EPRI round-robin results on stainless steel piping (Ref. 5.31). Consistent with the EPRI data, analyses were conducted only on stainless steel pipe, and in particular, they were conducted only for a 28-inch nominal diameter pipe case. This was a statistical analysis, where the mean and standard deviations of the UT flaw sizing were varied as a function of flaw depth, see Figure 5.10 for results from the EPRI round robin. (Note: in Figure 5.10, the location where the 1:1 line intersects the mean line determines when the mean UT and actual flaw depths were equal.) Comparisons based on the mean values are described first. This is essentially a deterministic evaluation. Secondly, comparisons were made involving the standard deviation normalized by the mean value (the coefficient of variance, COV). The COV values are important if a deterministic analysis was to consider using some conservative bound on a mean value to give a higher reliability. Frequently, mean minus one or two standard deviation values are used in bounding deterministic analyses.

The comparison of the mean values of the maximum moments using the UT flaw depth with the maximum moment using the actual flaw depth (deterministic comparisons) showed that the calculated maximum moment accounting for the UT flaw sizing inaccuracy was slightly lower for a/t values of less than 0.35, and then increases for larger a/t values. Figure 5.11 shows the results. This trend is consistent with the mean UT flaw depth accuracy trend, i.e., as the flaw depth increases the accuracy gets worse. The magnitude of the moment ratios changes with the flaw a/t, θ/π, and J-estimation scheme used. The SC.TNP1 analysis method, which has been found to give the best agreement with experimental maximum loads (Ref. 5.12), shows that the maximum over prediction of the actual loads range from close to zero percent (for short flaw lengths of any depth) to about 30 percent for the deepest and longest flaw evaluated.

The coefficient of variance (COV) is a measure of the statistical variability of a parameter. If the COV or standard deviation is small, then one might not need to apply a large safety factor to accommodate uncertainty. Conversely, a large COV may make a larger safety factor desirable. Good surface-cracked or through-wall-cracked pipe J-estimation schemes have a COV value around 10 percent for the accuracy of

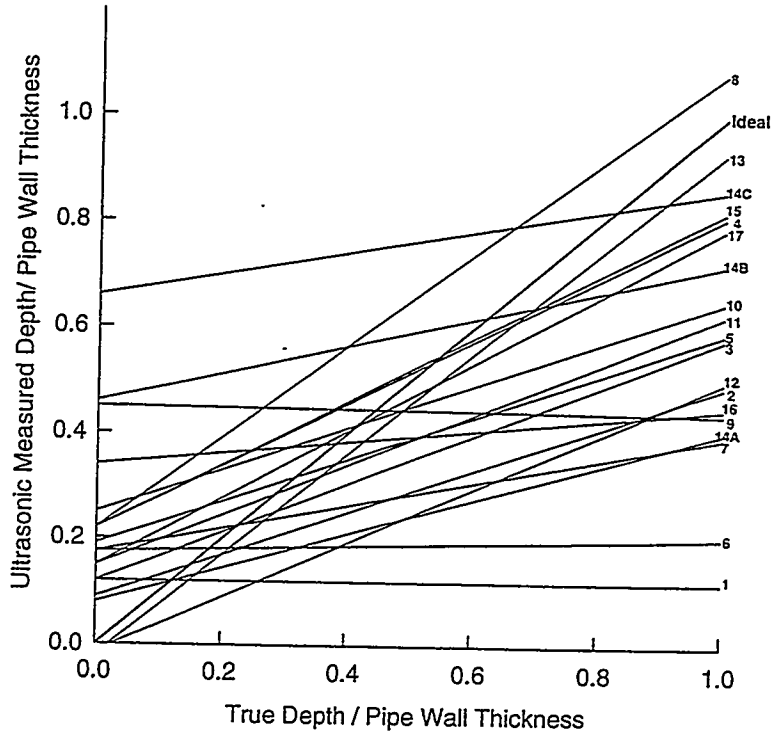

(a) Original EPRI data

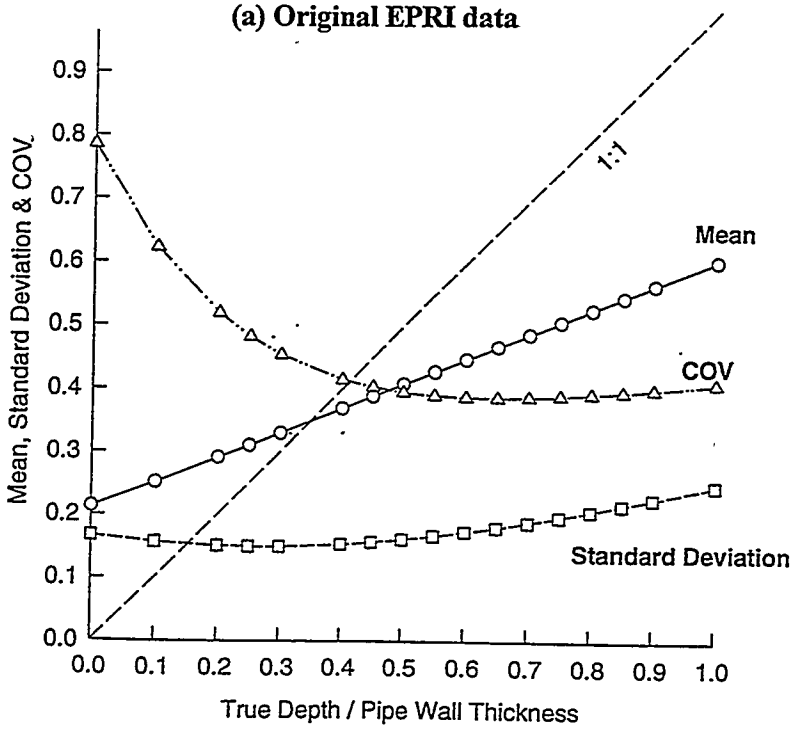

(b) Battelle determination of mean, standard deviation, and coefficient of variance (COV)

Figure 5.10 Statistical results of depth/thickness ratio from the 1989 EPRI Round-Robin data (Ref. 5.31)

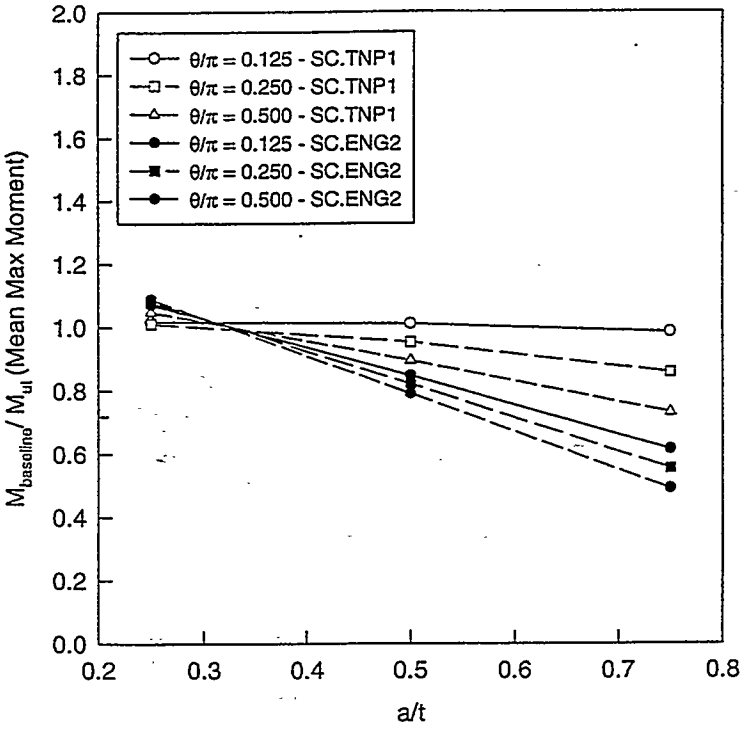

Figure 5.11 Ratio of actual maximum moment, $M_{baseline}$, to mean maximum moment, M_{UT}, for uncertainty in UT crack depth measurement as a function of a/t (28-inch nominal diameter Schedule 80 TP304 stainless steel pipe with the crack in the base metal)

maximum load predictions. The COV values for the UT flaw sizing were found to be 40 to 80 percent, depending on the flaw depth. Shallower flaws had higher COV values than deeper flaws.

A comparison of the COV values from the maximum-load statistical predictions showed that the COV values from the predictions of the maximum loads using the UT flaw sizing variability increase slightly as the flaw depth and lengths became larger. The COV values of the maximum loads due to UT variability were from 11 to 22 percent for the most accurate J-estimation scheme used (the SC.TNP1 analysis). This is a considerably lower COV range than the UT flaw sizing COV of 40 to 80 percent. This reflects some insensitivity in the fracture analyses to flaw depth variability. The larger UT flaw sizing COV was greater for ***shallower*** a/t values. However, the maximum load COV values were greater for ***deep and long*** flaws.

This diverse trend of larger COV values for shallow a/t flaw depths from UT (from the EPRI UT round-robin results) versus the maximum load COV values being larger for deep flaws comes from the fact that the maximum loads are more sensitive to deep flaws than shallow flaws. This is especially true for flaws that are longer. For short flaw lengths, the maximum moments are exceedingly insensitive to crack depth, especially in the Net-Section-Collapse and the SC.TNP1 analyses, see Figures 5.12a and 5.12b. Hence, for a short flaw a large variability on flaw depth will result in a small variability on maximum load.

Results such as these could be used in justifying variable safety margins for UT flaw sizing. For instance, the safety factor need not be as high for shallow flaws even though the COV is highest for them. Similarly, if the flaw length is short, the safety factor could be less than for a long flaw.

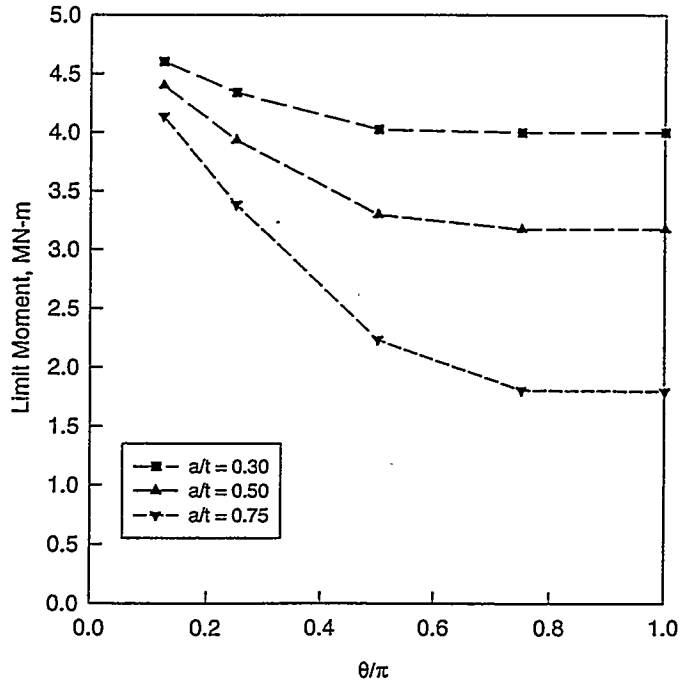

(a) Net-Section-Collapse analysis values

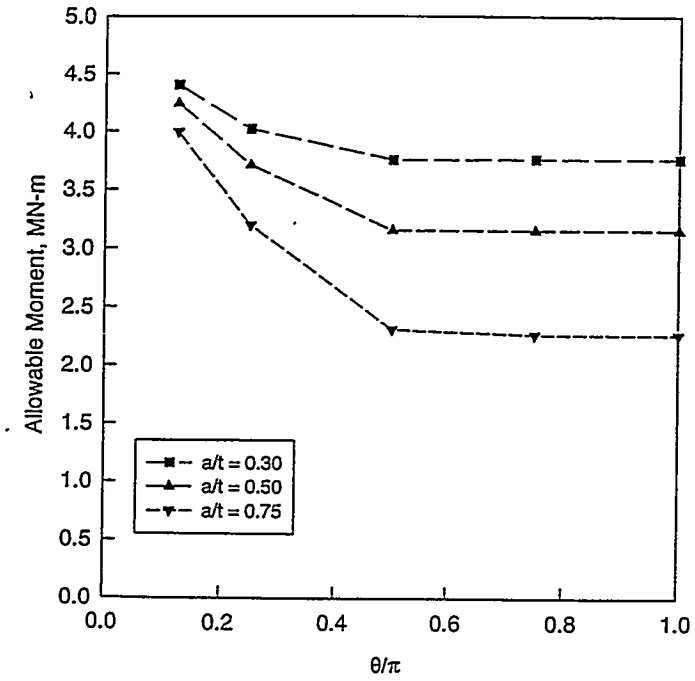

(b) SC.TNP1 J-estimation scheme values

Figure 5.12 Maximum moments for circumferentially surface-cracked 28-inch nominal diameter Schedule 80 pipe with the crack in the base metal

5.3.3 Ranking of Significance of Various Factors Investigated

The significance of the various technical issues investigated was ranked in importance of how these technical issues may change results relative to current analysis methodologies. Table 5.1 makes this ranking from both the deterministic and probabilistic results for the technical issues that affect LBB evaluations. Table 5.2 makes this ranking for the technical issues that affect in-service flaw evaluations.

These rankings are in the categories of very low, low, medium, high, and very high. An example of a very high ranking is the case of restraint of pressure induced bending on LBB, where for small diameter pipe the difference in the failure loads was a factor of 9 which was much greater than the maximum load safety factor of $\sqrt{2}$ used in LBB analyses. An example of the very low rating is the case of residual stresses on leak-rate analyses for a thick-walled pipe. Here the effects were essentially negligible, except at extremely low operating stresses thought to be lower than practical.

In some cases, it appeared from an initial review that the significance of the deterministic and probabilistic analyses did not agree. Upon further review, however, it was found that most of the deterministic and probabilistic analyses agreed on the significance of a technical issue. The cases where there were differences in the significance of a technical issue were found to be due to:

1. The deterministic model being more sophisticated than the model used in the probabilistic analysis, i.e., the effect of residual stresses on leak rates was such a case,

2. The material property input not being the same in the deterministic and probabilistic analyses, i.e., in the effects of cyclic and dynamic loading toughness and load-carrying capacity was such a case, and

3. What appeared to be a significant effect over a small range was thought to be less important from a deterministic view, but that same factor gave a major change in conditional failure probabilities, i.e., the effect of an off-centered crack on LBB being significant only if the crack was off-centered by more than 50 degrees was such a case.

All of these differences were closely evaluated to make our final ranking.

5.4 Comparison of Pre-Test Ultrasonic Examination of Test Flaws with Post-Test Measurements

It is easy to provide a detailed measurement of the flaw depth profile for the laboratory experiments from post-test inspection of a fracture surface. However, in actual practice the existence of a surface flaw is detected by inspection. The most common method of in-service flaw depth sizing is ultrasonics. As suggested by the uncertainty analyses described above, discrepancies between the actual flaw depth and indicated flaw depth can have a large impact on the load-carrying capacity of a flaw. Thus, if the ultrasonic inspection does not correctly size a flaw, inappropriate actions may be taken.

Table 5.1 Ranking of various technical issues investigated that affect LBB evaluations

Technical Issues Investigated	Comments	Significance
Evaluation of different crack morphology default values	For IGSCC	Low
	For corrosion fatigue	Medium
Evaluation of COD-dependent and COD-independent crack morphology models for tight-crack leak-rate analyses	Leak rates > 7.56 lpm (2 gpm)	Low
	3.5 lpm (0.926 gpm) <Leak rate < 4.5 lpm (1.2 gpm)	Medium
	Leak rate < 3.5 lpm (0.926 gpm)	High
Changes of normal operating and N+SSE Stress levels on failure probability	Low normal operating stresses	High
	High N+SSE stresses	Medium
Dynamic and cyclic load history effects on load-carrying capacity of through-wall-cracked pipe for LBB fracture analyses	Experimental results show analyses too conservative. (Low cycle fatigue crack growth not evaluated.)	Low
Evaluation of the effect of off-centered cracks for LBB evaluations	Cracks off centered < 50 degrees	Low
	Cracks off centered > 50 degrees	Medium
	Statistically varying off-center angle	Medium
Evaluation of the effect of restraint of pressure induced bending on LBB evaluations	Large diameter	Very low
	Small diameter	Very High
Evaluation of the effect of residual stresses on leak-rate analyses for LBB	Thin-walled pipe (i.e., tension to compression stresses through the thickness) at *low* operating stresses	High to very high
	Thin-walled pipe (i.e., tension to compression stresses through the thickness) at *high* operating stresses	Low
	Thick-walled pipe (i.e., tension to compression to tension stresses through the thickness) at typical operating stresses.	Very low

Table 5.2 Ranking of various technical issues investigated that affect in-service flaw evaluations

Technical Issues Investigated	Comments	Significance
Dynamic and cyclic loads history effect on load-carrying capacity of surface-cracked pipe for in-service flaw evaluations	Low yield-to-ultimate strength materials	Medium
	High yield-to-ultimate strength materials	Low
Effect of uncertainty in UT flaw sizing for in-service flaw evaluations	$a/t < 0.25$	Low
	$0.25 < a/t < 0.5$	Medium
	$a/t > 0.5$	High

As part of the two IPIRG-2 carbon steel elbow experiments, Experiments 2-1 and 2-2, the flaw profiles were measured using ultrasonics following the completion of precracking. The measurements were made in an effort to determine if the flaws had grown too deep during precracking, requiring replacement of the test elbows.

Figures 5.13 and 5.14 show the results of the pre-test measurements made using ultrasonic instrumentation along with the actual post-test measurements of the fracture surface. The Experiment 2-1 measurements were made by the Level III ultrasonic technician that did the routine inspection of the pipe system test specimen girth welds. The Experiment 2-2 measurements were made by a Siemens Power Corporation, Nuclear Division technician that had been certified by the EPRI NDE Center.

In both cases, the indicated crack depths were within 10 percent of the actual crack depth. The indicated crack depth trends appear to follow the actual crack depths, more or less, but in both cases, the indicated maximum crack depth was less than the actual crack depth. Because the crack depth was underestimated, predicted load-carrying capacity would be overestimated. Coupled with the knowledge of the sensitivity of analyses to crack depth, this result reinforces the sense that uncertainty in flaw sizing can dominate in-service flaw evaluation uncertainty.

Statistical data for UT flaw sizing accuracy of surface cracks in carbon steel pipe could not be found in the literature when we were conducting the uncertainty analysis discussed in Section 5.3.2.2. Hence, it was of interest to see how these data compared to the EPRI stainless steel pipe UT round-robin results. Figure 5.15 is a graph of actual a/t values versus UT a/t values. This figure gives the EPRI stainless steel UT mean a/t curve from Figure 5.10, a 1:1 line which corresponds to exact agreement, and the a/t values from Figures 5.13 and 5.14 for the carbon steel elbow. Additionally, UT versus actual flaw depth data were available for a microbiologically-induced corrosion (MIC) groove in an A53 Grade A pipe weld from an NRC Short Cracks in Piping and Piping Welds program experiment (Ref. 5.2). All these data are in Figure 5.15. The MIC inspections were done by a utility inspector certified by the EPRI NDE Center.

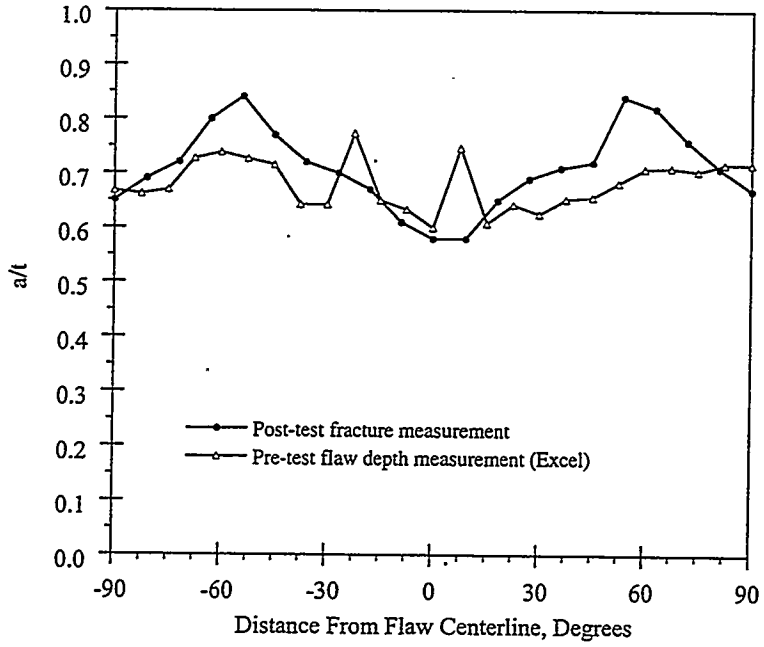

Figure 5.13 Pre- and post-test flaw depth measurements for Experiment 2-1, carbon steel elbow containing an internal fatigue-sharpened surface crack (Elbow IP2-FE18)

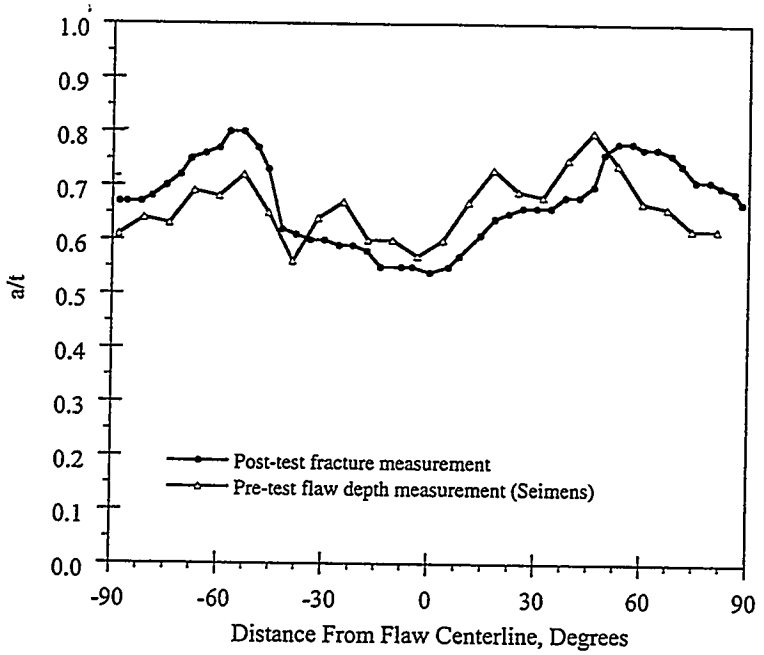

Figure 5.14 Pre- and post-test flaw measurements for Experiment 2-2, carbon steel elbow containing an internal fatigue-sharpened surface crack (Elbow IP2-FE16)

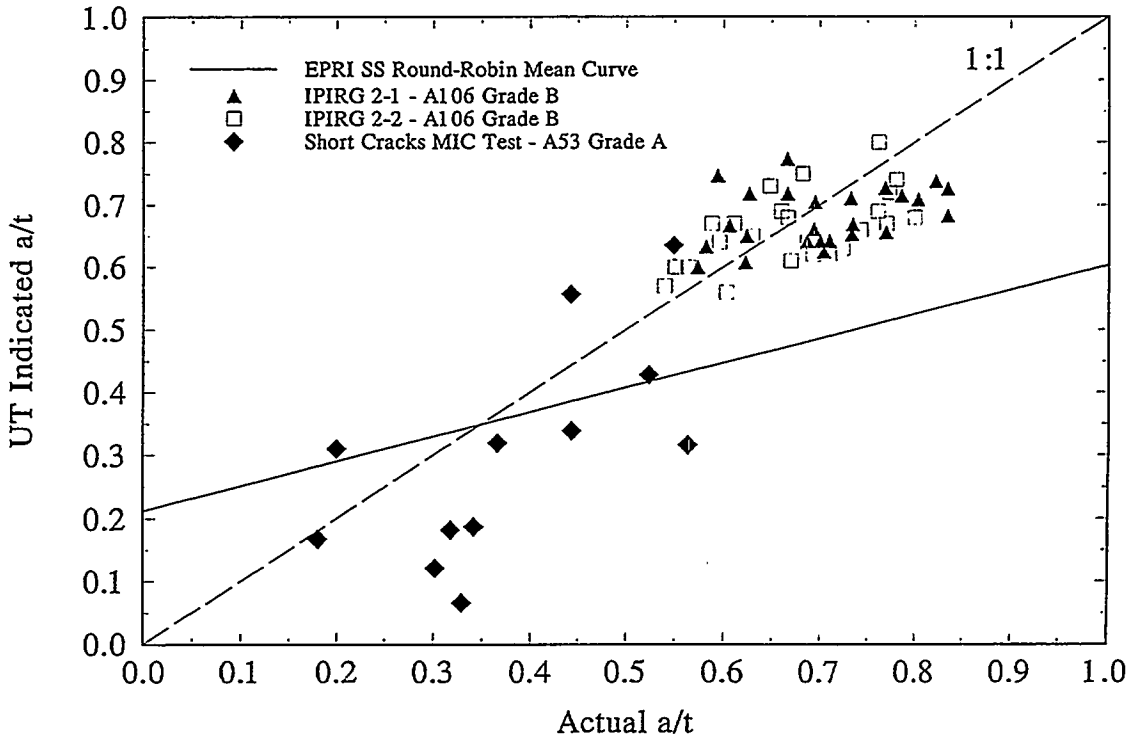

Figure 5.15 Comparison of UT flaw sizing of carbon steel piping data to EPRI UT round robin mean curve for stainless steel pipe

Figure 5.15 shows that the elbow inspection data are close to the 1:1 curve, and much better than the stainless steel mean curve. The MIC UT flaw depth data tended to undersize the actual flaw more than the crack data in the elbows. A mean curve of the elbow and MIC carbon steel pipe data gave a slope of 0.97 with a very slight negative intercept, so that it was virtually the same as the 1:1 curve. On first impression, it appears that the UT flaw sizing is more accurate for carbon steel pipe than stainless steel pipe. However, the data in Figure 5.15 should be qualified further. The elbow data was for the case where a relatively wide EDM cut was made with a tapered tip and a fatigue crack was grown a short distance from the EDM cut. The EDM cut provides a relatively good reflector for UT and hence the elbow data have a narrow scatter. The MIC data involved a blunt circumferential groove, but was more difficult to inspect because the width of the MIC corrosion affected the reflection of the UT wave off the inside surface of the pipe. Consequently, these data should probably not be used to draw any major conclusions on the accuracy of UT flaw sizing of cracks in carbon steel piping.

5.5 References

5.1 Wilkowski, G. M., and others, "Degraded Piping Program -Phase II, Summary of Technical Results and Their Significance to Leak-Before-Break and In-Service Flaw Acceptance Criteria," March 1984-January 1989, by Battelle Columbus Division, NUREG/CR-4082, Vol. 8, March 1989.

5.2 Wilkowski, G. M. and others, "Short Cracks in Piping and Piping Welds," NUREG/CR-4599, Vol. 4, No. 1, April 1995.

5.3 Kanninen, M. F. and others, "Mechanical Fracture Predictions for Sensitized Stainless Steel Piping with Circumferential Cracks," Final Report, EPRI NP-192, September 1976.

5.4 G. M. Wilkowski, and P. M. Scott, "A Statistical Based Circumferentially Cracked Pipe Fracture Mechanics Analysis for Design or Code Implementation," *Nuclear Engineering and Design*, Vol. III, pp 173-187, 1989.

5.5 Milne, I., Ainsworth, R. A., Dowling, A. R., and Stewart, A. T., "Assessment of the Integrity of Structures Containing Defects," CEGB Report R/H/R6 - Revision 3, 1986.

5.6 Kumar, V., and others, "An Engineering Approach for Elastic-Plastic Fracture Analysis," EPRI Report NP-1931, 1981.

5.7 Brust, F. W., "Approximate Methods for Fracture Analyses of Through-Wall Cracked Pipes," NRC Topical Report by Battelle Columbus Division, NUREG/CR-4853, February 1987.

5.8 "Evaluation of Flaws in Ferritic Piping," EPRI Report NP-6045, prepared by Novetech Corporation, October 1988.

5.9 Brust, F., Scott, P., Rahman, S., Ghadiali, N., Kilinski, T., Francini, R., Marschall, C., Muira, N., Krishnaswamy, P., and Wilkowski, G., "Assessment of Short Through-Wall Circumferential Cracks in Pipes - Experiments and Analyses," NUREG/CR-6235, April 1995.

5.10 Klecker, R., F. Brust, and G. Wilkowski, "NRC Leak-Before-Break (LBB.NRC) Analysis Method for Circumferentially Through-Wall Cracked Pipe Under Axial Plus Bending Loads," NUREG/CR-4572, BMI-2134, May 1986.

5.11 Scott, P. M., and Ahmad, J. A., "Experimental and Analytical Assessment of Circumferentially Surface-Cracked Pipes Under Bending," NUREG/CR-4872, April 1987.

5.12 Krishnaswamy, P., Scott, P., Mohan, R., Rahman, S., Choi, Y. H., Brust, F., Kilinski, T., Ghadiali, N., Marschall, C., and Wilkowski, G., "Fracture Behavior of Circumferential Short-Surface-Cracked Pipe," NUREG/CR-6298, November 1995.

5.13 Mohan, R., Brust, F. W., and Ghadiali, N., "Development of J-Estimation Schemes for Internal Circumferential and Axial Surface Cracks in Elbows," NUREG/CR-6445, June 1996.

5.14 Paul, D. D., Ahmad, J., Scott, P. M., Flanigan, L. F., and Wilkowski, G. M., "Evaluation and Refinement of Leak-Rate Estimation Models," NUREG/CR-5128 Rev. 1, June 1994.

5.15 Rahman, S., Brust, F., Ghadiali, N., Choi, Y. H., Krishnaswamy, P., Moberg, F., Brickstad, B., and Wilkowski, G., "Refinement and Evaluation of Crack-Opening Analyses for Short Circumferential Through-Wall Cracks in Pipes," NUREG/CR-6300, April 1995.

5.16 Scott, P.,Wilkowski, G., Sturm, D., and Stoppler, W., "Development of a Database of Pipe Fracture Experiments," *Proceedings of 18th MPA Seminar*, Stuttgart, Germany, October 1992.

5.17 Reynolds, M. B., "Reactor Primary Coolant System Rupture Study. Task C, Fracture Mechanics," Quarterly Progress Report 12, GEAP-5637, January - March, 1968, June 1968.

5.18 Miura, N., and others, "Application of Cyclic J-Integral to Low Cycle Fatigue Crack Growth of Japanese Carbon Steel Pipe," *LBB'95 Conference*, Lyon France, October 1995.

5.19 Stadtmüller, W. and Sturm, D., "Leak Before Break Behaviour of Austenitic and Ferritic Pipes Containing Circumferential Defects," *LBB'95 Conference*, Lyon France, October 1995.

5.20 Wilkowski, G. M. and Eiber, R. J., "Evaluation of Tensile Failure of Girth Weld Repair Grooves in Pipe Subjected to Offshore Laying Stresses," *Journal of Energy Resources Technology*, Vol. 103, pp 48-55, March 1981.

5.21 Hiser, A. L. and Callahan, G. M., "A User's Guide to the NRC's Piping Fracture Mechanics Database (PIFRAC)," NUREG/CR-4894, May 1987.

5.22 Wilkowski, G. M., Olson, R., Scott, P., Brust, F., Ghadiali, N., Kilinski, T., Rudland, D., and Hopper, A., "The IPIRG Programs - Advances in Pipe Fracture Technology," *LBB'95 Conference*, Lyon France, October 1995.

5.23 Ghadiali, N., Rahman, S., Choi, Y. H., and Wilkowski, G., "Deterministic and Probabilistic Evaluations for Uncertainty In Pipe Fracture Parameters In Leak-Before-Break and In-Service Flaw Evaluations," NUREG/CR-6443, July 1996.

5.24 Norris, D., and others, "PICEP: Pipe Crack Evaluation Program," EPRI Report NP-3596-SR, 1984.

5.25 Rahman, S., Ghadiali, N., Paul, D., and Wilkowski, G., "Probabilistic Pipe Fracture Evaluations for Leak-Rate Detection Applications," NUREG/CR-6004, April 1995.

5.26 Solicitations for public comment on "Standard Review Plan 3.6.3 LEAK-BEFORE-BREAK PROCEDURES," *Federal Register*, Vol. 52, No. 167, Notices, pp 32626 to 32633, Friday, August 28, 1987.

5.27 Scott, P., Olson, R., and Wilkowski, G., "The IPIRG-1 Pipe System Fracture Tests -- Experimental Results," ASME PVP Vol. 280, pp 135-152, June 1994.

5.28 Wilkowski, G. M., and others, "Analysis of Experiments on Stainless Steel Flux Welds," NUREG/CR-4878, April 1987.

5.29 Rahman, S., Olson, R., Rosenfield, A., and Wilkowski, G., "Summary of Results from the IPIRG-2 Round-Robin Analyses," NUREG/CR-6337, February 1996.

5.30 Rahman, S., Dong, P., Wilkowski, G. M., Brickstad, B., and Moberg, F., "Effect of Weld Residual Stresses on the Crack-Opening-Area Analysis of Pipes for LBB Applications," *LBB'95 Conference*, Lyon France, October 1995.

5.31 "Accuracy of Ultrasonic Flaw Sizing Techniques for Reactor Pressure Vessels," Electric Power Research Institute, EPRI-NP-6273, Palo Alto, California, 1989.

6.0 TASK 5 - INFORMATION EXCHANGE SEMINARS AND WORKSHOPS

One of the goals of the IPIRG-2 Program was to provide a forum for nuclear piping fracture experts to exchange information on state-of-the-art developments in pipe fracture analysis and experimentation. Through open discussion of the technical positions and concerns of the various member countries, the IPIRG-2 Program fostered a better understanding of the fracture issues facing piping experts on a world-wide basis as plants age or new plants are built. To fulfill this goal, a series of seminars and workshops was held in conjunction with several of the IPIRG-2 Technical Advisory Group (TAG) Meetings.

6.1 LBB Seminars

A Leak Before Break (LBB) seminar was held in Lyon, France, in conjunction with the 7th IPIRG-2 TAG meeting in October 1995. The seminar brought together nearly 200 pipe fracture researchers from around the world to present and/or listen to 37 papers and 21 poster sessions. Topics addressed included regulatory practices, pipe fracture research results, and application of LBB to new and existing plants. The proceedings of this conference are to be published as a NUREG/CP report.

6.2 Round-Robin Analyses

In conjunction with the IPIRG-2 Program TAG meetings, Battelle organized a series of round-robin workshops to compare analysis methodologies and solutions for a series of pipe fracture problems. Three one-day workshops were held in Columbus, Ohio, on August 5, 1993, March 4, 1994, and October 21, 1994. The general objectives were to enhance the IPIRG-2 members' understanding of the various technical and regulatory bases in other countries and to help develop a consensus on how to handle difficult analytical problems in leak-before-break (LBB) and pipe flaw evaluations for circumferentially cracked pipes and elbows.

At the suggestion of the IPIRG-2 members, four sets of round-robin problems were developed by Battelle for analysis by the TAG members and Battelle. They involved: (1) evaluations of fracture properties and pipe loads, (2) crack-opening and leak-rate evaluations, (3) dynamic analysis of cracked pipes, and (4) fracture evaluations of elbows. A total of 18 organizations presented analysis results for these problems.

Complete problem statements, solutions, and comparisons of solutions are documented in Reference 6.1. Key observations from the round-robin analyses are summarized below.

6.2.1 Problem Set A: Evaluations of Fracture Properties and Pipe Loads

Problem Set A involved three round-robin problems: (1) the evaluation of fracture properties of pipe at operating temperature from mill data, (2) an assessment of the differences in the international standards for determining J_{Ic} and J-R curves, and (3) the determination of the significance of the uncertainty in J-R curves and stress-strain curves for predicting the load-carrying capacity of pipes.

6.2.1.1 Prediction of High-Temperature Material Properties Using Ambient Temperature Mill Data

The high temperature yield strengths were estimated to be 78 to 93 percent of room temperature values with the actual value being 86 percent for the two different ferritic base metals that formed the basis of the problem statement. The high temperature ultimate strengths were estimated to be 90 to 100 percent of room temperature values with the actual values being 118 and 124 percent of the room temperature values. The higher actual ultimate strengths are probably due to dynamic strain aging.

Estimated stress-strain behavior and toughness showed wide scatter when compared to the actual data from the specimens that were used to create the problem statement. The predicted Ramberg-Osgood strain-hardening exponent (n) was either accurate or underestimated, depending on the analysis method and the particular ferritic pipe steel or weldment. The estimates of the Ramberg-Osgood coefficient (α) tended to be high, in general. From the Charpy V-notch data supplied in the transition region, the Charpy upper-shelf energy was overestimated. From the transitional Charpy data, the fracture toughness at crack initiation (J_{Ic}) and dJ/da were either underestimated or overestimated. The coefficient of variation of the J estimates varied from 20 percent at 1 mm (0.04 inch) of crack growth to 30 percent at 5 mm (0.2 inch) of crack growth.

6.2.1.2 Evaluation of J-R Curve Standards

Given load-displacement-crack growth data and specimen dimensions, the J-R curves calculated by the participants were very similar when using different international J-R curve calculation standards. Comparisons of J at several crack growths indicated that the standard deviation in computed J was of the order of ten percent of the mean. In addition, it was found that: (1) small differences might arise when comparing J-R curves with and without crack blunting, and (2) differences in the J-R curves using the newly proposed ASTM standard and ASTM E1152-87 were negligible for the materials evaluated.

6.2.1.3 Analyses of Cracked Pipes Using Various Quasi-Static J-R Curves

The predicted loads for through-wall-cracked (TWC) and surface-cracked (SC) pipes by the various participants were reasonably close to each other when the crack sizes were large. For short through-wall cracks and short and shallow surface cracks, the load predictions showed scatter that was larger than the scatter observed for long through-wall cracks and long and deep surface cracks.

Analyses of three ferritic large-diameter pipe fracture experiments (short TWC, long TWC, and short surface crack), which were conducted in the NRC's Degraded Piping Program (Phase II) (Ref. 6.2) and Short Cracks in Piping and Piping Welds Program (Refs. 6.3 and 6.4), were performed. The solutions showed that the loads predicted by the participants were in good agreement with the test data from these experiments, except for the short TWC pipe experiment in which case all participants underpredicted the maximum load.

6.2.1.4 Analyses of Cracked Pipes Using J-R Curves from Various Load Histories

J-R curves from specimens with quasi-static-monotonic load, dynamic-monotonic load, and dynamic-cyclic load were supplied to make predictions of the load-carrying capacity for TWC and SC pipes. The differences in J-R curves from various load histories can affect predictions of a pipe's load-carrying

capacity. The predictions based on quasi-static-monotonic and dynamic-cyclic J-R curves provided the largest and smallest values of the loads, respectively.

For the through-wall-cracked pipes, there was more scatter in the predicted loads when the crack size was smaller. There was far more scatter in predicted loads for the surface-cracked pipes than for the through-wall-cracked pipes.

6.2.1.5 Analyses of Cracked Pipes Using Various Quasi-Static Stress-Strain Curves

Predictions of initiation load were always low when a low stress-strain curve was used. No consistent trend was observed in the maximum load predictions using three different stress-strain curves that came from an earlier round-robin problem on predicting high temperature stress-strain curves from room temperature yield and ultimate data. Maximum load predictions based on lower stress-strain curves provided the largest values of maximum loads in many cases. This was true for solutions from all participants.

For a given stress-strain curve, the amount of the scatter in the predicted pipe maximum loads was comparable to the uncertainty in choosing the stress-strain curve itself. There was far more scatter in the results for predicted loads for surface-cracked pipes than for through-wall-cracked pipes, reflecting a greater diversity in analysis methods for surface-cracked pipes when compared to TWC pipes.

6.2.2 Problem Set B: Crack-Opening and Leak-Rate Evaluations

Problem Set B consisted of five problems: (1) evaluation of current models for crack-opening-area analysis of pipes, (2) evaluation of current models for predicting leak rates, (3) development of engineering models for predicting crack-opening for a pipe with an off-centered crack, (4) evaluation of the effects of weld residual stresses on the crack-opening predictions, and (5) crack-opening-area analysis of a girth weld crack in a nozzle with a thickness gradient on both sides.

6.2.2.1 Analysis of Crack-Opening Area

The predicted crack-opening displacement (COD) for a through-wall-cracked pipe by various participants agreed reasonably well. However, there was some scatter in the predictions, particularly in the problems that involved combined bending and tension. A quantitative measure of this scatter indicated that the largest coefficients of variation between the predictions were 6 and 10 percent for pipes under pure bending and combined bending and tension, respectively. The good agreement among the different participants comes mainly from consistent use of the GE/EPRI method.

Comparison of predicted results with an IPIRG-2 quasi-static pipe experiment (Experiment 1-8) that involved combined bending and tension showed that the experimental crack-opening displacement would be overpredicted by the solutions of all participants, at least at the loads considered. Hence, for a given leak rate, the crack size would be underpredicted for LBB applications in this case. (More comparisons between experimental and predicted COD values can be found in Reference 6.5. This report shows much more variability in predicting COD values in the elastic range, than the variability in predicting maximum loads.)

6.2.2.2 Estimation of Leak Rates

Models of crack-morphology parameters and the analysis input values used for corrosion-fatigue cracks and IGSCC by the participants varied considerably. As a consequence, the calculated leak rates for those cracks varied widely. For a prescribed set of crack-morphology parameters, the calculated leak rates for corrosion-fatigue cracks and IGSCC predicted by various participants also showed some scatter. However, it was somewhat less than that observed in cases where the crack-morphology parameters for a certain type of crack were chosen by the participants. Nevertheless, there was some concern about the scatter of the predictive models for general leak-rate calculations. Currently, there are few experimental data available to validate analysis methods with the crack morphologies that would be found in service. (A statistical database of crack morphology parameters determined from cracks removed from service is given in Reference 6.5.)

6.2.2.3 Analysis of Off-Centered Cracks

The results of all participants showed that the maximum COD shifts from the center of the crack when the crack becomes off-centered with respect to the bending plane. However, good predictions of crack-opening area could still be made by calculating center COD for a symmetrically-centered crack subjected to the resolved component of the applied moment and assuming an elliptic crack-opening profile. The results suggest that for off-centered cracks, when the crack opening is assumed to be elliptical with the length of the minor axis equal to the center COD, the actual COD from the finite element method would be underpredicted for one-half of the crack front and overpredicted for the other half of the crack front. Calculations of crack-opening area using an elliptical profile produced results in good agreement with those from explicit finite-element analysis. This is an important finding because the crack-opening area, which is more relevant for leak-rate prediction than COD itself, can be easily calculated just by knowing center COD (plus making elliptical assumption on the crack-opening profile) from simple GE/EPRI-type estimation formulae. For a given leak rate, the off-center crack will always be longer than a centered crack. This effect on crack length is described in Section 5.3.1.5.

6.2.2.4 Evaluation of Weld Residual Stresses

Finite element analyses were conducted to determine the effect of a weld residual stress field on crack-opening displacements. The residual stress field from ASME IWB-3640 and remote moments were applied to a large-diameter thick-walled pipe and a small-diameter thin-walled pipe. The results showed that the prescribed residual stress did not significantly affect the crack-opening for the large-diameter pipe (outer diameter = 402.6 mm [15.85 inch]), but could seriously affect the crack-opening for a small-diameter pipe (outer diameter = 102.0 mm [4.02 inch]). More specifically, for the large-diameter pipe, when the residual stresses were considered, the center-crack-opening displacement increased by 4.4 percent at the inside surface, decreased by 2.4 percent at the middle surface, and increased by 3.3 percent at the outer surface of the pipe. For the small-diameter pipe, when the residual stresses were included, the center COD at the inside, middle, and outside surfaces increased by 17.1 percent, decreased by 11.7 percent, and decreased by 31.7 percent, respectively. Further studies involving other crack sizes and residual stress distributions are needed to be certain that these findings are general.

6.2.2.5 Analysis of a Girth Weld Nozzle Crack at a Thickness Transition

For a girth weld crack at a nozzle, comparisons of finite element results submitted by the participants showed that the COD compared well when the applied bending moments were low. However, for larger moments, the COD solutions varied significantly. It was surmised that the principal reason for such differences may be due to the application of bending moments in the finite element analyses. For example, in the analysis by one participant, the bending moment was applied as a linearly-distributed axial stress on the nozzle cross-section which varies from tensile to compressive stresses at the outermost fibers (lumped formulation). The axial stresses were calculated from the simple beam theory. On the other hand, in the analysis by another participant, the bending moment was applied using consistent nodal forces on all nodes on the cross-section of the nozzle (consistent formulation). The nodal loads were calculated using the formulation of the 20-noded isoparametric solid elements. Another factor that may be responsible for differences in the COD for higher loads is the fact that there were also differences in mesh refinement in the finite-element models. Further studies are needed to resolve the consequences of different modeling assumptions.

6.2.3 Problem Set C: Dynamic Analysis of Cracked Pipes

In Problem Set C, the participants solved two problems: (1) generation of seismic time-histories consistent with a given response spectrum, and (2) determination of the accuracy of predictions for seismic pipe system tests with cracks.

6.2.3.1 Spectrum-Consistent Time Histories

Four different but "equal" displacement-time histories were created from a peak-broadened acceleration response spectrum. The maximum moments induced in a linear finite element model of the IPIRG piping system were similar (to within 20-percent with 2-percent damping), but the timing, number, and build-up of moment peaks were substantially different.

It is not clear that merely being consistent with a given input spectrum is any guarantee that one will have an upper-bound, lower-bound, or average crack-driving potential due to differences in loading rate and load history effects on the material's susceptibility to cyclic damage. Other prescriptions on spectrum matching are probably required to give bounding crack-driving behavior. This work showed that although the IPIRG-2 program seismic displacement-time history forcing function met all of the current ASME, NRC, etc. design requirements, it is not known if it is lower-bound, upper-bound, or average in terms of crack-driving force considerations.

6.2.3.2 Accuracy of Predictions for Seismically Loaded Cracked Pipe

From this problem, it was shown that there can be substantive differences between predicted moment-carrying capacities of flawed pipe, depending on which analysis methods are used and what material properties are known. More detailed knowledge of material properties at the crack location did not necessarily ensure a more accurate prediction of maximum moment.

It was also shown that nonlinearity caused by plasticity can dramatically alter the moment that can be applied at the crack. Whether the plasticity is restricted to the crack section or in remote piping, energy

input to the system will be absorbed and inertial stresses will not be as high as elastically calculated values using typical damping values.

6.2.4 Problem Set D: Fracture Evaluations of Elbows

Problem Set D involved evaluation of the accuracy of predicting displacements for an uncracked pipe elbow. This problem was selected for analysis because previous work in the IPIRG-1 Program suggested that there could be substantive differences in predicted displacements for elbows under pressure-only loading.

Many differences in solutions to elbow deflections under various loads can be traced to analysts not solving the same problem due to: (1) poorly documented finite element computer program features, (2) incorrect program inputs, (3) incomplete problem statements, and (4) finite element computer program errors.

The issue of pressure-only loading of elbows in finite element programs is somewhat problematic in that unless one has a very clear understanding of the theory for an element, one can get wrong answers that apparently look correct. Treatment of end cap loads and the surface that the internal pressure is applied to (mid-surface on shells, for instance) play a major role in the pressure load response of elbows modeled with finite elements.

6.3 Fracture Analyst's Group Meetings

A series of fracture analyst specialty meetings was organized in conjunction with the IPIRG-2 TAG meetings to promote discussions on fracture-related technical topics which the participants were actively researching or were interested in. The format of the analyst's group meetings permitted discussion of issues that dealt directly with IPIRG-2 experimental issues, or any peripheral fracture mechanics subject which was of interest to the group. The goals were two-fold: to check on the validity of selected solutions and to make progress on unsolved fracture mechanics questions.

Four Fracture Analyst's Group Meetings were held, all in Columbus, Ohio: August 6, 1993, February 28, 1994, October 17, 1994, and May 9, 1995. Topics discussed at each meeting were selected by the participants. In addition to the formally agreed upon discussion topics, time was always set aside for a general session in which any fracture-related topic could be presented. The format of the meetings permitted open discussion during all presentations. As a result of information presented during a particular meeting, discussions were often continued to subsequent meetings.

6.3.1 First Meeting

6.3.1.1 Fracture Evaluation of Elbows

A wide range of elbow fracture topics was discussed, including finite element analyses of leaking cracks in elbows, stress intensity factors along cracks in elbows, development of J-estimation schemes for surface cracks in elbows, numerical and experimental analysis of elbows, and surface-crack analyses of circumferential cracks in elbows. The important conclusions from the presentations were:

- Using elastic finite element analyses of cold-formed elbows containing circumferential through-wall cracks, it was found that for total crack sizes greater than about 100 degrees, a marked gradient in stress intensity factor exists through the pipe wall. This is caused by bulging induced by the internal pressure loading. For long deep surface cracks, the fabrication residual stresses markedly increase the value of the stress intensity factor compared to pressure alone.

- When loading, material properties, and thickness are equal, K in a plate is less than K in a pipe, and they are both less than K in an elbow.

- The J-integral from an elastic solution can be used to estimate J in the elastic-plastic range for circumferential surface cracks in elbows under pure bending.

- For axial flank cracks, the experimentally measured global load-displacement relationship is unaffected by the presence of the crack because the elbow behavior is dominated by ovalization.

- For circumferential through-wall cracks in elbows under bending, the effect of the crack is unimportant for half crack angles less than about 30 to 40 degrees; i.e., the failure load is the same as that without the crack. For cracks greater than 40 degrees, the failure loads decrease, as expected.

- For circumferential surface cracks in straight pipe loaded in bending, the line-spring model provides very good predictions of J and load-displacement relations, compared to full three-dimensional solutions, with a great reduction in costs (mainly due to labor cost reductions in creating 3D meshes). For a circumferential crack in an elbow, the line-spring model performed equally well.

6.3.1.2 Analyses of Cracks in Welds

Four presentations on cracks in welds were made. Topics included mismatching weld analysis, bimetallic and fusion line weld toughness, and J-estimation methods for welded cracked pipes. Conclusions that came from the presentations include:

- A novel J-estimation scheme for cracks in overmatched welds has been developed. The method separates J into a plastic-zone-corrected elastic term added to a plastic term, where the plastic term is estimated by multiplying J_p by a factor which is determined from the slip-line-field solution for a crack in a weld, assuming entirely weld metal. Solutions for center-cracked panels and an axisymmetric cracked pipe subjected to tensile load show good comparison with finite element solutions.

- Bimetallic weld specimen behavior has shown some interesting behavior: a Charpy specimen has shown fibrous delamination failures parallel to the face of the specimen, and J becomes independent of starter crack geometry after a few millimeters of crack growth.

- Regarding fusion line weld toughness, it appears that stainless steel SAW fusion line toughness may be lower than weld metal toughness, and that SAW welds are typically found to have "low" toughness.

- J-estimation scheme analysis of as-welded and solution-annealed stainless steel SAW pipes has indicated that, based on the C(T) specimen J-R curves, predictions of initiation and maximum loads were under predicted for both cases. Based on the pipe J-R curves, most predictions were reasonably accurate.

6.3.2 Second Meeting

6.3.2.1 Elbows

The subject of elbows was revisited, mainly in the context of the finite element analysis of uncracked elbows subjected to pressure loading. Round-Robin analyses and the Fracture Analyst's Group meeting results suggested that there could be wide discrepancies in finite element solutions for the same problem. After detailed discussion by the group, it was determined that there are limitations in some element types that can cause problems when response is dominated by pressure loading. Analysts have to be aware of such limitations when performing calculations.

6.3.2.2 Weld Fracture

As a closure to the discussions started at the previous meeting, some additional information was presented regarding fracture of welds. Additional information was presented on fusion line toughness testing, residual stress effects on weld fracture, and constraint effects on welded specimens. Conclusions coming out of these discussions were:

- The crack initiation toughness for the fusion line of stainless steel welds tends to fall between that for the base metal and the weld metal alone, however, the fusion line J-R curve became flat after 2 mm of crack extension where the J values then were below the weld metal curve. A slant notch test technique was found to be a viable method for determining the fusion line toughness of welds at 288 C (550 F).

- Residual stresses appear to increase both J and CTOA at low applied loads, which typically might occur at operating conditions in a nuclear plant. This suggests that residual stresses induced by the welding process may have a detrimental effect on service fatigue or stress corrosion crack growth at or near welds. However, at large loads, as may be experienced in a plant in overload conditions, the effect of residual stresses on J and CTOA is negligible.

- Analysis of welded SEN(B) and CCP specimens with different ratios of weld height, crack size, and material parameters shows that both J-Q theory and the local method, which is based on integrating a damage parameter through the nonlinear strain history, provide similar predictions for the weld behavior.

6.3.2.3 Cyclic Loading and Constraint

Five presentations were made on this topic. The topics ranged from an experimental study of cyclic load effects, to the development of a simplified engineering approach to model cyclic effects in large-scale piping systems, to the use of local approaches for understanding cyclic effects. The important points from the discussions were:

- Based on C(T) specimen testing: (1) as the stress ratio decreases, the J-R curve also decreases, where for stainless steel, reductions were most noticeable for $R < -0.8$, while for carbon steel, reductions in J occur for $R < -0.3$; and (2) using a cyclic J-R curve from a C(T) specimen to predict cyclic load behavior in a TWC pipe resulted in underprediction of loads, while using cyclic J-R curves to predict cyclic surface-crack pipe behavior leads to overpredictions of load and pipe rotation.

- Based on analyses of IPIRG-1 pipe experiments: (1) for carbon steel, dynamic loading reduces the J-R curve, while for stainless steel, little effect was observed; and (2) maximum and minimum loads for cyclic load cases were predicted quite well using isotropic hardening for the analyses, but crack-opening displacements were slightly underpredicted when compared with experimental results.

- A method for conducting nonlinear, cracked-pipe, fracture analyses using beam-type elements was presented that eliminates the objectionable features of pure kinematic-hardening law plasticity.

- In an attempt to provide an understanding of the results of cyclic load tests performed on pipe as part of the IPIRG program, the Gurson constitutive model for growth of a void in a material has been used. Gurson-type elements have been placed along the expected crack growth plane and then allowed to grow under load. The Gurson model has also been enhanced using the Leblond-Perrin modification to account for cyclic load effects. Analysis results were preliminary, but encouraging.

6.3.3 Third Meeting

6.3.3.1 Cyclic Loading and Constraint

The discussion on cyclic loading and constraint started at the second Analyst's Group Meeting was continued at the third meeting with an additional five presentations. The following major points were made during the discussions:

- A framework has been developed for including constraint effects in the R6 approach that has been tested on a number of two-dimensional cracked geometries. The approach consists of performing a fracture assessment in the usual R6 way, but the effects of constraint are included in the analysis through a normalized structural constraint parameter which is a function of the T-stress, Q-stress, etc.

- The effect of out-of-plane stresses (different from plane strain) on the fracture process was investigated using a double-edge-notch (DEN) specimen to see if longitudinal stresses adversely affects the toughness of an axial crack in a pressure vessel. The results of a limited number of tests suggest that the initiation value of J may be lower in the biaxial case when compared to the uniaxial case, but more testing is required.

- Using constraint arguments, an attempt was made to try to explain differences in fracture behavior between surface-cracked (SC) and through-wall-cracked (TWC) pipe. In general, surface-cracked pipe has a significantly lower transition temperature than a TWC pipe. Also, as the SC depth decreases so does the transition temperatures. The upper shelf toughness is also more than five times higher in a SC pipe than in a TWC pipe possibly due to a combination of constraint and anisotropy.

- At elevated temperatures, each time there is a change in stress state (from tension to compression or vice versa), the deformation caused by creep accelerates greatly. This leads to increased crack growth behavior under cyclic creep conditions. New constitutive models will be required to be able to predict this kind of behavior.

- The Leblond-Perrin modification of the Gurson-type void growth model was used to investigate cyclic elastic-plastic crack growth behavior of a TP304 stainless steel at 288 C (550 F). Using estimated properties, the Leblond-Perrin model was able to qualitatively predict experimentally observed behavior at $R = 0$ and $R = -1$.

6.3.3.2 Secondary Stresses

The topic of secondary stresses and how they should be dealt with in assessing nuclear piping was the focus of five presentations. Based on the discussions, it is evident that there is no uniform agreement among the different countries as to how best to account for secondary stresses for fracture consideration. Much more work is required to gain a consensus opinion.

The highlights of the discussions of the various presentations were:

- A new method for treating secondary stresses using the R6 approach has been proposed. The basic R6 approach is followed but a new parameter, ρ, which depends on the ratio of primary and secondary loadings, is added. Although the method has been tested, it has not been fully validated with a large database of service experience.

- Using the definition that secondary stresses are stresses through the thickness which produce no net force or moment and do not contribute to plastic J, it was shown that "Budden's Method", a relatively simple formulation for modifying the R6 approach, provided the best predictions when compared with other approaches.

- Using a factor of safety on all secondary stresses will severely limit the application of leak-before-break considerations in plants. Specifically, a problem would arise if weld residual stresses are included in the fracture analysis. Since weld residual stresses are usually assumed to be at yield, the addition of yield stresses makes the LBB fracture criteria virtually impossible to satisfy, which could cause all welds to be post-weld heat treated. Fortunately, experimental

pipe test data show that weld residual stresses are not important for high temperature pipe fracture behavior. However, they may be important in the crack-opening displacement calculations for LBB. (It is also well documented that weld residual stresses are important for subcritical crack growth considerations.) The important question of how to account for secondary stresses in a manner which does not cripple the operating plants remains a major concern.

- Recent changes in ASME Section III may necessitate reconsideration in how pipe flaw evaluations are performed in light of the fact that significant plasticity may actually exist. A method for treating cases where primary stresses are below yield and total stresses are above yield was proposed.

- Trying to find a rational way to handle the effect of secondary stresses on fracture, it was suggested that one approach would be to consider three classifications of stresses: (1) mechanical, (2) through-thickness thermal or residual stresses, and (3) displacement-controlled stresses such as thermal expansion. To calculate J, the mechanical stresses could be handled using an R6-type plasticity correction, the residual stresses could be handled using uncracked cylinder solutions, and the displacement-controlled stresses could be handled just like the mechanical stresses but with a different factor of safety.

6.3.3.3 Equivalent Crack Size Considerations

Equivalent crack size for surface cracks has become a topic of interest, particularly among the IPIRG members because of some non-uniform and off-center cracks in IPIRG experiments. Three presentations were made on this subject. The important points made during the discussions were:

- Using data from two different sets of experiments, it was found that estimating an equivalent surface crack length by dividing the actual crack area by the maximum crack depth produced the best maximum load predictions. Estimating the crack depth as the actual area divided by the maximum crack length produced the worst maximum load predictions.

- A method for predicting pipe failure for arbitrarily shaped circumferential cracks in pipe has been developed and verified. The development, based on Net-Section-Collapse, is valid for arbitrarily shaped cracks, including complex and multiple cracks, as long as Net-Section-Collapse dominates the failure process.

- The behavior of oddly shaped surface cracks depends on the type of piping component (straight pipe, elbow, fitting, etc.), the type of loading, whether there is a weld crown or not, the material strain-hardening characteristics, and the local constraint. In spite of the apparent complexity of the problem, the best approach for analyzing such cracks today is to use the actual crack area divided by the maximum crack depth.

6.3.4 Fourth Meeting

6.3.4.1 Secondary Stresses

Two presentations on secondary stresses, a topic originally discussed at the third Analyst's Group Meeting, were made to close out consideration of this issue. Summarizing the comments:

- A method for predicting the J-integral for two-dimensional laboratory specimens under thermo-mechanical loading conditions has been developed. Numerical results using this method showed that under thermo-mechanical load, the load history would have a strong influence on the applied J. However, the application of a thermal load before a mechanical load had no influence on the plastic component of J.

- The IPIRG-1 pipe system experiments showed that stresses due to thermal expansion and seismic anchor motion could contribute equally to fracture for a surface-cracked pipe system when the failure stresses were below yield of the uncracked pipe.

- If linear elastic stress analyses are to be used, ways must be found to develop and apply nonlinear corrections for stresses that involve thermal expansion, seismic anchor motion, and inertia for flaw evaluations.

6.3.4.2 Cyclic Loading and Constraint

The discussion of cyclic loading and constraint effects began at the second Analyst's Group Meeting and continued at the third. Finishing out the discussions, three additional talks were presented that made the following points:

- A two-parameter approach, based on J-h, J-Q, and J-Q_m concepts, was investigated to describe the crack-tip fields in stainless steel clad components where cracks extend from the stainless steel into the ferritic base metal. Analysis results show that under uniaxial loading, the initiation of ductile crack growth was insensitive to crack-tip constraint (stress triaxiality). For multiaxial loading, such as in pressurized thermal shock transients in pressure vessels, significant differences are observed between the parameters h, Q, and Q_m. Further investigations are required to better understand the biaxial loading effects in initiation and propagation of ductile crack growth.

- A Gurson-Tvergaard type of continuum damage model, modified to improve work-hardening behavior, has been used to predict crack growth in precracked specimens of various sizes, such as the C(T) and axisymmetric tensile cracked specimens. Results showed promise for laboratory specimens, but it will require a few more years for the computational effort, demanded by the local approach, to become acceptable for more practical applications, such as pressure boundary components of a power plant.

- Based on finite element modeling of cyclic plasticity in cyclic C(T) tests using kinematic and isotropic hardening rules, predicted results start to depart from the test data after a few cycles

of loading. Because such analyses are computationally intensive and not particularly accurate, efforts are under way to find better constitutive models.

6.3.4.3 Angled Crack Growth in Ferritic Pipes

Angled crack growth has been observed in ferritic steel cracked pipe fracture specimens and has been attributed to toughness anisotropy caused by elongated inclusions, banded microstructure, and crystallographic texture. Recognizing that this phenomenon needs to be considered in piping fracture evaluation, two authors presented information on this subject. The salient points of the presentations and resulting discussions were:

- An angular crack growth parameter, defined as the ratio of normalized angular fracture resistance to normalized angular driving force, has been proposed. Results using this new parameter have been compared for some ferritic pipes and laboratory specimens. More studies will be needed to verify the efficacy of this parameter.

- Regarding combined torsion and bending of circumferentially cracked pipe, a Von Mises based effective moment parameter from the initial circumferential crack gave solutions for fracture parameters, such as J, crack-opening displacement, and crack-opening area, that may be directly used to evaluate these parameters using pure bending solutions. This result is applicable to straight cracks as well as for angled cracks in which the crack-tip angle from the initial circumferential crack was in the neighborhood of 0 to 60 degrees.

6.4 Summary

The LBB Seminar, Round-Robin Analyses, and the Fracture Analyst's Group Meetings provided a unique opportunity for the IPIRG members to discuss contemporary fracture research problems. Although there were scheduled themes for each of the meetings, the opportunity existed to present results or progress reports on any fracture-related research topic. The principal benefit of the meetings was the opportunity to freely exchange ideas and viewpoints with peers in the international pipe fracture community.

6.5 References

6.1 Rahman, S., Olson, R., Rosenfield, A., and Wilkowski, G., "Summary of Results from the IPIRG-2 Round-Robin Analyses," NUREG/CR-6337, U.S. Nuclear Regulatory Commission, Washington, D.C., February 1996.

6.2 Wilkowski, G. M., and others, "Degraded Piping Program - Phase II, Summary of Technical Results and Their Significance to Leak-Before-Break and In-Service Flaw Acceptance Criteria," March 1984 - January 1989, NUREG/CR-4082, Vol. 8, March 1989.

6.3 Krishnaswamy, P., and others, "Fracture Behavior of Short Circumferentially Surface-Cracked Pipe," NUREG/CR-6298, November 1995.

6.4 Brust, F. W., and others, "Assessment of Short Through-Wall Circumferential Cracks in Pipes," NUREG/CR-6235, April 1995.

6.5 Rahman, S., and others, "Refinement and Evaluation of Crack-Opening Analyses for Short Circumferential Through-Wall Cracks in Pipe," NUREG/CR-6300, April 1995.

7.0 SUMMARY AND DISCUSSION OF RESULTS

In this section, the key results from the IPIRG-2 program are discussed. First the results from the material property evaluations are discussed, which include a discussion of the effects of dynamic loading on strength and the effects of cyclic and dynamic loading on toughness. Second, the pipe and elbow fracture analyses results are discussed. Finally, the results from other topics considered as part of this program, such as the uncertainty analyses, the computer codes generated in this program, and the seminars held during this program, are discussed.

7.1 Key Results from the Material Property Evaluations

The technical results from the cyclic and dynamic loading rate material property evaluations are discussed in this section. The results from the dynamic strength and toughness evaluations are discussed first, followed by a discussion of the cyclic effects on toughness. Finally, a brief discussion of the combined dynamic and cyclic effects on toughness concludes this section.

7.1.1 Discussion of Loading Rate Effects on the Tensile and Fracture Toughness Properties of Ferritic Nuclear Grade Piping Steels

In this investigation, a series of dynamic tensile and fracture toughness C(T) specimen tests were conducted on a variety of carbon steel materials. For the carbon steel materials evaluated in this investigation, the effects of increased loading rate on the stress-strain behavior were similar to those observed in the IPIRG-1 program (Ref. 7.1). All of the carbon steel materials tested showed a decrease in ultimate strength with an increase in strain rate. This behavior has been attributed to dynamic strain aging (DSA) effects (Ref. 7.2). It is hypothesized that as the strain rate increases, the interstitial atoms have less time to diffuse to the moving dislocations, thus increasing the local plastic strains and lowering the stress-strain curve. Interestingly, even though the ultimate strength decreased in all cases, the yield strengths either increased or were unchanged, with increasing strain rate.

The effects of dynamic loading on the fracture resistance were inconsistent between materials. While some ferritic base metal specimens showed a decrease in resistance with increasing strain rate, others were basically unaffected by an increase in strain rate. Furthermore, the ferritic submerged-arc weld showed a significant increase in resistance with increasing strain rate. This was consistent with what was observed for this weld procedure in IPIRG-1 (Ref. 7.1). The STS410 tungsten-inert-gas (TIG) weld showed no change in resistance with increasing strain rate.

There are two factors that were found to be related to dynamic toughness behavior; the materials' yield-to-ultimate strength ratio and the test temperature-to-room temperature Brinell hardness ratio. The trends from the existing database at 288 C (550 F) suggest that carbon steel materials whose yield-to-ultimate ratios are greater than 0.5 will have dynamic toughness values that are equal to or greater than their quasi-static values. This dependancy on yield-to-ultimate ratio may aid in the creation of a criterion that would help characterize a material's fracture toughness response to dynamic loading. However, the amount of data available to formulate such a criterion are still limited, making it difficult to reliably formulate such a criterion at this time.

The other factor that was examined was the change in Brinell hardness from the test temperature to room temperature, which was used as a dynamic strain aging screening criterion. Correlations with this parameter were generally good, but again there was more scatter in the data than desired. It may be that both of these parameters (the yield-to-ultimate strength ratio and test temperature-to-room temperature hardness) or a different parameter are needed to more accurately describe the change in toughness of ferritic steels at LWR temperatures and dynamic loading rates.

7.1.2 Discussion of Cyclic Effects on the Fracture Toughness of Nuclear Grade Steels

A series of cyclic C(T) specimen tests were conducted on six materials: three stainless steel base metals, a stainless steel SAW, a carbon steel base metal, and a carbon steel SAW. The DP2-A23 stainless steel base metal specimens were tested at a variety of stress ratios and cyclic plastic displacement increments (δ_{cyc}/δ_i). This displacement ratio is the inverse of the number of cycles to ratchet to the displacement at crack initiation in a monotonic test. The DP2-F30 carbon steel base metal, the DP2-A8I, and DP2-A8II stainless steel specimens, and the SAW specimens were conducted at various stress ratios, but only one cyclic plastic displacement increment ($\delta_{cyc}/\delta_i = 0.1$) which corresponds to 10 cycles to get to crack initiation. The J-R curve for each of these cyclic tests were calculated using the upper envelope of the load-displacement-crack growth record and the ASTM E813/1152 procedures. Detailed finite element analyses were conducted that verified that the upper envelope approach to calculating the cyclic J-R curve can be used to predict the fracture toughness response due to cyclic loading.*

7.1.2.1 Effects of Cyclic Loading on J at Crack Initiation (J_i)

DP2-A23 Stainless Steel and DP2-F30 Carbon Steel

For the DP2-A23 stainless steel base metal C(T) tests, it was possible to examine the effect of both the stress ratio (R) and δ_{cyc}/δ_i on J_i. For the larger cyclic plastic displacement increments ($\delta_{cyc}/\delta_i = 0.1$ and 0.2, 10 and 5 cycles to crack initiation, respectively), there was little effect of cyclic loading on J_i, until the stress ratio was less than approximately -0.8. However, for the smallest cyclic plastic displacement increment evaluated ($\delta_{cyc}/\delta_i = 0.025$, 40 cycles to crack initiation), the effect of cyclic loading on the initiation toughness is much more pronounced at the intermediate stress ratio of -0.6.

Since only one displacement increment was evaluated for the DP2-F30 carbon steel base metal material, only conclusions about the effect of stress ratio are made. In comparing the carbon steel results with the stainless steel results at the same cyclic plastic displacement increment ($\delta_{cyc}/\delta_i = 0.1$), the carbon steel seems to be more affected by cyclic loading at the intermediate stress ratios. Note, neither material was affected significantly by the R = 0 load history while both were affected significantly by the R = -1 load history. At a stress ratio of -0.3, the value of J_i from the cyclic C(T) test for the carbon steel material was approximately 60 percent of the value of J_i from the corresponding monotonic test. For the stainless steel evaluated, at the same combination of stress ratio and plastic displacement increment, the cyclic J_i value was nearly the same as the monotonic J_i value. This difference is probably the result of the relative toughness values for the two materials. The tougher, more ductile stainless steel is less susceptible to cyclic loading effects. Metallographic evaluations of a series of cyclic C(T) specimens showed that

* For details of these analyses, the reader is referred to NUREG/CR-6440.

differences in crack tip and void sharpening characteristics between the two materials may be responsible for the different sensitivities to cyclic damage.

For both the DP2-F30 carbon steel and the DP2-A23 stainless steel base metal tested, the cyclic-load C(T) experiments produced J_i values that were in reasonable agreement with the cyclic-load TWC pipe J_i values with similar load histories. Hence, using the TWC pipe δ_{cyc}/δ_i value in the C(T) test gave good similitude at crack initiation.

Submerged-arc welds

As was the case for the carbon steel base metal material, all of the cyclic weld specimens were tested with a cyclic plastic displacement increment of 0.1. In addition, only monotonic, R = -0.6, and fully-reversed (R = -1) stress ratios were considered. Dynamic monotonic loading increased the J_i value for the carbon steel weld (DP2-F40W) by a factor of approximately two when compared with the quasi-static monotonic loading condition, see Figure 2.5. Cycling this material at quasi-static rates at a stress ratio (R) of -1 lowered the J value at crack initiation by approximately 40 percent. When this weld was cycled at a stress ratio of -1 at dynamic loading rates, the J_i value was 10 percent less than the J_i value from the quasi-static, monotonic C(T) test. This observation tends to indicate that the degrading cyclic effects may contribute more to the overall combined effects due to dynamic, cyclic loading than do the enhancing dynamic effects. Similar observations were made for the carbon steel SAW, R = -0.6 tests and the stainless steel SAW, R = -0.6 and R = -1 tests. (See discussion on Combined Dynamic and Cyclic Effects below.)

DP2-A8I and DP2-A8II Stainless Steel Base Metals

These two materials showed considerable difference in the value of J_i under quasi-static, monotonic loading. In fact, the DP2-A8I material's J_i value was 56 percent higher than J_i for the DP2-A8II material. Under quasi-static, cyclic loading, the behavior of these two materials was similar. For quasi-static, R = -0.3 loading, both materials showed a slightly higher J_i value as compared with the quasi-static, monotonic specimens The quasi-static, R = -1 specimens for both materials had a significantly lower value of J at crack initiation as compared with the quasi-static, monotonic specimens. For the DP2-A8I material, the J_i value for quasi-static R = -1 loading was about 40 percent of the quasi-static, monotonic J_i value, while for the DP2-A8II material the J_i value for the quasi-static, R = -1 loading was 57 percent of the quasi-static, monotonic J_i value.

However, the behavior of these materials under dynamic, R = -0.3 loading was considerably different. For the DP2-A8I material, quasi-static, R = -0.3 loading produced a slight increase in J at crack initiation, but no significant difference in crack growth resistance up to about 4 mm (0.16 inch) of crack extension as compared with the quasi-static, monotonic specimen. For the DP2-A8II material, dynamic, R = -0.3 loading produced a significant decease in toughness at both crack initiation and during crack growth as compared with the quasi-static, monotonic resistance. Curiously, for the DP2-A8II material, the resistance under dynamic, R = -0.3 loading was very similar to the resistance under quasi-static R = -1 loading.

7.1.2.2 Effects of Cyclic Loading During Crack Growth

Even though the C(T) specimens were able to predict the J_i values from the TWC pipe experiments using the δ_{cyc}/δ_i scaling parameter, they were unable to predict the crack growth per cycle. The trends from Figure 2.2 suggest that δ_{cyc}/δ_i has to be doubled after crack initiation for the C(T) specimen to have the

same crack growth per cycle as the nominal 6-inch diameter TWC pipe tests that were conducted. An analysis performed* using the quasi-static, monotonic J-R curve and the GE/EPRI J-estimation scheme procedure suggests that this change in δ_{cyc}/δ_i is predictable. Figure 7.1 shows the results of this analysis. This figure shows that a C(T) experiment will have to be conducted with $\delta_{cyc}/\delta_i = 0.2$ in order to match the crack growth per cycle for the nominal 6-inch diameter TWC pipe experiments with $\delta_{cyc}/\delta_i = 0.1$. This analysis suggests that complete similitude can be obtained between the results of the C(T) and TWC pipe tests. A C(T) test can be run with one δ_{cyc}/δ_i value up to crack initiation and a second δ_{cyc}/δ_i value during crack growth. The change in the δ_{cyc}/δ_i value after crack initiation would be different for a surface-crack case as well as varying with pipe diameter. However, at this point, no similitude verification data exists where the δ_{cyc}/δ_i was changed after crack initiation to see if the same J-R curve can be obtained in a cyclic C(T) test as in the past TWC pipe tests.

7.1.2.3 Combined Dynamic and Cyclic Effects

The trends from this investigation suggest that both the dynamic and cyclic (R = -1) effect on toughness may be linearly related to the material's yield-to-ultimate strength ratio. If this is the case, then all that is required to make an estimate of the toughness of a material subjected to dynamic, cyclic (R = -1) loads are the quasi-static, monotonic J-R curve and the stress-strain curve. A method for estimating the dynamic, cyclic resistance ($J_{dyn,cyc}$) may be used that multiplies the quasi-static, monotonic resistance ($J_{QS,mono}$) by the relative decrease in resistance due to both cyclic ($J_{QS,cyc}/J_{QS,mono}$) and dynamic effects ($J_{dyn,mono}/J_{QS,mono}$). The results for the four materials where dynamic, cyclic (R = -1) data have been generated is shown in Figure 2.6. All of the J values shown in Figure 2.6 are taken at a crack extension of 30 percent of the original ligament, i.e., at the maximum limit of crack growth in the tests.

The open symbols in Figure 2.6 represent the results taken directly from the experimental data, i.e., the values of $J_{dyn,mono}/J_{QS,mono}$ and $J_{QS,cyc}/J_{QS,mono}$ were taken directly from the experimental data rather than using the σ_y/σ_u correlation. The solid symbols represent results calculated from the best fit of the data to the material's yield-to-ultimate strength ratio. The trends suggest that by multiplying the percent decrease in the monotonic resistance due to the cyclic and dynamic loading to the quasi-static, monotonic resistance produces a good approximation of the actual resistance due to dynamic, cyclic loading, which suggests that no synergism is present between these separate effects. However, when the linear relationship between the materials' yield-to-ultimate ratio and the relative decrease in quasi-static monotonic resistance due to cyclic and dynamic loading was used, the estimates of the dynamic, cyclic resistance were higher than the experimental values.

However, it should be noted that this trend may not be valid for all cyclic loading histories. As shown with the DP2-A8II material under dynamic, R = -0.3 loading, some interaction between the dynamic and cyclic effects may occur. For this material, since the dynamic, monotonic resistance showed an increase in toughness and the quasi-static R = -0.3 showed no significant change in toughness (after some crack growth), as compared with the quasi-static, monotonic resistance, the dynamic, R = -0.3 resistance should be slightly higher than the quasi-static, monotonic resistance if there is no interaction between the dynamic and cyclic effects. However, as shown earlier, the dynamic, R = -0.3 resistance for this material was

* For details of this analysis, the reader is referred to NUREG/CR-6440.

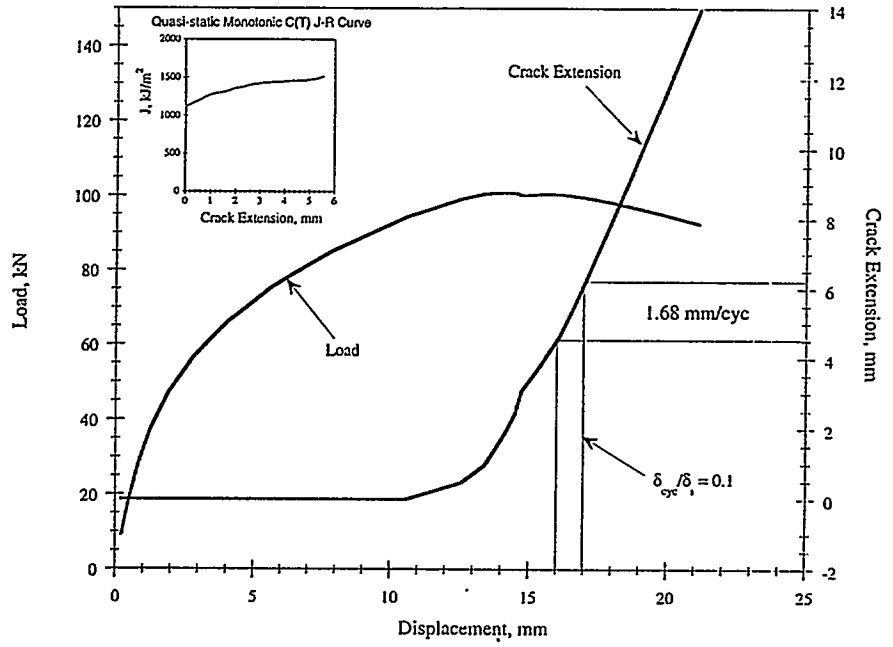

(a) GE/EPRI J-estimation scheme prediction of TWC pipe Experiment 4131-5 (Pipe DP2-A23) (J-R curve used in the calculation is inserted figure)

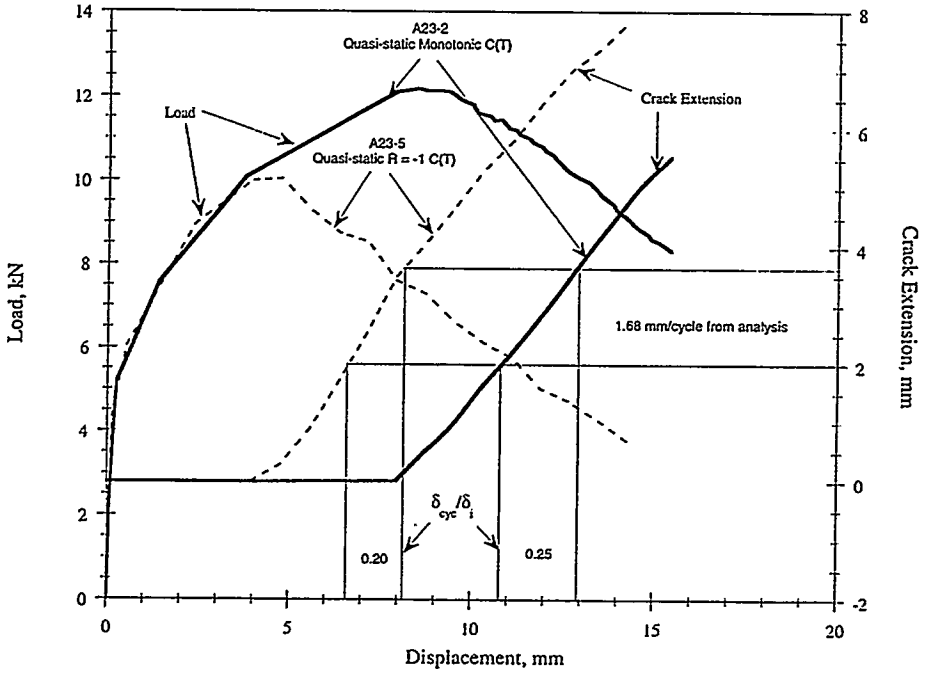

(b) C(T) specimen results

Figure 7.1 Load-displacement-crack growth records from a GE/EPRI TWC pipe prediction and C(T) specimens illustrating the need to change δ_{cyc}/δ_i after crack initiation to produce comparable cyclic crack growth between the two specimen types

considerably lower than the quasi-static, monotonic resistance. Therefore, more data are required before a suitable criterion can be developed to predict the resistance under dynamic, cyclic loading using quasi-static, monotonic properties.

7.2 Key Results from the Straight Pipe and Elbow Fracture Analyses

7.2.1 Straight Pipe Fracture Analyses

In this section, the results of the analyses of the straight pipe and elbow fracture experiments are discussed. Prior to discussing these results in detail, a discussion pertaining to the "intuitively consistent" crack size definition and material property data to use in the fracture analyses is presented.

7.2.1.1 Effect of the Choice of Flaw Size Definition on the Fracture Predictions

Few of the surface-cracked pipe experiments conducted as part of this program involved well-defined, constant depth flaw shapes, such as what is assumed for an ASME Code-type analysis. A number of the pipe experiments involved cracks which were significantly deeper at a location removed from the crack centerline where the bending stress was the highest. Furthermore, a number of the experiments involved cracks in welds. The prediction of the behavior of cracks in welds is complicated by the presence of weld crowns and counterbores. As a result, an assessment was made using what was believed to be an "intuitively consistent" definition of crack size to use in the fracture prediction analyses in order to account for these complications so that the results of these experiments could be compared on an equal basis. The discussion that follows provides the highlights of that assessment.

Assessment of the Effect of Off-Centered Cracks

Typically, the "intuitively consistent" definition of crack size was assumed to be a constant depth crack for the entire crack length and the depth was equal to the maximum crack depth, much in the spirit of the crack size used in a code-type flaw evaluation. However, for experiments which had a significant "off-centered" crack, such as Experiment 1-2, using the idealized ASME definition of crack size could result in predictions which are 20 to 30 percent lower than would be expected based on the previously established accuracy of the different fracture prediction methods (Ref. 7.3), unless measures were taken to account for the maximum crack depth location being "off-center". In comparing the experimental results with the analysis predictions for the cases where there was a significant "off-centered" crack, the experimental bending stresses were reduced by the cosine of the angle between the crack centerline and the location where the crack was deepest, see Figure 7.2. Alternatively, one could increase the predicted stress in the denominator by dividing the predicted stress by the cosine of the angle between the crack centerline and the location where the crack was deepest.

Assessment of the Effect of Weld Crowns and Counterbores

For the experiments which involved cracks in welds, the wall thickness was assumed to be the actual wall thickness of the pipe plus the weld crown height and the crack depth was referenced to the inside surface

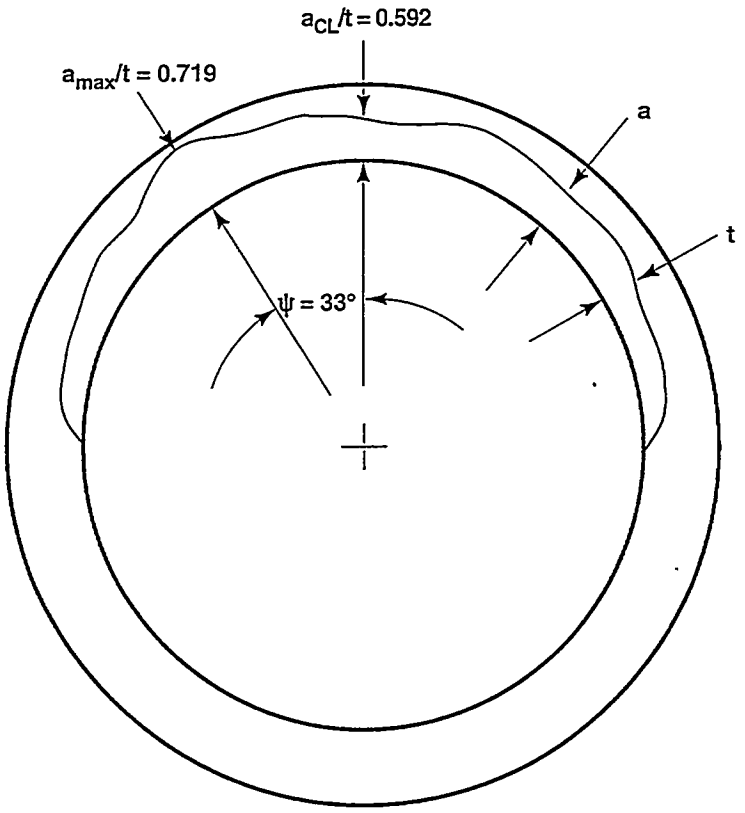

Figure 7.2 Sketch of an "off-centered" crack showing the angle ψ between the crack centerline where the bending stresses are highest and the location along the crack front where the crack is the deepest

of the pipe. This is somewhat different than what would be assumed for an ASME Code-type analysis in that Paragraph NB-3641.1 of Section III suggests that the wall thickness should be the wall thickness of the pipe less the material removed for counterboring. As such, it seems likely that an ASME Code-type analysis would reference the crack depth to the inside surface of the counterbore and not the inside pipe surface. In addition, the height of the weld crown would in all likelihood be ignored in such an analysis, which may be appropriate if the crack is not in the center of the weld. Also, in service, the weld crown may be ground off to ease UT inspection.

Comparisons of maximum moment predictions using the "intuitively consistent" and ASME Code definitions of crack size were made for seven experiments which involved cracks in welds, see Table 7.1. The predictions were made using the SC.TNP1 analysis method since that method, along with the DPZP method, was found to be most accurate when compared with experimental data (Ref. 7.3). As shown in Table 7.1, the predictions using the ASME Code definition of crack size were on average 20 to 40 percent lower than the predictions using the "intuitively consistent" definition of crack size for the case where the cracks were in girth welds.

Table 7.1 Comparison of maximum moment predictions between using the "intuitively consistent" and ASME Code crack size definitions for the SC.TNP1 analysis method for seven experiments which considered cracks in welds

Experiment Number	"Intuitively Consistent," kN-m	ASME, kN-m	ASME/ "Intuitively Consistent"
1-3[1]	691.3	411.0	0.595
1-4[1]	682.0	411.0	0.603
1.3-4	702.2	535.0	0.762
1-5	794.8	622.6	0.783
1-6	605.8	461.0	0.761
4141-4	454	349.9	0.771
1.3-5	425.4	355.7	0.836

(1) Using straight pipe dimensions and stress strain curve.

Both of these findings on the effects of "off-centered" cracks and weld crowns and counterbores show the degree of conservatism associated with using an idealized Code-type consistent depth flaw shape geometry to analyze real cracks shapes, typical of those found in service. Obviously, if a crack found in service is significantly "off-center" and in a weld, then the effect of using the idealized constant depth flaw shape geometry will be compounded.

7.2.1.2 Determination of Appropriate Material Properties to Use in Dynamically-Loaded Pipe Test Predictions

The current practice in dynamic pipe fracture analyses is to determine the peak uncracked pipe dynamic loads, and use them in a fracture analysis. Typically, quasi-static material properties are used in the fracture analyses. As shown in this report, loading rates typical of seismic events can cause the strength and toughness of nuclear piping materials to change. Consequently, it is important to determine the appropriate material properties to use in a dynamic analysis.

The determination of the loading rate for the J-R curve is relatively simple. This is because large amplitude dynamic loads will occur near the first natural frequency of the pipe system of interest. Hence, the J-R curve specimen should be tested so that the time to reach crack initiation corresponds to one quarter of the period of the first natural frequency. This approximates to the rate of loading if the crack initiated in one large amplitude cycle of an earthquake time-history where this is not a gradual cyclic build-up.

It was shown in Section 4 of this report that reasonably accurate predictions could be made using quasi-static J-R curves in conjunction with quasi-static stress-strain data to analyze the quasi-static pipe experiments. For dynamic pipe experiments, dynamic J-R curve data in conjunction with quasi-static stress-strain data seemed to result in predictions most closely aligned with results reported previously for the various fracture prediction methods (Ref. 7.3).

Even though the quasi-static stress strain curve appeared to produce the most consistent predictions, a sound technical justification is required before a conclusion can be drawn about using the quasi-static stress-strain curve in dynamic predictions. To make this justification, a comparison between the load-displacement responses of the quasi-static and dynamic, monotonically-loaded TWC pipe and C(T) experiments for both the 6-inch nominal diameter STS410 and the A106 Grade B material were made. None of comparisons showed any differences in the load-displacement response up to crack initiation. Even for the carbon steels whose initiation toughnesses were different under quasi-static and dynamic loading, the load-displacement response was identical up to crack initiation. This result indicates that the global strain rate response in the dynamic experiments conducted in this program is identical to the strain rate response of the quasi-static experiments. There was only one exception to the experimental observations of quasi-static and dynamic load-displacement curves prior to crack initiation being reasonably close. This was for the IPIRG-2 16-inch nominal diameter through-wall-cracked pipe tests. In this case, the quasi-static pipe test exhibited a lower yield load and more strain-hardening than the dynamic test. This trend was consistent with static versus dynamic stress-strain curves. A complication with this test, however, was a large difference in angled crack growth. Evidence from past video tapes of experiments with angled crack growth showed the crack tip plastic zone formed at an angle prior to crack growth. This angled plastic zone may have affected the load-displacement curve shape. Therefore, the bulk of the experimental evidence indicates that the quasi-static stress-strain curve is sufficient for dynamic fracture predictions at the rates investigated in this program for cracked pipe. Perhaps if the pipe was uncracked or had a much smaller crack than used in this program, then the uncracked pipe would be experiencing plastic strains at high rates. In that case, perhaps the dynamic stress-strain curve is needed.

7.2.1.3 Discussion of Straight-Pipe Fracture Analyses Results

In this section, the results from the pipe fracture analyses conducted in this program will be discussed. These analyses include maximum moment predictions for: (1) the 6-inch nominal diameter, cyclic and dynamic TWC pipe experiments conducted in this program and the IPIRG-1 program, (2) a series of cyclic and dynamic sensitivity studies aimed at studying the effects of dynamic and cyclic loads on larger diameter TWC pipes, and (3) maximum moment predictions for both the single-frequency and simulated-seismic, pipe-system experiments. This section concludes with a discussion of the inherent inaccuracies associated with the current fracture prediction and failure avoidance criteria.

Discussion of the Results from the 6-inch Diameter Separate Effects Pipe Experiments

As part of IPIRG-2, a total of five 6-inch nominal diameter, through-wall-cracked, separate effects pipe fracture experiments were conducted. Four evaluated the fracture behavior of a Japanese STS410 carbon steel pipe material. The purpose of this series of tests was to ascertain whether or not this Japanese pipe steel was as susceptible to dynamic and cyclic loading effects as was the A106 Grade B pipe material evaluated in IPIRG-1 (Ref. 7.4). The results from the material characterization tests (i.e., tensile and C(T) specimen tests) on the STS410 material indicated that this material was not as susceptible to dynamic loading rate effects as was the particular A106 Grade B pipe material evaluated in IPIRG-1. The purpose of the fifth experiment was to evaluate the fracture behavior of the A106 Grade B pipe material evaluated in IPIRG-1 at an intermediate stress ratio (i.e., R = -0.6). In this section, both the effects of dynamic and cyclic load histories will be discussed. In addition to these five separate effect pipe experiments, there was a series of twelve, 6-inch nominal diameter, separate effects, pipe experiments conducted as part of IPIRG-1 (Ref. 7.4).

To investigate the effect of pipe diameter on the maximum moment for cyclically-loaded pipe, a series of

SUMMARY AND DISCUSSION OF RESULTS Section 7

Table 7.3 Comparison of fracture ratios (experimental to predicted maximum loads) for two quasi-static, cyclic (R = -1) pipe experiments (1.2-4 and 1.2-5) for two analysis methods (LBB.ENG2 and LBB.NRC) using four different J-R curves

				Calculated Fracture Ratios Using Different J-R Curves			
Expt. No.	Material	J-estimation Scheme Method	Accuracy Established from Reference 7.5 (Mean/Std Dev)	Mono C(T)	C(T) R = -1 $\delta_{cyc}/\delta_i = 0.2$	C(T) R = -1 $\delta_{cyc}/\delta_i = 0.1$	C(T) R = -1 $\delta_{cyc}/\delta_i = 0.025$
1.2-4	A106B	LBB.ENG2	1.04/0.134	0.972	NA	1.205	NA
1.2-4	A106B	LBB.NRC	1.01/0.106	0.825	NA	1.052	NA
1.2-5	TP304	LBB.ENG2	1.04/0.134	1.254	1.398	1.392	1.493
1.2-5	TP304	LBB.NRC	1.01/0.106	1.008	1.097	1.071	1.123

predictions were made for the circumferential TWC in the base metal of both stainless steel and carbon steel pipe. As shown in Section 4, the calculations suggest that as the pipe diameter was increased, the maximum moment at all stress ratios was decreased. Interestingly, for the stainless steel base metal, the percent decrease in load-carrying capacity between J-R curves at different stress ratios was 20 percent, ranging from 20 to 27 percent decrease for 152m (6-inch) to 1.3m (51.2-inch) diameter pipe, respectively. The decrease in load-carrying capacity in the carbon steel was greater at large diameters than at small diameters.

It should be noted though that this analysis does not fully account for the effect of the cyclic through-wall crack growth on the predictions. For large diameter pipes, the number of cycles to reach maximum moment will be large when compared with the number of cycles to reach maximum moment for the smaller diameter pipes. As such, the remaining ligament, as a function of the pipe circumference, will decrease much faster for the small diameter case than it will for the large diameter case. Thus, it is possible that a cyclic load history may have less of an effect on the moment-carrying capacity of a large diameter pipe than it does on a small diameter pipe. In order to quantify this hypothesis, a cyclic dJ/da crack growth analysis was conducted. The results of such an analysis illustrate that the likelihood of attaining the required number of cycles to reach a maximum moment condition during a single seismic event, with its typical 5 to 30 large amplitude cycles, is much higher for a small diameter pipe than for a large diameter pipe, see Figure 7.3. The results from Figure 7.3 also indicate that a seismic event with a stress ratio of -1 is likely to take a TWC pipe beyond its maximum load-carrying capacity for all pipe sizes considered. However, surpassing maximum moment does not constitute a double-ended-guillotine break; instability of the crack would depend on many factors, for example, the ratio of the primary to secondary stresses.

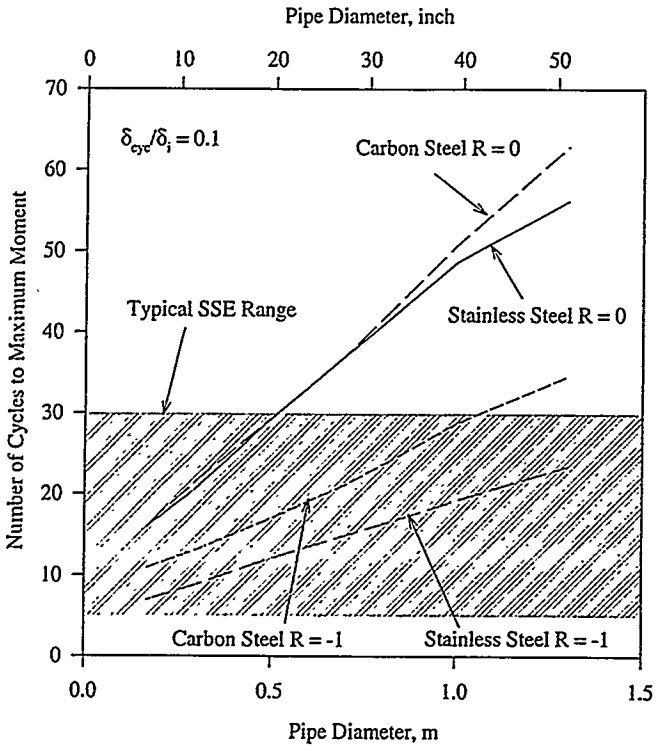

Figure 7.3 Calculated number of cycles to maximum moment as a function of pipe diameter based on a cyclic dJ/da crack growth analysis

Discussion of Analysis Results from Single-Frequency and Seismic Pipe-System Experiments

Effect of Seismic Load History

As part of the EPRI/NRC Piping Reliability Program (Ref. 7.6), seismic load histories were applied to uncracked pipe systems. From those results, it was shown that an uncracked piping system could withstand seismic histories many times greater than the design basis earthquakes (Safe-Shutdown Earthquake [SSE]) typically used in the design of nuclear power plants. As a result of this finding, the ASME Section III Code allowable stresses were increased to take credit for this apparent conservatism. (Note, the U.S. NRC has yet to endorse these rule changes.) Furthermore, as a result of the experiments conducted as part of Reference 7.6, it was shown that the failure mode of an uncracked piping system was fatigue ratcheting, and not fracture.

One of the questions left unresolved at the conclusion of the EPRI/NRC (Ref. 7.6) and IPIRG-1 (Ref. 7.7) programs was what effect a seismic load history would have on the fracture behavior of a cracked piping system. All of the cracked pipe-system experiments conducted as part of IPIRG-1 used a single-frequency, increasing amplitude forcing function. At the end of IPIRG-1, the state-of-the-art of pipe fracture analyses

was such that it was possible to predict the fracture behavior of one of these single-frequency cracked-pipe-system experiments using a nonlinear spring representation of the nonlinear crack behavior with a high degree of confidence, given that appropriate material property data were available and the dimensions of the pipe and crack were adequately defined*. Using SC.TNP1 analyses to calculate the moment-rotation response of the cracked pipe section, it was possible to predict the response of single-frequency pipe-system experiments with such fidelity that the cycle number on which the crack would penetrate the pipe wall could be predicted with high accuracy.

As the IPIRG-2 program was being formulated, it was unknown how well this analysis methodology worked for the case of a seismic load history with its rich frequency content and greater number of load cycles. In order to address this question, two simulated-seismic, surface-cracked, pipe-system experiments were conducted as part of this program. The seismic load history applied to the piping system was designed to be compatible with U.S. NRC Standard Review Plan (SRP) 3.7.1 (Seismic Design Parameters), U.S. NRC Reg. Guide 1.60 (Design Response Spectra for Seismic Design of Nuclear Power Plants), U.S. NRC Reg. Guide 1.61 (Damping Values for Seismic Design of Nuclear Power Plants), ASCE Standard 4-86 (Seismic Analysis of Safety-Related Nuclear Structures and Commentary on Standard for Seismic Analysis of Safety-Related Structures), and ASME Boiler and Pressure Vessel Code, Appendix N. The load history was derived from an analysis of a PWR nuclear plant on a soil foundation with many simplifying assumptions. The frequency content and spectral amplitudes were reasonably consistent with actual plant design. Figure 7.4 shows the response spectra for this simulated-seismic load history. The damping values shown are representative of values for floor response spectra for nuclear power plants and are not equivalent to the damping associated with the IPIRG pipe loop. From Figure 7.4, it can be seen that the IPIRG simulated-seismic load history contains frequencies up to 40 Hz, with most of the large amplitude cycles occurring in the 1 to 10 Hz range.

As part of this program, it was shown that the fracture ratios** for the simulated-seismic, surface-cracked, pipe-system experiments were higher than the fracture ratios for the companion, single-frequency, pipe-system experiments. Initially this finding was somewhat perplexing in that the number of load cycles associated with the simulated-seismic experiments was significantly higher than the number of cycles associated with the single-frequency experiments. Furthermore, the effective stress ratio ($R_{effective}$), accounting for the stress contribution due to internal pipe pressure, was more negative for the simulated-seismic experiments than it was for the single-frequency experiments. As such, it was expected that cyclic degradation, and consequential reduction in load-carrying capacity, for the simulated-seismic experiments would be greater than for the single-frequency experiments. This apparent inconsistency has been

---

* The biggest limitation associated with this type of analysis is not the fidelity of the fracture prediction models, but the definition of the crack depth from nondestructive evaluation (NDE) techniques.

** "Fracture ratio" is defined as the experimental-to-predicted maximum stress.

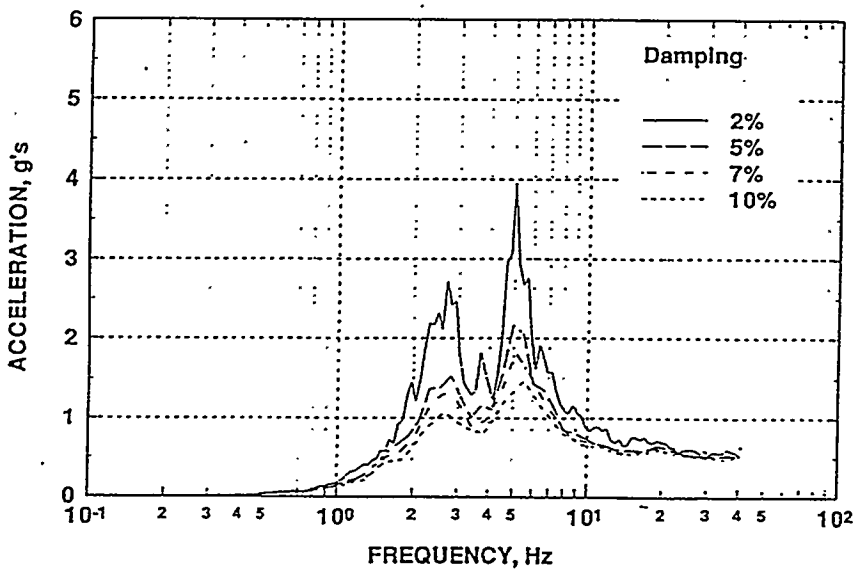

Figure 7.4 Response spectra for the simulated-seismic forcing function used in IPIRG-2

attributed to the fact that the cycles prior to maximum load for the simulated-seismic, pipe-system experiments were primarily elastic, see Figure 7.5a, while the cycles prior to maximum load for the single-frequency experiments exhibited a significant amount of plasticity, see Figure 7.5b. The fact that the cycles prior to maximum load for the simulated-seismic experiments were essentially elastic implies that these experiments could probably be analyzed much in the same manner as one would analyze a dynamic monotonic experiment. This was due to the particular forcing function used for the IPIRG-2 simulated-seismic experiments. If some other simulated-seismic history was used with a more gradual buildup of the large amplitude cycles, then the extent of cyclic degradation that occurred during these simulated-seismic experiments may have increased.

As part of Problem Set C of the IPIRG-2 Round Robin Analyses (NUREG/CR-6337), four different but "equal" displacement-time histories were created from the same peak-broadened acceleration response spectrum. The maximum moment calculated from an elastic finite element analysis of the IPIRG piping system were similar for each (to within 20 percent), but the timing, number, and build-up of the moment peaks were substantially different. It is not clear that merely being consistent with a given input spectrum is a sufficient design specification due to differences in loading rate and load history effects. This work

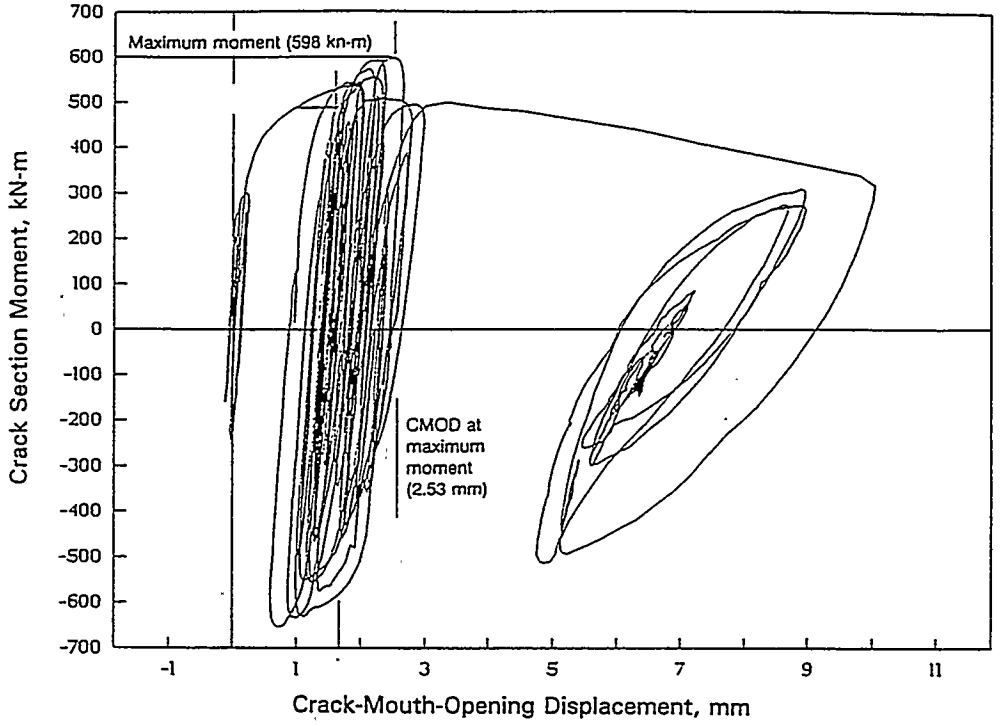

(a) Experiment 1-1

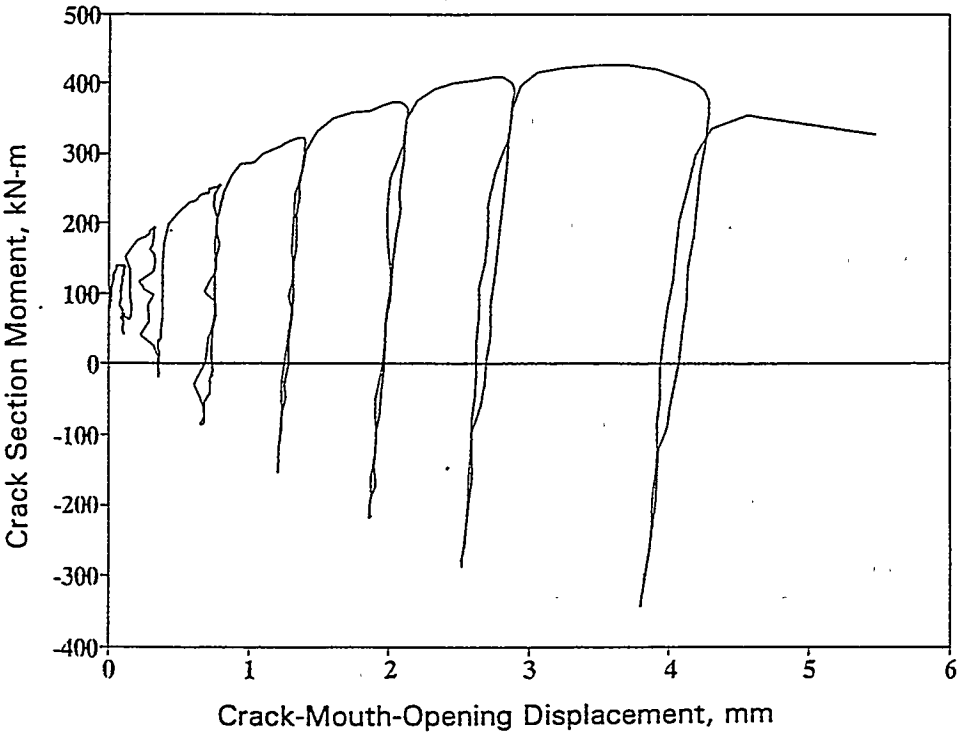

(b) Experiment 1.3-3

Figure 7.5 Comparison of moment-CMOD response for the stainless steel base metal, simulated-seismic, pipe-system experiment conducted as part of IPIRG-2 (Experiment 1-1) and the stainless steel base metal, single-frequency, pipe-system experiment conducted as part of IPIRG-1 (Experiment 1.3-3)

showed that although the IPIRG-2 program seismic displacement-time history forcing function met all of the current ASME, NRC, etc. design requirements, it is not known if it is lower-bound, upper-bound, or average in terms of crack driving force considerations. A more severe loading than the IPIRG-2 seismic time history would include a gradual build-up of cycle amplitudes to the peak amplitude, and perhaps more of the large amplitude cycles. The frequency of occurrence of this more severe type of seismic history compared to the frequency of occurrence of a seismic event with a large amplitude cycle with little build-up (closer to the IPIRG-2 time history) is unknown at this time.

Surface Cracks in Elbow Girth Welds

Another question left unresolved at the end of the IPIRG-1 program was the effect of a change in pipe system geometry near the crack location, such as at the junction of an elbow and a straight pipe section, on the fracture behavior of a cracked pipe system. The specific question of interest to a number of the IPIRG-2 participants was whether or not one could use fracture analysis methods previously developed and verified for cracks in straight pipe runs to analyze cracks at geometric discontinuities, such as at an elbow/straight pipe girth weld. In order to address this question, two elbow/straight pipe girth weld experiments were conducted as part of Task 1 of the IPIRG-2 program with surface cracks in the girth welds. In addition, there were two straight pipe-to-straight pipe girth weld experiments conducted as part of the Degraded Piping (Ref. 7.9) and IPIRG-1 (Ref. 7.7) programs, to which the results from the two elbow/straight pipe girth weld experiments from IPIRG-2 could be compared. The same carbon steel C-Mn-Mo-Ni submerged-arc weld procedure was used in fabricating the test welds for all four of these experiments.

It was shown in Section 4.0 that the calculated fracture ratios (experiment/predicted maximum loads) for the companion straight pipe experiments from References 7.7 and 7.9 agreed very closely with those for the elbow/straight pipe girth weld experiments from this program, especially for the case when the straight pipe dimensions and the straight pipe stress-strain curve were used in the analyses of the elbow/straight pipe girth weld experiments. In fact, for the SC.TNP1 analysis method (which was shown in Reference 7.3 to be the best predictor of maximum stresses), the calculated fracture ratios for the four experiments agreed within 5 percent of each other, see Table 4.10. This finding suggests that straight-pipe analyses can be used to predict the load-carrying capacity of surface cracks located in elbow/straight pipe girth welds. As such, no new analysis methods for predicting the load-carrying capacity for this geometry condition need to be developed.

Although the existing analysis methods did a consistent job of predicting the load-carrying capacity of surface cracks in elbow/straight pipe girth welds, these same methods did a poor job of predicting the crack section rotations for this crack location. Figure 7.6 shows a comparison of the experimental moment-rotation response with the SC.TNP1 predicted moment-rotation response for the elbow girth weld pipe-system experiment (1-3). Figure 7.7 shows a similar comparison for the short surface-cracked, straight pipe-to-straight pipe, stainless steel weld, pipe-system experiment (1-5). As can be seen in Figures 7.6 and 7.7, the SC.TNP1 analysis method did a good job of predicting the maximum moments for both experiments. Furthermore, it did a good job of predicting the rotations for the straight-pipe, girth weld experiment (1-5). However, it did a very poor job of predicting the rotations for the elbow girth weld experiment (1-3). The predicted rotations for Experiment 1-3 were a factor of ten less than the

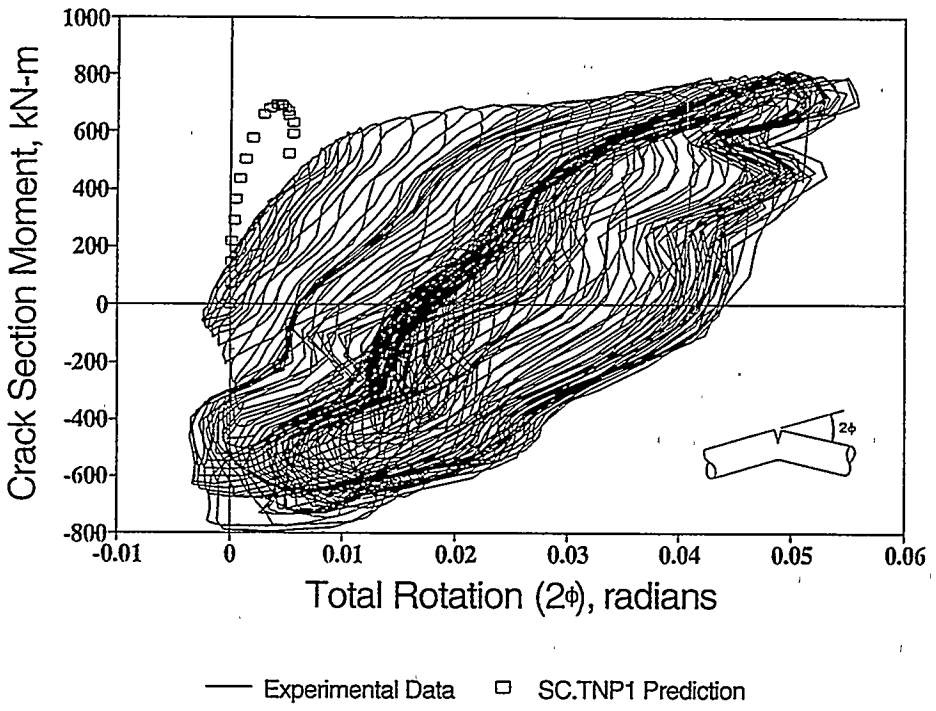

Figure 7.6 Comparison of the experimental moment-rotation response with the SC.TNP1 predicted moment-rotation response for Experiment 1-3

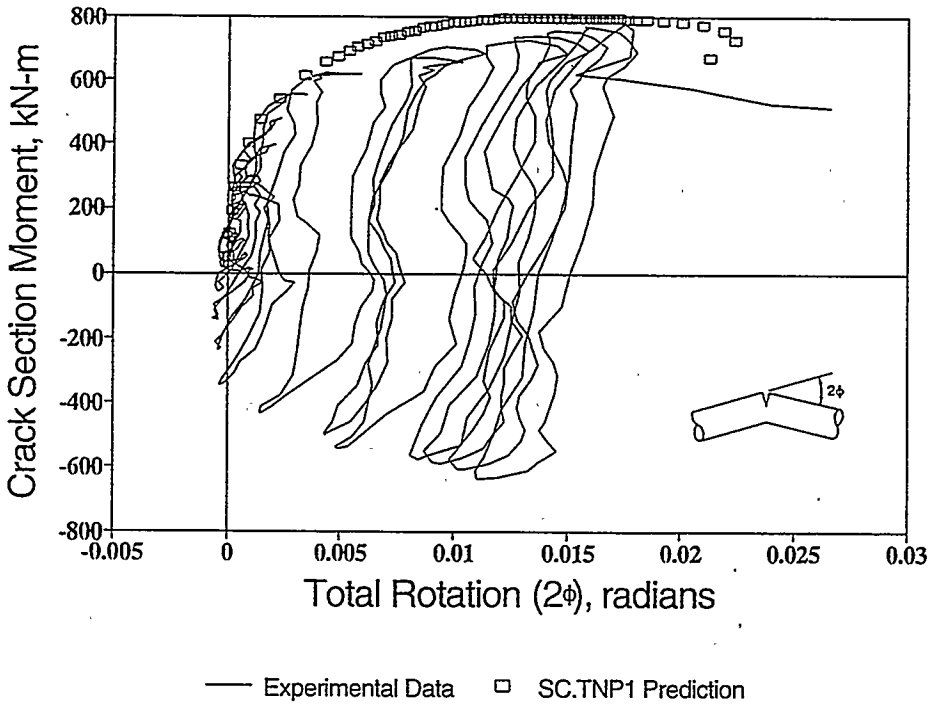

Figure 7.7 Comparison of the experimental moment-rotation response with the SC.TNP1 predicted moment-rotation response for Experiment 1-5

experimentally measured rotations for this experiment. Furthermore, the experimentally measured rotations for the elbow girth weld experiment were a factor of approximately three greater than the experimentally measured rotations for the straight-pipe, girth weld experiment. The larger rotations for the elbow girth weld case resulted in significantly higher predictions of J at crack initiation from the pipe η-factor analyses of these elbow girth weld experiments.

Finally, it should be noted that for a through-wall crack close to an elbow or nozzle in a pipe system, elastic finite element analyses results presented in the Uncertainty Report (NUREG/CR-6443) showed there can be a restraint of the pressure-induced bending. For large cracks, as in small and intermediate diameter pipe for LBB analyses, this restraint of pressure-induced bending will cause the crack-opening displacement to be much smaller than all existing estimation schemes and leak-rate codes assume. For a surface crack, the magnitude of the pressure-induced bending is much smaller and hence is of lesser importance.

Accuracy of Analyses for Weld Crack Experiments

In the prior sections, results from experiments on pipes with cracks in the center of carbon steel and stainless steel welds were discussed. These evaluations mainly looked at different geometric or loading conditions, i.e., can surface-cracks in elbow girth welds be analyzed using straight pipe solutions, what are the effects of short versus long crack, and what are the differences between dynamic/cyclic loading versus quasi-static loading. As discussed earlier: (1) for the elbow girth weld surface crack case, the straight pipe solutions appeared adequate, (2) the existing surface-cracked pipe analyses have the same degree of accuracy for the short and long surface cracks evaluated, and (3) for the welds examined, the effect of dynamic/cyclic loading was negligible, and perhaps even helpful for the carbon steel weld tested.

Another aspect of interest is the relative accuracy of the analyses for the stainless steel and carbon steel weld crack experiments. In these analyses, the "intuitively consistent" flaw size definition included the weld crown in the pipe thickness since the crack was in the center of the weld. Including the weld crown in the analyses of these experiments results in an analysis similar to the case where weld crowns have been removed in service for UT inspection. (In the IPIRG programs, no weld crowns were removed.) Consequently, for the same experiments discussed in the IPIRG-1 program, the predicted maximum moments were much different. This is not unexpected, since the weld crown height increases the ligament significantly for the deep surface cracks evaluated.

An interesting point is that the accuracy of the predicted maximum loads for the stainless steel SAW experiments was consistent with base metal experiments when the weld crown height is considered. The only surface-cracked girth weld pipe experiment with the weld crown ground off that we are aware of was a stainless steel experiment in the Short Cracks in Piping and Piping Welds program, Experiment 1.2.3.16 in Reference 7.3. The experimental maximum load for that case was exactly in agreement with the predictions for the analysis methods that were the most accurate for the base metal surface-cracked pipe experiments. This observation is consistent with the analyses in this program when the weld crown is included in the fracture evaluations for the stainless steel SAW experiments.

For the carbon steel SAW experiments, if the weld crown is included in the thickness, the experimental maximum loads are overpredicted by 10 to 20 percent; see the DPZP and SC.TNP1 analyses prediction in Table 4.10. For the carbon steel weld experiments, ignoring the weld crown resulted in predicted failure loads that were 25 to 30 percent below the experimental results (as in the IPIRG-1 predictions).

Although accounting for the weld crown heights was needed to better understand the trends from the experimental data, from this assessment, it appears prudent to not include the weld crown height in the thickness for service applications. After all, it may not be known if the flaw is centered exactly under the weld crown anyway. However, this raises the question of the accuracy of the fracture predictions if the weld crown was not present, particularly for the carbon steel weld case. Furthermore, if the weld was inspected, then more than likely the weld crown would be removed. In hindsight, it might have been better to conduct all the experiments without the weld crowns ground off.

Effect of Shorter Crack Sizes

During the Degraded Piping (Ref. 7.9) and IPIRG-1 (Ref. 7.7) programs, the nominal crack sizes used in the pipe experiments were relatively large, i.e., 37 percent of the pipe circumference in length for through-wall-cracked pipe experiments and 50 percent of the pipe circumference in length and 66 percent of the pipe wall thickness in depth for surface-cracked pipe experiments. For surface-cracked pipe, the nominal crack size used in the IPIRG-1 and Degraded Piping Programs is near the limit of flaw sizes considered for evaluation in Table H-5310-1 of Section XI for ferritic pipe and Table IWB-3641-1 of Section XI for austenitic pipe. These larger crack sizes were chosen for these experiments to facilitate analyses of the experiments since the maximum loads were low enough that the stresses in the uncracked pipe were typically elastic, i.e., all of the plasticity was concentrated at the crack section.

While larger crack sizes facilitated analyses, they were not representative of the crack sizes typically considered in Leak-Before-Break (LBB) or in-service flaw evaluation analyses. For U.S. LBB analyses, the size of the postulated through-wall crack is fixed by a prescribed minimum detectable leak rate, where the leak rate is based on leak detection capabilities. In U.S. NRC Standard Review Plan (SRP) 3.6.3 (Ref. 7.10), a margin of 10 on leakage detection is required unless a detailed justification can be provided which accounts for the effects of potential uncertainties, e.g., particulate plugging, measurement techniques, personnel qualifications, and frequency of monitoring. For large diameter pipes, these criteria typically result in a postulated through-wall crack size of 6 to 8 percent of the pipe circumference.

It was decided to include a series of shorter crack experiments (both through-wall and surface-cracked pipe) in the IPIRG-2 program to demonstrate that the analysis methods previously developed and validated for the long crack case were adequate for the case of shorter cracks. As part of the U.S. NRC Short Cracks in Piping and Piping Welds Program (Refs. 7.3 and 7.5), a number of shorter surface-cracked and through-wall cracked pipe experiments were conducted, but the loading conditions were always quasi-static, monotonic, four-point bending. No dynamic or cyclic loadings, such as real plant piping will experience under seismic loading, were included.

The cracks in the test specimens for the two IPIRG-2 short surface-cracked pipe experiments were located in stainless steel pipe-to-pipe girth welds. The nominal crack size for these experiments was 25 percent of the pipe circumference in length and 50 percent of the pipe wall thickness in depth. The welds were submerged-arc welds made according to a procedure that was supplied to Battelle by the General Electric (GE) Corporation as part of the Degraded Piping Program (Ref. 7.9). Companion quasi-static, monotonic, four-point bend and companion single-frequency, pipe-system, long surface-crack pipe experiments were conducted as part of the Degraded Piping (Ref. 7.9) and IPIRG-1 (Ref. 7.7) programs, respectively. In Section 4.0 it was shown that when allowances were made in the analysis of Experiment 1-5 for the lowering of the J-R curve due to cyclic loading, that the SC.TNP1 calculated fracture ratios for the four pipe experiments all agreed within 3 to 7 percent of each other, see Table 4.11. This is well within the

experimental scatter typically observed for these types of experiments. This tends to indicate that the surface-cracked pipe analysis methods, which had previously only been verified using quasi-static, monotonic, pipe fracture data, are probably adequate for shorter surface-cracks subjected to dynamic, cyclic load histories. This result is consistent with the toughness testing results that showed that for this stainless steel weld, dynamic loading increased the toughness, KR = -0.6 cyclic loading decreased the toughness, and the net result was that the combined dynamic/cyclic loading J-R curve was only slightly below the quasi-static monotonic J-R curve (see Section 2.0).

For the case of the IPIRG-2 through-wall-cracked, simulated-seismic, pipe-system experiment (1-7), it was found that the fracture ratios using the GE/EPRI (Ref. 7.11), LBB.NRC (Ref. 7.12), and LBB.ENG2 (Ref. 7.13) J-estimation schemes agreed very closely with the average fracture ratios reported for these three methods for six quasi-static pressure and bend experiments previously analyzed during the Short Cracks Program (Ref. 7.5). From Table 4.31 of Reference 7.5, it can be seen that the average fracture ratio for the six previously conducted pressure and bend, through-wall-cracked experiments was 1.31 for the GE/EPRI method, 1.17 for the LBB.NRC method, and 1.18 for the LBB.ENG2 method. These values compare well, within 2 to 7 percent, with the corresponding values for Experiment 1-7, i.e., 1.25 for the GE/EPRI method, 1.15 for the LBB.NRC method, and 1.11 for the LBB.ENG2 method, see Table 4.12. Consequently, based on this comparison, it appears that the previously developed through-wall-cracked analyses, which had previously only been verified using quasi-static, monotonic, pipe fracture data, work equally well for the case of a short through-wall-cracked, dynamic, cyclic pipe-system experiment.

An interesting observation for the pressure and bend cases compared to the pure bending pipe solutions is that there seems to be an extra degree of conservatism inherent in the combined load case. We believe that this may come from the assumptions in the analyses that the pipe is free to rotate from the induced pressure axial loads. In reality, for a pipe system, or in a pipe pressure and bend test, the pipe ends are restrained or loaded in a fixed displacement fashion. Hence, the pressure-induced rotation is limited which reduces the crack-driving force.

7.2.1.4 Inherent Inaccuracies Associated with the Current Fracture Analyses and Failure Avoidance Criterion

ASME Z-Factor Procedures

The ASME Code Section XI flaw evaluation procedures found in Appendix C (austenitic materials) and Appendix H (ferritic materials) specify that the flow stress be defined in terms of the Code Design Stress Intensity (S_m) value from Table 2A of Part D of Section II of the ASME Code. (The Appendix H criteria allows use of the average of the yield and ultimate strengths for the flow stress definition.) For the ferritic materials, the flow stress based on S_m is defined as $2.4S_m$. For the austenitic materials, the flow stress is defined as $3S_m$. In Section 4.0 of this report, the S_m value was established in two ways: (1) using values from Table 2A of Part D of Section II of the ASME Code to determine the S_m using actual properties, i.e., S_m(Code), and (2) using the criteria specified in Article 2110 of Appendix III of Section III Division 1 of the 1989 Edition of the ASME Code, i.e., S_m(Actual). The S_m(Actual) definition was used to analyze each pipe test as if the material properties of the test specimen pipe had strength properties as specified in the Code. This allows a more technically sound evaluation of the actual flaw evaluation procedures embodied in the Code. Figure 7.8 is a bar chart showing a comparison of the flow stresses using actual tensile data, i.e., the average of yield and ultimate strengths, the S_m(Code) values, and the S_m(Actual) values for five pipe/elbow materials used in the IPIRG-2 program. From Figure 7.8, it can be seen that the flow stress

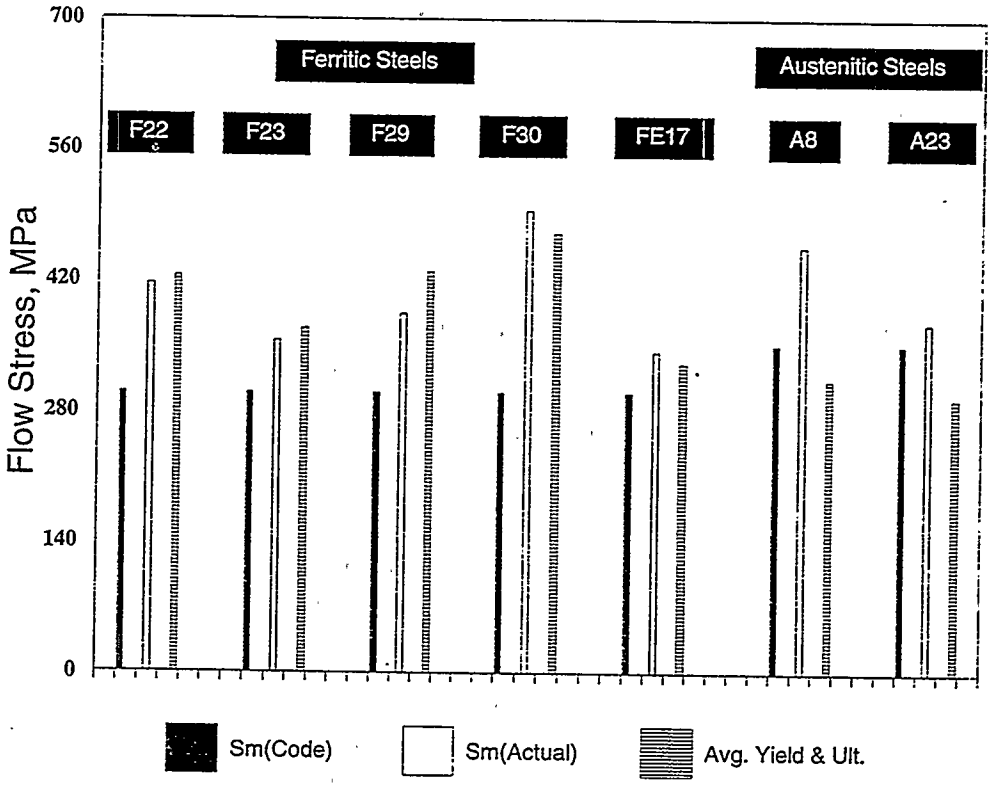

Figure 7.8 Comparison of flow stresses using actual tensile data (average of yield and ultimate) and flow stresses based on S_m(Code) and S_m(Actual) values

based on S_m(Actual) was within 12 percent of the flow stress based on the average of the measured yield and ultimate strength values for the four ferritic materials considered. In fact, for three of the four ferritic materials, the flow stress based on S_m(Actual) was within 4 percent of the flow stress based on measured values. On the other hand, the flow stresses based on S_m(Code) were 10 to 40 percent less than the flow stresses based on measured tensile properties. These findings support the contention that using the S_m(Actual) definition for flow stress provides a reasonable means for evaluating the technical basis of the Code procedures by analyzing the pipe experiments as if the pipes used had the properties defined in Section II of the ASME Code, at least for the case of the ferritic experiments.

For the austenitic material (i.e., DP2-A8), the flow stress based on the average of the yield and ultimate strengths was approximately 10 percent less than the flow stress ($3S_m$) based on the S_m(Code) value and was approximately 30 percent less than the flow stress ($3S_m$) based on the S_m(Actual) value. This finding is significant in that the actual strength properties of this stainless steel material at 288 C (550 F) are lower than what Table 2A of Part D of Section II of the Code permits one to use. This finding is even more significant when one considers the fact that the other stainless steel pipe material used in the IPIRG-1 program (i.e., DP2-A23), had even lower strength properties (Ref. 7.1). This suggests that the ASME Code definition of flow stress, i.e., $3S_m$, for Type 304 stainless steel may frequently overestimate the strength of this material. This may be part of the reason why the calculated fracture ratios for the

Appendix C approach for the two elevated temperature, stainless steel base metal, pipe-system experiments (i.e., Experiments 1.3-3 and 1-1) are low, see Table 4.13.

As can be seen in Table 4.13, the calculated fracture ratios using the Appendix C procedures for the two elevated temperature, stainless steel base metal experiments (i.e., Experiments 1.3-3 and 1-1) were only 0.977 and 1.154 when the S_m(Code) definition of flow stress was used. When the S_m(Actual) definition of flow stress was used in the analyses of these experiments, the calculated fracture ratios were even lower, i.e., 0.728 for Experiment 1.3-3 and 0.865 for Experiment 1-1. These values are significantly below the fracture ratios calculated for the stainless steel weld experiments and the carbon steel experiments, which were analyzed using a Z-factor approach to account for the crack being in a lower toughness material. Based on the analyses of the stainless steel weld experiments, it appears that some of the conservatism associated with the Z-factor approach may offset the fact that the strength of this particular stainless steel at 288 C (550 F) is less than the strength properties specified in Section II of the Code.

Figures 7.9 and 7.10 illustrate the basic inaccuracies/conservatisms associated with the use of ASME Appendices C and H elastic-plastic Z-factor approaches. As part of Reference 7.3, Z-factors based on the DPZP analyses were calculated as a function of pipe diameter and compared with the ASME Code Z-factors from Appendices C and H. (Note, the DPZP analysis was found to be one of the most accurate of the analysis methods, see Reference 7.3.) The DPZP-calculated Z-factors used the lower bound default J_{Ic} values specified in the technical basis documents for Appendices C and H for the different material categories considered by these approaches and both the "best-fit" and 95-percent confidence level DPZP correlation curves. As can be seen in Figure 7.9 for the austenitic case, the "best-fit" Z-factor curves from the DPZP analysis are well below the Z-factor curves from the IWB-3640 and Appendix C criteria. (There is much better agreement between the Appendix C Z-factors and the DPZP 95-percent confidence level curve Z-factors, especially for the shielded-metal-arc weld (SMAW) case, see Figure 7.9.) Considering the case of a 16-inch nominal diameter pipe, such as evaluated in the IPIRG-2 Task 1 experiments, Figure 7.9 shows that the ratio of the IWB-3640 Z-factor for submerged-arc welds to the DPZP "best fit" Z-factor for submerged-arc welds is approximately 1.5. Combining this inaccuracy with the fact that the flow stress of this pipe (DP2-A8), based on the average of the yield and ultimate strengths, is 10 percent less than the flow stress based on a S_m(Code) definition, results in an overall inaccuracy of approximately 1.35 (i.e., 0.9 times 1.5). As can be seen from Table 4.13, the calculated fracture ratios for the four elevated temperature, stainless steel SAW experiments for the Appendix C method for the case when the flow stress was defined as $3S_m$(Code) ranged from approximately 1.4 to 1.5, which considering the complications of analyzing a crack in a weld, agrees fairly well with the level of inaccuracy one might expect based on the preceding discussion. Furthermore, comparing these fracture ratios for the stainless steel SAW experiments with the calculated fracture ratios for the two elevated temperature, stainless steel base metal, pipe-system experiments, with a Z-factor of 1.0, for the same flow stress definition, shows that the fracture ratios for the weld experiments relative to that of the base metal experiments was approximately 1.25 to 1.55. This demonstrates the degree of inherent conservatism associated with the Z-factor correction embodied in Appendix C for austenitic flux welds.

A similar story can be told for the case of the ferritic Z-factor approach embodied in IWB-3650 and Appendix H. From Figure 7.10, it can be seen that the ASME Code Z-factor for a crack in the base metal

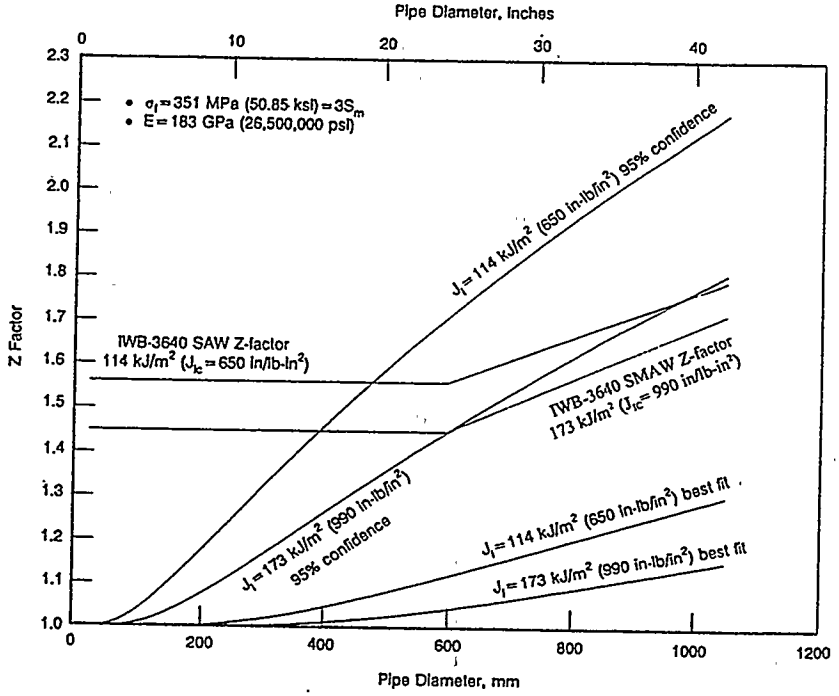

Figure 7.9 Comparison of ASME Section XI Appendix C Z-factors with calculated Z-factors from the Dimensionless-Plastic-Zone-Parameter analysis using both the "Best-Fit" and "95-percent Confidence Level" curves

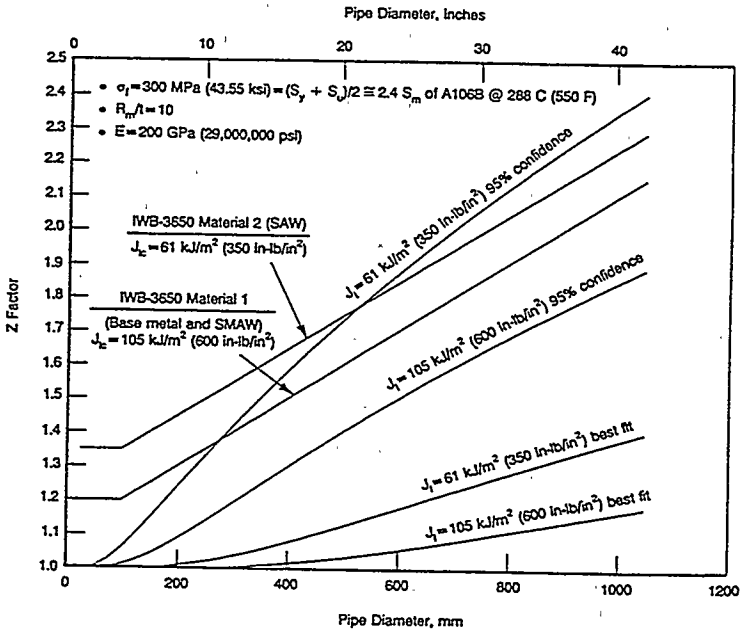

Figure 7.10 Comparison of ASME Section XI Appendix H Z-factors with calculated Z-factors from the Dimensionless-Plastic-Zone-Parameter analysis using both the "Best-Fit" and "95-percent Confidence Level" curves

of a 16-inch diameter carbon steel pipe would be approximately 1.5. On the other hand the DPZP "best-fit" Z-factor for the same crack in the same pipe would only be about 1.03. Consequently, the ASME Z-factor for a base metal crack in a 16-inch diameter ferritic pipe is approximately 45 percent greater than the DPZP Z-factor using the "best fit" curve in Figure 7.10. Combining this inaccuracy with the fact that the flow stress for this pipe (DP2-F29), based on the average of the measured yield and ultimate strengths, is 43 percent higher than the flow stress based on a S_m(Code) definition, results in an overall fracture ratio of approximately 2.1 (i.e. 1.45 times 1.43). As can be seen in Table 4.13, the calculated fracture ratios for two of the three carbon steel base metal experiments using the Appendix H criteria with the flow stress based on S_m(Code) agree very closely with this level of inaccuracy, i.e., fracture ratios of 1.94 and 2.18.

Similarly, for the case of the ferritic straight pipe-to-pipe girth weld experiments, the ratio of the Code Z-factor to the DPZP "best fit" Z-factor is approximately 1.53 for cracks in a 16-inch diameter pipe. Combining this with the fact that the flow stress based on actual properties is approximately 43 percent higher than the flow stress based on S_m(Code) values suggests that the fracture ratios for these two experiments (i.e., Experiments 4141-8 and 1.3-4) should approach 2.2. In reality, the fracture ratios for these two experiments for the Appendix H approach when using the S_m(Code) value for flow stress were 2.47 and 2.67, respectively, which agree fairly well with the value of 2.2. The slightly higher fracture ratios for these experiments may be due to the presence of the weld crown which was ignored in the analyses. Furthermore, the higher value of the fracture ratio for Experiment 1.3-4 (i.e., the dynamic pipe-system experiment) may be due to the fact that the toughness of this carbon steel weld (DP2-F29W) increases by a factor of two at dynamic rates, but is lowered by cyclic loading where the combined dynamic/cyclic (R = -0.6) J-R curve is more than 20 percent higher than the quasi-static, monotonic, J-R curve.

As a result of this discussion, it appears that contrary to what has been published in the past (Refs. 7.3 and 7.7), the degree of inaccuracy, or conservatism, associated with the Appendix H approach may not be significantly greater than that for the Appendix C approach. The higher fracture ratios for the Appendix H approach when compared with the Appendix C approach are significantly affected by the fact that the strength of the carbon steel pipe material evaluated (DP2-F29) is significantly higher than what one might expect based on Code properties, while the strength of the stainless steel pipe material evaluated (DP2-A8), is slightly less than what one might expect based on Code properties.

In conclusion, both the Appendix C and Appendix H elastic-plastic Z-factor approaches have a degree of inaccuracy or conservatism of approximately 1.5 for 16-inch diameter pipe for a material with strength properties near the strength properties provided in Section II. As can be seen in Figures 7.9 and 7.10, this degree of inaccuracy or conservatism would increase as the pipe diameter increases. The results of these analyses suggest that the Code definitions of the flow stress in terms of S_m could be increased for ferritic pipes and lowered for austenitic pipes to better account for statistical scatter in material strength relative to Code values.

R6 Revision 3 Option 1 and ASME Code Case N-494-3 Methods

As is the case for the ASME criteria, the R6 method is more of a failure avoidance criteria than a fracture prediction criteria. Consequently, there is a degree of conservatism built into this method. As can be seen in Table 4.13, the calculated fracture ratios for the R6 method using actual strength and quasi-static, monotonic, J-R curves are on average comparable to those for the ASME criteria. For the twelve straight-pipe experiments considered in Table 4.13, the average fracture ratio for the R6 method is approximately

1.6. On average, the R6 fracture ratios for stainless steel experiments are slightly higher than the Section XI Appendix C fracture ratios for these same stainless steel experiments. Conversely, the R6 fracture ratios for the carbon steel experiments are less than the Section XI Appendix H fracture ratios for these same carbon steel experiments. The explanation for this observation is that the R6 method uses actual material property data instead of Code specified strength values. Based on this evaluation, it appears that the degree of inaccuracy, or conservatism, associated with the R6 Revision 1 Option 1 method is comparable to that for the ASME Appendices C and H approaches, if differences in material property data are accounted for.

It is interesting to note from Table 4.13 that the degree of inaccuracy or conservatism associated with the ASME Code Case N-494-3 approach for austenitic and ferritic pipes is comparable to that for the R6 method. Like the R6 method, the FAD-based ASME Code Case N-494-3 approach uses actual yield and ultimate strength data instead of Code-specified strength parameters, i.e., S_m values.

It is also of note from Table 4.13 that the fracture ratios for the R6 analyses are significantly higher than fracture ratios from the Net-Section-Collapse analyses for the same experiments, see Tables 4.9, 4.10, and 4.11. This was the case even though a number of these experiments were expected to have failed under limit-load conditions, such that the R6 analyses and the NSC analyses should have resulted in approximately the same fracture ratios. In investigating the cause of this apparent discrepancy, it was concluded that the problem had to do with the manner in which the R6 Option 1 method was coded in the NRCPIPES, Version 3.0 program. In Version 3.0, of NRCPIPES, as well as in prior versions, for combined pressure and bending cases, the L_r term is defined as $\sigma_b/\sigma_b^{NSC(\sigma y)}$, where σ_b is the applied bending stress, and $\sigma_b^{NSC(\sigma y)}$ is the bending stress calculated by the Net-Section-Collapse analysis, accounting for the axial (pressure) stress using the yield strength in place of the flow stress in the analysis. This is probably not correct for the case where the axial stress becomes a significant amount of the total stress at failure. For such cases, the L_r term should probably be related to the total stress (bending plus membrane) instead of just the bending stress.

To illustrate this point, consider Figure 7.11. Figure 7.11 is a plot of the ratio of the maximum bending stress as calculated from NRCPIPES, Version 3.0, using the R6 analysis method-to-the NSC stress as a function of the ratio of the pressure stress-to-the maximum bending stress calculated using the NRCPIPES R6 analysis for various applied pressure levels. The far right-hand data points for each of the three curves shown in Figure 7.11 represent the test conditions for the IPIRG pipe-system experiments, i.e., 15.5 MPa (2,250 psi) internal pipe pressure. The bottom curve in Figure 7.11 is for Experiment 1.3-3 from IPIRG-1 analyzed using the dynamic, monotonic J-R curve data from pipe material DP2-A8I, the middle curve is for Experiment 1-1 from IPIRG-2 analyzed using the dynamic, monotonic J-R curve from pipe material DP2-A8II, and the top curve is for Experiment 1-1 analyzed using the room temperature, quasi-static, monotonic J-R curve for pipe material DP2-A8. This was the highest J-R curve available for such an analysis, and was used to see the effect of the problem with the L_r coding for a very high toughness material which would fail under limit-load conditions. (Note, based on a Dimensionless-Plastic-Zone-Parameter (DPZP) type calculation, the toughness levels for DP2-A8I and DP2-A8II should have been high enough that their failures should have been governed by limit-load conditions, however, as can be seen in Figure 7.11, the NRCPIPES R6 predicted stresses did not reach the NSC stresses even for the case of zero internal pipe pressure.) Of note from Figure 7.11 is the fact that as the pressure stress term increases, the NRCPIPES R6 predicted maximum stress decreases with respect to the NSC stress. Conversely, as the pressure term goes to zero, the maximum bending stress from the NRCPIPES R6 analysis approaches the NSC stress. This was especially true for the case where the higher, room

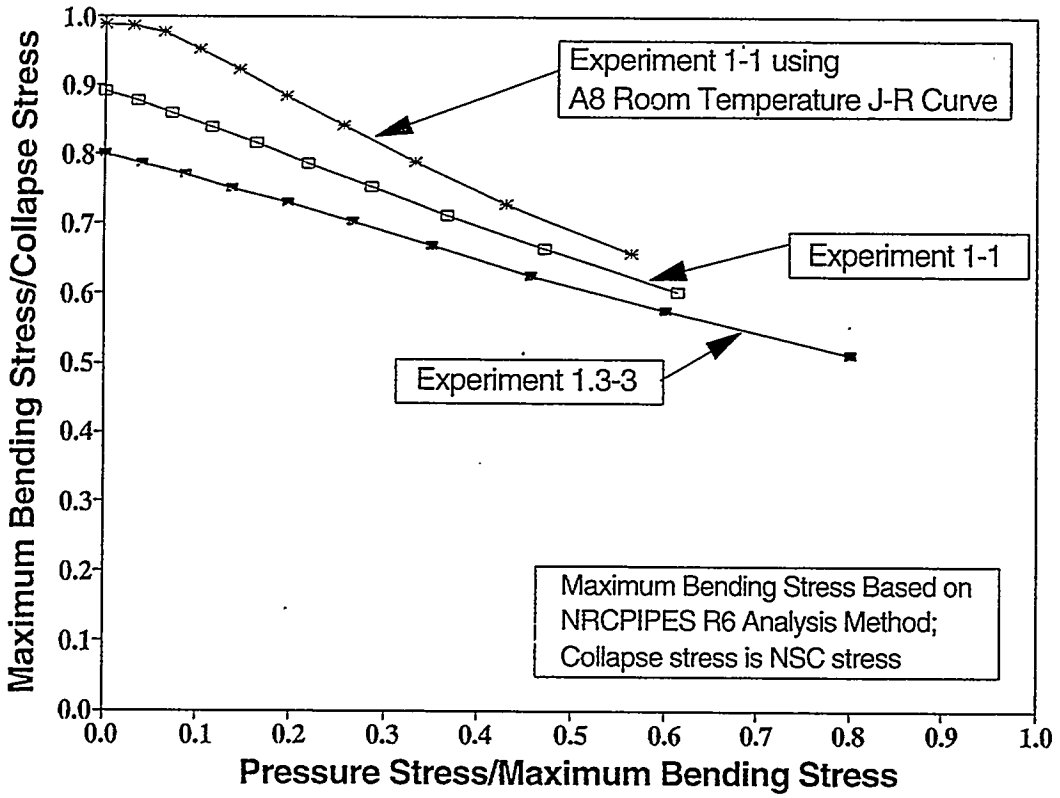

Figure 7.11 Ratio of the maximum bending stress using the NRCPIPES R6 analysis-to-the NSC stress as a function of the ratio of the pressure stress-to-the maximum bending stress using the NRCPIPES Version 3.0 R6 analysis

temperature J-R curve was used to analyze Experiment 1-1. These findings support the contention that the reason the NRCPIPES R6 fracture ratios in Table 4.13 were so much higher than the NSC fracture ratios had to do with the coding of the L_r term in NRCPIPES, Version 3.0 for the combined loading conditions. This aspect should be fixed in the next version of NRCPIPES.

7.2.2 Key Results From the Flawed Fittings Fracture Analyses

Several efforts were undertaken as part of the flawed fitting work in IPIRG-2. These involved: a literature survey and development of elbow and tee fracture experiment databases, development of J-estimation schemes for surface-cracked elbows, quasi-static and dynamic pipe-system fracture experiments, and development of a codifiable flaw evaluation analysis for surface cracks in elbows. These are briefly discussed below.

7.2.2.1 Discussion Pertaining to the Development of a Database of Flawed Fitting Data

During Task 2 of this program, a database of full-scale elbow experiments was developed. The format for this database, ELBOWCK.WK1, is similar to the format for the circumferentially-cracked pipe fracture database, CIRCUMCK.WK1, developed as part of the Short Cracks in Piping and Piping Welds Program

(Ref. 7.14). This elbow database contains the experimental test conditions (i.e., elbow sizes, crack sizes, loading conditions, etc.), experimental results (moments at crack initiation and maximum load), and material property data (tensile and fracture toughness data) for 76 elbow experiments conducted worldwide. In addition to the elbow data developed as part of this program, ELBOWCK.WK1 contains elbow data developed by MPA-Stuttgart, Westinghouse, General Electric, Commissariat A L'Energie Atomique (CEA), and Electricité de France (EDF). The database includes both circumferential through-wall-cracked and circumferential surface-cracked elbow data, as well as some uncracked elbow data. A subset of this database was used in conjunction with the IPIRG-2 elbow data to validate the elbow fracture prediction analysis methods developed as part of Task 2, and to assess whether existing straight-pipe analysis methods are adequate for the analysis of cracks in elbows. A second, much smaller, database for tees was also developed as part of this effort. This tee database, TEECK.WK1, includes 18 tee experiments conducted at General Electric, MPA-Stuttgart (Germany), and Nuclear Research Institute (NRI-Czech Republic)*.

In addition to the development of these databases, a literature survey was conducted to consolidate into a single document existing references pertaining to analysis methods and experimental data for flawed fittings. This survey includes approximately 140 references.

7.2.2.2 Development of J-Estimation Schemes for Cracked Elbows

Three new J-estimation schemes for cracked elbows** were developed in this program. Two methods (SC.ELB1 and SC.ELB2) were developed for the case of a circumferential surface crack along the extrados of an elbow. The difference between the two methods is the definition of the limit moment, M_o. The SC.ELB1 analysis uses the Net-Section Collapse (NSC) (Ref. 7.15) moment as a reference moment solution while the SC.ELB2 method uses a reference moment solution from the GE/EPRI method (Ref. 7.11). A third estimation scheme (SC.ELB3) was developed for the case of an axial surface crack along the flank of an elbow. All three estimation schemes consider internal pressure and in-plane bending as the loading mechanisms. The methodologies were developed much in the spirit of the GE/EPRI method (Ref. 7.11) for straight pipe in that they incorporate a series of h-functions which are used for the calculation of the plastic component of J.

The library of h-functions developed for these methods is limited at this time. For the case of circumferential surface cracks along the extrados, h-functions have only been developed for a 180-degree crack. For the case of axial cracks along the flank, h-functions have only been developed for the case of a 30 degree crack. Although crack lengths are limited, the elastic F-function and plastic h_1-function values were developed over a range of a/t values from 0.3 to 0.75, hardening exponents (n) from 3 to 10, and R_m/t ratios of 5 to 20. Over 100 finite element analyses were conducted to develop these f- and h-functions. Prior to conducting these analyses, line-spring and 3D brick element FEM analyses were conducted. Extremely good comparison existed, hence the more economical line-spring FEM analysis approach was used in the production runs. For the axial crack estimation method, the validation of the new h-functions was restricted to comparisons with other studies which used the line-spring element to model axial surface cracks (Ref. 7.16). Obviously, if these methods are going to be useful, additional h-functions for more

---

* For further details regarding these elbow and tee data, the reader is referred to NUREG/CR-6444.

** For further details regarding these elbow J-estimation schemes, the reader is referred to NUREG/CR-6445.

crack lengths need to be developed. The need for such development work will be discussed in greater detail in the following sections.

7.2.2.3 Discussion of the Results from the Full-Scale Flawed Fitting Experiments

Four cracked elbow experiments were conducted as part of this program. Each involved a 180-degree internal circumferential surface crack along the extrados of a 16-inch diameter, Schedule 100, 90-degree, long radius elbow. Two of these experiments involved cracks in A106-90 (Grade B) carbon steel elbows and two involved cracks in WP304L stainless steel elbows. For each material, there was a quasi-static, monotonic bend experiment and a dynamic, cyclic pipe-system experiment. In addition to the full-scale elbow experiments, a series of quasi-static and dynamic tensile and quasi-static and dynamic C(T) specimen tests were conducted for each material. These material data were used in the analyses of the full-scale cracked elbow experiments. The purpose of these full-scale experiments was to develop experimental data to validate the new elbow J-estimation schemes and to address the question as to whether existing analysis methods previously developed for straight pipe were adequate for the case of a circumferential crack along the extrados of an elbow.

Comparisons of results from the elbow data and the various analysis methodologies are shown in Figures 7.12 and 7.13. As can be seen in Figure 7.12 for the carbon steel elbows, both of the new extrados crack J-estimation schemes (SC.ELB1 and SC.ELB2) agree with the straight-pipe Net-Section-Collapse (NSC) and SC.TNP1 analysis methods for the case where a circumferential surface crack along the extrados of the elbow is less than approximately 60 percent of the pipe wall thickness in depth. For circumferential cracks deeper than 60 percent of the pipe wall thickness, the SC.ELB1 method diverges from the other three solutions. Furthermore, it can be seen in Figure 7.12, that the straight pipe NSC and SC.TNP1 analysis methods and the elbow SC.ELB2 method underpredicted the experiment moments for both carbon steel elbow experiments. Conversely, the SC.ELB1 method over predicted the carbon steel experimental results. For the case of the stainless steel elbows, see Figure 7.13, all four methods (SC.ELB1, SC.ELB2, SC.TNP1, and NSC) under predicted the maximum experimental moments. As indicated in Section 4.0, the fracture ratios for all four elbow experiments, based on the straight pipe SC.TNP1 method, are within the previously established scatter band of fracture ratios (Ref. 7.3) for the SC.TNP1 analysis method, see Table 4.14. This tends to indicate that the straight pipe SC.TNP1 method is adequate for predicting the load-carrying capacity of circumferential cracks along the extrados of an elbow, at least for the range of R/t ratios, elbow diameters, crack sizes, etc. evaluated in these experiments.

The bottom line from this discussion is that the SC.ELB2 method results in a reasonable under prediction of the experimental moments for elbows with 180 degree, circumferential extrados-type surface cracks. Even so, the need for such an analysis method and the development of more h-functions for more crack sizes may not be that great since an existing straight-pipe J-estimation scheme method (SC.TNP1) already exists which results in just as good a prediction as does the SC.ELB2 method, at least for the range of experimental test parameters evaluated in these experiments. For both materials and for all of the crack sizes considered in Figures 7.12 and 7.13, the difference in predictions between the SC.ELB2 elbow solution and the SC.TNP1 straight-pipe solution is less than 10 percent, which is within the typical experimental scatter observed for these types of experiments.

An assessment of the validity of the new elbow J-estimation scheme for the case of the axially-oriented elbow flank crack is more difficult than the circumferential crack case. None of the existing straight-pipe

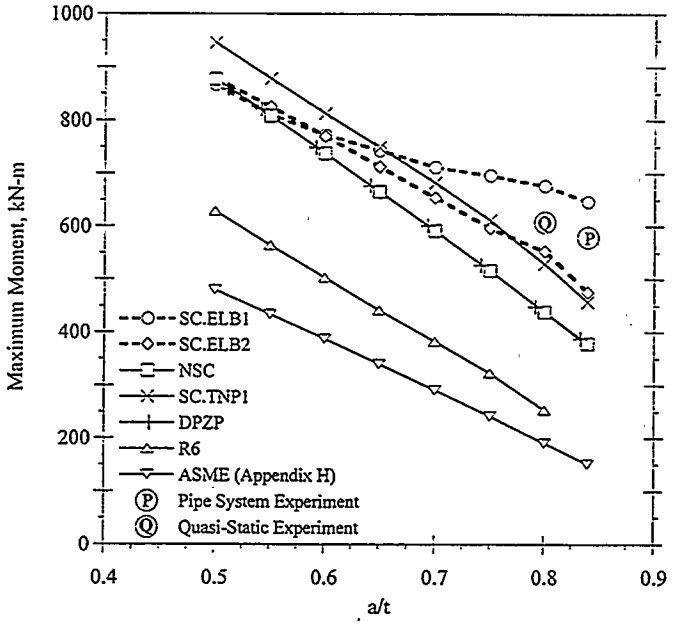

Figure 7.12 Prediction of maximum moment as a function of crack depth for the Net-Section-Collapse, SC.TNP1, DPZP, R6, ASME Appendix H, SC.ELB1, and SC.ELB2 analysis methods with experimental moments from the two carbon steel elbow experiments (Experiments 2-1 and 2-2) shown for comparison

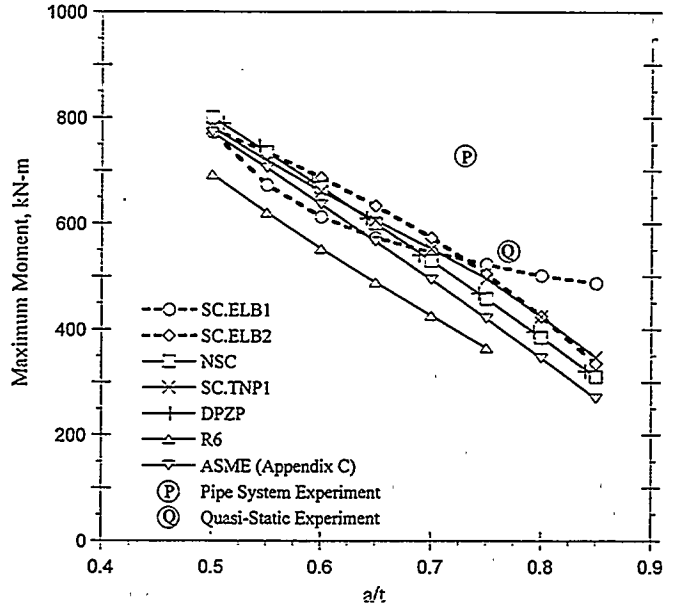

Figure 7.13 Prediction of maximum moment as a function of crack depth for the Net-Section-Collapse, SC.TNP1, DPZP, R6, ASME Appendix C, SC.ELB1, and SC.ELB2 analysis methods with experimental moments from the two stainless steel elbow experiments (Experiments 2-3 and 2-4) shown for comparison

J-estimation scheme analysis methods are applicable for this flaw geometry. Furthermore, no data exist in the elbow database with the same crack length which can be used to validate the new elbow axial flaw J-estimation scheme. The only validation available for this flaw geometry is through comparisons with past work, or to perform comparable analyses using 3-dimensional finite element analyses. Consequently, the development of additional h-functions for different crack sizes for this flaw geometry and the development of experimental data to validate those h-functions may be of importance.

7.2.2.4 Simplified Flaw Evaluation Criteria for Fittings

To overcome the crack length limitation in the elbow J-estimation schemes, and develop a simplified approach that could be easily codified, a methodology of determining a geometric multiplier between straight-pipe and fittings was developed and checked against a few elbow fracture experiments. This geometric stress magnification factor approach was originally developed by Folias (Ref. 7.17) in comparing failure stresses of through-wall cracks in flat plates to straight pipes.

To implement this methodology into a code-type approach, two possible approaches could be undertaken. The first is the simplest, but perhaps the more conservative. This approach is to take the ASME Section III stress indices and use them as a simple multiplier on the straight pipe solutions. In the work done, both the B_2 and C_2 stress indices were evaluated, however, the B_2 stress indices were found to be more accurate. In this case,

$$M^{elbow} = M^{pipe}/B_2 \tag{7-1}$$

The second approach involves the definition of a new parameter, Υ^f_x (where f is the type of fitting, and x is the crack orientation). This parameter is equal to the ratio of the moments of the circumferentially surface-cracked straight pipe to that for the flawed elbow at the same applied J values for the same crack size, diameter, and R/t ratio. The straight-pipe J solutions were calculated using the SC.TNP1 and SC.TNP2 (Ref. 7.3) J-estimation schemes. The Υ^f_x parameter was found to be linearly related to the B_2 stress indices. In this case, a more accurate solution comes from

$$M^{elbow} = M^{pipe}/\Upsilon^f_x \tag{7-2}$$

The Υ^f_x functions are the straight line equations for the upper and lower bounds of the scatter bands for the B_2 indices from Figures 7.14 and 7.15. For the case of an axial, flank, surface crack in an elbow the function Υ^e_a using the SC.TNP1 and SC.TNP2 solutions and the B_2 indices would be

$$\Upsilon^e_a = 0.601B_2 + 0.755 \tag{7-3a}$$

using the SC.TNP1 straight-pipe analysis, and

$$\Upsilon^e_a = 0.462B_2 + 0.618 \tag{7-3b}$$

using the SC.TNP2 straight-pipe analysis method.

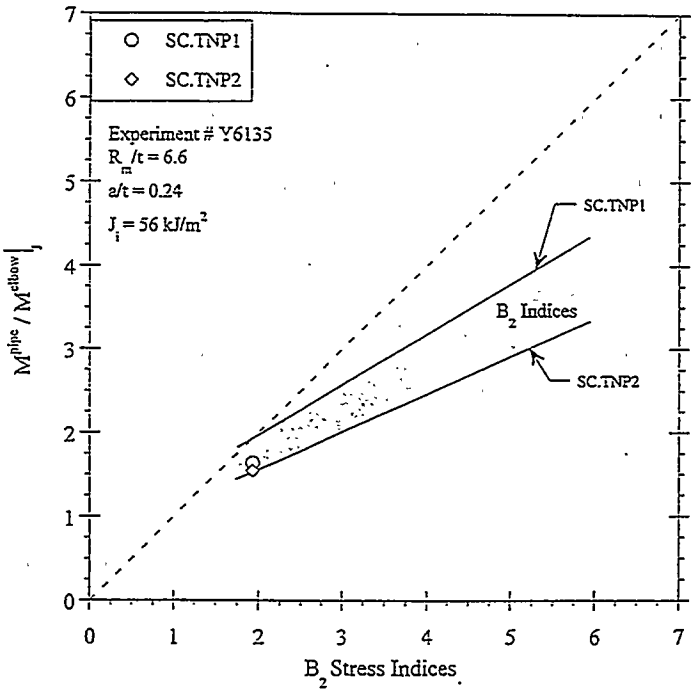

Figure 7.14 Ratio of moments for the straight pipe to moments for an axial-flank-cracked elbow as a function of the stress index B_2 with the experimental data for EDF Experiment Y6135 shown for comparison

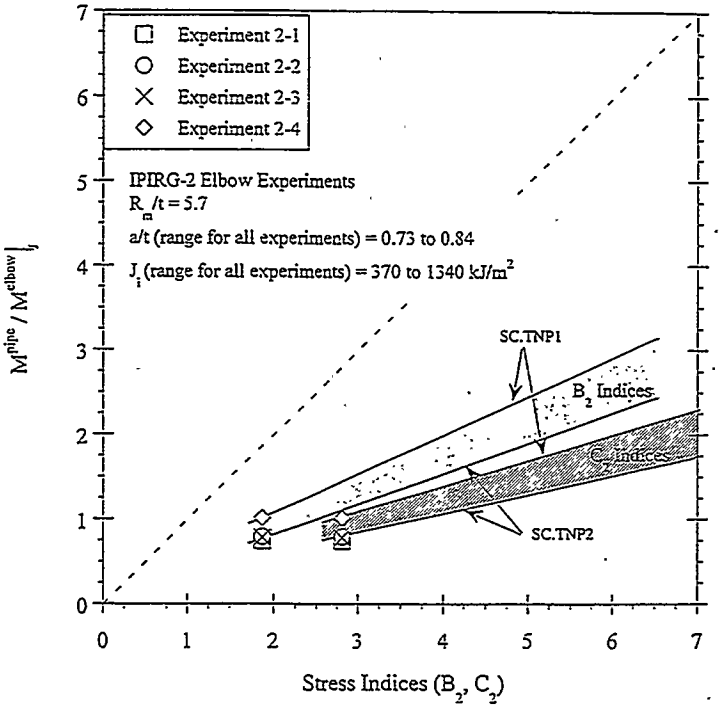

Figure 7.15 Ratio of moments for the straight pipe to moments for a circumferential-cracked elbow as a function of the stress index B_2 with the IPIRG-2 elbow experimental data shown for comparison

For the case of a circumferential, extrados, surface crack in an elbow (Υ^e_c), using the SC.TNP1 and SC.TNP2 solutions for the straight pipe, and the SC.ELB2 solution (which is virtually identical to the SC.ELB1 results) for the elbow, would be

$$\Upsilon^e_c = 0.465B_2 + 0.136 \tag{7-4a}$$

using the SC.TNP1 straight-pipe analysis, and

$$\Upsilon^e_c = 0.351B_2 + 0.121 \tag{7-4b}$$

using the SC.TNP2 analysis method.

The Υ^e_a and Υ^e_c values are shown in Figure 7.16 for both the SC.TNP1 and SC.TNP2 straight-pipe analysis solutions. Generally the experimental results agreed better with the SC.TNP2 Υ^e_a and Υ^e_c values, except for the one IPIRG-2 stainless steel circumferential surface-crack elbow experiment, i.e., Experiment 2-4, which agreed better with the SC.TNP1 Υ^e_a values, see Figures 7.14 and 7.15.

In order to further codify this type of flawed fitting failure avoidance criterion, the following should be done. First, although some of the experiments analyzed had materials with different strain-hardening

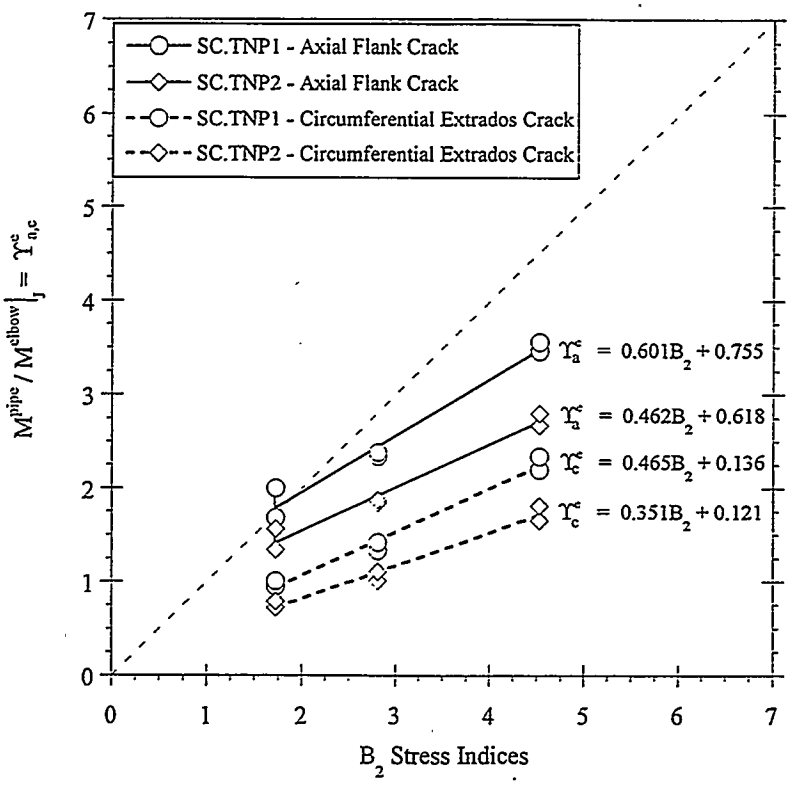

Figure 7.16 The parameter Υ^e_x (equal to $M^{pipe}/M^{elbow})|_J$) as a function of the stress index B_2 for both the axial flank (Υ^e_a) and circumferential extrados (Υ^e_c) crack cases for both the SC.TNP1 and SC.TNP2 straight pipe analysis methods

exponents or cracks of different sizes, additional sensitivity studies should be conducted to see the sensitivity of the Υ^f_x function to these parameters over a wider range. Additional experimental data in the IPIRG-2 ELBOWCK database could be used to assess the accuracy of these functions.

Secondly, Υ^f_x functions could be developed for different cracked fitting cases. It is not necessary to develop a large matrix of finite element solutions to come up with an estimation scheme, but rather selected finite element runs for cracked fittings could be conducted to establish the necessary Υ^f_x functions. Some experimental data for cracks in tees exist in the IPIRG-2 TEECK data base that could be used to assess such an approach, or the more conservative approach of using the B_2 indices as in Equation 7-1.

Finally, an additional benefit to the Υ^f_x function approach, is that since this approach is best for very high J values, these functions can be used as a stress multiplier for limit-load solutions. Hence, this approach can be used for blunt flaws in fittings, such as those that might be caused by erosion corrosion.

7.3 Key Results from Other Issues Studied in the IPIRG-2 Program

7.3.1 Discussion of Results from Uncertainty Analysis

Section 5.3 presented the results from a series of deterministic and probabilistic analyses which evaluated the significance of a number of technical issues that may affect LBB or in-service flaw evaluations. For most of these issues the results from both deterministic and probabilistic analyses were presented. The deterministic analyses were conducted independently of the probabilistic analysis, which offered the opportunity to validate conclusions from each of these studies.

The significance of the various technical issues investigated were ranked in importance of how they may impact current analysis methodologies. Table 7.4 makes this ranking from both the deterministic and probabilistic results for technical issues that affect LBB evaluations. Table 7.5 makes this ranking for technical issues that affect in-service flaw evaluations. For both tables, the issues are ranked from the most significant to the least significant. These rankings are in the categories of very high, high, medium, low, and very low. An example of a very high ranking is the case of restraint of pressure induced bending on LBB, where for small diameter pipe, the LBB maximum load was a factor of 9 lower when this effect was considered. This is much greater than the maximum load safety factor of $\sqrt{2}$ used in LBB analyses. An example of the very low rating is the case of residual stresses on leak-rate analyses for a thick-walled pipe. Here the effects were essentially negligible, except at unrealistically low operating stresses.

In some cases, it appeared from an initial review that the significance of the deterministic and probabilistic analyses did not agree. Upon further review, however, it was found that most of the deterministic and probabilistic analyses agreed when all factors were considered. The cases where there were differences in the significance of a technical issue were found to be due to: (1) the deterministic model being more sophisticated than that used in the probabilistic analysis, (2) the material property input not being the same in the deterministic and probabilistic analyses, and (3) what appeared to be a significant effect over a small range was thought to be less important from a deterministic view, but that same factor gave a major change in conditional failure probabilities. All of these differences were closely evaluated to make the final ranking given in Table 7.4.

Table 7.4 Ranking of various technical aspects investigated in uncertainty study that affect LBB evaluations

Technical Aspect Investigated	Comments	Significance
Effect of restraint of pressure induced bending on LBB	Small diameter	Very High
Effect of residual stresses on leak-rate analyses for LBB	Thin-walled pipe (i.e., tension-to-compression stresses through the thickness) at *low* operating stresses	High to very high
LBB failure probability	Low normal operating stresses	High
COD-dependent crack morphology model leak-rate analyses	Leak rate < 3.5 lpm (0.926 gpm)	High
Effect of off-centered cracks for LBB	Cracks off centered > 50 degrees	Medium to high
LBB failure probability	High N+SSE stresses	Medium
COD-dependent crack morphology model for leak-rate analyses	3.5 lpm (0.926 gpm) <leak rate < 4.5 lpm (1.2 gpm)	Medium
Effect of off-centered cracks for LBB	Statistically varying off-center angle in probabilistic analyses	Medium
Crack morphology default values	For corrosion fatigue cracks	Medium
Effect of residual stresses on leak-rate analyses for LBB	Thin-walled pipe at *high* normal operating stresses	Low
Crack morphology default values	For IGSCC	Low
COD-dependent crack morphology models for leak-rate analyses	Leak rates > 7.56 lpm (2 gpm)	Low
Dynamic/cyclic history effect on toughness for LBB analyses	Experimental results show analyses too conservative	Low
Evaluation of the effect of off-centered cracks for LBB evaluations	Cracks off centered < 50 degrees	Low
Effect of restraint of pressure induced bending on LBB	Large diameter	Very low
Effect of residual stresses on leak-rate analyses for LBB	Thick-walled pipe at typical operating stresses	Very Low

Table 7.5 Ranking of various technical aspects investigated in uncertainty study that affect in-service flaw evaluations

Technical Aspect Investigated	Comments	Significance
Uncertainty in UT flaw sizing on failure loads from in-service flaw evaluations	For $a/t > 0.5$	High
Dynamic/cyclic history effect on toughness for surface-cracked pipe (in-service flaw evaluations)	Low yield-to-ultimate strength materials	Medium
Uncertainty in UT flaw sizing on failure loads from in-service flaw evaluations	For $0.25 < a/t < 0.5$	Medium
Dynamic/cyclic history effect on toughness for surface-cracked pipe (in-service flaw evaluations)	High yield-to-ultimate strength materials	Low
Uncertainty in UT flaw sizing on failure loads from in-service flaw evaluations	For $a/t < 0.25$	Low

7.3.2 Discussion of Computer Codes and Databases

During the course of the IPIRG-2 program, several computer codes were improved or developed. These computer codes were:

NRCPIPE - Version 3.0 for Windows,
NRCPIPES - Version 3.0 for Windows,
IP2ELBOW - Version 1.0 for Windows, and
SQUIRT - Version 2.4 for DOS.

NRCPIPE, NRCPIPES, and IP2ELBOW are fracture prediction codes for straight pipe and elbows. SQUIRT is a leak-rate code for LBB applications. A brief description of these codes and the modifications and development efforts associated with each are provided in Section 5.1.

In addition, a number of fracture databases were either made available to the fracture community, created, or improved during the course of this program. These databases are:

AXIALCK,
CIRCUMCK,
ELBOWCK,
TEECK, and
PIFRAC.

The first four of these databases deal with full-scale pipe and fitting fracture data, and are in spreadsheet format, i.e., Lotus 1-2-3. The PIFRAC database contains pipe and fitting material property data (i.e., over 800 σ-ϵ curves and J-R curves) and is in dBase III + software format.

These databases are described in Section 5.2.

7.3.3 Seminars and Workshops

One of the goals of the IPIRG-2 Program was to provide a forum for nuclear piping fracture experts to exchange information on state-of-the-art developments in pipe fracture analysis and experimentation. Through open discussion of the technical positions and concerns of the various member countries, the IPIRG-2 Program fostered a better understanding of the fracture issues facing piping experts on a world-wide basis as plants age or new plants are built. To fulfill this goal, a series of seminars and workshops were held in conjunction with several of the IPIRG-2 Technical Advisory Group (TAG) Meetings.

7.3.3.1 LBB'95 Seminar

A Leak-Before-Break (LBB) seminar (LBB'95) was held in Lyon, France, in conjunction with the 7th IPIRG-2 TAG meeting in October 1995. This seminar, which was structured similarly to the three previously held LBB seminars in 1985, 1987, and 1989 (Refs. 7.18, 7.19, and 7.20), brought together nearly 200 pipe fracture researchers from around the world to present and/or listen to 37 technical papers and poster papers. Topics addressed included; regulatory practices, pipe fracture research results, and application of LBB to new and existing plants. The proceedings for this seminar are published in Reference 7.21 and will be also published as a NUREG/CP report.

7.3.3.2 IPIRG-2 Round Robin Analyses

In conjunction with the IPIRG-2 program TAG meetings, a series of round-robin workshops to compare analysis methodologies and solutions for a series of pertinent pipe fracture problems were organized. The general objective of these workshops were to enhance the IPIRG-2 members' understanding of the various technical and regulatory bases in other countries and to help develop a consensus on how to handle difficult analytical problems associated with LBB and in-service flaw evaluations for circumferentially-cracked pipes and elbows.

At the suggestion of the IPIRG-2 TAG members, four sets of round-robin problems were developed by Battelle for analysis by the TAG members and Battelle. These problem sets involved: (1) evaluations of fracture properties and pipe loads, (2) crack-opening and leak-rate evaluations, (3) dynamic analysis of cracked pipes, and (4) fracture evaluations of elbows.

Complete problem statements, solutions, and comparisons of solutions are summarized in Reference 7.22. Key observations from the round-robin analyses are summarized in Section 6.2 of this report.

7.3.3.3 IPIRG-2 Analysts Group Meetings

In addition to the round-robin analyses, a series of fracture analyst speciality meetings was organized and held in conjunction with the IPIRG-2 TAG meetings. The purpose of the analyst group meetings was to

promote discussions on fracture-related technical topics which the participants were actively researching or

8.0 CONCLUSIONS

In this section, the conclusions reached as a result of the research conducted in the IPIRG-2 program are discussed. The conclusions which are related to the major issues that provided motivation for the IPIRG-2 program will be discussed first. After discussing these issues and conclusions, other key observations or conclusions which were made during the course of this research, but were not directly related to these major issues, are discussed. To aid the reader in differentiating the supporting background documentation from the actual conclusions, the conclusions are given as indented paragraphs in the text.

8.1 Conclusions Related to the Major Issues Which Formed the Rationale and Basis for the Formation and Conduct of the IPIRG-2 Program

As discussed in Section 1.2 of this report (Rationale and Objective Behind the IPIRG-2 Program), there were a number of gaps in the pipe fracture technology at the end of the IPIRG-1 (Ref. 8.1) and Short Cracks in Piping and Piping Welds (Ref. 8.2) programs which still needed to be addressed. Addressing these issues was the motivation behind the development of the IPIRG-2 program. These issues included:

(1) The development of a better understanding of dynamic and cyclic load effects on material properties and the impact of such properties on the behavior of cracked pipe sections,

(2) The behavior of cracked pipe sections subjected to more complex load histories, such as may occur during a seismic event,

(3) The behavior of smaller crack sizes, including both short surface cracks and short through-wall cracks, when subjected to dynamic/cyclic load histories, and

(4) The behavior of cracks in and adjacent to fittings, such as elbows.

8.1.1 Developing a Better Understanding of Dynamic and Cyclic Load Effects on Material Properties and Their Impact on the Behavior of Cracked Pipe Sections

One of the key aspects of the IPIRG program was to assess the behavior of cracked pipe in a pipe system under loads simulating a seismic or some other dynamic load history. Prior to discussing the pipe-system fracture behavior, it is first important to understand the effects of load histories on the strength and toughness of typical nuclear piping steels at rates typical of a seismic event. Two specific types of loading effects influence the material properties. The first is the effect of dynamic loading and the second is the effect of cyclic loading. Seismic and other non-repeating dynamic loading events (i.e., pressure relief valve blowdown loads, water hammer, etc.) will always involve dynamic loading, whereas they may or may not involve cyclic loads. In this section, conclusions related to the effect of dynamic loading are discussed first, then cyclic loading conclusions are discussed, and finally the conclusions related to the synergism between the two on toughness are given.

8.1.1.1 Effect of Loading Rate on Tensile and Fracture Toughness Properties

During the IPIRG-1 program, Ref. 8.3, it was learned that dynamic loading rates had different effects on austenitic steels and ferritic steels. The ferritic steels are frequently affected by dynamic strain aging (DSA), which at LWR temperatures affects the strength and toughness of the material (Ref. 8.4). First, the effects of dynamic loading on strength will be discussed, followed by the effects of dynamic loading on toughness.

Effect of Dynamic Loading on the Strength of Nuclear Grade Pipe Materials at LWR Temperatures

In the IPIRG-1 program, it was decided to conduct tensile tests at quasi-static strain rates of 10^{-4}/s to 10^{-5}/s as well as at higher strain rates that might be representative of a seismic event. Strain rates of 1/s and 10/s were chosen somewhat arbitrarily, since the strain rate in a cracked pipe during a dynamic event varies from very high at the crack tip, to almost quasi-static in the uncracked pipe remote from the crack. The results in Reference 8.3 showed that at 288 C (550 F), austenitic steels and their welds tended to have slightly higher stress-strain curves at the higher strain rates. The ferritic steels tested in IPIRG-1 and this program, however, consistently showed a decrease in the ultimate strength with little change in the yield strength at the higher strain rates. The ferritic pipe behavior was attributed to DSA.

The change in the ferritic material stress-strain curve on pipe fracture behavior could be defined using visco-plastic analyses to properly account for the loss of strength with increasing loading rate (the opposite of most materials), or by defining an effective strain rate for use in either FEM, simplified closed-form J-estimation schemes, or limit-load analyses.

The selection of the effective strain rate to use in a pipe fracture analysis to account for these observed differences in strength is not easy using existing analytical methods. This effective strain rate was determined experimentally by examining the load-displacement record of quasi-statically loaded and dynamically loaded C(T) specimens and pipe specimens. The shape of the load-displacement curves up to the point of crack initiation is theoretically [from either Key Curve methodology or the use of the GE/EPRI estimation scheme method (Refs. 8.5 and 8.6)] a function of the specimen geometry and the strain-hardening exponent of the material. Such comparisons of static and dynamic C(T) specimen data, as well as static and dynamic pipe fracture specimen data have been made. The C(T) specimens involved a variety of ferritic steels that showed various degrees of DSA sensitivity in the J-R curves. No significant difference was seen in the shape of the load-displacement curves prior to crack initiation in the sets of identical specimens. Similarly, 6-inch nominal diameter TWC pipe experiments were examined, and there was no major change in the shape of the load-displacement curve between the quasi-static and dynamic experiments up to the point of crack initiation.

Consequently, it appears that the quasi-static stress-strain curve is sufficient for use in pipe fracture analyses of cracked pipe at seismic loading rates. The higher strain-rate effects near the crack tip are captured by the J-R curve.

Effect of Dynamic Loading on Toughness at LWR Temperatures

In the IPIRG-1 program, it was estimated that the time to crack initiation in an inertially loaded pipe fracture experiment was roughly 0.2 seconds (Ref. 8.3). This loading time to crack initiation was used in subsequent C(T) fracture tests in Reference 8.3 and in the IPIRG-2 program. More recently, in the later part of the IPIRG-2 program, it was found that:

> The time to crack initiation in a seismic event could be as fast as one-quarter of the period of the first natural frequency of the pipe system of interest. This provides a relatively simple criterion for establishing dynamic toughness testing requirements.

This quarter period testing time corresponds to the time to crack initiation in one large amplitude cycle (as occurred in this program in some of the pipe-system experiments) rather than estimating the equivalent monotonic time to initiation during multiple plastic cycles (as was calculated in the IPIRG-1 program). For the IPIRG pipe system, this time to crack initiation corresponded to about 0.062 seconds, or about three times faster than that used in the IPIRG C(T) specimen tests. Fortunately, loading rate effects typically require an order of magnitude change to exhibit significant differences, hence, the factor of three on loading rate should not be significant on the toughness. However, hard data to support this hypothesis do not exist.

The effects of dynamic loading were found to be quite variable for austenitic and ferritic steels.

> The toughness of austenitic steels (i.e., TP304, aged CF8M, and a TP304 SAW) either stayed the same or increased with loading rate. The ratio of the dynamic to quasi-static toughness was found to be linearly related to the material's yield-to-ultimate strength ratio. Higher yield-to-ultimate strength ratio steels had a higher dynamic toughness at 288 C (550 F).

Some ferritic steels showed an increase in toughness while others showed a decrease in toughness at the dynamic loading rates. This is believed to be due to the material's susceptibility to DSA. This random behavior is probably due to the lack of cooling rate specifications in the fabrication of such steels, where the atomic (free) nitrogen and carbon atoms responsible for DSA could be tied up with better cooling rate control. The results of the data generated in the IPIRG-1 and this program showed that:

> For ferritic steels, there was a mild correlation between the dynamic to quasi-static toughness with the yield-to-ultimate strength ratio of the material, and perhaps a correlation with the ratio of the high temperature to room temperature Brinell hardness. Many ferritic base metals had lower dynamic values than quasi-static toughness values, but the few weld metals tested had higher dynamic toughnesses. At this point, it is hard to say whether or not there is a lower bound to the dynamic toughness, or that welds will always have a higher dynamic toughness, but from the eight materials examined, the greatest reduction observed in a dynamic J-R curve was about 55 percent, as compared to the quasi-static J-R curve.

8.1.1.2 Effect of Cyclic Loading on Fracture Toughness Properties

Cyclic loading can cause either low cycle fatigue crack growth or an interrupted ductile tearing process with some additional damage at the crack tip due to the compressive loads. Neither of these effects are

considered in either typical pipe flaw evaluation criteria or LBB analyses. In the IPIRG program, a cyclic J-R curve, which was easier to implement into an analysis than a Dowling ΔJ low cycle fatigue analysis (Ref. 8.7), was used.

The upper envelope method of calculating the cyclic J-R curve showed good agreement with FEM far-field J-R curves, and was subsequently used in all the analyses of the cyclic C(T) and pipe specimen tests. Metallographic sectioning of interrupted C(T) tests showed that the cyclic loading caused crack-tip sharpening and flattening of voids ahead of the crack tip, both of which contribute to reducing the toughness locally at the crack tip. The results to date show:

> Cyclic loading reduces the toughness of all nuclear piping materials evaluated. The magnitude of the toughness degradation depends on: the stress ratio (the minimum/maximum stresses), the cyclic plasticity prior to crack initiation or amount of cyclic crack growth, the monotonic toughness of the material, and the yield-to-ultimate strength ratio of the material.

The more negative the stress ratio, the lower the cyclic toughness. The stress ratio for uncracked pipe can be calculated from the (N-SSE)/(N+SSE) stress ratio, which assumes the normal stress (N) bending plane is in the same direction as the SSE bending plane. However, work in Reference 8.8 showed that the stress ratio for cracked pipe can be substantially more negative than the stress ratio for an uncracked pipe.

The cyclic plasticity, similar to ratcheting for uncracked pipe, is an important parameter, but is difficult to quantify. Since seismic time-histories are probabalistic in nature, this effect is also probabalistic. If the seismic event exhibits a large amplitude cycle preceded only by small amplitude elastic cycles (i.e., the January 1995 Kobe, Japan or the January 1994 Northridge, California earthquakes), then accounting for cyclic effects on toughness is not required, and only accounting for the dynamic loading rate effects on toughness is required. However, typical seismic design analysis requires a time-history with a build up of 5 seconds with a 10 to 20 second duration of large motion, and then a decay over 5 seconds. In the worst case, that 5 second build-up could involve a gradual increase of cycles at the first natural frequency of the pipe system. For a pipe system with a natural frequency of 4 Hz, this could involve 20 cycles (some of which would be elastic). Hence, this plastic increment could be estimated as an upperbound. In the cyclic C(T) tests conducted, it was assumed that there would be 10 plastic cycles to crack initiation, which is reasonable with this simple bounding evaluation.

> A lower bound on the cyclic J-R curve for seismic evaluations can be approximated by the IPIRG C(T) tests with an stress ratio of -1 and the cyclic plastic increment corresponding to 10 cycles to crack initiation, i.e., $\delta_{cyc}/\delta_i = 0.1$).

There was a significant finding from the IPIRG cyclic J-R curve evaluations involving carbon steel base metals, stainless steel base metals, a stainless steel weld, and a carbon steel welds:

> Cyclic (R = -1) loading appears to correspond to a lower bound J-R curve level that is related to the materials' yield-to-ultimate strength. The lower the yield-to-ultimate strength, the greater the toughness degradation from cyclic loading.

8.1.1.3 Similitude Between C(T) and Cracked Pipe Under Cyclic Loading

One of the questions raised during the course of the IPIRG-2 program was on the similitude between J-R curves from pipe and C(T) specimens during cyclic loading.

From C(T) and through-wall-cracked pipe tests, the cyclic J-R curve values were found to be in reasonable agreement at crack initiation using the same stress ratio and normalized cyclic plastic displacement increment (δ_{cyc}/δ_i). Once crack growth starts, the δ_{cyc}value needs to be changed to keep the same Δa values per cycle and to account for geometric differences between C(T) specimens and cracked pipes. This change in the δ_{cyc} value can be calculated from pipe and C(T) specimen J-estimation schemes, and would be considerably different for a through-wall-cracked pipe than a surface-cracked pipe.

8.1.1.4 Synergism Between Dynamic and Cyclic Loading on Toughness at LWR Temperatures

In the IPIRG-1 and IPIRG-2 program, several sets of C(T) specimen and through-wall-cracked pipe data were available where there were quasi-static, monotonic (standard load history), quasi-static/cyclic, dynamic/monotonic, and dynamic/cyclic load histories. Results from these tests showed:

The combined dynamic/cyclic load effect on the J-R curve ($J_{dyn,cyc}$) can be estimated from a simple multiplication of the dynamic effect (dynamic/quasi-static toughness values both under monotonic loading, F_{dyn}) times the cyclic effect (cyclic/monotonic loading at quasi-static rates, F_{cyc}) times the standard quasi-static monotonic toughness, $J_{QS,mono}$, i.e.,

$$J_{dyn,cyc} = F_{dyn}\, F_{cyc}\, J_{QS,mono}$$

Hence, there are no significant synergistic effects.

8.1.2 Effect of More Complex Load Histories on the Fracture Behavior of Cracked Pipe Sections

As part of Task 1, it was shown that the fracture ratios (i.e., the ratio of the experimental-to-predicted stress [bending plus membrane]) for the simulated-seismic, surface-cracked, pipe-system experiments were higher than the fracture ratios for the companion, single-frequency, pipe-system experiments. Even though the effective stress ratios for the simulated-seismic experiments were lower than they were for the companion single-frequency, pipe-system experiments, the apparent effect of the cyclic load history on the fracture behavior was less for the simulated-seismic experiments. This apparent discrepancy was attributed to the fact that the cycles prior to maximum load for the simulated-seismic, pipe-system experiments were primarily elastic prior to a large amplitude cycle (large δ_{cyc}/δ_i), while the cycles prior to maximum load for the single-frequency experiments exhibited a gradual build up of cyclic plasticity (small δ_{cyc}/δ_i). The fact that the cycles prior to maximum load were essentially elastic for the simulated-seismic experiments implies that these experiments could probably be analyzed much in the same manner as a dynamic, monotonic experiment would be analyzed.

Consequently, the degradation of the load-carrying capacity of the cracked-pipe sections due to the simulated-seismic load history applied in the IPIRG-2 program was less severe than that for the single-frequency load history.

Note, however, that this conclusion must be qualified in that it may only be valid for the simulated-seismic forcing function used in these experiments. If some other simulated-seismic load history was used, with a more gradual buildup of large amplitude cycles, then the extent of cyclic degradation that occurred during the simulated-seismic experiments may have increased. Since time-histories for seismic events are probabilistic in nature, there is some frequency of occurrence for both the initial-large-amplitude and gradual-buildup type of seismic forcing functions. The determination of the frequencies of occurrence was beyond the scope of this program.

It was, therefore, concluded that independent of the seismic load history, the dynamic effects on toughness always need to be considered, whereas the cyclic effects on toughness will occur only in some subset of seismic events.

8.1.3 Behavior of Smaller Crack Sizes When Subjected to Dynamic/Cyclic Load Histories

During the Degraded Piping (Ref. 8.9) and IPIRG-1 (Ref. 8.1) programs, the crack sizes evaluated in the pipe experiments were relatively large. Larger crack sizes were chosen for these experiments to facilitate analyses, since the maximum loads were low enough that the stresses in the uncracked pipe were typically elastic. While these larger crack sizes facilitated the analyses, they were not representative of crack sizes typically considered in Leak-Before-Break (LBB) or in-service flaw evaluation analyses. Smaller crack sizes, more typical of those considered in LBB or in-service flaw evaluation analyses, were tested as part of the Short Cracks in Piping and Piping Welds Program (Ref. 8.2), but only quasi-static, monotonic bending, with and without internal pipe pressure was considered. No dynamic or cyclic loadings, such as will be introduced during a seismic event, were evaluated. In order to fill this void in the experimental database, a series of short surface-cracked and short through-wall-cracked quasi-static bend and dynamic, pipe-system experiments were conducted.

In the short surface-cracked pipe experiments, the crack was in the center of a stainless steel SAW. Because of the higher yield-to-ultimate strength ratio of the weld, this weld was not very sensitive to combined dynamic, cyclic loading effects on toughness (i.e., the dynamic loading increased the toughness almost as much as the cyclic loading lowered the toughness). The use of the cyclic, dynamic J-R curve brought the single-frequency pipe system results more in line with the quasi-static behavior.

For the through-wall-cracked A106 Grade B pipe experiments, there was a 20 percent higher maximum moment in the quasi-static test than the companion pipe-system test. Since the dynamic toughness of this particular length of A106 Grade B was the same as the quasi-static toughness, and the seismic load history did not induce cyclic degradation, it was concluded that the lower failure load was attributed to the fact that the crack grew at a much larger helical angle in the quasi-static test than in the pipe-system test. Past results (Ref. 8.10) showed that helical crack growth increases the load-carrying capacity of through-wall cracked pipe in combined pressure and bending. Since the pipe-system result was accurately predicted with the existing analyses, which for this case did not require dynamic or cyclic

effects on the J-R curve, and the quasi-static test result reached loads above the scatter typically observed for these types of analyses, it was concluded:

> The existing pipe fracture mechanics analyses are sufficient for predicting the maximum loads for short through-wall and surface cracks in a pipe system, and
>
> Helical crack growth improves the load-carrying capacity for pipe loaded under combined pressure and bending.

It is speculated that ferritic pipes that are susceptible to helical crack growth may not experience as much of a beneficial effect when loaded under torsional loading; however, this is not a concern for primary nuclear piping since it does not experience high torsional loads (Ref. 8.10).

8.1.4 Behavior of Cracks Adjacent to Elbows

A question not addressed in the IPIRG-1 program was the effect of a crack at a geometric discontinuity, such as at the junction of an elbow and a straight pipe section, on the fracture behavior of a cracked-pipe system. The specific question was whether or not the fracture analysis methods previously developed and verified for cracks in straight pipe could be used to analyze cracks at such geometric discontinuities. In order to address this question, two experiments with surface cracks in the girth weld joining an elbow to a straight pipe were conducted. Data from these tests showed that the fracture ratios (experiment/predicted maximum stresses) for these elbow-girth weld experiments agreed very closely with the fracture ratios for two companion straight-pipe experiments from the Degraded Piping (Ref. 8.9) and IPIRG-1 (Ref. 8.1) programs. The maximum loads in the pipe-system tests were slightly higher than the quasi-static tests. This reflects the fact that this particular carbon steel weld had a much higher dynamic toughness than quasi-static toughness, with a smaller decrease in the toughness due to cyclic loading. This gave a combined dynamic, cyclic J-R curve that was slightly higher than the quasi-static monotonic J-R curve. As a result of the analyses of these experiments, it was concluded:

> The analysis methods previously developed and verified for straight pipe work, equally well for the case of a surface crack in a weld joining a straight pipe to an elbow. Consequently, no new analysis methods need to be developed for predicting the load-carrying capacity for this geometric condition.

It should be noted that the above conclusion is relevant to surface cracks. However, for a circumferential through-wall crack close to an elbow or nozzle, there would be restraint of the pressure induced bending that can have a considerable effect on the crack-opening displacement for small and intermediate diameter pipe for LBB applications, see Reference 8.11 and Section 8.2.4.

8.1.5 Behavior of Cracks in Elbows

In addition to studying the behavior of elbow-to-straight pipe girth weld cracks, experiments were also conducted to evaluate the behavior of circumferential surface cracks located along the extrados of elbows. A total of four cracked-elbow experiments were conducted as part of Task 2 of the IPIRG-2 program. Each involved a 180-degree internal circumferential surface crack on the extrados of a 16-inch diameter, 90-degree, long radius elbow. Two of the experiments involved cracks in A106-90 carbon steel elbows and two involved cracks in WP304L stainless steel elbows.

Also as part of this effort, two new J-estimation schemes for the case of extrados surface cracks were developed (SC.ELB1 and SC.ELB2), and one new J-estimation scheme was developed for an axial crack on the flank of an elbow (SC.ELB3) (Ref. 8.12). These J-estimation schemes were developed from a matrix of 108 FEM analyses to define the GE/EPRI-type elastic and plastic functions.

In addition, a failure avoidance criterion for cracked fittings was developed. The basic concept behind this criterion involved determining the relationship between the moments for a straight pipe and an elbow with the same flaw size and at the same applied J. Criteria were developed for both axially and circumferentially oriented cracks in fittings. To implement this methodology into a code-type document, two possible approaches were developed. The first was the simplest and more conservative, and involved using the ASME Section III B_2 stress indices directly as a stress multiplier on the straight pipe solutions. The second approach attempts to account for the conservatism associated with directly using the B_2 indices through the definition of a new stress multiplier parameter, Υ^f_x (where f is the type of fitting and x is the crack orientation). The parameter Υ^f_x was found to be linearly related to the B_2 indices, and was effectively the ratio of the moments from the elbow J-estimation scheme developed in this program relative to the straight-pipe solutions with the same size crack and at the same applied J value. It was theoretically shown that the moment ratio, at constant J values, was independent of the J value chosen assuming the elastic contributions were small.

Comparisons were made between the IPIRG-2 circumferentially cracked elbow experiments and three analyses: straight pipe J-estimation schemes, the elbow J-estimation schemes, and the Υ^f_x approach. In addition, the results of an axially flawed aged cast stainless elbow experiment were compared to the Υ^f_x analysis approach. The experiment was conducted by Electricité de France, EDF, (Ref. 8.13). The results showed that:

For the circumferentially cracked elbow, with an R/t ratio similar to that evaluated in the IPIRG-2 experiments ($R_m/t = 6$), the straight-pipe J-estimation scheme solution (SN.TNP1) was adequate for predicting the maximum moments. However, the elbow J-estimation scheme (SC.ELB2) or the Υ^f_x analysis approach may be needed for larger R/t ratio elbows.

For the axially cracked elbow case, the Υ^f_x analysis worked well.

The Υ^f_x analysis approach is a promising simple method to analyze flaws in elbows (and perhaps other fitting geometries) and can be readily codified.

8.2 Other Key Observations and Conclusions from the IPIRG-2 Program

8.2.1 Effect of Flaw Size Definition on the Predictions of the Load-Carrying Capacity of a Cracked Pipe Section

A number of the 16-inch diameter surface-cracked pipe experiments evaluated as part of this program involved initial crack geometries which were irregular in shape, i.e., the cracks were not uniform in depth and the deepest part of the crack was not at the crack centerline where the applied bending stress was the highest. In addition, a number of these experiments involved cracks in welds that have features, such as

weld crowns and counterbores, which complicate the analyses. As a result, an assessment was made to determine the most appropriate flaw size to use in a fracture prediction analysis. As a result, an assessment was made to determine the most appropriate flaw size to use in a fracture prediction analysis, and it was concluded that:

The ASME Section XI idealized constant depth flaw shape definition, where the length is assumed to be the total flaw length and the depth is assumed to be the maximum flaw depth along the entire length of the flaw, yields a conservative estimate of the load-carrying capacity of the flawed pipe.

For flaw evaluation, the weld crown height and the material removed by counterboring should not be included with the pipe thickness when making moment predictions to insure a conservative underprediction. (In reality, it is probably not known if the flaw is in the center of the weld or near the weld toe.)

A second conclusion is that if the weld crown was ground off, then these results imply that the analysis for the stainless steel weld experiments is still sufficiently accurate, but this may not be true for the carbon steel weld. In hindsight, it might have been better to conduct the IPIRG experiments with the weld crowns removed, since typically for UT flaw sizing, the weld crown is ground off.

8.2.2 Inherent Inaccuracy Associated with the ASME Section XI Z-Factor Approaches

As a result of analyses of the 16-inch diameter surface-cracked pipe experiments, it was concluded:

Contrary to what has been published in the past (Refs. 8.14 and 8.15), when accounting for the actual material strength, the degree of inaccuracy or conservatism associated with the ASME Section XI Appendix H flaw evaluation approach for ferritic pipes was similar to the degree of inaccuracy for the Appendix C approach for austenitic pipes.

The higher fracture ratios (experimental/predicted maximum stresses) for the Appendix H approach, when compared with the Appendix C approach, may be the result of the strength of the carbon steel pipe material evaluated in some of the 16-inch diameter pipe experiments (DP2-F29) being significantly higher than Code properties, while the strength of the stainless steel pipe evaluated (DP2-A8) is slightly less than Code properties.

The $2.4S_m$ definition of flow stress for ferritic steels underestimates the strength of the A106 Grade B carbon steels evaluated in this and related programs (Refs. 8.1, 8.2, and 8.9) while the $3S_m$ definition of flow stress for the austenitic steels overestimates the strength of the TP304 stainless steels evaluated in this and related programs (Refs. 8.1, 8.2, and 8.9) when Code specified values of S_m are used in the analyses.

Both the Appendix C and Appendix H elastic-plastic Z-factor approaches have a degree of conservatism associated with them of approximately 1.5 for 16-inch diameter pipe for a material with strength properties near the strength properties provided in Section II of the ASME Code. This conservation will increase as the pipe diameter increases.

8.2.3 Inherent Inaccuracy Associated with the R6 Revision 3 Option 1 and ASME Code Case N-494-3 FAD Approaches

Both the R6 Revision 3 Option 1 and ASME Code Case N-494-3 failure avoidance criteria are Failure Assessment Diagram (FAD) based approaches which allow use of actual yield and ultimate strength data in the analyses as well as Code-specified strength values.

It was concluded that there is a similar degree of conservatism associated with R6 Revision 3 Option 1 and ASME Code Case N-494-3 if the same material property data and a consistent flaw size definition is used for both analyses. Furthermore, the degree of conservatism was comparable to that for the ASME Appendices C and H approaches, if one accounts for the differences in material property data. It is of further note that there is a problem with the coding of the L_r term for the R6 analyses in the NRCPIPES code for the case where the pressure stress is a significant factor of the bending stress.

8.2.4 Conclusions from Uncertainty Analyses

The significance of a number of technical issues and how they relate to Leak-Before-Break and in-service flaw evaluations were ranked in order of importance. The technical issues which were found to be highly significant or important for LBB evaluations were:

(1) It was found that the failure probability in LBB analysis was governed more by the normal operating stress than the N+SSE stresses. At a location with low normal operating stresses, it is more difficult to satisfy LBB criteria. Implications from this area are:

- LBB criteria need to be more explicit in the evaluation criteria. The intent of NRC SRP 3.6.3 on LBB, although not explicitly stated, is to use the location with the highest N+SSE stresses. Perhaps the location with the highest normal operating stress should be selected, since that is the location where cracks are most likely to form. Choosing locations with the lowest normal operating stresses would give more conservative analyses, but cracks are less likely to occur there, and furthermore, the undesirable message given to piping designers is to have high normal operating stress in the pipe systems.

- Secondly, these results show that attention should be given to factors that affect the crack and leak rate at normal operating stresses.

(2) The effect of restraint of pressure-induced bending was found to be very significant for small, and insignificant large diameter pipe.

For a 4-inch nominal diameter pipe, accounting for restraint of pressure-induced bending reduces the LBB failure loads by a factor of nine, which greatly exceeds the $\sqrt{2}$ safety factor on load. The effect on intermediate pipe diameters, although not investigated, may not be as profound, but certainly could override the safety factor.

(3) The effect of residual stresses was determined to have a significant effect on the crack-opening displacement (and resulting crack size for a given leak rate) if the residual stress field results in through-thickness bending stresses. In this case:

The residual stress will rotate the crack faces resulting in pinching off the flow for part or all of the crack length, depending on the applied stresses.

(4) At low crack opening to surface roughness ratios, some leak-rate codes have problems with the friction factor equation becoming mathematically undefined when extrapolated beyond the existing data. Warning messages were implemented into the SQUIRT Code, but in some other codes the user may not be aware of this problem. A new COD-crack morphology model was proposed in Reference 8.16 and was used in comparison to the standard SQUIRT Code predictions. This comparison showed that for leak rates less than 3.5 liters/minute (0.92 gpm), leak-rate predictions differed by a factor of two or greater.

The technical issues which were found to be highly significant or important for in-service flaw evaluations were:

(1) A statistical analysis was undertaken to assess the statistical flaw sizing errors relative to pipe fracture loads. The 1989 EPRI UT round-robin results (Ref. 8.17) on stainless steel pipe were used in this evaluation. The results showed:

For either short-crack lengths ($\theta/\pi < 0.25$) and/or shallow cracks ($a/t < 0.25$), the pipe fracture failure loads were not sensitive to the UT flaw sizing error.

UT flaw sizing error was more significant on pipe fracture failure loads for deep long cracks.

The standard deviation (or coefficient of variance) of the pipe fracture failure loads was much less than that from the UT flaw sizing, i.e., the pipe fracture failure loads are not as sensitive as the UT flaw depth variability.

(2) Cyclic load effects on the toughness of stainless steel base metal caused elastic-plastic fracture rather than limit-load failure, hence for Service Level C and D loads, an EPFM correction (Z-factor) is needed in the ASME Section XI pipe flaw evaluation criteria for austenitic base metals.

8.3 References

8.1 Schmidt, R. A., Wilkowski, G. M., and Mayfield, M. E., "The International Piping Integrity Research Group (IPIRG) Program--An Overview," *SMiRT-11 Proceedings*, Paper G23/1, August 1991.

8.2 Wilkowski, G. M., and others, "Short Cracks in Piping and Piping Welds," Seventh Program Report--March 1993 - December 1994, NUREG/CR-4599, Vol. 4, No. 1, January 1995.

8.3 Marschall, C. W., and others, "Loading Rate Effects on Strength and Fracture Toughness of Pipe Steels Used in Task 1 of the IPIRG Program," NUREG/CR-6098, September 1993.

8.4 Marschall, C. W., and others, "Effect of Dynamic Strain Aging on the Strength and Toughness of Nuclear Ferritic Piping at LWR Temperatures," NUREG/CR-6226, July 1994.

8.5 Ernst, H., Paris, P.C., Rossow, M., and Hutchinson, J.W., "Analysis of Load-Displacement Relationship to Determine J-R Curve and Tearing Instability Material Properties," *Fracture Mechanics*, ASTM STP677, pp 581-599, 1979.

8.6 Kumar, V., and others, "An Engineering Approach for Elastic-Plastic Fracture Analyses," EPRI Report NP-1931, 1981.

8.7 Dowling, N.E., and Begley, J.A., "Fatigue Crack Growth During Gross Plasticity and the J-Integral," *Mechanics of Crack Growth*, ASTM STP 590, pp 82-103, 1976.

8.8 Olson, R., Wolterman, R., and Wilkowski, G., "Margins for Dynamic FEM Analysis of Cracked Pipe Under Seismic Loading for the DOE New Production Reactor," ASME PVP Vol. 280, pp 119-134, June 1994.

8.9 Wilkowski, G. M., and others, "Degraded Piping Program - Phase II, Summary of Technical Results and Their Significance to Leak-Before-Break and In-Service Flaw Acceptance Criteria," March 1994 - January 1989, NUREG/CR-4082, Vol. 8, March 1989.

8.10 Mohan, R., and others, "Effects of Toughness Anisotropy and Combined Tension, Torsion, and Bending Loads on Fracture Behavior of Ferritic Nuclear Pipe," NUREG/CR-6299, April 1995.

8.11 Ghadiali, N., and others, "Deterministic and Probabilistic Evaluations for Uncertainty in Pipe Fracture Parameters in Leak-Before-Break and In-Service Flaw Evaluations," NUREG/CR-6443, BMI-2191, June 1996.

8.12 Mohan, R., Brust, F.W., Ghadiali, N., and Wilkowski, G., "Development of a J-Estimation Scheme for Internal Circumferential and Axial Surface Cracks in Elbows," NUREG/CR-6445, BMI-2193, June 1996.

8.13 Le Delliou, P., Semete, P., and Ignaccolo, S., "Fracture Mechanics Analysis of Cast Duplex Stainless Steel Elbows Containing a Surface Crack," 1996 ASME PVP Conference, *Fatigue and Fracture-1996*, Volume MF-1, June 1996.

8.14 Scott, P. M., and others, "The IPIRG-1 Pipe System Fracture Tests: Analytical Results," PVP Vol. 280, pp 153-163, June 1994.

8.15 Krishnaswamy, P, and others, "Fracture Behavior of Short Circumferentially Surface-Cracked Pipe," NUREG/CR-6298, November 1995.

8.16 Rahman, S., and others, "Probabilistic Pipe Fracture Evaluations for Leak-Rate Detection Applications," NUREG/CR-6004, April 1995.

8.17 "Accuracy of Ultrasonic Flaw Sizing Techniques for Reactor Pressure Vessels," Electric Power Research Institute, EPRI-NP-6273, Palo Alto, California, 1989.

NRC FORM 335 (2-89) NRCM 1102, 3201, 3202

U.S. NUCLEAR REGULATORY COMMISSION

BIBLIOGRAPHIC DATA SHEET

(See instructions on the reverse)

1. REPORT NUMBER (Assigned by NRC, Add Vol., Supp., Rev., and Addendum Numbers, If any.)
NUREG/CR-6452
BMI-2195

2. TITLE AND SUBTITLE
The Second International Piping Integrity Research Group (IPIRG-2) Program - Final Report

3. DATE REPORT PUBLISHED
MONTH: March
YEAR: 1997

4. FIN OR GRANT NUMBER
D2060

5. AUTHOR(S)
A. Hopper, G. Wilkowski, P. Scott, R. Olson, D. Rudland, T. Kilinski, R. Mohan, N. Ghadiali, and D. Paul

6. TYPE OF REPORT
Technical

7. PERIOD COVERED *(Inclusive Dates)*
10/91 - 4/96

8. PERFORMING ORGANIZATION – NAME AND ADDRESS *(If NRC, provide Division, Office or Region, U.S. Nuclear Regulatory Commission, and mailing address; if contractor, provide name and mailing address.)*
Battelle
505 King Avenue
Columbus, OH 43201-2693

9. SPONSORING ORGANIZATION – NAME AND ADDRESS *(If NRC, type "Same as above"; if contractor, provide NRC Division, Office or Region, U.S. Nuclear Regulatory Commission, and mailing address.)*
Division of Engineering Technology
Office of Nuclear Regulatory Research
U. S. Nuclear Regulatory Commission
Washington; D. C. 20555-0001

10. SUPPLEMENTARY NOTES
T. Hayrich, NRC Project Manager

11. ABSTRACT *(200 words or less)*

The IPIRG-2 program was an international group program managed by the U.S. NRC and funded by organizations from 15 nations. The emphasis of the IPIRG-2 program was the development of data to verify fracture analyses for cracked pipes and fittings subjected to dynamic/cyclic load histories typical of seismic events. The scope included: (1) the study of more complex dynamic/cyclic load histories, i.e., multi-frequency, variable amplitude, simulated seismic excitations, than those considered in the IPIRG-1 program, (2) crack sizes more typical of those considered in Leak-Before-Break (LBB) and in-service flaw evaluations, (3) through-wall-cracked pipe experiments which can be used to validate LBB-type fracture analyses, (4) cracks in and around pipe fittings, such as elbows, and (5) laboratory specimen and separate effect pipe experiments to provide better insight into the effects of dynamic and cyclic load histories. Also undertaken were an uncertainty analysis to identify the issues most important for LBB or in-service flaw evaluations, updating computer codes and databases, the development and conduct of a series of round-robin analyses, and analyst's group meetings to provide a forum for nuclear piping experts from around the world to exchange information on the subject of pipe fracture technology.

12. KEY WORDS/DESCRIPTORS *(List words or phrases that will assist researchers in locating the report.)*
Pipe, elbow, fracture mechanics, fracture leak-before-break, nuclear, J-integral, crack surface crack, through-wall crack, leak rate, probabilistic analysis, cyclic loading, dynamic loading, seismic, carbon steel, stainless steel, welds, dynamic strain aging, circumferential crack, axial crack, ASME Section XI, limit load, residual stresses, J-R curve, ultrasonic testing, pipe-system toughness, R6

13. AVAILABILITY STATEMENT
Unlimited

14. SECURITY CLASSIFICATION
(This Page)
Unclassified
(This Report)
Unclassified

15. NUMBER OF PAGES

16. PRICE

NRC FORM 335 (2-89)